The University of Nottingham

UNITED KINGDOM · CHINA · MALAYSIA

An Investigation into the Impact of Hydrothermal Carbonisation on the Suitability of Biomass for Fuel Switching

Robert John Stirling, MChem

Thesis submitted to the University of Nottingham for the degree of Doctor of Engineering

September 2018

Abstract

Biomass has the potential to be a useful low-carbon replacement for coal in a number of applications. Hydrothermal carbonisation (HTC) is a pre-treatment technology which has the potential to alleviate many of the drawbacks of replacing coal with biomass, as it improves many of the fuel properties of biomass. This study was conceived as a means to investigate the impact of HTC on the suitability of biomass for this purpose, and to investigate the chemisty of HTC so that the process could be more deeply understood. HTC experiments were performed using a Parr reactor heated by a sand bath, and numerous analytical techniques were used to investigate the composition and properties of the biocoal produced. Major analytical techniques used include thermogravimetric analysis, elemental analysis, gas chromatography, XRF spectrometry, textural analsyis, and NMR. Devolatilisation of samples in a drop tube furnace was also used so that chars generated under high heating rates equivalent to what is seen in pulverised fuel combustion could be investigated.

The impact of HTC process parameters on the yield and composition of biocoal was investigated, and HTC temperuature was found to have the largest impact. Increasing temperature decreased the yield of HTC, and resulted in a biocoal with a lower moisture and volatile matter content, with a higher fixed carbon content. Temperature also had a significant effect on the energy yield and energy densification of biocoal, with increasing temperature decreasing the

yield and increasing the densification. A good compromise was found at a midpoint temperature of 225°C, before the energy yield dropped considerably. Anaerobic digestion was calculated to have significant potenital for increasing the energy yield of HTC, especially when there is sinigicant loss of organic matter to the process liquor. The feedstock was also found to have a significant effect on the outcomes of HTC, primarily linked to the biochemical compostion of the feedstock.

The removal of alkali and alkaline earth metals was found to have a strong impact on the char reactivity of biocoal, with surface area and biocoal composition providing secondary impact. Biocoal produced from soft wood biomass was shown to have a char reactivity similar to that of high-volatile bituminous coal, but HTC of biomass with higher levels of alkali and alkaline earth metals resued in a biocoal with a reactivity lower than that of the feedstock biomass, but higher than that of high-volatile bituminous coal. A coal-equvalent fuel was generated by torrefaction of soft wood biocoal.

The role of water in the aromatisation reactions occuring during HTC in comparison to torrefaction was investigated. Lower levels of aromatisation were seen in HTC than in torrefaction, indicating that the water present in HTC suppresses aromatisation.

HTC was found to have little impact on the yield of activated carbon production, and was found to lower the surface area of activated carbon due to deposition of organic matter in the pores of the feedstock.

Publications

Journal publications

R.J. Stirling, C.E. Snape, W. Meredith, The impact of hydrothermal carbonisation on the char reactivity of biomass, Fuel Process. Technol. 177 (2018) 152–158. doi:10.1016/j.fuproc.2018.04.023.

Oral presentations

Stirling, R.; Snape, C.; Meredith, W. (2016) 'Hydrothermal carbonisation of biomass to produce reduced-ash fuel', 2nd International Congress and Expo on Biofuels & Bioenergy, August 2016, Sao Paulo, Brazil.

Stirling, R.; Snape, C.; Meredith, W. (2017) 'Char reactivity of hydrothermally-treated biomass', 2017 International Conference on Coal Science & Technology and 2017 Australia-China Symposium on Energy, September 2017, Beijing, China.

Stirling, R.; Snape, C.; Meredith, W. (2018), 'The effect of hydrothermal carbonisation on the char reactivity of biomass', 22nd International Symposium on Analytical and Applied Pyrolysis, June 2018, Kyoto, Japan.

Poster presentations

Stirling, R.; Snape, C.; Meredith, W. (2018), 'The effect of hydrothermal carbonisation on the char reactivity of biomass', 26th European Biomass Conference and Exhibition, May 2018, Copenhagen, Denmark.

Acknowledgements

This work was supported by the UK Engineering and Physical Sciences Research Council (EPSRC) through the Centre for Doctoral Training in Carbon Capture and Storage and Cleaner Fossil Energy [grant number EP/L016362/1] as part of the Flex-E-Plant project (grant number EP/K021095/1).

I would like to acknowledge my supervisors, Professor Colin E. Snape and Dr. Will Meredith. I am very grateful for their guidence.

I would also like to thank Adrian Quinn, Dr. Clement Uguna, Dr. Lee Stevens, Dr. Jaqueline Deans, and Teresa Needham for their assistance in laboratory work and analysis.

I sincerely appreciate my colleagues in the centre for doctoral training for their support and friendship over the last four years.

Finally, I would like to thank my family. Their unwavering support has been invaluable, and I am forever grateful to them.

Table of contents

Figures

Tables

Equations

Chapter 1 Introduction

1.1 Reducing global emissions – global and national targets

Anthropogenic carbon dioxide (CO_2) emissions have now been globally accepted as the primary cause of accelerated global warming, and as such numerous countries are committing to drastically reducing their emissions. This commitment has been made legally binding though legislation such as the Paris Agreement, which has been signed by the majority of the largest economies of the World. This agreement stipulates a long-term goal of limiting the global temperature increase to below 2°C, with additional focus on attaining a limit of 1.5°C above pre-industrial global temperature (Schleussner et al., 2016).

On a national level, the United Kingdom has committed to a goal of reducing emissions to 80% of pre-industrial levels by 2050 though the Climate Change Act (Lockwood, 2013). This target has been broken down into stages, with the UK publishing carbon budgets stating reduction targets for specific periods. The most recent UK pledge, the fifth carbon budget, sets a target of 57% reduction of CO_2 emissions 1990 levels by 2030 (Committee on Climate Change (CCC), 2017). There has been a steady decline in UK CO_2 emissions, with steep reductions in 2014 and 2016. In 2017, UK emissions were 42% below 1990 levels (Committee on Climate Change (CCC), 2017), with the first and second carbon budgets (2008-12) was satisfied, and the third carbon budget having already been surpassed years in advance of the deadline. In spite of these significant achievements, the UK is currently not on track to meet the fourth

and fifth carbon budgets, and in June 2017 there had been no significant policy plans published since the unveiling of the fifth carbon budget. Clearly much more work needs to be done to ensure that emission targets are met and dangerous climate change (above 2°C warming) is avoided.

1.2 Current status of emissions

There are multiple major sources of CO_2 emissions globally. Generation of electricity and heat is the largest contributor to global emissions, but transport and industry are also large contributors. These three sectors accounted for 42 %, 24 %, and 19% of global emissions in 2015 (IEA, 2017a), and are therefore the key areas that need to be addressed if significant emissions reductions are to be realised.

Fossil fuels still form the base of power generation portfolios, as can be seen in Figure 1.1. The use of fossil fuels globally has only marginally reduced in the 45 years between 1971 and 2016, going from 86% to 81%. This reduction was mainly due to a significant reduction in the use of oil for energy generation, largely replaced by natural gas and nuclear energy. The use of coal power increased slightly over this time.

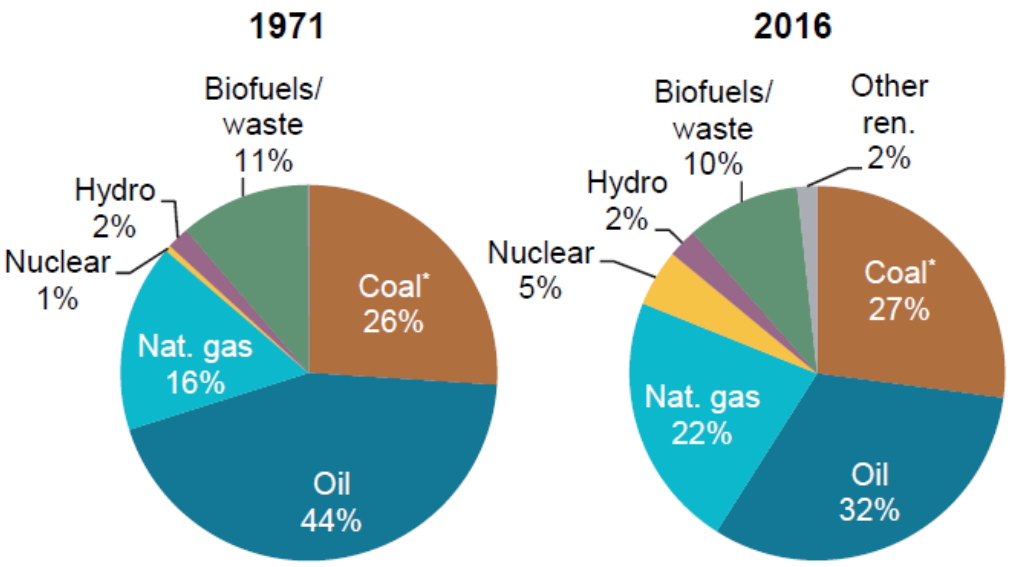

Figure 1.1 Global primary energy supply by fuel in 1971 and 2016 (IEA, 2018b)

Fossil fuels are especially heavily involved in fast-growing emerging countries such as India and China. These two countries are responsible for two thirds of the global electricity production rise in 2016, and were separated by the United States in the top three producers of electricity in the world (IEA, 2017b). The immense population of these countries mean that there is a large demand for electricity, which results in fossil fuel combustion being by far the largest power generation source in the world. China and the Asia-Pacific region in particular will have an extremely significant impact on global emissions through power generation, as it still has a large reliance on coal. The Asia-Pacific region derives 49% of energy from coal, and China itself represents nearly 25% of global electricity generation (IEA, 2017b). Some of the largest economies in the World are still growing significantly and rely on fossil fuels for the majority of their energy, so fossil fuels will remain a significant factor in the global energy mix

for the near future. This can be seen in Figure 1.2 Percentage of global fossil fuel use by nation , which shows China and the USA as the main users of coal power, with the USA also being large users of oil and natural gas power.

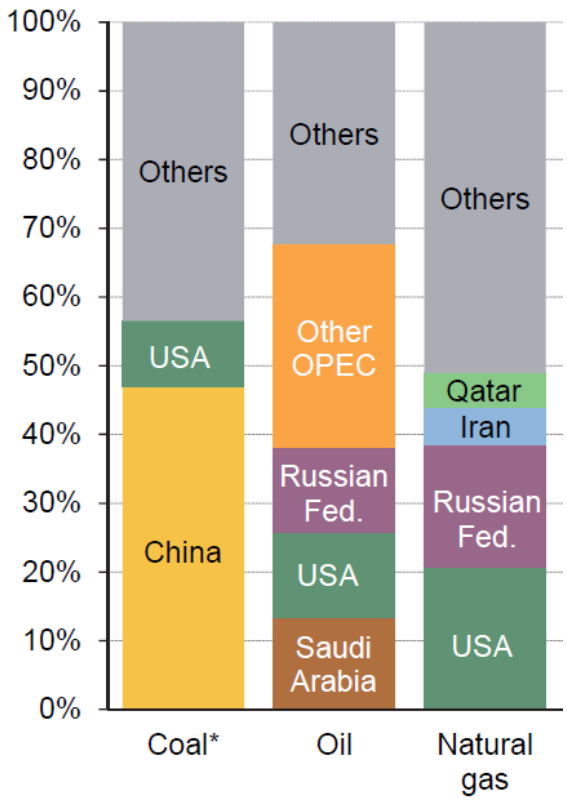

Figure 1.2 Percentage of global fossil fuel use by nation (IEA, 2018b)

A breakdown of CO_2 emissions by region and country can be seen in Figure 1.3 and Figure 1.4, respectively. The figures confirm that some of the largest economies in the world, which are heavily reliant on fossil fuels for power generation, contribute an extremely large portion of global CO_2 emissions. China is the largest CO_2 emitter by far, as a result of using approximately 45% of global coal power.

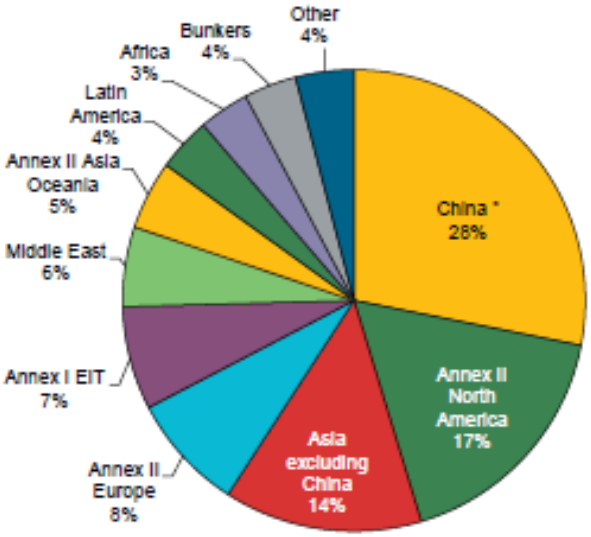

*China – China and Hong Kong

Figure 1.3 Percentage of global fossil fuel use by nation (IEA, 2018b)

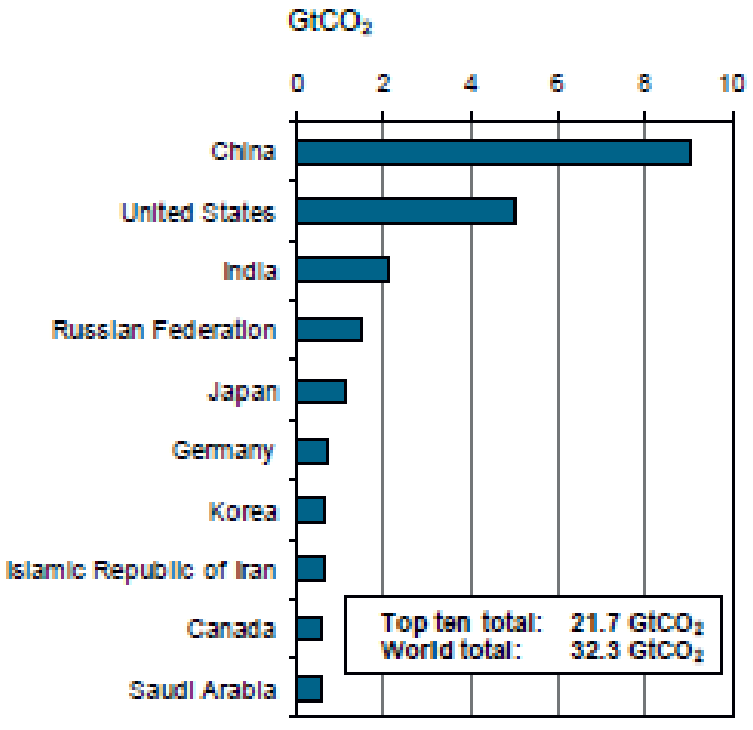

Figure 1.4 CO2 emissions by country (IEA, 2017a)

The UK has been committed to reducing CO_2 emissions in the recent past. A graph depicting UK CO_2 emissions reductions can be seen in Figure 1.6, which

shows that the greatest reduction in CO_2 emissions has been a result of changes in power generation. This is a result of the country adopting renewable energy and low-carbon fossil fuel combustion. In the UK, nearly all of the emission reductions stem from the power sector, and 75% of emission reductions have been the result of abandoning coal as a source of electricity (Committee on Climate Change (CCC), 2017). Alternatives that have been implemented include gas combustion (with higher efficiency resulting lower CO_2 emissions per unit of energy), and numerous renewable energy sources. The emissions associated with transport and buildings have risen in 2015 and 2016. Both of these sectors are seeing increased emissions due to increased demand and slowed development and deployment in efficient alternatives. Industrial emissions have been falling, but this is mainly due to a reduction in production (not due to policy) rather than development of low-carbon alternatives (Committee on Climate Change (CCC), 2017). A focus on low carbon alternatives as well as policy implementation is needed to ensure and bolster the continued decline of CO_2 emissions.

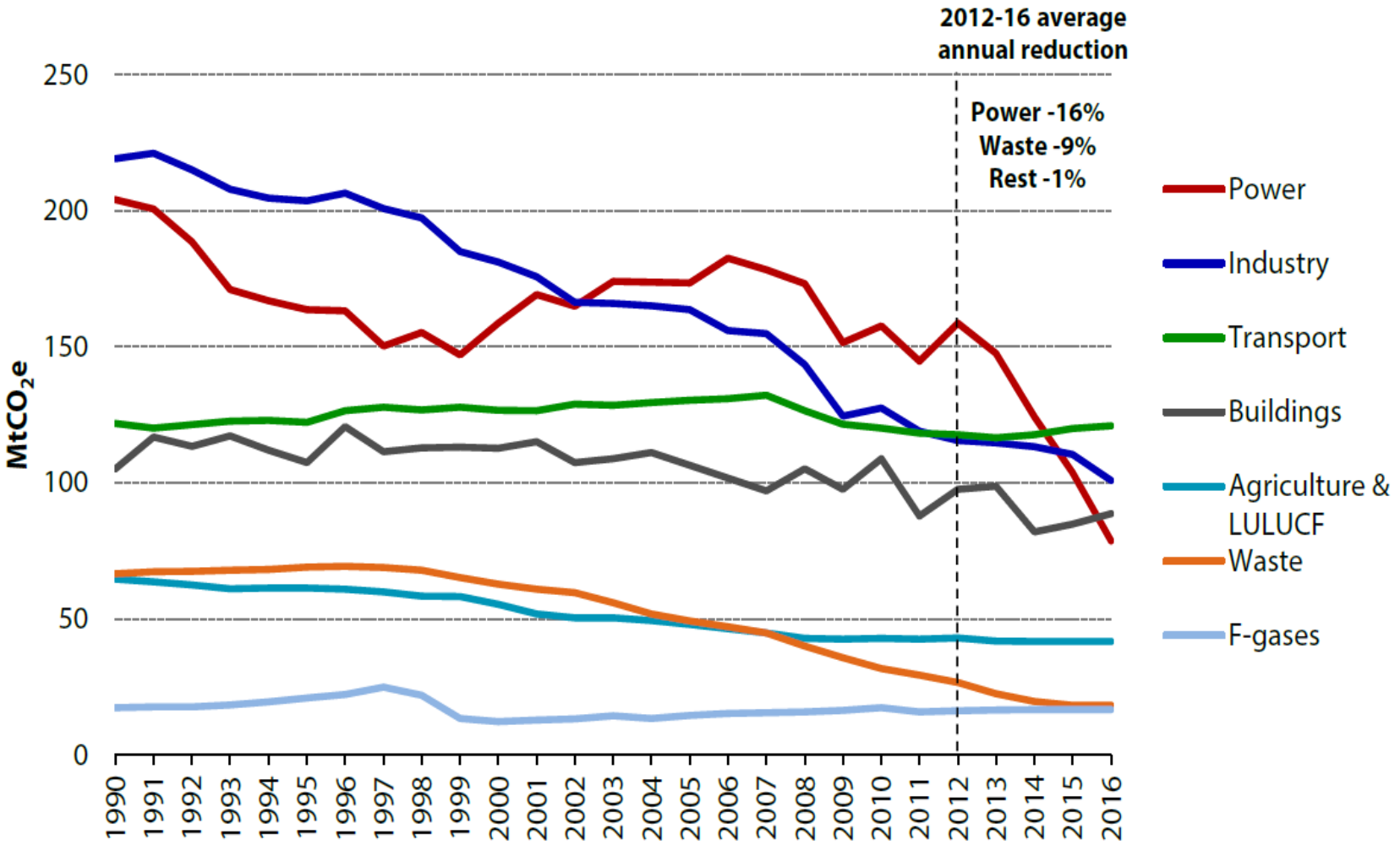

Figure 1.5 UK emissions reduction by sector from 1990 to 2016 (Committee on Climate Change (CCC), 2017)

1.3 Potential of biomass utilisation to reduce CO2 emissions

Biomass is an important energy source for the future. This is defined as any organic material derived from plants (McKendry, 2002), or animals (Iakovou, Karagiannidis, Vlachos, Toka, & Malamakis, 2010). It is the fourth largest energy resource available on Earth (Ladanai & Vinterbäck, 2009), and as such has a large part to play in securing future sustainable energy production if utilised correctly. The theoretical biomass energy supply could be as high as 1100 EJ (26273 Mtoe) (Iakovou et al., 2010), which is much more than current global energy use. In 2016, total energy supply was 13761 Mtoe (IEA, 2018). A breakdown of biomass energy potential in certain scenarios can be seen in Table 1.1, ranging from a scenario where little land is used for energy crops and no human consumption behaviour changes occur, to one where there is a very large supply of energy crops and there is a low human population. It shows that a number of favourable conditions would have to occur to have biomass supply the entirety of the global energy demand in 2016, but it highlights that biomass has great potential to be a significant contributor to global low-carbon energy supply under a range of conditions.

Table 1.1 Projection of global biomass energy potential under different scenarios (Slade, 2011)

Global biomass potential (EJ (Mtoe))	Essential pre-conditions
0 – 100 **(0 – 2388)**	• Little or no land for energy crops (<0.4Gha total) • High meat diet/low input agriculture • Limited expansion of cropland area and high level of environmental protection • Use only agricultural residues
100 – 300 **(2388 – 7165)**	• Crop yields keep pace with demand, <0.5Gha land for energy crops • Low population/vegetarian diet/limited deforestation • Agricultural, forestry, and waste residues used (<100EJ)
300 – 600 **(7165 – 14331)**	• Crop yields outpace demand, 1.5Gha land for energy crops (1Gha good agricultural land) • Low population/vegetarian diet/extensive deforestation/conversion to managed forestry • Agricultural, forestry, and waste residues used (<100EJ)
600 – 1200 **(14331 – 28662)**	• Crop yields outpace demand, >2.5Gha land for energy crops (>1.3Gha good agricultural land) • High/very high input farming, limited, and landless, animal production with dung recovery • Low population (<9bn) • Vegetarian diet or extensive deforestation/conversion to manage forestry • Agricultural, forestry, and waste residues used (<100EJ)

Utilisation of biomass in place of fossil fuels can also have an impact on carbon dioxide emissions. Biomass is carbon neutral (Agbor, Zhang, & Kumar, 2014), which means that the utilisation of it results in a net zero carbon dioxide emission, as the CO_2 released is balanced by that absorbed during biomass growth (McManus, 2010). As such, biomass utilisation can theoretically result in a reduction of the carbon emissions of an energy consuming system if it replaces fossil fuels as the energy or CO_2 source. This is known as fuel switching (Jun Li, Brzdekiewicz, Yang, & Blasiak, 2012).

The carbon neutrality of biomass disregards any additional emissions associated with processing and transport of biomass. The transport emissions associated with different biomass feedstocks used in the UK can be seen in Table 1.2. It shows that the source of biomass has a great effect on the emissions associated, with palm residues from Indonesia and Malaysia having over 60 times more transport emissions associated than biomass sources locally in the UK. A significant net reduction in emissions through fuel switching is still feasible as long as emissions associated with processing are minimised through careful process optimisation.

Table 1.2 Transport emissions associated with different biomass feedstocks used in the UK (DEFRA, 2007)

Feedstock	Likely country of origin	Mode of transport	Total transport emissions (kg CO_2/tonne biomass)
Energy crops	UK	Road	1.7
Shea residues	Africa	Ship	55.4
Sunflower pellet	Romania	Road and ship	47.1
Sewage sludge and waste derived fuels	UK	Road	3.4
Cereal co-products and pellets	UK	Road	1.7
Tallow	UK	Road	1.7
Olive waste	Greece, Italy, Spain	Road and ship	21.2
Wood	UK, Canada, Latvia, Scandinavia	Road and ship	1.7 – 42.9
Palm residues	Indonesia, Malaysia	Road and ship	106.5 – 107.4

Biomass derived energy (bioenergy) has an advantage over other renewable energy sources such as solar or wind power in that it is not intermittent and inflexible, as it is not dependent on the weather. It is therefore similar to fossil fuels in being a flexible and responsive source of energy, being able to easily meet fluctuating energy demand. A further advantage of bioenergy is that it have multiple end uses, being able to provide electricity, heat, and transport fuel (McManus, 2010), with biomass also being able to act as a feedstock in the manufacture of chemicals (Kruger, Kicherer, Kormann, & Raupp, 2018) and other industrial processes. These uses for biomass will be outlined below.

As was shown in section 1.2, power and heat generation is the largest CO_2 emitting sector globally. Therefore, this is where biomass can have the largest effect in terms of reducing overall global CO_2 emissions. Biomass already has a long history of use in heating being the traditional source of heat for cooking and space heating.

1.3.1 Power generation

The combination of relatively inefficient power generation and significant CO_2 emissions associated with coal combustion systems means that unabated coal combustion for power generation will soon become unacceptable in a low carbon energy portfolio. As some of the largest economies in the world (China and India) are still heavily reliant on coal power, and another (USA) is returning

to utilising coal, finding a way to reduce the CO_2 emissions of coal-based power generation is pivotal to ensuring the continued reduction of global CO_2 emissions. Replacing coal with solid biomass fuels would reduce the greenhouse gas (GHG) emissions of coal-fired power plants, which would make thermal power more compatible with a low carbon economy. The introduction of biomass into fossil fuel power generation can be done either partial replacement through co-firing, or full replacement through retrofitting existing coal-fired boilers or building dedicated biomass boilers. Co-firing in particular is viewed as an attractive solution to quickly introduce biomass into the energy sector, and can be utilised through a number of methods, including direct co-firing, indirect co-firing, and parallel co-firing. Untreated biomass is thought to have a potential to replace more than 50% of coal in co-firing (Agbor et al., 2014).

Biomass power generation can also be combined with carbon capture and storage (CCS), this is called bioenergy with CCS (BECCS) (Bui, Fajardy, & Mac Dowell, 2017). Combining the carbon neutral combustion of biomass with CO_2 capture results in net negative CO_2 emissions if the entire process is carefully optimised and deployed. Negative CO_2 emissions are necessary in the majority of scenarios if we are to limit global warming to below the 1.5°C target (Muri, 2018), and BECCS will be competitive in liberalised energy markets in the near to medium term, further emphasising the vital role that biomass will play in future energy mixes (Bui et al., 2017).

1.3.2 Heating and domestic use

Another sector where biomass can have a significant effect on emissions is heating. Biomass heating systems have the potential to produce 100% renewable domestic hot water and heating (Verma, Bram, & De Ruyck, 2009). The high thermal conversion efficiency of biomass makes it optimal for heat generation (Pantaleo, Candelise, Bauen, & Shah, 2014), which combined with carbon neutrality means that there is potential for large reductions in CO_2 emissions when replacing fossil fuel based heating. Use of biomass heating can be very profitable, and can possess financial paybacks in the month time frame (McManus, 2010). Profitability is especially high in the case of high heat load rates where fossil fuel costs are high (Pantaleo et al., 2014), meaning that there is a tangible incentive to implementation. In the case of residential and tertiary sector (trade, commerce, and services (Schlomann et al., 2006)), the profitability is dependent on the distribution costs and heat demand (Pantaleo et al., 2014). Emissions can also become an issue if situated in areas with existing air pollution problems (McManus, 2010) (Verma et al., 2009). Biomass can also be utilised in combined heat and power (CHP) stations to maximise efficiency, although there are higher investment costs than in conventional heating (Pantaleo et al., 2014). CHP implementation alongside district heating and cooling (DHC) is expected to be an important factor in reducing emissions (Kummamuru Venkata et al., 2016).

1.3.3 Biomass derived gas (biogas)

As well as being used as a coal replacement in solid fuel power generation and heating, biomass can be transformed into a gaseous fuel using gasification. The gasification process converts biomass into a gas primarily containing hydrogen, methane, carbon monoxide, and carbon dioxide, which has numerous beneficial decarbonising applications (Heidenreich & Foscolo, 2015). Gas can also be produced from biomass from other processes such as pyrolysis (Perkins, Bhaskar, & Konarova, 2018) and anaerobic digestion (AD) (Patrizio, Leduc, Chinese, Dotzauer, & Kraxner, 2015).

1.3.4 Transport

As has been stated in section 1.2, transport emissions form a large portion of global emissions that remains relatively untouched by emissions reduction. Biomass can form a pivotal part of the solution to this problem, with a number of processes being investigated and implemented converting the solid feedstock into transport fuels. Pyrolysis is a process that results in solid, liquid and gaseous products through thermal decomposition of biomass in the absence of oxygen. The temperature, and especially residence time of pyrolysis affects the distribution of product phases. Fast pyrolysis results in bio-oil (75–80% polar organics, 20–25% water (Ail & Dasappa, 2016)) which can be used as a transport fuel with after further processing (Perkins et al., 2018). The Fischer-Tropsch (FT) process is a fairly established and advanced process which can convert synthesis gas produced from pyrolysis or gasification into transport

fuels (Ail & Dasappa, 2016). The fuel produced in FT has similar combustion properties to conventional fuels. Economically and environmentally favourable biofuel production is feasible, especially in some developing countries such as India where there are climates that are optimal for biomass growth, alongside lower labour and capital costs (Ail & Dasappa, 2016). Methane from biomass can also be used as compressed natural gas (CNG) as a transportation fuel (Patrizio et al., 2015).

1.3.5 Industrial applications

Biomass can be processed using pyrolysis to produce feedstocks for the chemicals industry (Perkins et al., 2018). Biomass derived naphtha or biogas can directly compete with those derived from crude oil or natural gas in producing basic organic chemicals which can be further processed into other products. Biomass derived raw materials like sugars, ethanol and plant oils can also be converted into dedicated products (Kruger et al., 2018).

Biomass also can also be processed into activated carbon, which has numerous potential applications such as pollution control (Mohamad Nor, Lau, Lee, & Mohamed, 2013) and catalysis (Baccar, Bouzid, Feki, & Montiel, 2009). The limitation on potential feasible application by the high cost of activated carbon can be eased by use of low-cost biomass wastes as a feedstock (Baccar et al., 2009).

The iron- and steel-making industries use a significant amount of coal. This is responsible for the majority of CO_2 emissions from the steel industry. Biomass can be used either as a full or partial replacement of coal in this application, although the biomass needs processing prior to use. Untreated biomass can be blended with coal to make a bio-coke (Ng, MacPhee, Giroux, & Todoschuk, 2011). A 20% replacement of coal coke with biomass in a pig iron plant can result in an emission reduction in 15% (Fick, Mirgaux, Neau, & Patisson, 2014).

1.4 Current utilisation of biomass

Bioenergy is the largest current renewable energy source, as can be seen in the distribution of energy and renewable energy supplies displayed in Figure 1.6 and Figure 1.7, respectively. Figure 1.7 also shows that solid biofuels make up by far the largest phase of biofuel used. A 2016 World Energy Council report stated that bioenergy represented over 75% of the renewable energy in the energy mix, supplying 10% of global energy (Kummamuru Venkata et al., 2016). Countries that have high investment in renewable also invariably have significant utilisation of biomass. For example, roughly one quarter of the U.S non-fossil energy production is bioenergy, and the use of biomass is increasing (Young, Anderson, Naughton, & Mullan, 2018).

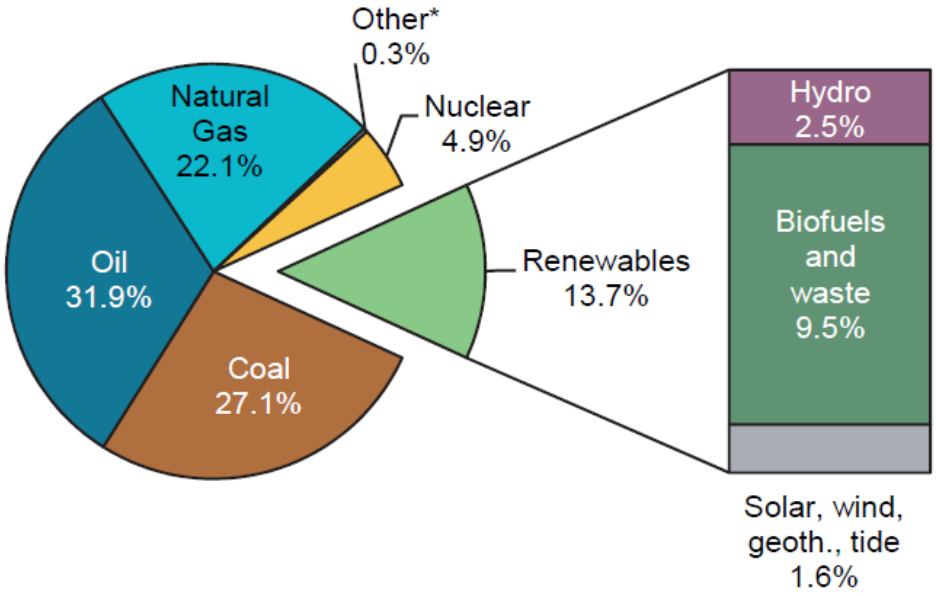

* Other includes non-renewable wastes and other sources not included elsewhere such as fuel cells.

Note: Totals in graphs might not add up due to rounding.

Figure 1.6 Distribution of primary energy supply, 2016 (IEA, 2018a)

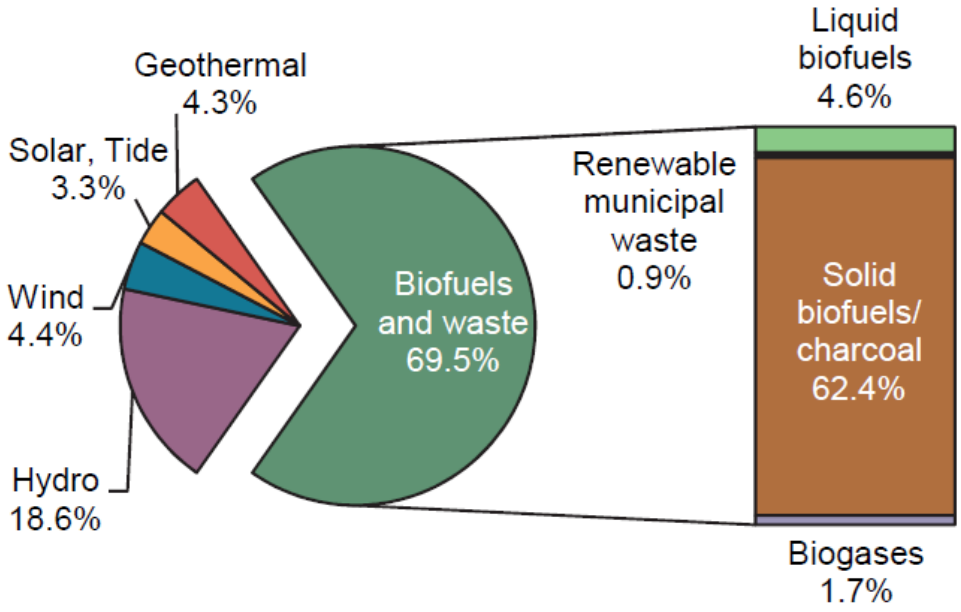

Note: Totals in graphs might not add up due to rounding.

Figure 1.7 Distribution of renewable energy supply, 2016 (IEA, 2018a)

The distribution of both traditional (cooking, space heating) and modern biomass use (energy, heating, and transport etc.) globally can be seen in Figure 1.8. Traditional biomass use is more prevalent than modern biomass use, and is the vast majority use in developing areas like Sub Saharan Africa (Kummamuru Venkata et al., 2016). In developed countries, modern biomass use is nearly the sole use of biomass, and will only increase in the future, providing a solid foundation for renewable energy based, low-carbon economies. The mode of utilisation of biomass varies geographically, with biofuels being a focus in South America, wood and charcoal fuel in Asia and Africa, and CHP generation in Europe.

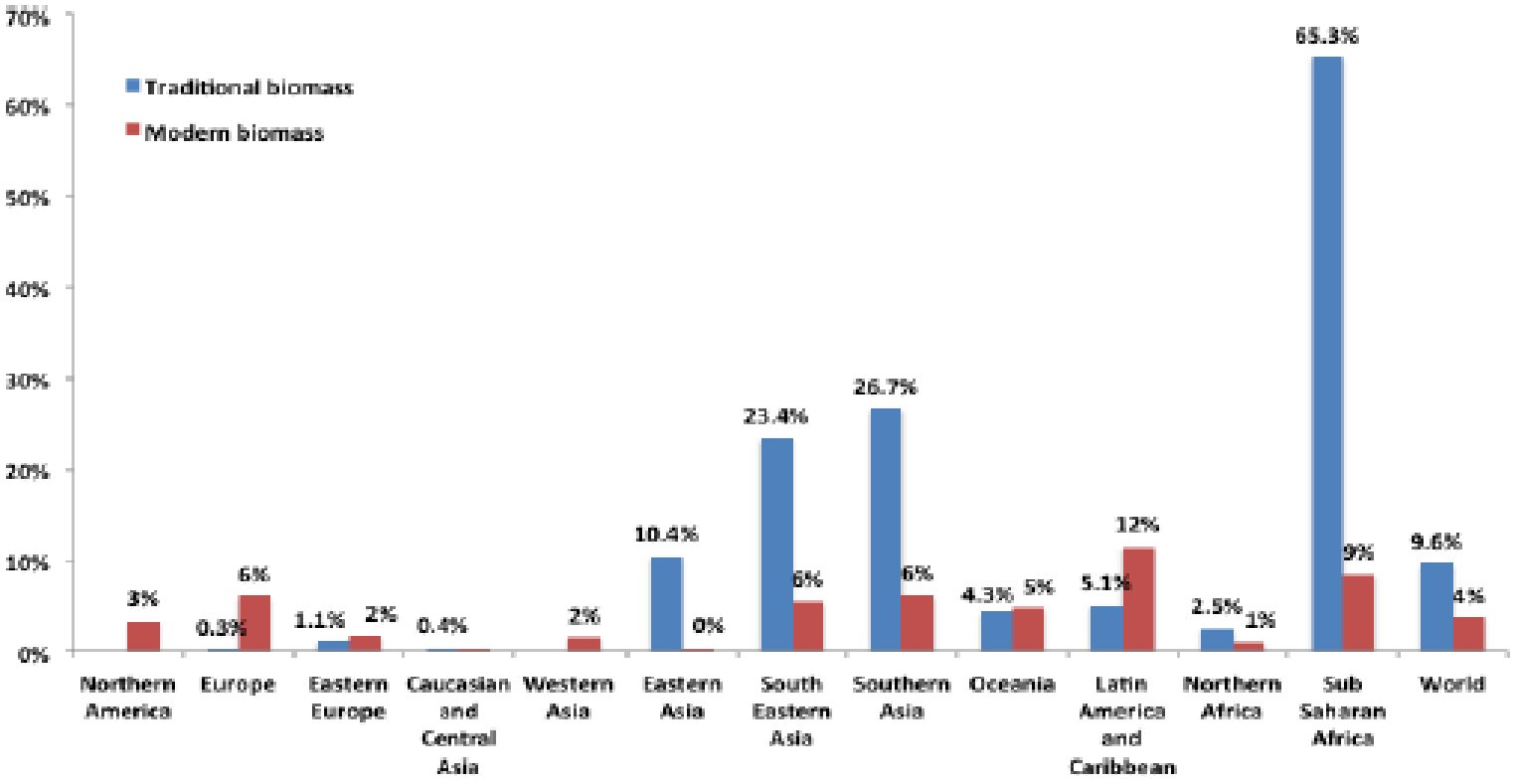

Figure 1.8 Share of biomass in final energy consumption (World Energy Council, 2016)

1.4.1 Power generation

The world leaders in biomass power plants are the USA, China, India, Germany, and the UK. In 2015, the proportion of biomass installed capacity in global of bioenergy among all renewable energy technologies was 5.3%, and in terms of electricity generation this value is 8.6% (Freiberg, Scharfe, Murta, & Seidler, 2018).

In 2010, Chinese biomass power generation capacity was 5.5 GW, with the majority coming from straw and waste biomass direct-fired power generation. China plans to have increased this capacity to 30GW by 2020 (Xingang, Zhongfu, & Pingkuo, 2013). In 2017, the reported capacity was 14.88 GW (SXCoal, 2018).

There is also some involvement in developing biomass power generation in the UK. Drax power station, in North Yorkshire, England, practices indirect co-firing. This involved power generation utilising separate biomass (wood pellets) and coal boilers. Four out of the six 660MW boilers have been converted to burn biomass (E&T, 2019). Drax aim to achieve full conversion to biomass power by 2025. In addition to co-firing projects, there are also large-scale fluidised bed reactors burning solely biomass, for instance the Steven's Croft plant in Lockerbie, Scotland (McIlveen-Wright et al., 2011).

Large-scale deployment of negative-emissions BECCS deployment is currently an idea rather than a practicality. In 2015, there were 15 pilot and one

commercial BECCS plant globally (Burns & Nicholson, 2017). Drax are currently working towards establishing the first BECCS pilot plant in Europe (Drax, 2017).

1.4.2 Heating and domestic use

Traditional biomass combustion is still being used heavily in developing countries as a primary source of heat, both for space heating and cooking (Sander, Waqar Haider, & Hyseni, 2011). Biomass is also used extensively in rural china for cooking and heating (J. Chen et al., 2017). In terms of modern heat generation using biomass, industrialized countries are generating heat from biomass mostly industrial co-generation of heat and power, private residential heating, and district heat and electric power generation. These generally involve advanced biomass combustion, gasification and pyrolysis processes (Young et al., 2018).

In the EU, small-scale pellet stoves and boilers are being used reliably, with testing and certification of biomass products. EU regulations have been published with more scheduled. These concern efficiency emissions, safety, and residential installations. Financial incentives are a key driver in this market (Verma et al., 2009).

In the US, many private and public facilities use woody biomass as fuel in decentralized heating systems to facilitate on-site disposal of manufacturing by-products and support of local forest management and forest industry. In

2014, there were 401 known biomass heating systems installed in US institutions (Young et al., 2018).

1.4.3 Transport

Global production of biofuels is continuing to increase, but is slowing down. Worldwide biofuels production in 2016 totalled 82,306 thousand tonnes of oil equivalent, which represented a 2.6% growth from 2015 (British Petroleum, 2017). This was a larger increase than was seen in 2015, but much less than the average growth rate per annum from 2005-15 of 14.1% (British Petroleum, 2017). The largest increases in biofuels production from 2006 and 2016 were seen in North and South America, with Europe and Eurasia contributing significantly in the increasing use of biodiesel, but not bioethanol. The rest of the world has had a much smaller impact but has seen a large increase in biodiesel use (British Petroleum, 2017).

1.4.4 Industrial applications

Over the last ten years, there has been increasing governmental and private interest in fundamental research and process development for generating chemicals from biomass. Recent research has been focused on areas such as novel catalysts, protein engineering, synthetic biology and metabolic pathway engineering to transform sugars, lignin, and waste products such as glycerol into valuable commodity chemicals (Wheeldon, Christopher, & Blanch, 2017) (Sheldon, 2014). A selection of these advancements have been commercialised

or are currently en-route to becoming traditional industrial practice (Sheldon, 2014).

There is also research being conducted currently attempting to facilitate use of biomass in the steel production industry. Applications studied include sintering solid fuel, coke making, blend components, steelmaking recarburiser, nut coke replacement and pre-reduced feed reductants (Mathieson, Rogers, Somerville, Ridgeway, & Jahanshahi, 2011).

1.5 Limitations of biomass

Although biomass has the potential to have a significant impact on the reduction of global carbon dioxide emissions as a fossil fuel replacement, there are a number of limitations it possesses that prove problematic. There are technical, logistical, and economic factors that hinder biomass utilisation, which are described below.

1.5.1 Differing properties to fossil fuels

One of the main difficulties faced when utilising biomass as a fossil fuel replacement is that it often possesses different fuel properties to the targeted fuel. This severely limits the potential of biomass. This can be clearly seen in the case of using biomass as a coal replacement in power generation. Coal is more energy dense, more friable, more hydrophobic, less reactive, and has

lower concentrations of corrosive alkali and alkaline earth elements than biomass (Vassilev, Vassileva, & Vassilev, 2015).

The lesser energy density of biomass has impacts on the throughput of processes and also increases the transport energy needed (Miedema, Benders, Moll, & Pierie, 2017). This has a significant impact on the cost of the process (Searcy, Flynn, Ghafoori, & Kumar, 2007), and would result in an increase in transport emissions per unit of energy. The greater energy consumed in the grinding biomass due to lesser friability (due to the fibrous nature of biomass) means that more energy is expended in using the replacement rather than coal, resulting in greater cost and emissions. Effective grinding of biomass can be very important in determining the performance of the fuel, as the particle size of a fuel can affect the flame stability. Large particles can act as heat sinks, affecting the balance of heat loss and release (Aidan Mark Smith, Whittaker, Shield, & Ross, 2018). The heterogeneity of biomass means that it is less predictable in terms of heating value and composition from batch to batch, hindering any attempts to maximise efficiency in energy recovery technologies such as combustion and anaerobic digestion (Zhao, Shen, Ge, Chen, & Yoshikawa, 2014). The higher volatile matter content and higher reactivity of biomass affects the temperature profile and flame stability in combustion, neutralising efficiency measures if used in existing coal fired boilers. The lower decomposition temperature for biomass can also cause issues in pulveriser mills, which would need to be operated a lower temperatures to avoid decomposition of the biomass during grinding (Aidan Mark Smith et al., 2018).

Biomass and coal also exhibit different burn profiles when combusted. Unprocessed miscanthus exhibits a two-stage combustion profile (showing two peaks in consumption rate as temperature is increased), one where the volatile matter is consumed and a second when the char ignites (Aidan Mark Smith et al., 2018). Coal exhibits a near single-stage profile, where char combustion provides the main peak in decomposition rate, and volatile matter burning appears as a small 'shoulder' on the curve (Aidan Mark Smith et al., 2018). The lower ignition temperature of biomass means that there can be a poor burn interaction when co-firing with coal (Aidan Mark Smith et al., 2018). The hydrophilic nature of biomass makes it susceptible to biodegradation, impacting the potential longevity of biomass stockpiles.

One of the major disadvantages of biomass use in power generation is that it has higher concentrations of alkali metals, alkaline earth metals and chlorine than coal. Table 1.3 compares the ash composition of bituminous coal to a number of biomass feedstocks. It can be seen that in general, biomass has higher concentrations of calcium, potassium, phosphorous, magnesium, sulphur, and sodium than bituminous coal. Alkali metals (especially potassium and sodium), alkaline earth metals, sulphur and chlorine affect ash chemistry (Aidan M. Smith, Singh, & Ross, 2016), and the higher concentrations of these elements in biomass causes slagging and fouling in boilers (Bhuiyan, Blicblau, & Naser, 2017), vastly reducing their efficiency and lifetime (Agbor et al., 2014).

Table 1.3 Comparison of the ash composition of various biomass feedstocks and bituminous coal (Vassilev, Baxter, Andersen, & Vassileva, 2010)

Feedstock	Ash composition (%)									
	SiO_2	CaO	K_2O	P_2O_5	Al_2O_3	MgO	Fe_2O_3	SO_3	Na_2O	TiO_2
Poplar wood	3.9	57.3	18.7	0.9	0.7	13.1	1.2	3.8	0.2	0.3
Miscanthus	56.4	10.8	19.8	5.5	0.8	3.0	0.9	2.3	0.5	0.0
Bagasse	46.8	4.9	7.0	3.9	14.6	4.6	11.1	3.6	1.1	2.0
Sewage sludge	33.28	13.0	1.6	15.9	12.9	2.5	15.7	2.1	2.3	0.8
Olive residue	22.3	12.9	42.8	6.1	4.1	5.8	2.0	3.7	0.1	0.2
Bituminous coal	54.1	4.9	1.6	0.2	24.8	1.6	6.7	2.2	0.8	1.1

Slagging is where ash melts upon exposure to radiant heat, for example a flame in a pulverised fuel boiler. Ash removal in boilers is designed for the ash being in a powdery state, and problems arise when molten slag solidifies (Aidan Mark Smith et al., 2018). The main cause of slagging is alkali metals acting as a flux for aluminosilicate ash (Aidan Mark Smith et al., 2018). These elements react with silica, producing alkali silicates, which soften and melt at low temperatures (even as low as 700°C), resulting in slag (Saddawi, Jones, Williams, & Le Coeur, 2012). Chlorine (which is in itself corrosive to stainless steel) will also react with alkali metals and silicates to form slag (Aidan M. Smith et al., 2016). Different alkali and alkaline earth metals have a different effect on the melting temperature of ash. In general, potassium and sodium reduce the melting temperature of ash, whereas magnesium and calcium increase the melting temperature (Aidan Mark Smith et al., 2018).

Fouling occurs when potassium, sodium, and chlorine partially evaporate from the radiant heat in boilers. They then form alkali chlorides, which condense on lower temperature surfaces, like those found on heat exchangers. These reduce the efficiency of the heat exchangers, but also react with sulphur, forming alkali sulphates and releasing corrosive chlorine (Aidan Mark Smith et al., 2018).

Most of these factors also hinder biomass use in industry. For example, use of biomass in steel production requires biomass to have high lower heating value (LHV), high carbon content, and good mechanical properties (Fick et al., 2014). Biomass does not typically possess these properties.

Liquid fuel derived from biomass needs significant upgrading before use. Bio-oil from pyrolysis tends to have high moisture and oxygen content, which results in a low heating value and high corrosion rates due to acidity (Perkins et al., 2018). The degree of processing necessary has a great impact on the viability of bio-oil as a fossil fuel replacement.

As is the case with bio-oil, bio-gas tends to have a low heating value, impacting its competitive edge against fossil fuel alternatives (Hosseini & Wahid, 2014).

1.5.2 Biomass variability

The four main types of biomass (woody, herbaceous, aquatic, and manures (McKendry, 2002)) all differ significantly from each other. This variation can have detrimental effects on the effectiveness of biomass as a fossil fuel replacement, as the variability would hinder any attempts at process optimisation. Biomass also varies between sub-classifications, batches, as well as from within parts of the same plant (Rabemanolontsoa & Saka, 2013).

1.5.3 Sustainability of use

The variability of biomass described in section 1.5.2 often means that operators opt to use a single source of biomass. Often dry, high-quality woody biomass is chosen due to its higher energy content, and low moisture, ash, nitrogen, and sulphur content. If wood continues to be the sole biomass used as the demand for biomass increases substantially, biomass energy will become unsustainable (Baruya, 2015). If other biomass sources are used, then biomass can be sustainable. There is a significant potential for using wastes and energy crops to bolster biomass supply, ensuring that the beneficial impact of biomass can be maximised. The UK biomass power potential in 2050 can be seen in Table 1.4.

Table 1.4 UK biomass potential in the year 2050 (Welfle, Gilbert, & Thornley, 2014)

Biomass	Power potential in 2050 (TWh)
Energy crops	>100
Household waste	>115
Agricultural residues	>80

In order to facilitate use of these biomass sources, numerous technical and logistical barriers have to be addressed. In the case of energy crops, producing energy crops on marginal land can lessen the competition with agriculture for more fertile land (Milbrandt & Overend, 2009). There are a number of countries with significant quantities of marginal land, providing them with great potential for bolstering their own biomass supply and also giving opportunities to supply to neighbouring countries. These countries and their marginal land area can be seen in Table 1.5. Where water is scarce, competition with food agriculture for water is also a significant issue (Gheewala, Berndes, & Jewitt, 2011).

Table 1.5 Marginal land area of selected countries (Milbrandt & Overend, 2009)

Country	Total land area (km^2)	Total marginal land (km^2)	Total marginal land (%)
Australia	7,694,273	1,036,239	13.5
Chile	722,511	95,645	13.2
Mexico	1,953,851	255,862	13.1
United States	9,426,295	1,214,007	12.9

Utilisation of waste biomass is another solution for lessening competition for land (McManus, 2010), and is thought of as one of the key energy resources in

meeting increasing energy demand while maintaining the sustainability of biomass (Nanda, Azargohar, Dalai, & Kozinski, 2015). Although use of waste biomass has promise, high moisture and ash content can be an issue for certain waste biomass feedstocks like human and animal waste (Werther & Ogada, 1999) (Vamvuka & Alloimonos, 2017).

There are a number of supply chain sustainability issues involved in biomass utilisation. There are challenges associated with constructing an interconnection scheme and the industry chain not being technically and commercially developed (Raychaudhuri & Ghosh, 2016). In terms of utilisation of waste biomass, one of the key issues is the difficulty of collection, transportation and storage (Iakovou et al., 2010).

1.6 Pre-treatment technologies

For biomass to have a positive effect on the emissions of coal-fired power plants, it needs to constitute a large proportion of the fuel combusted (Miedema et al., 2017), much more than the current limit. Pre-treatment of biomass has the potential to deliver this by altering the qualities of biomass to make them mirror those of coal. These could also have potential advantages in further processing of biomass, making them more suitable for generating biofuels, biogas, or chemicals.

Pyrolysis was described in section 1.3 as a way of turning biomass into various solid, liquid, and gaseous products. This can be seen as pre-treatment for producing solid fuel as the char from pyrolysis can be used in combustion or as a soil amendment (Peters, Iribarren, & Dufour, 2015). In addition to this, the liquid fraction can be converted into fuels and chemicals (Czernik & Bridgwater, 2004). The pyrolysis conditions can be finely tuned to maximise the yield of the desired product, to maximise efficiency of the pre-treatment. The divisions in pyrolysis are slow, moderate, and fast pyrolysis. Typical process parameters and product yield distributions of these can be seen in Table 1.6. Catalysts can be used to increase the yield and quality of specific fractions (Sharma, Pareek, & Zhang, 2015).

Table 1.6 Comparison of typical parameters and yields of different modes of pyrolysis (Libra et al., 2011)

Pyrolysis mode	**Temperature (°C)**	**Residence time**	**Product yield (%)**		
			Solid	Liquid	Gas
Slow	400	1h-1week	35	30	35
Medium	500	10-20s	20	50	30
Fast	500	1s	12	75	13

Other common pre-treatment technologies include torrefaction and leaching. Torrefaction of biomass can be thought of as mild pyrolysis (Chew & Doshi, 2011), and results in a homogenous, friable fuel that has similar composition to coal in terms of fixed carbon and moisture content (Nunes, Matias, & Catalão, 2014). Torrefaction can result in a more efficient feedstock, with torrefaction combined with pelleting being reported to perform better as a supply chain

than utilisation of untreated wood, as the conversion of the fuel to energy was more efficient (Miedema et al., 2017). The main disadvantages of torrefaction as a pre-treatment are that it requires dry, high-quality biomass as a feedstock (Nunes et al., 2014) and that it does little to remove alkali and alkaline earth metals from biomass (Hidayat et al., 2017), meaning that thermal conversion of torrefied biomass would still have slagging and fouling issues. Leaching uses biomass immersion in water or other solvents to significantly reduce the ash content of biomass. Leaching using strong acids is particularly effective, having been shown to be able to remove over 99% of potassium from a high alkali and alkaline earth metal biomass as well as effective removal of other alkali and alkaline earth metal species (Jiang et al., 2013). The main disadvantage of leaching is that it results in a product with a very high moisture content that would be expensive to dewater (C. Yu et al., 2014).

Hydrothermal processing is similar to pyrolysis and torrefaction, with the primary difference being that water is involved in the process. This can have a significant effect on the composition and distribution of products in comparison to these other pre-treatments. As with pyrolysis, the parameters of hydrothermal treatment can be tailored to maximise the yield of the desired product. There are three main divisions of hydrothermal treatment, hydrothermal carbonisation (HTC), hydrothermal liquefaction (HTC), and supercritical water gasification (SCWG) (Tekin, Karagöz, & Bektaş, 2014) (Yakaboylu, Harinck, Smit, & de Jong, 2015). The differences between the three processes are mainly the process parameters and the desired products.

Hydrothermal carbonisation converts biomass into a solid product using relatively mild conditions (Román, Nabais, Laginhas, Ledesma, & González, 2012), while hydrothermal liquefaction (HTL) and supercritical water gasification (SCWG) use increasingly harsh conditions to produce liquid and gaseous products, respectively (Libra et al., 2011). The product of HTC is has been called both biocoal (B. Erlach, Harder, & Tsatsaronis, 2012) and hydrochar (Xuejiao Chen, Lin, He, Zhao, & Li, 2017). For this thesis, in the context of combustion the solid product of HTC will be referred to as biocoal, and for other applications it will be referred to as hydrochar. This study aims to add to the knowledge of the potential HTC in producing useful solid fuels.

1.7 Aims and objectives

The primary aim is this study is to investigate the potential of hydrothermal carbonisation to produce a biomass feedstock with favourable characteristics for fuel switching and production of biomaterials. Specific objectives of the project are as follows:

- Perform design of experiments (DoE) study on HTC of miscanthus to describe in detail the impact of temperature, residence time, and water to biomass ratio on the yield of HTC, composition, and energy content of the products of HTC.

- Perform hydrothermal treatments on a wide range of biomass to understand the effect of feedstock on product yield and composition.

- Assess the impact of HTC on the char reactivity of biomass in comparison to other pre-treatments, and identify the sources behind these impacts.

- Perform NMR studies on biocoal and torrefied biomass to investigate the differences in the chemistry of the two processes and assess the role of water in HTC reaction pathways.

- Investigate the use of hydrochar as a feedstock for producing activated carbon, focussing in particular on activation yield and porosity of the activated carbon.

1.8 Thesis structure

The thesis is divided into 7 chapters, which are organised as follows:

- Chapter 2 is a literature review which introduces hydrothermal carbonisation, compares the process to rival pre-treatments, and highlights where further research needs to be conducted

- Chapter 3 describes the materials and methods employed during the EngD research, encompassing the feedstocks used, sample preparation, analysis, and the calculations used.

- Chapter 4 describes the impact of HTC parameters and biomass feedstock on the yield, composition, and energy content of the products of HTC.

- Chapter 5 compares the char reactivity of biocoals to untreated biomass, torrefied biomass, leached biomass, and bituminous coal. The chapter describes the role of alkali/alkaline earth metal content, surface area, and fuel composition on the char reactivity of biomass fuels.

- Chapter 6 compares mass, carbon, and aromatic carbon balances of HTC with torrefaction, and discusses the role of water HTC reactions.

- Chapter 7 describes the impact of HTC on the yield, composition and porosity of activated carbon produced from olive cake.

- Chapter 8 describes the overall conclusions of the EngD, and recommendations for future work.

Chapter 2 Literature review

The purpose of this literature review is to provide an overview of HTC of biomass. Firstly, the review will detail biomass composition, properties, and limitations; then secondly the chemistry involved in HTC, and the fuel properties of biocoal in comparison to the products of other pre-treatment alternatives. Finally, the energetics and economics of HTC will be discussed, and the current state of HTC will be defined.

2.1 Biomass composition

As was stated in section 1.3, biomass can be defined as any organic materials derived from plants (McKendry, 2002) or animals (Iakovou et al., 2010). It is a heterogeneous mixture of organic substances, with a small amount of inorganic impurities (Tekin et al., 2014). There are a vast number of biomass sources, all with distinct differences in composition. The types of biomass will be split into general classifications of Lignocellulosic, aquatic, and waste biomass in this review. The composition of these will be described below.

2.1.1 Lignocellulosic biomass

Woody and herbaceous biomass can be grouped together as lignocellulosic biomass (Maddi, Viamajala, & Varanasi, 2011). Lignocellulosic biomass is plant based, with the main constituents being cellulose, hemicellulose, lignin, and extractives (Tekin et al., 2014). The proportions of these vary significantly between biomass feedstocks, with the contents of cellulose, hemicellulose, and lignin in biomass being 40–60%, 15–30%, and 10–25%, respectively. (D. Chen et al., 2018). This variation can be seen in **Figure** 2.1, which displays the composition of various lignocellulosic biomass feedstocks, in terms of holocellulose (total cellulose and hemicelluloses) and lignin. The remaining weight fraction is comprised of acid-soluble hydrocarbons (extractives) (Gani & Naruse, 2007).

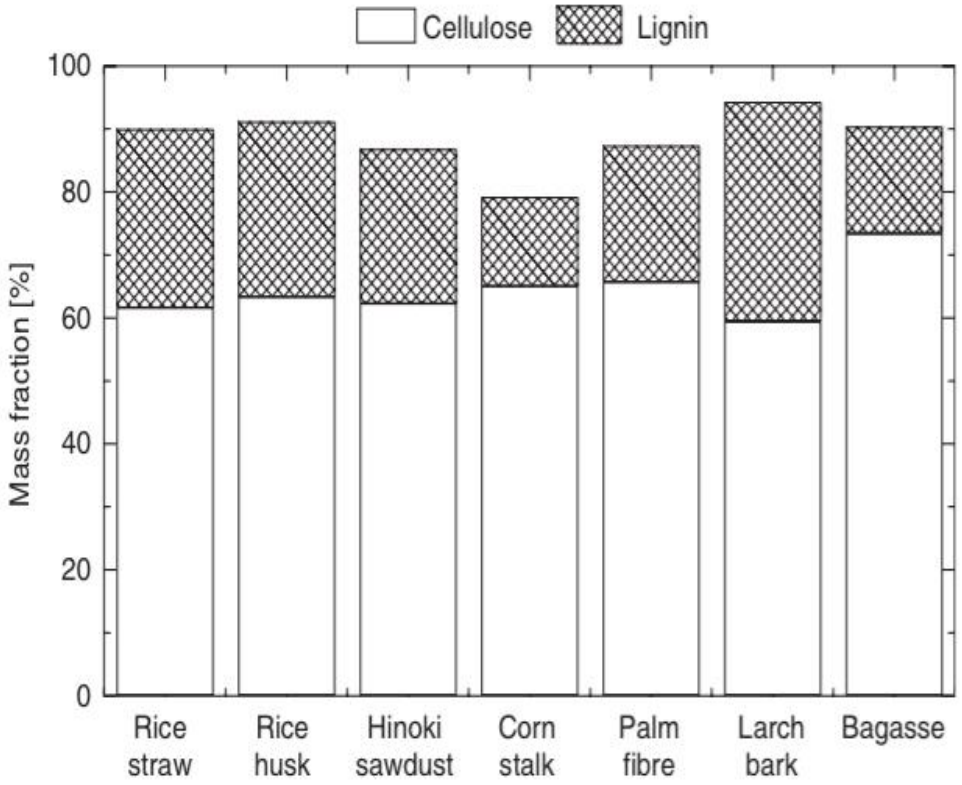

Figure 2.1 Holocellulose and lignin content of various lignocellulosic biomass types (Gani & Naruse, 2007)

Cellulose is a long chain polysaccharide with the general formula $(C_6H_{10}O_5)_n$, where the main structural monomer is the hexose glucose (Borrero-lópez, Masson, Celzard, & Fierro, 2018). The structure of cellulose can be seen in Figure 2.2. Cellulose is considered to be a nearly inexhaustible biomass source, being the most abundant natural polymer in the world. It is insoluble in most solvents due to a tight fibrous structure resultant of hydrogen bonding (Tekin et al., 2014).

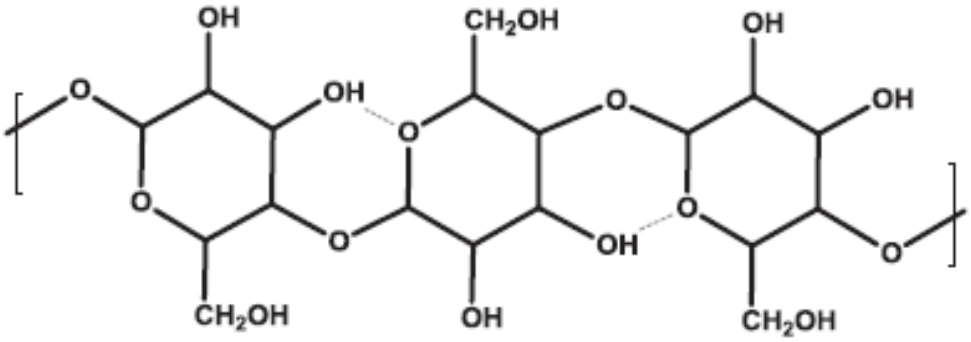

Figure 2.2 Structure of cellulose (Tekin et al., 2014)

Hemicellulose is also a polysaccharide, but has a lower degree of polymerisation than cellulose. It is an amorphous heteropolysaccharide with a high degree of branching off of a straight-chain spine comprised of mostly of the polymers xylan and gulucomannan (Tekin et al., 2014). The main structural monomer is the pentose xylan (Borrero-lópez et al., 2018). Some hemicellulose monomers can be seen in Figure 2.3.

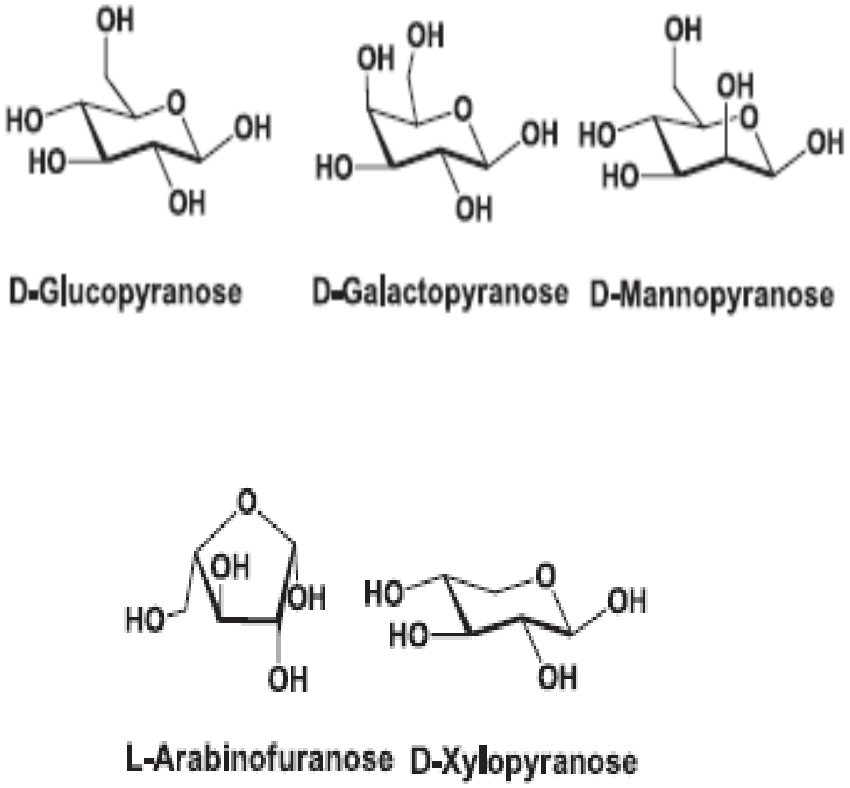

Figure 2.3 Primary constituents of hemicellulose (Tekin et al., 2014)

Lignin is an amorphous polymer consisting of various phenylpropane based monomers, which are mainly linked through ether bonds (Tekin et al., 2014). These monomers have varying amount of additional hydroxyl and methoxy functional groups. As with cellulose, lignin has very little solubility in water (Tekin et al., 2014). Some lignin monomers can be seen in Figure 2.4, and a piece of a lignin polymer can be seen in Figure 2.5.

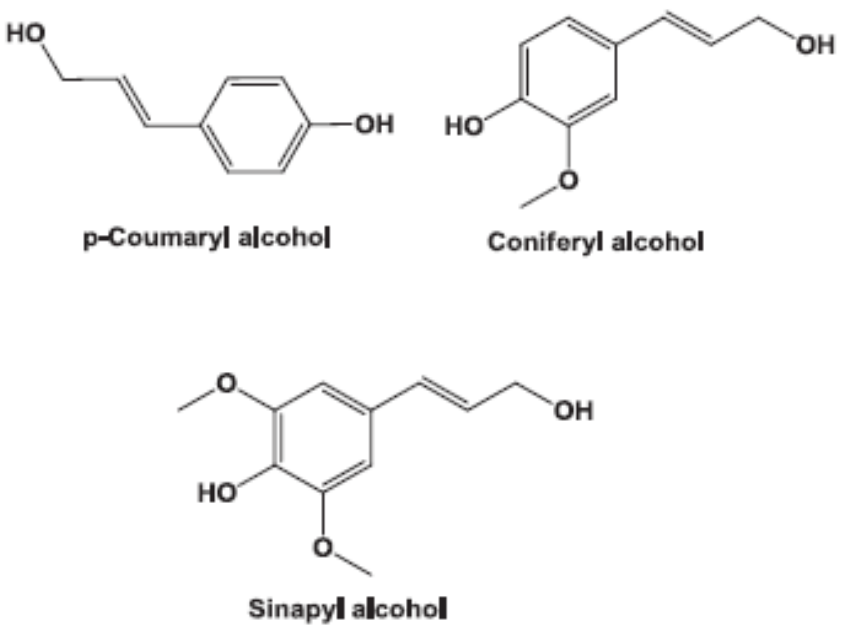

Figure 2.4 Basic lignin monomers (Tekin et al., 2014)

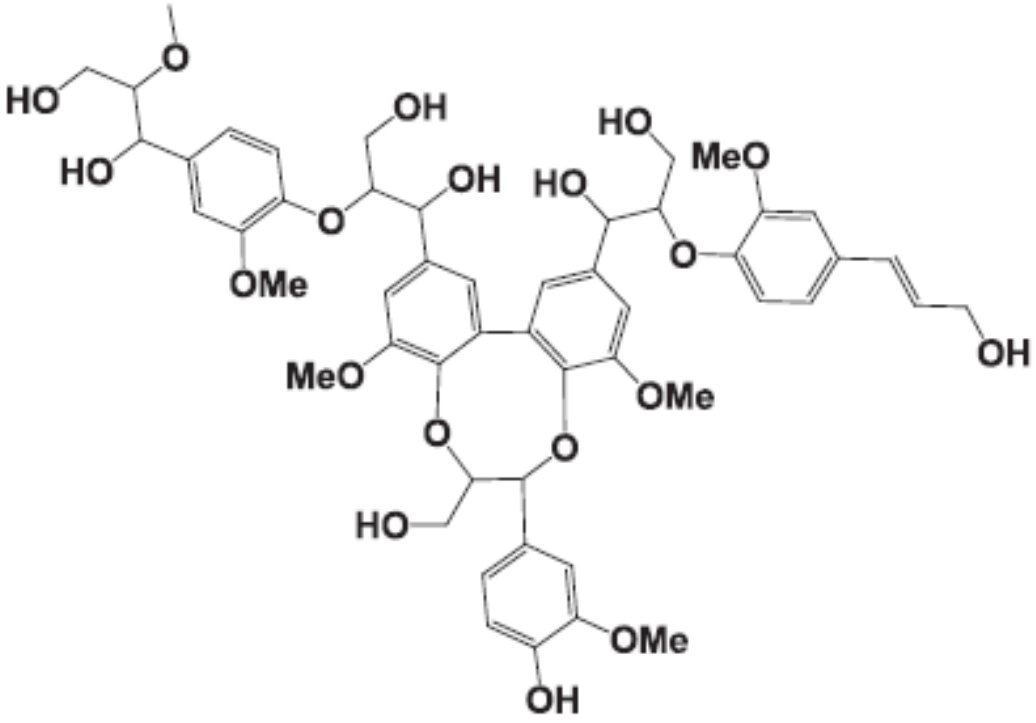

Figure 2.5 Sample fraction of lignin (Tekin et al., 2014)

Extractives are a wide range of chemicals that are extractable by solvents. These include proteins, fats, fatty acids, sugars, phenols, terpenes, resin acids, and resin. (Tekin et al., 2014).

The structure of plant cell walls can be seen in Figure 2.6. It shows that cellulose forms in bundles, which are then covered by hemicellulose (providing structural integrity to the cells). These are bound together by lignin (Kashaninejad, 2011). Lignin is also key in regulating the flow of fluids, protecting the plant from micro-organisms, and storing energy (Tekin et al., 2014). Lignin has the highest energy content of the three main components so has a large impact on the overall heating value of the biomass (Tekin et al., 2014).

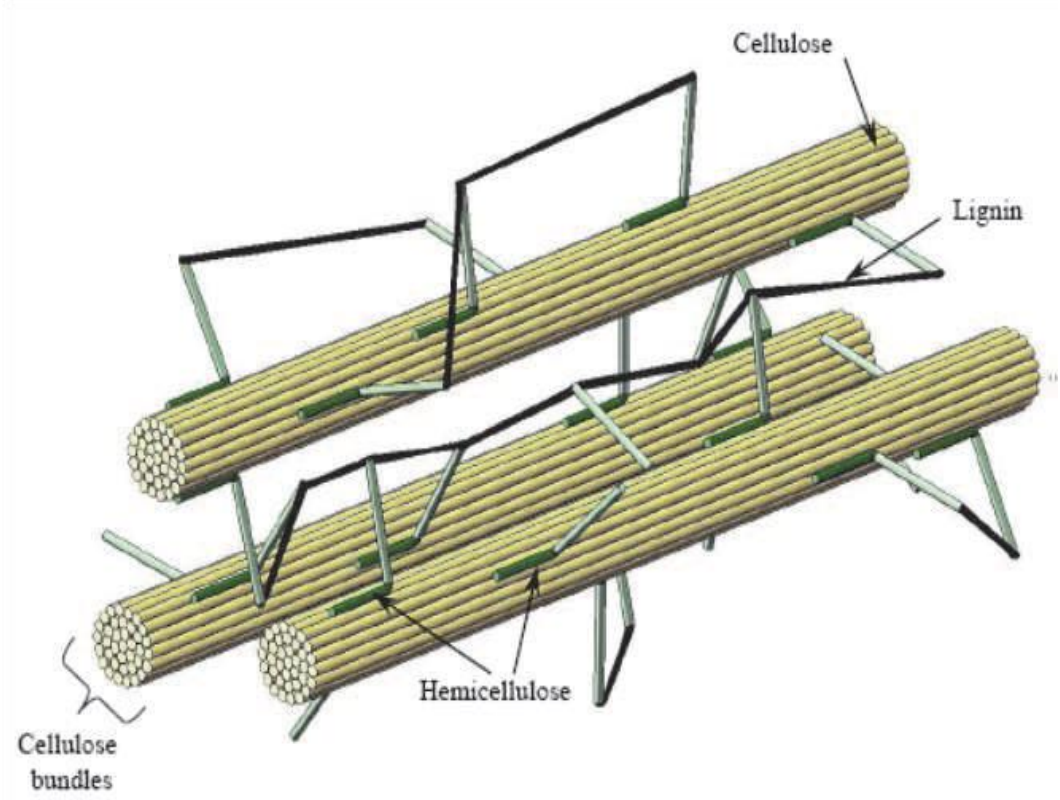

Figure 2.6 Cellulose, hemicellulose, and lignin in plant cell walls (Kashaninejad, 2011)

Each component of lignocellulosic biomass has a different thermal stability. Hemicellulose is the least stable of the main components of biomass, and as such is the first to degrade upon heat treatment (Tekin et al., 2014). A study on the pyrolysis of hemicellulose, cellulose, and lignin found that hemicellulose and cellulose decomposed quickly at relatively low pyrolysis temperatures. The decomposition of hemicellulose generally occurred at 220–315°C, and cellulose at 315–400°C (Yang, Yan, Chen, Lee, & Zheng, 2007). Lignin proved more difficult to decompose, with decomposition occurring in a wide temperature range of 160–900°C, with high levels of solid residue formed (Yang et al., 2007).

This shows that lignin is the most unreactive of the three major components and forms the basis of the solid product of thermal pre-treatments of lignocellulosic biomass.

A review of the proximate and ultimate (elemental) analysis of a large selection of lignocellulosic biomass types can be seen in Table 2.1 and Table 2.2. The wide variation in moisture content of biomass on an as received basis is mainly due to the excessive moisture content of some of the waste biomasses. This in turn results in the ranges seen for other fraction being very large. The proximate analysis on a dry basis gives a better indication of the how the useful fractions of biomass compare. Lignocellulosic biomass is characterised by high volatile matter content, low fixed carbon content and low ash content when compared to coals (Vassilev et al., 2015). The high upper limit for herbaceous biomass fixed carbon is due to one outlier biomass feedstock, walnut shells, having a fixed carbon content of 37.9%, which is well above that of any of the other herbaceous biomass feedstocks. None of the other herbaceous biomass types had a fixed carbon content larger than 27%, which would make the range similar to that of woody biomass. In terms of elemental composition, the two biomass feedstock categories are similar, although herbaceous biomass has a larger range of carbon content, and a larger nitrogen content. The sulphur content in both biomass types is very low.

Table 2.1 Proximate composition range of lignocellulosic biomass (Vassilev, Baxter, Andersen, & Vassileva, 2010)

Lignocellulosic biomass type	Proximate analysis (%)			
	Moisture	Volatile matter	Fixed carbon	Ash
Woody (ar[1])	4.7 – 62.9	30.4 – 79.7	6.5 – 24.1	0.1 – 8.4
Woody (db[2])	-	69.5 – 86.3	12.3 – 26.3	0.1 – 16.5
Herbaceous (ar[1])	4.4 – 47.9	41.5 – 76.6	9.1 – 35.3	0.8 – 18.6
Herbaceous (db[2])	-	59.3 – 85.5	12.4 – 37.9	0.9 – 20.1

[1]ar – as received
[2]db – dry basis

Table 2.2 Elemental composition range of lignocellulosic biomass (Vassilev et al., 2010)

Lignocellulosic biomass type	Elemental content (daf[1]) (%)				
	Carbon	Oxygen	Hydrogen	Nitrogen	Sulphur
Woody	48.7 - 57.0	32.0 - 45.3	5.4 - 10.2	0.1 - 0.7	0.0 - 0.4
Herbaceous	42.2 – 58.4	34.2 – 49.0	3.2 – 9.2	0.1 – 3.4	0.0 – 0.6

[1]daf – dry, ash free

The ash composition range of the two lignocellulosic biomass categories are shown in Table 2.3. This shows that lignocellulosic biomass ash is typified by high alkali and alkaline earth metal content. As was discussed in section 1.5, this causes slagging and fouling issues in thermal conversion.

Table 2.3 Ash content range of lignocellulosic biomass (Vassilev et al., 2010)

Lignocellulosic biomass type	Ash composition (%)									
	SiO_2	CaO	K_2O	P_2O_5	Al_2O_3	MgO	Fe_2O_3	SO_3	Na_2O	TiO_2
Woody	1.86–68.18	5.79–83.46	2.19–31.99	0.66–13.01	0.12–15.12	1.10–14.7	0.37–9.54	0.36–11.66	0.22–29.82	0.06–1.20
Herbaceous	2.01–94.48	0.97–44.32	2.29–63.90	0.54–31.06	0.10–14.60	0.19–16.21	0.22–36.27	0.01–14.74	0.09–26.20	0.01–2.02

2.1.2 Aquatic biomass

Aquatic biomass is derived from the aquatic plant algae, and is comprised of lipids, carbohydrates, and proteins (Tekin et al., 2014). Aquatic biomass can be divided into two classifications – macroalgae and microalgae (Kröger & Müller-Langer, 2012).

Macroalgae are aquatic plants formed of branches, leaves, and sometimes roots. It can be further classified into brown, red and green macroalgae, and these denote different types of multicellular eukaryotes which originate from separate evolution pathways (Kröger & Müller-Langer, 2012). Macroalgae does not have significant levels of lignocellulose in its composition (Aidan M. Smith & Ross, 2016), and in the absence of lignin it utilises polymers bound by alkali and alkaline earth metals for support. This results in high ash contents and significant concentrations of alkali and alkaline earth metal ions (Aidan M. Smith & Ross, 2016). Macroalgae has a similar moisture content; lower volatile matter content; and similar fixed carbon content to most non-waste lignocellulosic biomass (Vassilev et al., 2010).

Microalgae are unicellular (eukaryote or prokaryote), and are sized on the nanometre to millimetre scale (Kröger & Müller-Langer, 2012). Microalgae can be grown and then harvested as a slurry, which means naturally the feedstock has a high moisture content (Biller et al., 2012).

2.1.3 Waste biomass

Waste biomass spans the majority of biomass categories, as many process which utilising biomass will end up with some form of waste biomass by-product. Some applications of biomass result in contaminants such as metals being concentrated in the residue (Nzihou & Stanmore, 2013), so waste biomass is quite often characterised by a high contaminant level.

Human communities generate large volumes of waste that is mostly sent to landfill, known as municipal solid waste (MSW). MSW includes food waste, paper, plastics, textiles, rubber, leather, wood, glass, and metals (Kathirvale, Muhd Yunus, Sopian, & Samsuddin, 2004). MSW varies significantly in composition and contains numerous troublesome contaminants. For example, plastics can cause issue trough containing organic chlorine (Prawisudha, Namioka, & Yoshikawa, 2012).

Sewage sludge is can also be utilised as waste biomass. The organic composition of sewage sludge is mainly comprised of carbohydrates and proteins, with lignin comprising a small fraction (He, Giannis, & Wang, 2013; Huang et al., 2013). Sewage sludge also has a high ash content, with significant concentrations of silicon (Aidan M. Smith et al., 2016). Biosolids are the end result of dewatering and pollutant/pathogen treatment of wastewater in wastewater treatment plants, and can be utilised as a waste biomass. These are mostly composed of water, organic matter, and significant quantities of ash (M. M. Yu et al., 2015).

Biochemical processes can also produce waste products than can be used as biomass fuel. For example, anaerobic digestion results in a wet cake, which can be used as a biomass feedstock. Anaerobic digestion is a biological process that consumes organic matter in the absence of oxygen, producing a biogas composing of mostly methane and carbon dioxide. The process consumes the labile fraction of the organic matter (for example carbohydrate-like molecules), leaving an increased concentration of the more recalcitrant compounds (for example lignin and non-hydrolysable lipids) in the digestate cake (Tambone, Genevini, D'Imporzano, & Adani, 2009). As with sewage sludge, anaerobic digestate has a high ash content, with significant concentrations of silicon (Aidan M. Smith et al., 2016).

2.2 Comparison of biomass and coal

As has been stated in section 1.5, biomass is less energy dense than coal. This is due to the lower carbon density of biomass (Demirbaş, 2001; Aidan Mark Smith et al., 2018). Energy density is important in a fuel as it can have a significant impact on transport emissions and costs (Mauro, Rentizelas, & Chinese, 2018).

Due to the fibrous nature of lignocellulosic biomass it has lower friability than coal. This means that more energy is expended grinding biomass and some coal

mills are unsuitable for preparing biomass for PF combustion (Wils, Calmano, Dettmann, Kaltschmitt, & Ecke, 2012).

A key difference between coal and biomass ash is that biomass ash has higher concentrations of alkali and alkaline earth metals than coal ash. The increased slagging and fouling effects of this has been stated before in Sections 1.5.1 and 2.1.1. In addition to this, alkali and alkaline earth metals catalyse combustion (Yi et al., 2018). This results in biomass being much more reactive than coal, which can limit the efficiency as a coal replacement in both combustion and industrial applications. The presence of oxygen in reactive forms such as carboxylate, methoxy, and alcohol functional groups also makes biomass more reactive (Vassilev et al., 2015). Additionally, biomass and coal display differing combustion profiles, which can result in inefficiencies when co-fired, such as poor burn interaction (Aidan Mark Smith et al., 2018).

2.3 Hydrothermal carbonisation

2.3.1 Overview

As was stated in section 1.6, hydrothermal treatment is similar to pyrolysis in that you can tailor the reaction conditions to target a specific product. The various ranges of the three main hydrothermal treatments can be seen in Table 2.4, and a phase diagram of water showing which phase water is in under the parameters of each hydrothermal process can be seen in Figure 2.7. As was stated in section 1.6, Hydrothermal carbonisation uses mild temperature and

pressure to produce a solid product (Román et al., 2012), while hydrothermal liquefaction (HTL) and supercritical water gasification (SCWG) produce liquid and gaseous products, respectively, by subjecting the biomass to increasingly harsh conditions (Libra et al., 2011). The transition between carbonisation and liquefaction conditions occurs at temperatures above 250°C (Aidan M. Smith et al., 2016).

Table 2.4 Typical process conditions for hydrothermal treatments

Process	Temperature (°C)	Pressure (MPa)	Residence time	Desired product phase	Reference
Steam Explosion	180-240	1-3.5	2-10 min	Solid	(Stelte, 2013) (Tabil, Adapa, & Kashaninejad, 2009)
HTC	180-250	1-10	1-12 hours	Solid	(Libra et al., 2011)
HTL	<350	4-22	30min*	Liquid	(Tews et al., 2014)
SCWG	>350	>22	Minutes*	Gas	(Matsumura et al., 2005)

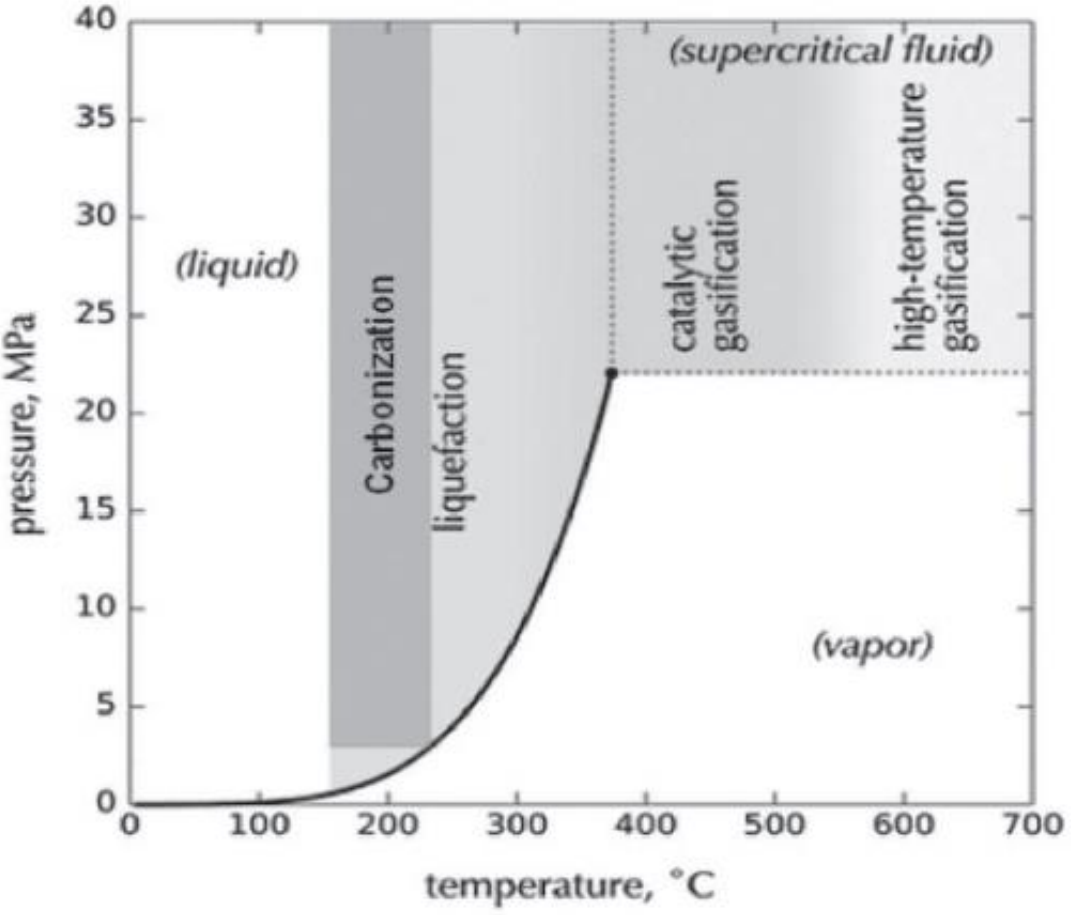

Figure 2.7 Phase diagram of water showing typical hydrothermal process temperature ranges (Gude, 2018)

Hydrothermal carbonization (HTC) of biomass can be described as 'wet torrefacton' (Bach & Skreiberg, 2016). A more apt description for HTC is artificial coalification, as it resembles natural coal production more than purely char production (B. Erlach et al., 2012). Steam explosion is a hydrothermal pre-treatment that operates in a similar temperature range to HTC. The main difference between the two is the phase of water during the process. In steam explosion the water used is gaseous, and in HTC the increased pressure results in the water remaining in the liquid state at the operating temperature (which is above the boiling point of water). The steam in steam explosion is used to burst open the fibres of the biomass, as well as using heat to remove moisture

and some volatile matter, resulting in a biomass feedstock with better pelletizing properties, higher heating value (HHV), and low moisture absorption (Stelte, 2013). The process is also used as a precursor to chemical and biochemical conversion of biomass (Stelte, 2013) (Jiebing Li, Gellerstedt, & Toven, 2009). Utilising water in the liquid phase in HTC allows for further thermochemical degradation of the biomass (Kruse & Dahmen, 2015), resulting more energy dense, coal like substance. Using liquid water also results in leaching of soluble inorganics out of the biomass, typically alkali and alkaline earth metals as well as chlorine (Reza, Lynam, Uddin, & Coronella, 2013) (Aidan M. Smith et al., 2016). In addition to biocoal, HTC produces water containing soluble organics, CO_2, and other gaseous products (B. Erlach et al., 2012).

2.3.2 Advantages of biocoal over biomass

Biocoal compares more favourably to coal than biomass – possessing greater friability (due to loss of fibrous structure); having a higher bulk and energy density; having a higher ignition temperature and better overall combustion performance; lessened variability and heterogeneity of fuel; lower alkali/alkaline earth metal and chlorine content; and greater ease of drying (Coronella, Lynam, Reza, & Uddin, 2014; Liu, Quek, Kent Hoekman, & Balasubramanian, 2013; Oliveira, Blöhse, & Ramke, 2013; Reza, Lynam, et al., 2013; Aidan M. Smith et al., 2016).

Producing biocoals from biomass reduces the variation between the biomass sources and biocoals derived from different biomass feedstocks all typically

possess similar characteristics (Liu et al., 2013). This is incredibly important to using biomass for thermal power, making the results predictable so efficiency can be maximized and ensuring that a large resource pool can be used.

2.3.3 HTC Chemistry

Although HTC has been likened to torrefaction and pyrolysis, the chemistry of HTC is substantially different. The primary difference between HTC and pyrolysis is that the HTC reaction pathways begin with hydrolysis, with the resulting fragments initiating the other pathways in degradation (Libra et al., 2011). Under HTC conditions, hydrogen bonding is weakened, resulting in water autoionizing. This produces hydronium (H_3O^+) and hydroxide (OH^-) ions. Hydronium ions then act as catalysts in the HTC reactions (Ruiz, Rodríguez-Jasso, Fernandes, Vicente, & Teixeira, 2013).

After initial hydrolysis, further reactions take place. These include dehydration, condensation, aromatization, and decarboxylation (Hoekman, Broch, Felix, & Farthing, 2017; Oliveira et al., 2013). These reactions do not occur in succession but rather happen simultaneously (Fang, Zhan, Ok, & Gao, 2018). The different generic reaction pathways that occur in HTC and pyrolysis are shown in Figure 2.8.

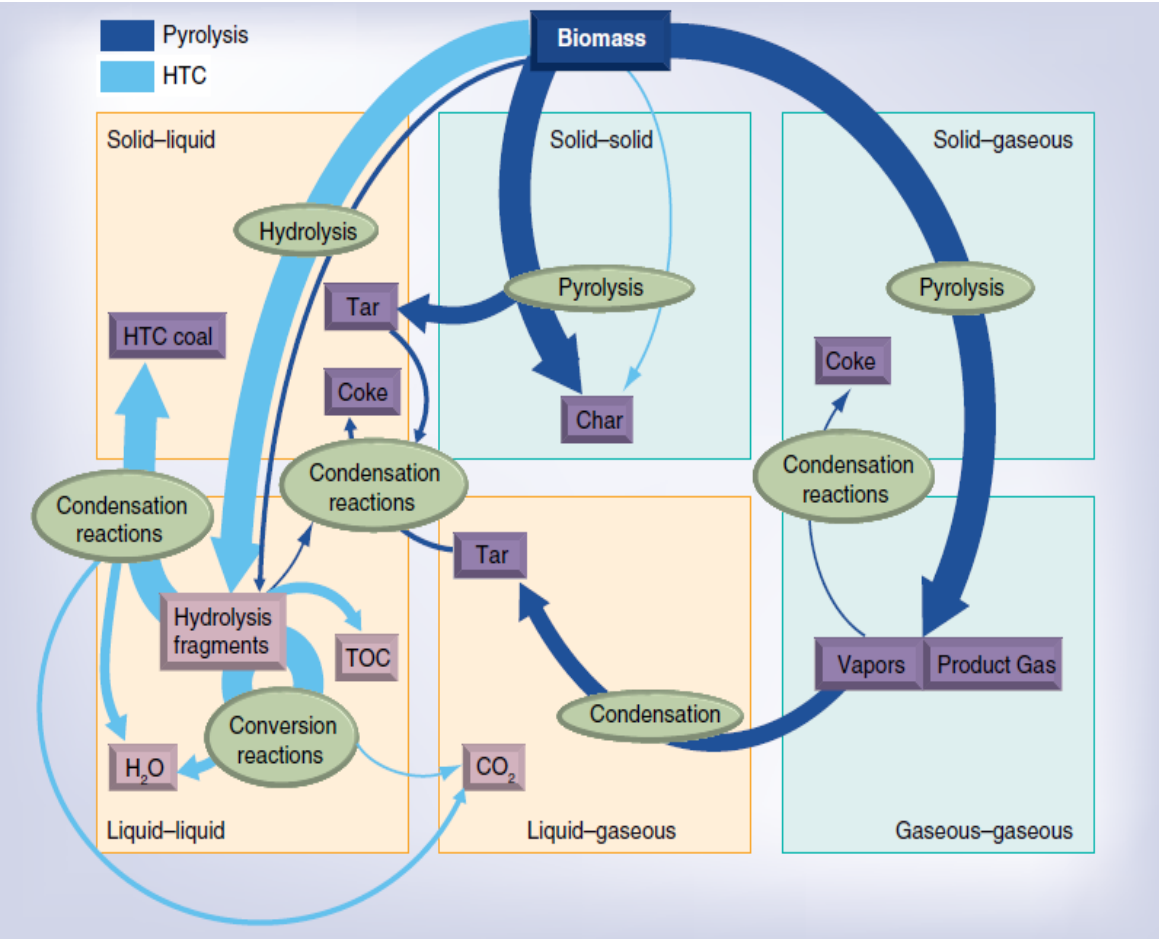

Figure 2.8 Comparison of general reaction mechanisms of pyrolysis and HTC (Libra et al., 2011)

In an investigation into the effect of HTC at various temperatures on the composition of biomass in terms of hemicellulose, cellulose and lignin, it was found that hemicellulose was completely degrades in almost all cases studied (the single case in which some hemicellulose remained was in HTC of miscanthus at 200°C, where less than 7% of the original hemicellulose was found) (Reza, Lynam, et al., 2013). The degradation of hemicellulose occurs through hydrolysis of the β-(1-4) glycosidic bonds, producing the constituent sugar monomers. The main structural unit of hemicellulose is xylan. These pentoses degrade further to form furfurals, alongside other products (Reza, Lynam, et al., 2013). The furans produced in the hydrolysis then polymerise and

aromatise, producing carbon solids. This is strongly suggested by the morphologies and chemical structures of carbon material generated by hydrothermal treatment of saccharides being directly related to those generated from pure furans (Titirici, Antonietti, & Baccile, 2008). Some further possible degradation pathways in hydrothermal decomposition of hemicellulose can be seen in Figure 2.9. Here, xylan is used as a model compound for hemicellulose (Bach & Skreiberg, 2016).

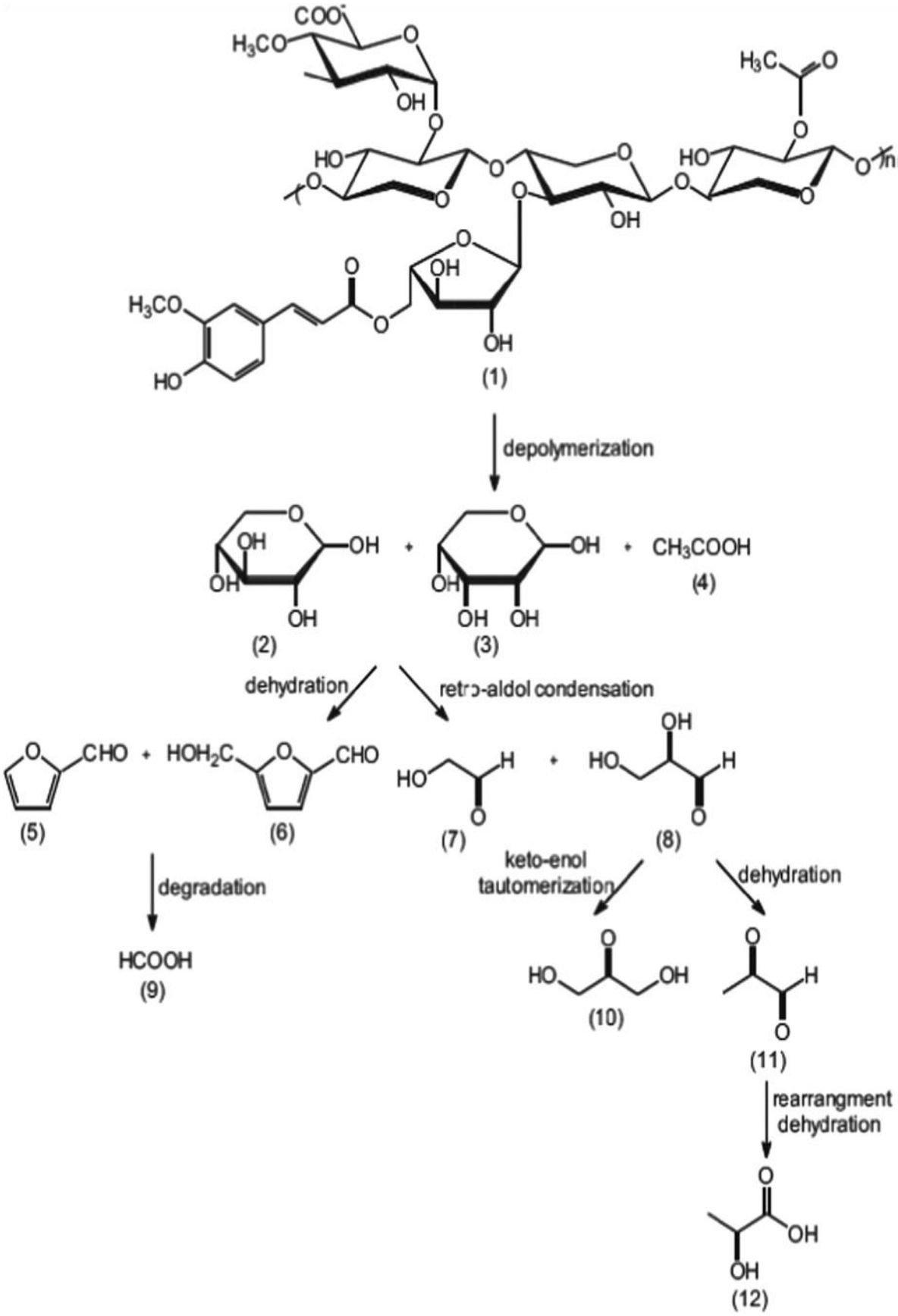

Figure 2.9 Potential hydrothermal decomposition pathways for a hemicellulose model compound, xylan (Bach & Skreiberg, 2016)

Cellulose begins to react under HTC conditions at 200°C (Coronella et al., 2014), but is more resistant to decomposition, needing slightly harsher conditions than hemicellulose (Reza, Lynam, et al., 2013). Under hydrothermal carbonisation conditions, cellulose decomposes into oligomers, some of which hydrolyse to produce glucose (Reza, Lynam, et al., 2013). HTC of Glucose alone results in the glucose undergoing dehydration, producing 5-hydroxymethylfurfural (HMF), levulinic acid, dihydroxyacetone and formic acid. Polymerisation of the HMF produces a polyfuranic structure, which then forms an aromatic solid product (Falco, Baccile, & Titirici, 2011). This is not the primary reaction pathway seen in degradation of cellulose by HTC, as the oligomers form nano/micro-scale cellulosic spherical envelopes to minimise the surface area in contact with water (Falco et al., 2011). This results in the bulk of the cellulose experiencing a homogenous thermal environment resembling pyrolysis conditions. As a result of these conditions, the cellulose experiences intramolecular condensation, dehydration, and decarboxylation reactions, producing a carbon solid composed of large aromatic macromolecules (Falco et al., 2011). The reaction pathways of glucose and cellulose can be seen graphically in Figure 2.10.

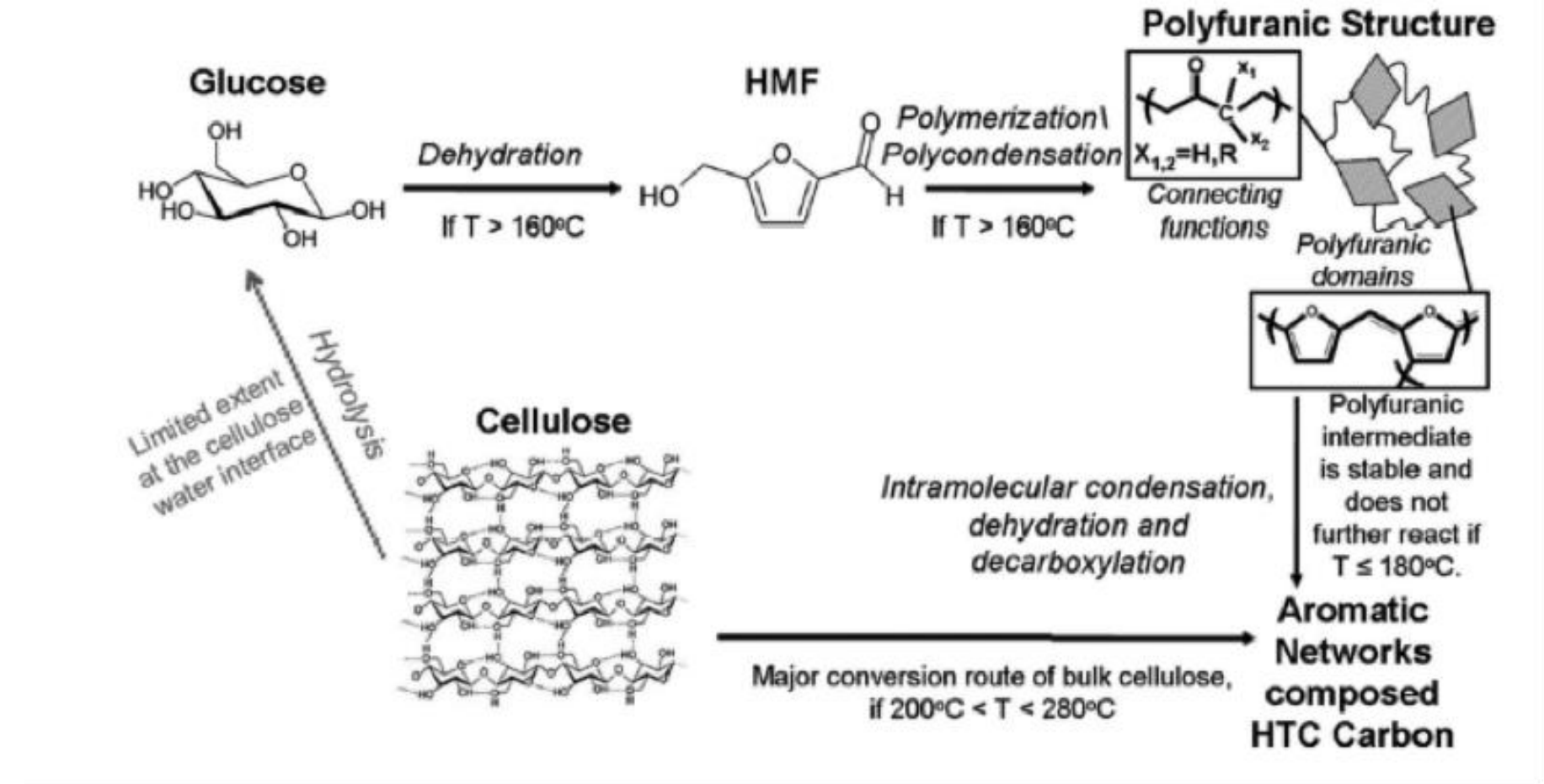

Figure 2.10 HTC chemistry of cellulose and glucose (Falco et al., 2011)

Lignin decomposition requires harsher conditions (Liu et al., 2013), with the biopolymer being shown to be largely unaffected by HTC process between 200°C and 260°C (Reza, Lynam, et al., 2013). As a result of this, biocoals generally retain the natural macrostructure of the biomass feedstock (Falco et al., 2011). Although lignin is mostly unaffected, there is some degradation via demethylation, decarboxylation, and cleavage of β-O-4 bonds (Yue, Marcus, Yan, Liu, & Xiang, 2018). Lignin fragments are very reactive and condense easily, forming solid hydrochar (Fang et al., 2018). However the presence of hemicellulose degradation products can stabilise the lignin fragments, slowing down condensation reactions leaving lignin fragments in the aqueous phase (Fang et al., 2018).

Lipids can hydrolyse into glycerol under HTC conditions, and the degradation products remain in the liquid fraction. This likely happens through hydrolysis of triglyceride (Yue et al., 2018).

The reaction pathways of cellulose, lignin, and lipids can be seen in Figure 2.11, where furfural residue is used as the source of these compounds.

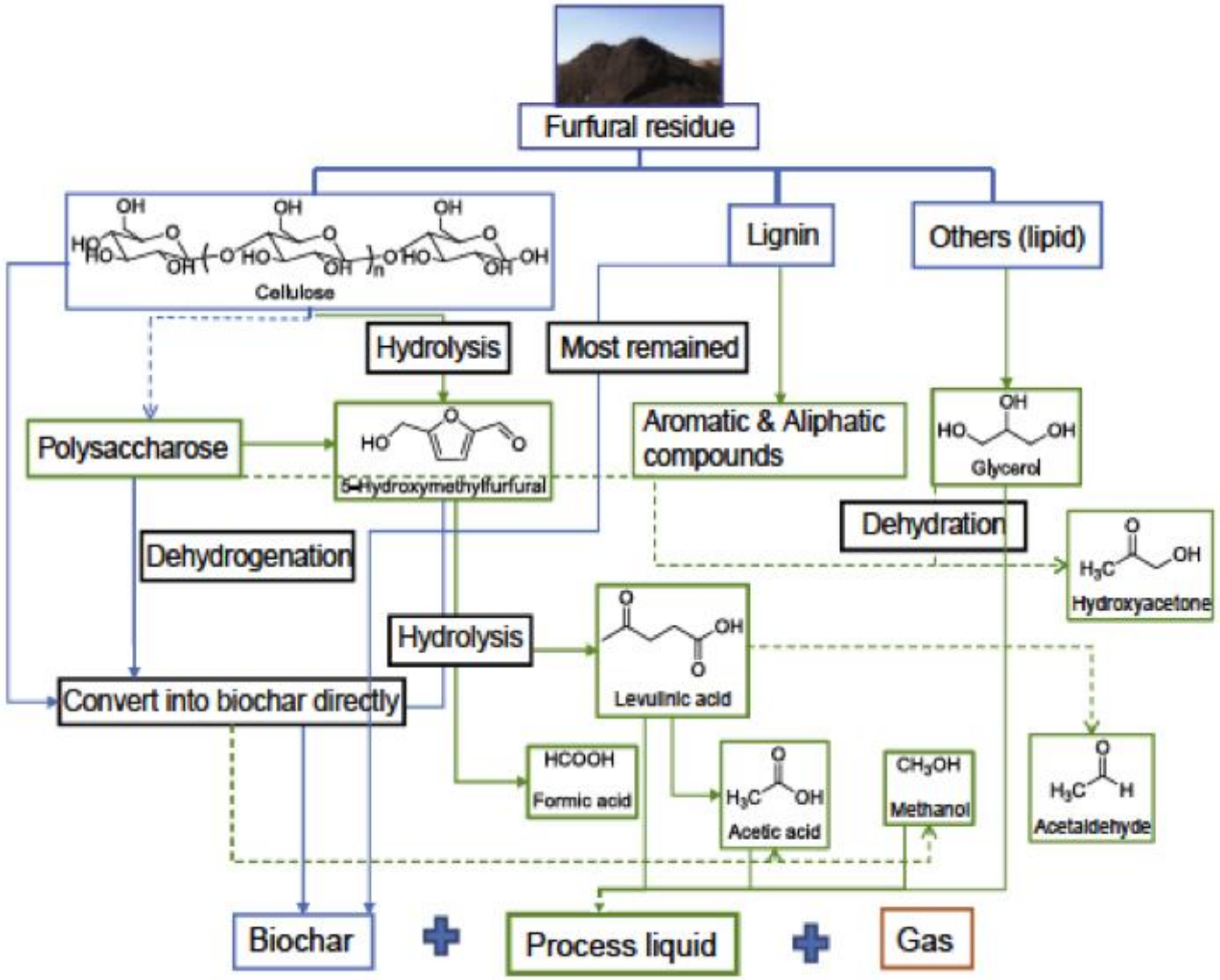

Figure 2.11 Hydrothermal reaction pathways of cellulose, lignin and lipids from furfural residue (Yue et al., 2018)

HTC of starches yields a furan rich hydrochar, indicating that the oligomers formed during degradation do not bind to each other as tightly as those produced in HTC of cellulose (Falco et al., 2011). This results in further hydrolysis into the monosaccharide building blocks, allowing for the generation of a polyfuranic hydrochar. The looser binding also means that hydrolysis occurs at lower temperatures than hydrolysis of cellulose (less than 180°C) (Falco et al., 2011).

Proteins easily degrade under HTC conditions, hydrolysing to form amino acids, which will further hydrolyse to form ammonium (Kruse, Koch, Stelzl, & Zeller, 2016). This is shown through an FTIR study of human waste hydrochar conducted by Spitzer et al., where the –NH peak from the solids was found to diminish significantly after HTC at 180°C, and disappear completely after HTC at 210°C (Spitzer, Mau, & Gross, 2018). Nitrogen is not completely removed, indicating that some nitrogen compounds may recombine with the hydrochar. Maillard reactions may be the mechanism for this (Kruse et al., 2016).

Repolymerisation of the degradation products of the biochemical components of biomass may be limited in low temperature HTC. It has been shown that miscanthus can experience a significant mass loss during HTC without a significant increase in carbon density, indicating decomposition of the biomass

without much repolymerisation of the fragments (Aidan Mark Smith et al., 2018).

2.3.4 The impact of HTC on the inorganic content of biomass

As was discussed in section 1.5, the high concentration of alkali metals, alkaline earth metals, sulphur, and chlorine in biomass cause slagging and fouling issues in thermal conversion. Therefore, the fate of the inorganic content of biomass during HTC is of great importance. Potassium, sodium, sulphur, and chlorine are especially strong influencers of ash chemistry (Aidan M. Smith et al., 2016).

The properties of water under HTC conditions are much different than under ambient conditions. As the temperature and pressure of water is increased, the high polarity of water reduces until it resembles that of hexane (Aidan M. Smith et al., 2016).

Table 2.5 shows the effect of HTC temperature on inorganic content removal by HTC of various biomass types. Some inorganic species are removed from cellulose and hemicellulose when they decompose, and more are removed when the large surface area of lignin is exposed to the water and subject to leaching. The higher temperature and acidic pH of the process liquor can aid in leaching (Reza, Lynam, et al., 2013). Although the cases shown in Table 2.5 all show greater removal of inorganic content with increasing HTC temperature, some other cases show less efficient inorganics removal. In these cases, the

hindrance of inorganic content removal could be due some of the elements being absorbed into the porous lignin matrix left behind by the HTC (Reza, Lynam, et al., 2013), or less efficient leaching through a less polar water solvent.

Table 2.5 HTC ash yield of various biomass feedstocks (Reza et al., 2013)

Biomass	HTC temperature (°C)	Inorganic content removal (%)
Corn stover	200	27.0
	230	38.1
	260	59.5
Miscanthus	200	26.4
	230	40.4
	260	46.9
Switch grass	200	5.4
	230	31.8
	260	39.5
Rice hull	200	0.0
	230	5.1
	260	24.7

It can be seen that effectiveness of inorganic content removal is feedstock dependent. In the study described in Table 2.5, it was found that corn stover was more susceptible to inorganic content removal by HTC, followed by miscanthus, switch grass, and rice hull. In the case of rice hull, the inorganic content was completely unaffected by HTC at 200°C, and it took an HTC temperature of 260°C to remove a quarter of the ash content. The varying composition of biomass inorganic content can explain this, as the solubility of different inorganic elements in water under HTC conditions will vary.

The effectiveness of removal of individual inorganic elements by HTC at different temperatures can be seen in Figure 2.13. The concentration of the inorganic elements in the samples was determined by inductively coupled plasma – atomic emission spectrometry (ICP-AES). It can be seen that silicon is largely unaffected by HTC under the conditions studied, and the reduction through HTC seen can mostly be attributed to loose dirt removal (Reza, Lynam, et al., 2013). The lesser inorganic content removal for rice hull in comparison to the other biomass feedstocks shown in Table 2.5 can be attributed to the inorganic content consisting of nearly 73% silicon (Reza, Lynam, et al., 2013). In some cases, the silicon content of biocoal reduces more sharply between 230˚C and 260˚C, which can be attributed to lignin degradation (Aidan M. Smith et al., 2016). Removal of iron, aluminium and titanium is also not trivial (Aidan M. Smith et al., 2016). It has been seen that HTC of biomass with ash containing high levels of silicon and iron can result in a biocoal with a higher ash content than the feedstock biomass (Aidan M. Smith et al., 2016). This also can be due to high solubilisation of organic content seen in HTC of waste biomass (Aidan M. Smith et al., 2016)

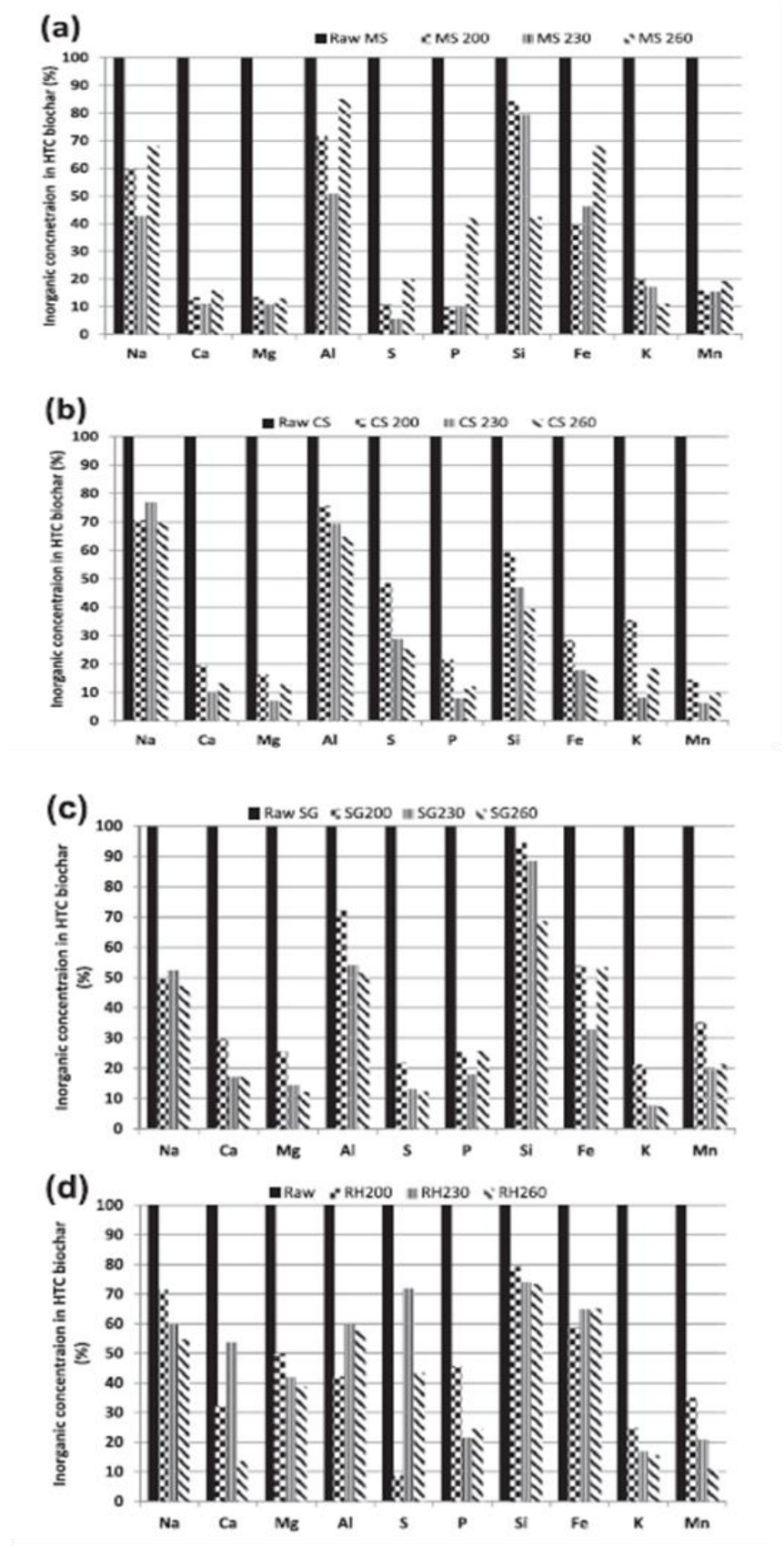

Figure 2.12 Inorganic elemental yield of HTC of various biomasses: (a) miscanthus, (b) corn stover, (c) switch grass, and (d) rice hull (determined by ICP-AES) (Reza et al., 2013)

Potassium, sodium, calcium, sulphur, and phosphorous are more easily removed by HTC. Potassium and sodium are generally the most easily removed, often showing the largest reduction out of the main inorganic species studied, due to these metals being present in the biomass as ionic salts (Aidan M. Smith et al., 2016). The ease of potassium removal is displayed in Figure 2.12, although sodium removal appears more difficult in that specific case. This result is also seen in HTC of Chinese fan palm (Yao & Ma, 2018). The concentration of selected inorganic elements in fan palm and fan palm biocoals produces at various temperatures, determined by inductively coupled plasma – optical emission spectrometry (ICP-OES), can be seen in Table 2.6. It can be seen that in these experiments, potassium is easily removed, with the potassium concentration in the biocoals being an order of magnitude lower than that of the untreated fan palm. In the case of sodium, the concentration in the biocoals is only slightly less than what is seen in the untreated fan palm. Some sodium has been removed on an absolute basis, as the concentration of sodium has been slightly lowered in spite of HTC removing a significant quantity of the organic matter, but the level of removal is much less than that seen in potassium. The ease of potassium removal is also shown in HTC of empty palm oil fruit bunches (EFB), where HTC was found to remove 91.9% and 88.6% at 180°C and 220°C (Novianti et al., 2015). The lesser removal at 220°C was theorised to be due to readsorption of potassium into the porous biocoal structure (Novianti et al., 2015).

Table 2.6 Concentration of selected inorganic elements in fan palm and fan palm biocoals produces at various temperatures (determined by ICP-OES) (Yao & Ma, 2018)

Sample (Chinese fan palm)	Inorganic element concentration (mg/kg)							
	K	Ca	Na	Mg	Cu	Zn	Fe	Al
Untreated	3333.8	2925.0	276.3	702.5	6.0	21.3	313.8	253.8
Biocoal (180˚C)	160.0	1527.5	210.0	82.5	9.5	15.0	427.5	321.3
Biocoal (210˚C)	176.3	1248.8	152.5	60.0	8.8	20.0	362.5	406.3
Biocoal (240˚C)	130.0	1128.8	210.0	58.8	10.0	16.3	433.8	363.8

Although the data shown in Figure 2.12 shows some cases where magnesium, calcium, and phosphorous are easily removed from biomass, other studies indicate that these species are more difficult to remove than potassium and sodium (Aidan M. Smith et al., 2016; Aidan Mark Smith et al., 2018). The biomass feedstock processed affects the impact of increasing HTC temperature on removal of these elements. For example, in the case of HTC of willow, increasing HTC temperature from 200˚C to 250˚C results in worse removal of calcium and magnesium, whereas this temperature increases aids removal of these elements from miscanthus (Aidan M. Smith et al., 2016). The ineffective calcium removal is seen in HTC of Chinese fan palm, shown in Table 2.6, although magnesium is removed with relative ease. The reason behind the less effective removal of magnesium and calcium is lesser proportions of these elements are present in biomass as ionic salts. Ionic salts constitute 60-90% and 20-60% of the concentration of magnesium and calcium, respectively (Aidan M. Smith et al., 2016). A large proportion of the remaining magnesium present is found organically associated with chlorophyll and the biomass macromolecule;

and the majority of the remaining calcium is present as part of amorphous or crystalline compounds. The ease of removal of magnesium in Chinese palm fan shown in Table 2.6, and some of the cases (miscanthus, corn stover, and switchgrass) shown in Figure 2.12, suggests that the magnesium present in these biomass feedstocks are present mostly as salts. Phosphorous is present both as ionic and organic compounds (such as proteins, phospholipids, and nucleic acids), and as such can experience more limited removal from biomass than sodium and potassium (Aidan M. Smith et al., 2016). The ease of removal of sodium and potassium in comparison to magnesium, calcium, and phosphorus indicate that the compound that the inorganic species is incorporated in likely strongly affects the efficacy of removal through HTC (Aidan M. Smith et al., 2016).

It has been seen that removal of magnesium, calcium, and phosphorous can be hindered at higher temperatures. This is also seen in the ash removal data for HTC of miscanthus displayed in Figure 2.12. This could be due to increasing surface functionality of the biocoal. The large number of carboxylic groups on the biocoal surface could result in the biocoal adsorbing the metal species from the process liquor through cation exchange (Aidan M. Smith et al., 2016), as was discussed as a potential explanation for the lower potassium removal in HTC of empty palm oil fruit bunches when the HTC was performed at 220˚C rather than 180˚C (Novianti et al., 2015). Other hypotheses for the reduced removal efficiency include build-up of hydrolysis products on the outer surface of the biocoal (reducing the extraction efficiency of salts with poorer solubility),

and divalent cations (for instance calcium and magnesium) being incorporated into the macromolecule through promoting cross linking of oligomers (Aidan M. Smith et al., 2016). Another potential factor in increasing HTC temperature reducing alkali and alkaline earth metal removal could be due to the polarity of water becoming more non-polar with increasing temperature. As was stated previously in this section, under HTC conditions, the polarity water is similar to hexane (Aidan M. Smith et al., 2016).

It has been shown increasing residence time increases the removal of alkali metals from miscanthus. Limited calcium removal is also seen in this study, with the ash becoming predominantly based on silicon and calcium with increasing residence time (Aidan M. Smith & Ross, 2019). There was shown to be significant extraction of phosphorous and sulphur in HTC with very short residence times, but the species were reincorporated when the residence times were longer. Longer residence times were suggested to favour Maillard reactions, which reincorporated sulphur in the biocoal (Aidan M. Smith & Ross, 2019).

HTC is also effective in removing the chlorine content of biomass (Reza, Lynam, et al., 2013), although some chlorine can be retained in the biocoal through weak chlorine-hydrogen interactions on the biocoal surface resulting in worse chlorine removal than can be achieved through washing (Aidan M. Smith & Ross, 2019).

The heavy metal content of various biomasses and biocoals is shown in Table 2.7. It can be seen that HTC is generally effective at reducing the heavy metal content of biomass, though lead and arsenic are fairly inert under HTC conditions.

Table 2.7 Heavy Metal Content of Various Biomasses and Biocoals (Reza et al., 2013)

Biomass	HTC temperature (˚C)	Heavy Metal Content (mg)							
		Ni	Ag	Pb	Zn	Cu	As	Cd	Cr
Corn Stover	Untreated	20.3	14.1	36.6	45.3	13.8	44.4	9.0	14.0
	200	4.5	4.0	24.9	14.7	8.4	35.2	2.2	6.3
	230	5.1	2.7	12.3	12.6	9.1	25.9	1.1	5.4
	260	5.6	1.8	20.2	18.7	10.6	26.3	1.1	5.8
Miscanthus	Untreated	12.6	10.4	29.3	35.1	4.0	7.3	30.2	6.8
	200	2.1	2.8	29.4	5.2	0.7	0.7	25.8	0.8
	230	3.1	3.1	35.1	8.8	3.3	0.5	29.9	0.7
	260	5.8	2.4	24.2	10.3	7.9	6.0	22.7	1.2
Switch Grass	Untreated	14.8	16.8	30.4	37.0	8.3	11.4	51.9	11.0
	200	3.8	2.3	34.9	8.3	10.0	0.8	30.4	0.9
	230	2.3	2.0	24.0	4.6	4.2	1.2	31.5	1.0
	260	9.2	2.1	30.8	11.7	15.4	8.4	18.2	1.2
Rice Hull	Untreated	1.3	4.8	34.4	5.9	3.1	1.2	16.2	1.9
	200	3.2	2.8	34.2	4.6	3.0	1.3	14.2	1.5
	230	2.9	2.4	35.4	4.1	1.8	1.6	18.9	0.7
	260	2.7	2.2	34.7	5.4	5.9	1.5	2.8	1.7

2.3.5 Effect on HTC conditions on yield and fuel properties of biocoal

A study investigating the effect of temperature, residence time, and particle size on the yields and energy densification of Loblolly pine through HTC can be seen in Table 2.8. The mass yield was calculated as the dry mass ratio of biocoal to biomass; the energy densification by the ratio of the higher heating value (HHV) of product and feedstock (dry, ash free basis); and the energy yield by the mass yield multiplied by the energy densification (Lynam, Reza, Yan, Vásquez, & Coronella, 2015). It shows that HTC temperature is the dominant factor in determining the yield, with the yield greatly decreasing with increasing temperature. Residence time, water to biomass (W/B) ratio, and particle size all have a significantly smaller effect on the mass yield of the char and energy densification. These observations are also seen in other studies (Yan, Hoekman, Broch, & Coronella, 2014). In the case of loblolly pine, increased residence time had a negative effect on the mass yield, and decreasing the particle size may have had a detrimental effect on the mass yield, which may indicate mass transfer limitations in the reaction (Lynam et al., 2015). However, particle size is not as impactful as HTC temperature. In terms of energy yield, temperature is still the primary determinant, but the other parameters have a slightly larger effect than that seen for the mass yield. The water to biomass ratio in particular seems to have a larger effect on the energy yield than the mass yield, with higher W/B ratio lowering the energy yield of HTC. Other studies have also noted increasing W/B ratio having a negative effect on the yield of HTC (Román et al., 2012).

Table 2.8 Reaction parameter effects on the mass and energy yield of loblolly pine (Lynam et al., 2015)

Temperature (˚C)	Residence Time (min)	Water/Biomass ratio	Particle Size (mm)	Mass yield	Energy yield	Energy Densification
200	5	5	0.16	86.1	95.5	1.11
200	5	10	0.24	87.2	93.5	1.07
200	20	5	0.24	85.7	98.4	1.15
200	20	10	0.16	79.0	88.1	1.12
260	5	5	0.24	57.0	81.8	1.44
260	5	10	0.16	53.6	66.3	1.24
260	20	5	0.16	50.0	71.0	1.42
260	20	10	0.24	42.0	61.9	1.48

HTC increases the energy density of biomass, and increasing HTC temperature further increases the energy densification (Álvarez-Murillo, Román, Ledesma, & Sabio, 2015a). This is due to the removal of oxygen and hydrogen through dehydration and decarboxylation resulting in concentration of carbon in the biocoal. A higher carbon concentration means a more energy dense biocoal (Aidan Mark Smith et al., 2018).

It can be seen that that much of the energy content of biomass can be retained when the reaction parameters are mild. The energy yields are much lower at higher temperatures, but the energy density is far greater in these biocoals. There is therefore a trade-off between product quality (energy density) and product yield in HTC (Yan et al., 2014).

The type of biomass also affects the result of HTC, as the biochemical composition of biomass will have an effect on the yield and composition of the products. For example, biomass with high lignin content will have higher yields, as lignin is generally unaffected by HTC and remains in solid form (Liu et al., 2013). The lignin structure also has an impact on the yield and composition of the HTC products (Tekin et al., 2014). Examples of variation include HTC of algae producing much lower yields than HTC of lignocellulosic biomass (Aidan M. Smith et al., 2016); and HTC of some waste biomass feedstocks with high inert ash content (such as sewage or anaerobic digestate) producing misleading results, due to high ash retention, masking significant solubilisation of organic content (Aidan M. Smith et al., 2016). Blending of biomass feedstocks can have a beneficial effect on HTC outcomes (Oliveira et al., 2013).

Recycling of water can increase the mass and energy yield of the biocoal, as the degradation products have a longer residence time under process conditions to cross-link, polymerize and join the biocoal in solid form (Stemann & Ziegler, 2011). In HTC of miscanthus at 260°C, it was shown that recirculation of process liquor increases that the mass yield of biocoal by 5–10% and the energy yield by up to 15% compared to a single-run HTC experiment (Kambo, Minaret, & Dutta, 2018). The impact of water recirculation on mass and energy yields is mostly seen in the first recirculation (Weiner, Poerschmann, Wedwitschka, Koehler, & Kopinke, 2014). Other studies have shown that although mass and energy yields are increased through process liquor

recirculation, the effects on HHV are minor. Some studies report no change in HHV, some slightly improved HHV, and some slightly lowered HHV (Xinfei Chen et al., 2018; Uddin, Reza, Lynam, & Coronella, 2013; Weiner et al., 2014)

The proximate analysis of coconut fibres, eucalyptus leaves, their respective biocoals and lignite can be seen in Table 2.9. The biocoals have a lower volatile matter and a higher fixed carbon content than the feedstock biomass, with these values being intermediate between the values for biomass and lignite. The lower volatile matter content is a result of decomposition of reactive (volatile) components of biomass under HTC conditions. Reactive components that degrade or are removed under HTC conditions include hemicellulose, cellulose, lipids, and proteins (Falco et al., 2011; Kruse et al., 2016; Reza, Lynam, et al., 2013; Yue et al., 2017). These fractions will degrade and be evolved under the conditions of volatile matter determination, so are classified as volatile matter (Tekin et al., 2014; Yang et al., 2007). Lignin does not decompose to the same degree under the conditions of volatile matter determination (Yang et al., 2007), so will form the bulk of the fixed carbon determined. The lignin content of biomass has a significant impact on the fixed carbon content of the biocoal produced (Aidan M. Smith & Ross, 2019). Further material that generates fixed carbon is produced by degradation products repolymerising and joining the solid phase as aromatic carbon (Aidan M. Smith & Ross, 2019).

Table 2.9 Proximate analysis of coconut fibre, eucalyptus leaves, and their respective biocoals (Liu et al., 2013)

Biomass	Temperature (°C)	Residence time (s)	Proximate analysis (db[1]) (%)		
			Volatile matter	Fixed carbon	Ash
Coconut Fibre	Untreated		80.9	11.0	8.1
	220	30	69.8	24.0	6.2
	250	30	67.9	27.1	5.0
Eucalyptus Leaves	Untreated		79.2	10.3	10.5
	220	30	72.5	20.2	7.3
	250	30	70.1	23.0	6.9
Lignite	Untreated		48.8	41.0	10.3

Increasing HTC temperature further decreases volatile matter content and further increases fixed carbon content. This can be attributed to the higher temperature resulting in increased degradation of reactive (volatile) components, as cellulose only significantly degrades at HTC temperatures about 200°C (Coronella et al., 2014). A lower cellulose content in the biocoal will result in a lower volatile matter content and a higher fixed carbon content. Increasing residence time also increases the fixed carbon content of the biocoal produced, indicating increased repolymerisation has occurred (Aidan M. Smith & Ross, 2019).

The elemental analysis of coconut fibres and eucalyptus leaf biomass feedstocks are compared to that of their respective biocoals and lignite in Table 2.10. The data shows HTC removes hydrogen and oxygen, resulting in a biocoal with a higher carbon content than the untreated biomass feedstock. The removal of these elements is due to dehydration and decarboxylation reactions

prevalent under HTC conditions (He et al., 2013; Aidan M. Smith et al., 2016). This effect is strengthened with increasing HTC temperature as the reactions occur to a greater extent. It can be seen that the carbon content of biocoal produced at 220°C is similar to that of lignite. Residence time also has an effect on the elemental composition of biocoal. It has been shown that miscanthus biocoal produced over 24 hours at 200°C is more coal-like in terms of elemental composition than biocoal produced over 0 hours (heated to desired temperature then left to cool immediately) at 250°C (Aidan M. Smith & Ross, 2019).

Table 2.10 Ultimate analysis of coconut fibre, eucalyptus leaves, and their respective biocoals (Liu et al., 2013)

Biomass	Temperature (°C)	Residence time (s)	Ultimate analysis (%)				
			C	H	N	S	O
Coconut Fibre	Untreated		47.8	5.6	0.9	0.2	45.5
	220	30	62.5	5.3	0.9	0.3	31.1
	250	30	67.1	5.2	1.0	0.3	26.4
Eucalyptus Leaves	Untreated		47.0	6.2	1.23	0.8	44.8
	220	30	61.1	6.1	1.4	0.7	30.7
	250	30	62.3	5.5	1.4	0.4	30.4
Lignite	Untreated		61.6	5.7	1.7	0.8	30.1

The Van Krevelen diagram shown in Figure 2.13 compares the O/C and H/C ratios of maize silage anaerobic digestate, cellulose, their respective biocoals, lignite, coal, and anthracite. It can be seen that biocoals have a lower H/C and O/C ratios than their respective biomass, and some of which possess similar values to lignite and coal. As process severity increased, the H/C and O/C ratios came closer to the values for coal. This agrees with the elemental analysis data shown in Table 2.10.

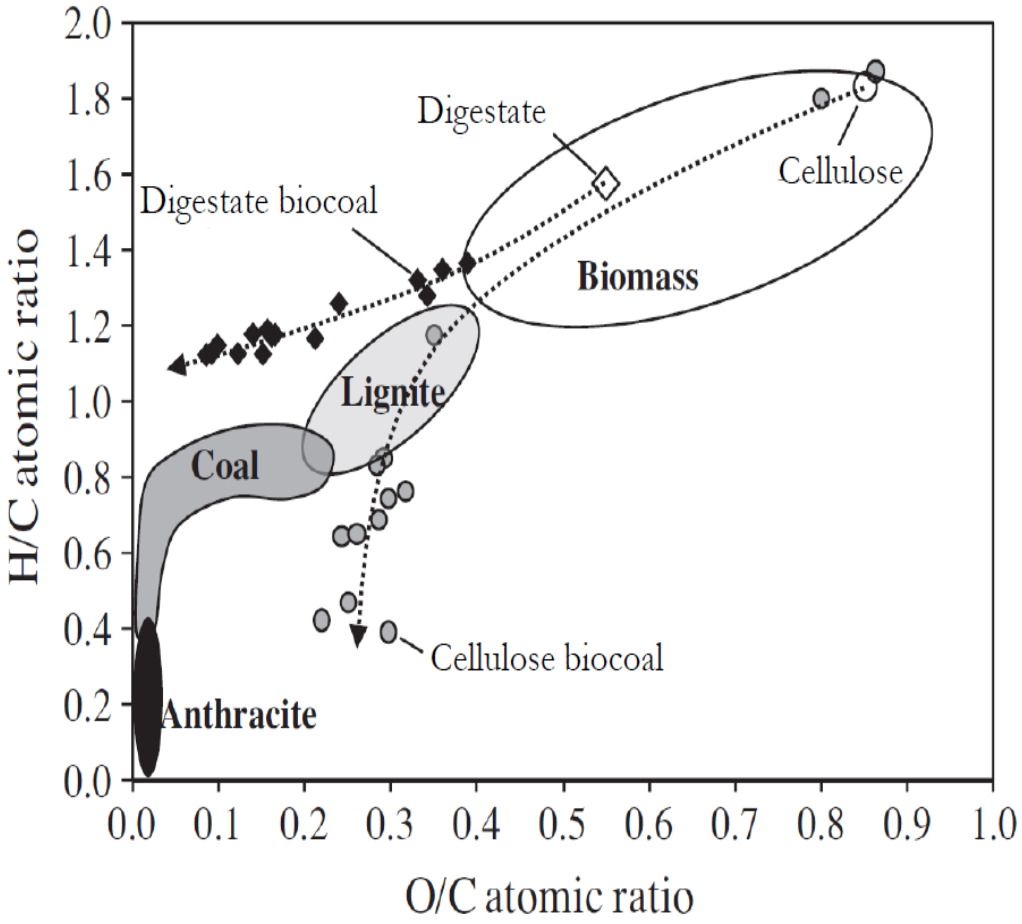

Figure 2.13 Van Krevelen graph comparing cellulose, maize silage anaerobic digestate, and their respective biocoals (Mumme et al., 2011)

The two biomass feedstocks reacted differently to HTC and increasing process severity. Firstly, HTC generally had a larger effect on the O/C and H/C ratios of cellulose than anaerobic digestate. For cellulose, the large shift in O/C and H/C matches the reaction pathways described earlier, with dehydration and decarboxylation reactions evolving oxygen and hydrogen and repolymerisation reactions allowing for significant carbon retention. The smaller change seen in HTC of anaerobic digestate could be due to the reactive (labile) fraction of the biomass being consumed by digestion (Tambone et al., 2009), leaving behind a

feedstock that is less responsive to HTC. The O/C ratio of anaerobic digestate was reduced much more than the H/C ratio by HTC, indicating that decarboxylation reactions were more prevalent than dehydration (Mumme et al., 2011). The results here show that the feedstock used can have a significant impact on the composition of the biocoal produced.

The changes that biomass undergoes through HTC, both in the chemistry of the organic and inorganic content, has a significant impact on the combustion properties of biocoal. Reducing the O/C and H/C ratios, as well as the volatile matter content enhances the combustion properties of biomass, meaning lesser pollutant emissions and a more efficient burn (Aidan M. Smith et al., 2016). Additionally there will be lower energy losses associated with smoke and water vapour evolution during combustion (Aidan M. Smith et al., 2016). HTC also alters the combustion characteristics of biomass. HTC increases the initiation temperature for volatile matter and char decomposition, with the increase in volatile matter combustion initiation temperature being the result of hemicellulose removal (Aidan M. Smith & Ross, 2019). HTC also alters the combustion profile of biomass, changing from the two-stage profile shown in untreated biomass to the one-peak combustion profile shown by coal (Aidan Mark Smith et al., 2018). HTC temperature is a key factor in the degree of change in combustion profile. Miscanthus biocoal produced at 200°C exhibits a two-stage combustion profile, whereas miscanthus biocoal produced at 250°C has a nearly single-stage profile, although with a lower initiation and peak burn temperature than that of coal (Aidan Mark Smith et al., 2018), due to the higher

volatile matter of biocoal (Liu, Quek, Kent Hoekman, Srinivasan, & Balasubramanian, 2012). This can be seen in Figure 2.14.

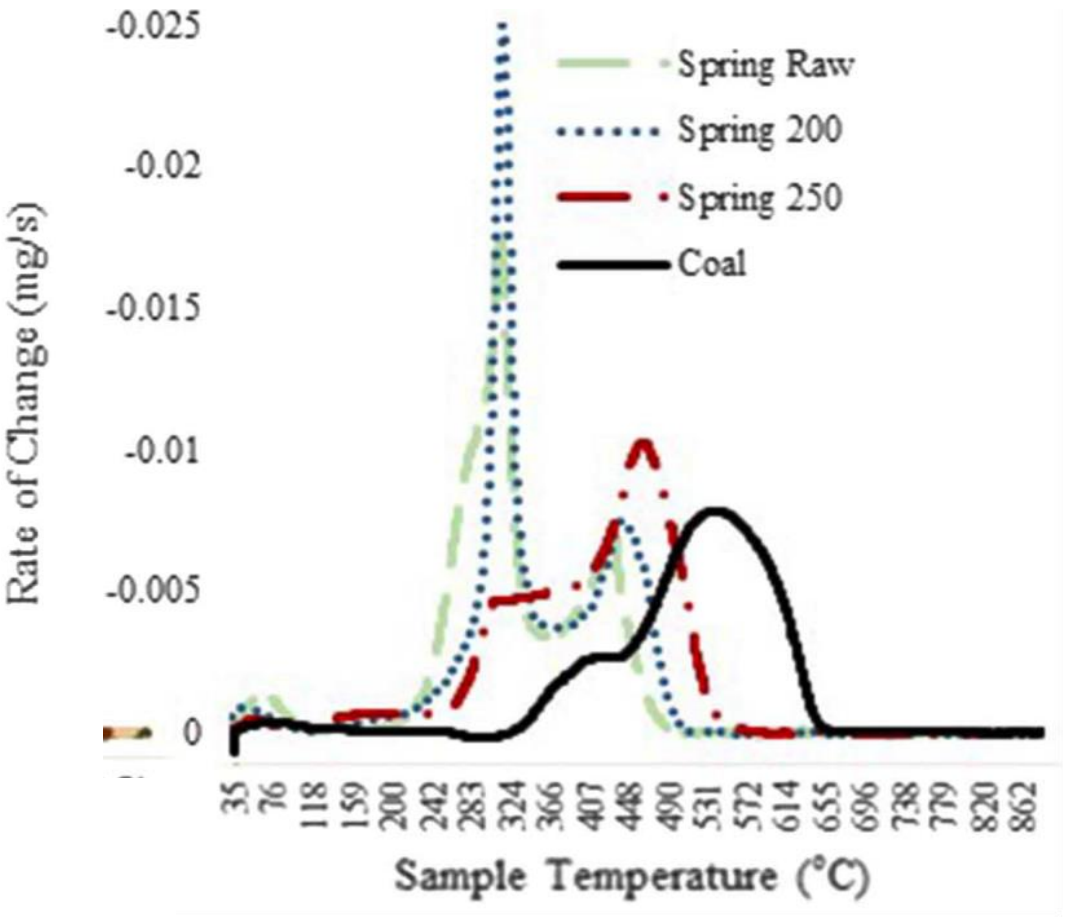

Figure 2.14 Combustion profiles of untreated (Spring Raw) miscanthus, miscanthus biocoal produced at 200°C (Spring 200), miscanthus biocoal produced at 250°C (Spring 250), and Coal.

HTC residence time also has an impact on the combustion properties of biocoal. Biocoal reactivity has been shown to decrease with increasing residence time, and the char initiation temperature increases with increasing residence time (Aidan M. Smith & Ross, 2019).

As was discussed in sections 1.5.1 and 2.3.4, alkali and alkaline earth metals influence ash chemistry, altering the melting temperature. Therefore it follows that removal of these species through HTC affects the chemistry of biocoal ash. In general, sodium and potassium decrease the fluxing (melting) temperature of ash, whereas magnesium and calcium increase it (Aidan Mark Smith et al., 2018). This means that removal of these species can sometimes have counteracting effects on the ash melting temperature, and therefore the slagging propensity of biocoal ash.

2.4 Applications of biocoal

The largest application of biocoal is as a replacement for coal and biomass in combustion, either in power generation or heating. The advantages of biocoal in these applications have already been addressed. Lignite is currently used as a fuel for industrial drying facilities and combine heat and power (CHP) plants, as a cheaper alternative to natural gas, and is also combusted in some European power plants (Pehnt & Henkel, 2009). Since biocoal is similar to lignite, it could also be used in this manner. Biocoal could also be utilised in blast furnaces in steel production, although only if the hydrochar is further processed to produce a feedstock with higher fixed carbon content (Hernandez et al., 2018). Further energy applications of biocoal/hydrochar include gasification to produce gaseous fuel, synthesis of fuels cells, electrode capacitors, and batteries for energy storage (Fang et al., 2018; Reza et al., 2014).

As was stated previously in section 1.6, when the product is used for applications other than combustion, it is referred to as hydrochar. Hydrochar can be utilised as a soil amendment, both for carbon sequestration and for enhancing soil fertility and water retention (Fang et al., 2018). Biochars produced from pyrolysis are already well known chemically inert materials which can be used in soil to sequester carbon, and hydrochar may be used in a similar manner if proven to be suitably chemically inert (Fang et al., 2018; Reza et al., 2014; Titirici, White, Falco, & Sevilla, 2012). Hydrochar could be useful for enhancing soil fertility, reducing the amount of fertiliser lost in surface run-off. The mechanism of this would involve hydrochar adsorbing nutrients into its pores, which then will be released steadily (Fang et al., 2018). Addition of hydrochar into soils can increase the water retention of the soil by decreasing the bulk density and increasing the porosity of the soil (Fang et al., 2018). Hydrochar aiding water retention initially does not follow due to the hydrophobic nature of hydrochar, but when mixed in soil over an extended duration in an oxidative atmosphere, the hydrochar will become hydrophilic through formation of carboxylic and phenolic functional groups (Kambo & Dutta, 2015a). Hydrochar can also help protect soils from infections by root pathogens (Kambo & Dutta, 2015a).

Hydrochar can also be utilised as an absorbent for removing contaminants from aqueous solutions. Hydrochar would be a relatively low-cost adsorbent, and has a wide range of sorption ability (being able to adsorb polar and non-polar chemicals due to possessing a wide range of functional groups) (Fang et al.,

2018). The sorption capacity can be tailored by adjusting the HTC conditions, and potential contaminants in the form of volatile organic carbon in the hydrochar can be easily removed by washing. To achieve the desired characteristics the hydrochar can be activated to form activated carbon. Hydrochar can be effective in heavy metal, phosphate, organic pollutant, and pathogen removal as well as CO_2 sorption (Fang et al., 2018; Kambo & Dutta, 2015a; Oliveira et al., 2013).

Hydrochar can also be useful in chemical production, as it can be used as a catalyst support. Hydrochar can be functionalised to use as catalysts through impregnation. Iron-based catalysts can be made in a single step by dissolving iron salts in HTC process liquor prior to heating with sawdust. This produces carbon spheres with the iron nanoparticles embedded in the matrix (Gai et al., 2017). Iron impregnated hydrochar catalysts can also be produced from immersing hydrochar in an aqueous salt solution after HTC processing (Gai et al., 2017; Liu et al., 2016). These can be used for a number of applications, including inhibiting tar formation in pyrolysis and gasification. This method of catalyst preparation could be done using other metal or metal oxide nanoparticles to tailor the hydrochar catalyst to a given application (Gai et al., 2017). In addition to this, hydrochar can also be sulphonated by heating in concentrated sulphuric acid after HTC processing for potential use in biodiesel production (Kang, Ye, Zhang, & Chang, 2013). Activation of hydrochar could also be used to tailor the properties of the catalyst support (Jain, Balasubramanian, & Srinivasan, 2016a).

There are a number of medical applications for hydrochar currently under research. These include producing quantum dots for organ imaging and increasing antioxidant activity and levels of nutraceutical compounds in watermelon extracts (Fang et al., 2018).

2.5 Comparison to rival pre-treatments

The major rival pre-treatments to HTC, in terms of producing a solid fuel, include washing, torrefaction, pyrolysis, leaching, and steam explosion.

A crucial advantage of HTC over dry pre-treatments (torrefaction and pyrolysis) is the capacity to process wet biomass. Pyrolysis and torrefaction need dry, high quality biomass to operate efficiently (Liu et al., 2013; Titirici, Thomas, & Antonietti, 2007). The capability to process wet biomass allows for utilisation of wastes and algal biomass (Libra et al., 2011). This would widen the feedstock pool, enhancing the sustainability of biomass use. The capability of HTC to process wet biomass also removes the need for drying before processing. This is an energy intensive step, so utilising a process that doesn't require drying would be useful in ensuring the sustainability of pre-treatment.

A comparison of the typical process parameters and yields of pyrolysis, torrefaction, and HTC is shown in Table 2.11. Slow pyrolysis and torrefaction

will be discussed in comparison to HTC, as these processes yield significant quantities of solid products.

Table 2.11 Comparison of Pyrolysis, torrefaction and HTC (Libra et al., 2011)

Process	Temperature (˚C)	Residence time	Product Distribution (Wt %)		
			Solid	Liquid	Gas
Slow Pyrolysis	400	1h-1week	35	30	35
Intermediate Pyrolysis	500	10-20s	20	50	30
Fast Pyrolysis	500	1s	12	75	13
Torrefaction	200-300	0.5-1 hour	70-80	-	30-20
HTC	180-250	(1-12h processing time)	50-80	5-20	2-5

Torrefaction and HTC operate under similar conditions and have similar solid yields. Slow pyrolysis is performed at higher temperatures, and has a much lower solid yield than HTC and torrefaction. HTC has a wider variation of solid yield and produces more liquid than torrefaction. The majority of the liquid

yield are organic molecules dissolved in water (Libra et al., 2011), some of which would become part of the solid yield if process liquor was recycled (Stemann & Ziegler, 2011). This would put the solid yield of HTC on the higher end of the range shown, making the two processes very similar in solid yield.

Biocoals differ from pyrolysis biochars in terms of organic composition. Figure 2.14 and Figure 2.15 show ^{13}C NMR spectra of a range of biochars and biocoals, and Table 2.12 displays the relative contribution of alkyl carbon, O-alkyl carbon, aryl carbon, and carboxyl carbon to total signal intensity of the solid-state ^{13}C NMR spectra of these fuels in addition to untreated biomass. The biochars were produced by Advanced Gasification Technology (AGT), Blackcarbon, and Pyreg. The temperatures used in the production of these biochars were 1200°C, 760°C, and 850°C, respectively (Wiedner et al., 2013).

The biocoal samples were produced by CS CarbonSolutions Deutschland GmbH. Two of the maize silage biocoal samples – 'Maize silage 1' and 'Maize silage 2' – were processed in a commercial scale, continuous HTC reactor. In this reactor, the biomass was heated at 230°C for at least 15 minutes, followed by heating at 180°C for at least 75 minutes. All other biocoals were produced using a prototype reactor which mimicked the temperature and residence time profiles of the commercial reactor, with the exception of the biocoal sample 'Maize silage 3', which was processed at 170°C for 90 minutes. Some of the 'Maize silage 3' sample was then processed under the same parameters mimicking the

commercial scale process to produce the 'maize silage 4' biocoal (Wiedner et al., 2013). The HTC conditions used to make the biocoals are summarised in Table 2.13.

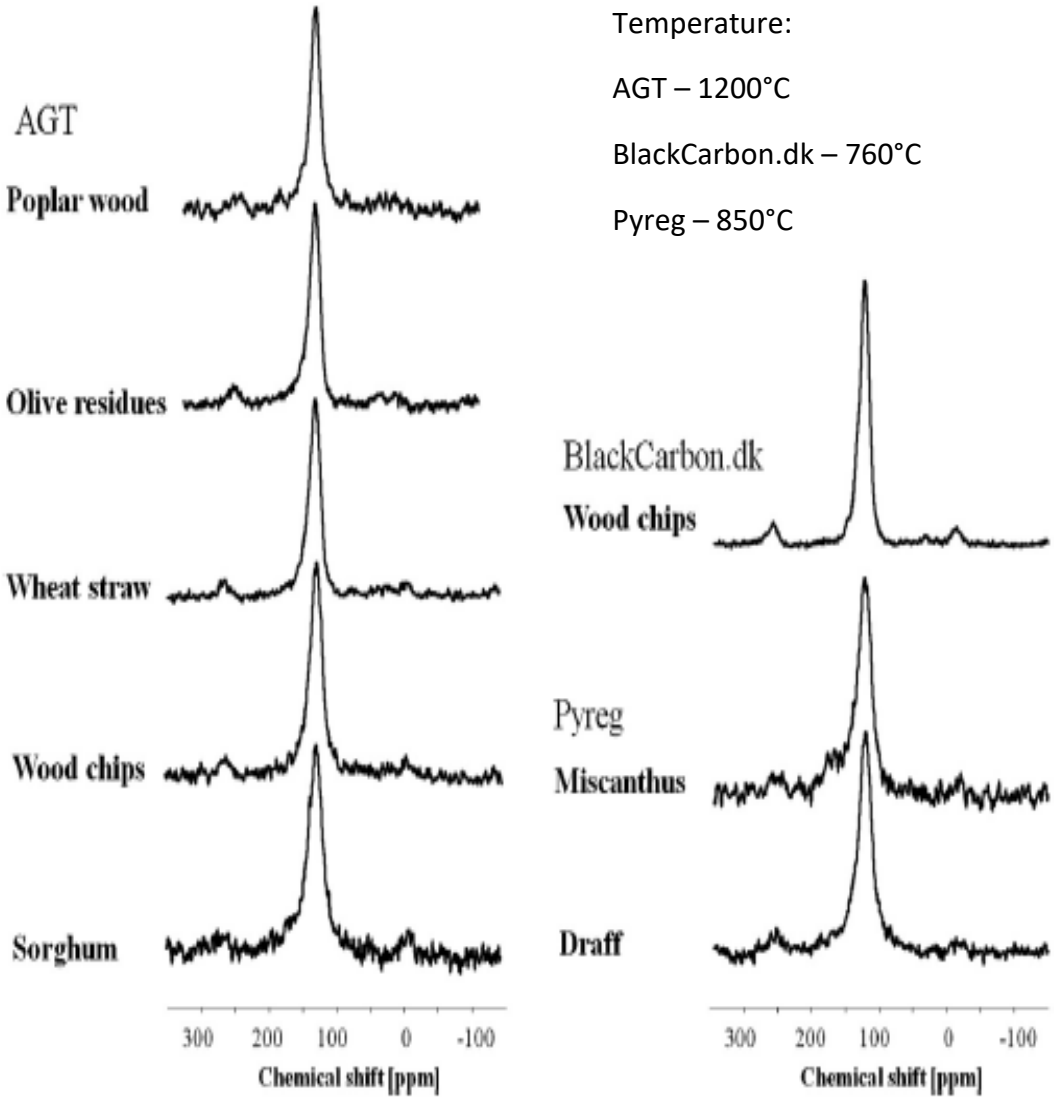

Figure 2.14 ^{13}C NMR spectra on Advanced Gasification Technologies (AGT) biochar, and pyrolysis biochar from BlackCarbon (BC) and Pyreg processes (Wiedner et al., 2013)

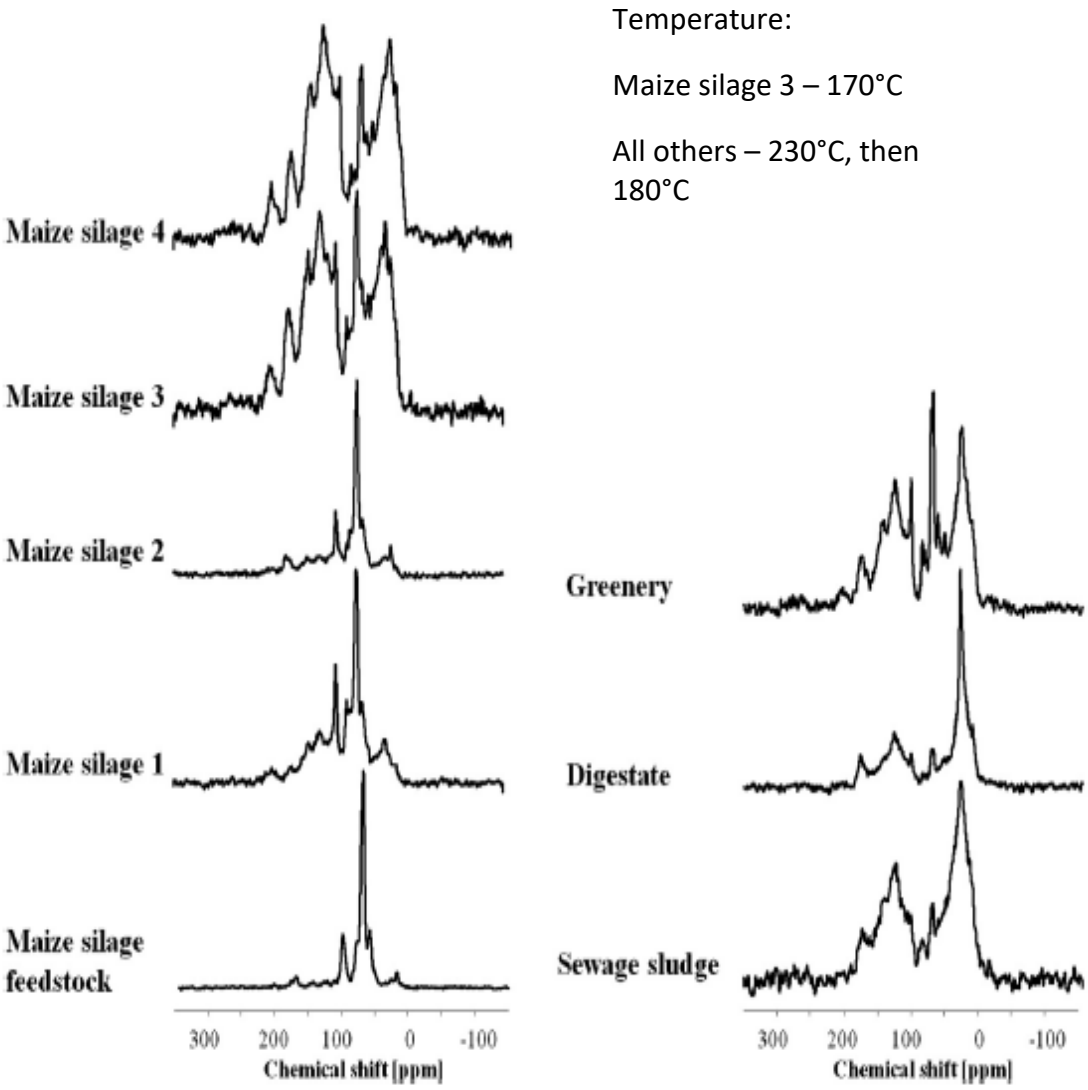

Figure 2.15 ^{13}C NMR spectra for a selection of biocoals (Wiedner et al., 2013)

Table 2.12 Carbon composition of varied biomass feedstocks, biochars, and biocoals (Wiedner et al., 2013)

Sample	Alkyl C 0-45 ppm		O-Alkyl C 45-110ppm	Aryl C 110-160ppm	Carboxyl C 160-220
Poplar	6	78	13	2	
Wheat Straw	5	81	11	4	
Olive Cake	10	71	14	4	
Maize Silage	6	83	6	5	
Poplar biochar (AGT)	0	0	100	0	
Wheat straw biochar (AGT)	0	0	100	0	
Wood chips biochar (AGT)	0	0	100	0	
Sorghum biochar (AGT)	0	0	100	0	
Olive cake biochar (AGT)	0	0	100	0	
Wood chips biochar (BlackCarbon.dk)	0	0	100	0	
Draff biochar (Pyreg)	0	0	100	0	
Miscanthus biochar (Pyreg)	0	0	100	0	
Wood Chips biochar	0	0	100	0	
Maize silage 1 biocoal	13	57	23	7	
Maize silage 2 biocoal	12	63	15	10	
Maize silage 3 biocoal	23	29	38	11	
Maize silage 4 biocoal	48	20	24	9	

Biogas digestate biocoal	48	20		24		9	
Grass greenery biocoal	8	51		26		15	
Sewage sludge biocoal	39	24		19		18	

Table 2.13 HTC conditions used in biocoal production (Wiedner et al., 2013)

Biocoal	**Feedstock**	**Temperature (°C)**		**Time (min)**		**Pressure (MPa)**	
		Stage 1	Stage 2	Stage 1	Stage 2	Stage 1	Stage 2
Maize silage 1	Maize silage	230	180	15	75	2.8	1
Maize silage 2	Maize silage	230	180	15	75	2.8	1
Maize silage 3	Maize silage	170	N/A	90	N/A	0.79	N/A
Maize silage 4	Maize silage 3	230	180	15	75	2.8	1
Leftover food	Leftover food	230	180	15	75	2.8	1
Biogas digestate	Biogas digestate	230	180	15	75	2.8	1
Greenery	Greenery	230	180	15	75	2.8	1
Sewage sludge	Sewage sludge	230	180	15	75	2.8	1

In the feedstock biomass, the likely source of the O-alkyl carbon moieties is polysaccharides (for example hemicellulose and cellulose). In the case of aromatic carbon moieties, the likely sources are lignin, tannins and other aromatic molecules. Alkyl carbon moieties are likely derived from lipids, cutin, suberin and other aliphatic biomacromolecules (Wiedner et al., 2013).

The organic composition of the untreated biomass treatments follow what was discussed in section 2.1.1 – that lignocellulosic biomass is mostly comprised of holocellulose (indicated by O-alkyl carbon moieties) and lignin (indicated by aryl carbon moieties). The conversion to 100% aryl carbon in the biochars indicates that the biomacromolecules in the biomass have decomposed completely, leaving behind only aromatic carbon.

The milder conditions of HTC result in the biocoals having significant proportions of alkyl carbon, O-alkyl carbon, and carboxyl carbon. The proportion of the carbon moieties in biocoal is between that of the untreated biomass and the biochar. This indicates that there are still significant concentrations of polysaccharides and biomacromolecules (or their fragments). The reduction in the concentration of O-alkyl carbon from 83% in the untreated maize silage to between 20-63% in the maize silage biocoals shows the degradation of hemicellulose and (in some cases) cellulose during HTC. The increase in the concentration of aryl carbon from 6% in the untreated maize silage to 15-38% in the maize silage biocoals show the increasing lignin content of the biocoals (as lignin is mostly left unaffected as other components

decompose), in combination with aromatisation of hemicellulose and cellulose degradation products. This is consistent with the chemistry of HTC described in section 2.3.3. The wide array of peaks found in biocoal is similar to those found in low-rank coals (Wiedner et al., 2013).

HTC can be considered a combination of torrefaction and leaching, as it operates in the same temperature range as torrefaction while also utilising water (Acharya, Dutta, & Minaret, 2015). Both torrefaction and leaching improve certain aspects of biomass performance as a fuel, but neither alleviate all of them (Saddawi et al., 2012). HTC could potentially do this. HTC increases fixed carbon content and decreases moisture and volatile matter contents (Bach & Skreiberg, 2016) like torrefaction, but also is also effective in removing alkali and alkaline earth metals from biomass (Reza, Lynam, et al., 2013). Torrefaction is not effective in removing alkali and alkaline earth metals from biomass (Hidayat et al., 2017).

Washing with deionised water at room temperature can remove some of the inorganic content of biomass by dissolving simple ionic salts, such as alkali metal chlorides (Aidan M. Smith et al., 2016). Washing can be particularly effective for herbaceous biomass, and has been shown to remove up to 92% of sodium, 62% of potassium, and 100% of chlorine (Saddawi et al., 2012). As was stated in section 2.3.3, washing can be more effective in chlorine removal than HTC as some chlorine be retained in the biocoal through weak chlorine-hydrogen interactions on the biocoal surface (Aidan M. Smith & Ross, 2019).

Hot leaching has been shown to remove 50-90% of the calcium, sulphur, phosphorous, magnesium and potassium in biomass (Reza, Lynam, et al., 2013). Although effective in alkali and alkaline earth metal removal, leaching produces less desirable outcomes in other fuel properties. For example, leaching of rice straw, wheat straw, switchgrass, and miscanthus was found to have little impact on heating value even though the ash content decreased (C. Yu et al., 2014). This means that leaching is removing organic fractions in addition to the inorganic content. In addition to this, leaching leaves biomass with a large moisture content (C. Yu et al., 2014), resulting in the product needing extensive drying to become suitable for use. Biocoal is hydrophobic (Reza et al., 2014), therefore is relatively easy to dry, typically only requiring mechanical dewatering (Reza et al., 2014), rather than drying through heating (Rahbari, 2011). This means that less energy will be needed to make the product suitable for combustion. In addition to this, HTC does not require grinding of biomass prior to treatment whereas leaching typically does (Rahbari, 2011). The key advantage of HTC over torrefaction and leaching is that it combines the beneficial qualities of these processes and avoids some of their drawbacks. In addition to this, the favourable efficiency of the process has the potential to be further improved upon through process augmentation like utilising microwave heating (Elaigwu & Greenway, 2016).

The advantages of HTC over steam explosion include that it produces better grinding quality (biocoal is more friable than steam exploded biomass), and that

HTC extracts metals from the biomass (Reza, Lynam, et al., 2013) due to using liquid water rather than steam.

2.6 Energetic and economic analysis of HTC

The heat of reaction for HTC has been reported to be between 0 and -5.8MJ/$kg_{feed,dry}$ (Funke & Ziegler, 2011). The heat of reaction of HTC will have only a minor effect on the overall energy balance of the system as heating and pressurising the system requires a comparatively large energy supply due in part to the significant heat capacity of water (Calzavara, Joussot-Dubien, Boissonnet, & Sarrade, 2005; Funke & Ziegler, 2011). The large energy requirement poses a significant potential issue of HTC. There are a number of measures that can be taken to maximise the energy efficiency of HTC. Firstly, heat can be recovered by recycling process liquor. This was also shown in section 2.3.5 to have the potential to increase the yield of HTC, so water recirculation has a twofold positive impact on HTC efficiency. Recirculation of water would also minimise the water footprint of HTC (Stemann, Putschew, & Ziegler, 2013).

Another solution to the problem of energy recovery is integration of the HTC plant to the end-use of HTC products. Integrating HTC with a combined heat and power (CHP) plant means that there is no longer a need for a complex heat recovery scheme in the HTC process., which would aid operability (Berit Erlach, Wirth, & Tsatsaronis, 2011). Integration of these two processes would also

enhance economic viability by reducing the overall investment cost for the plants and would increase the CHP plant annual operating time where heat load varies seasonally (for example northern Europe) (Saari, Sermyagina, Kaikko, Vakkilainen, & Sergeev, 2016). The process liquor can also be recycled into an adjacent biogas production plant to make use of the dissolved organic content (Erdogan et al., 2015a).

Catalysis is a further option for making HTC more economical, although this eliminates the advantage of HTC being a non-chemical, environmentally friendly process. It has been seen that metal ions (Fe especially) and nanoparticles (FeO_x) can accelerate the process (Titirici et al., 2007), and other potential catalysts include citric acid (Wiedner et al., 2013), acetic acid (J. Xu, Thomsen, & Thomsen, 2010), lithium chloride (Lynam, Coronella, Yan, Reza, & Vasquez, 2011), and sodium salts (Ming et al., 2013). Some issues that would need to be addressed include recovery of miscible catalysts and distribution of solid catalysts.

The ability to process waste biomass is a very important aspect in ensuring the economic viability of HTC. Waste biomass is typically unwanted and can be acquired at little or no cost. The main logistical issue of large-scale use of waste biomass is the widespread nature of the producers, the uncertainty of supply, and perishable nature of the products. This makes supply chain management complicated, requiring a robust and flexible supply chain (Iakovou et al., 2010).

Figure 2.16 shows a process flow diagram (PFD) used for modelling HTC of poplar wood in a semi-continuous HTC plant. The process design includes a heat recovery system based on recycling of hot compressed water to reduce the external energy consumption, and the assumed capacity of the plant is 2000 kg/h of dry biomass. The simulation was performed using *Engineering Equation Solver* (EES) software (Stemann & Ziegler, 2011).

In the model, biomass is mixed with hot compressed water in the lock hopper, before being heated to a temperature of 156°C by steam from the first flash tank. The slurry is then mixed with hot compressed water from the piston press, resulting in an increase in temperature to 196°C and a final W/B ratio of 7:1. After this, very little external heat is needed to fully heat slurry to 205°C, where then the heat of reaction alone is enough to heat the slurry to the desired process temperature of 210°C (Stemann & Ziegler, 2011). The external thermal energy required amounts to 1.03 GJ/h. This represents 2.7% of the energy of the biomass input and 3.4% of the energy of the biocoal output. Additionally, the char can be dried to a moisture content of 7% using solely the heat of the process (Stemann & Ziegler, 2011).

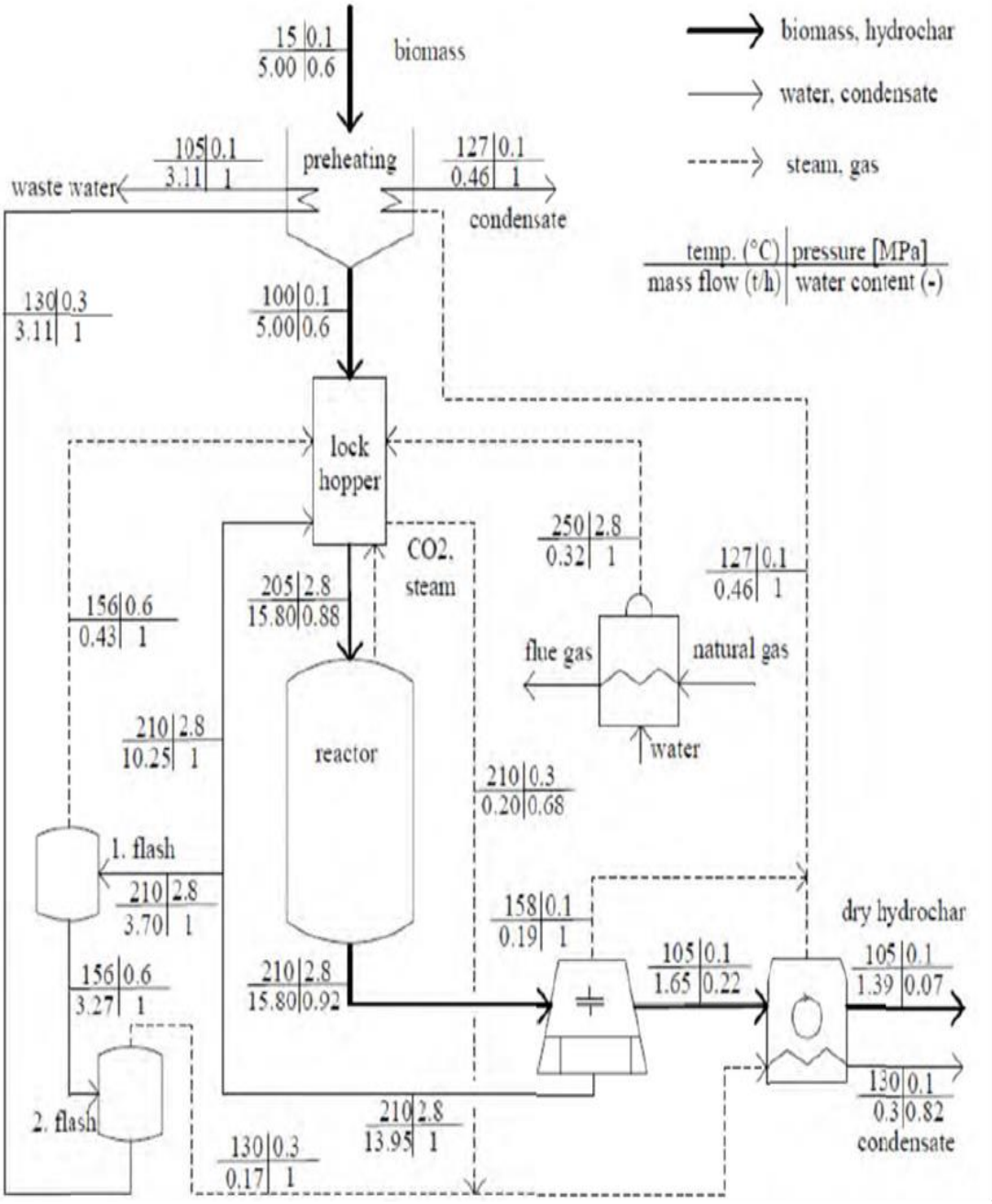
biomass, hydrochar
water, condensate
steam, gas
temp. (°C) | pressure [MPa]
mass flow (t/h) | water content (-)
15 | 0.1
5.00 | 0.6
biomass
preheating
105 | 0.1
3.11 | 1
waste water
127 | 0.1
0.46 | 1
condensate
130 | 0.3
3.11 | 1
100 | 0.1
5.00 | 0.6
lock hopper
CO2, steam
250 | 2.8
0.32 | 1
127 | 0.1
0.46 | 1
205 | 2.8
15.80 | 0.88
156 | 0.6
0.43 | 1
flue gas
natural gas
water
210 | 2.8
10.25 | 1
reactor
210 | 0.3
0.20 | 0.68
1. flash
210 | 2.8
3.70 | 1
158 | 0.1
0.19 | 1
dry hydrochar
105 | 0.1
1.65 | 0.22
105 | 0.1
1.39 | 0.07
156 | 0.6
3.27 | 1
210 | 2.8
15.80 | 0.92
2. flash
210 | 2.8
13.95 | 1
130 | 0.3
0.17 | 1
130 | 0.1
0.3 | 0.82
condensate

Figure 2.16 A PFD used for simulating HTC of poplar wood in a semi-continuous HTC plant (Stemann & Ziegler, 2011)

The moisture content of the feedstock biomass was also considered in the model. A feedstock with a higher moisture content would result in less water being recycled, if the desired W/B ratio is to be met. This results in less heat recovery, and more external energy would be needed to heat the slurry to reaction temperature. Therefore, the efficiency of the plant on an HHV basis will decrease if a feedstock with a high moisture content is used, as more external energy is required. Although, if the efficiency of the plant is calculated on an LHV basis, the efficiency of the plant increases with increasing moisture content, as the LHV of the feedstock biomass decreases sharply with increasing moisture content (Stemann & Ziegler, 2011).

A PFD used to model HTC of empty palm oil fruit bunches (EFBs) in an industrial scale plant is shown in Figure 2.17. The simulation was performed using *Aspen Plus V7.1* software (Stemann, Erlach, & Ziegler, 2013). The temperature, pressure, residence time, and W/B ratio used in the simulation was 220°C, 30 bar, 4 hours, and 6.67 respectively. The capacity of the plant was 5.7 t/h, producing 1.3 t/h of biocoal (10% moisture content) (Stemann, Erlach, et al., 2013). The inputs to the plant were 1.5% electrical energy, 6.2% thermal energy, and 92.3% energy from feedstock. The energetic efficiency of the process (on an HHV basis) was calculated to be 71.2%. It was calculated that 33% of the energy of the feedstock would be required to dry the untreated

biomass from 65% to 10% moisture content, therefore HTC would be more energetically efficient than solely drying in this case (Stemann, Erlach, et al., 2013). The cost of biocoal production was calculated using the simulated data, with the cost amounting to 7.9-9.7 €/GJ_{HHV}. If carbon credits at a value of 10 €/t CO_2 were applied, the cost of production would lower to 6.1-7.8 €/GJ_{HHV} (Stemann, Erlach, et al., 2013).

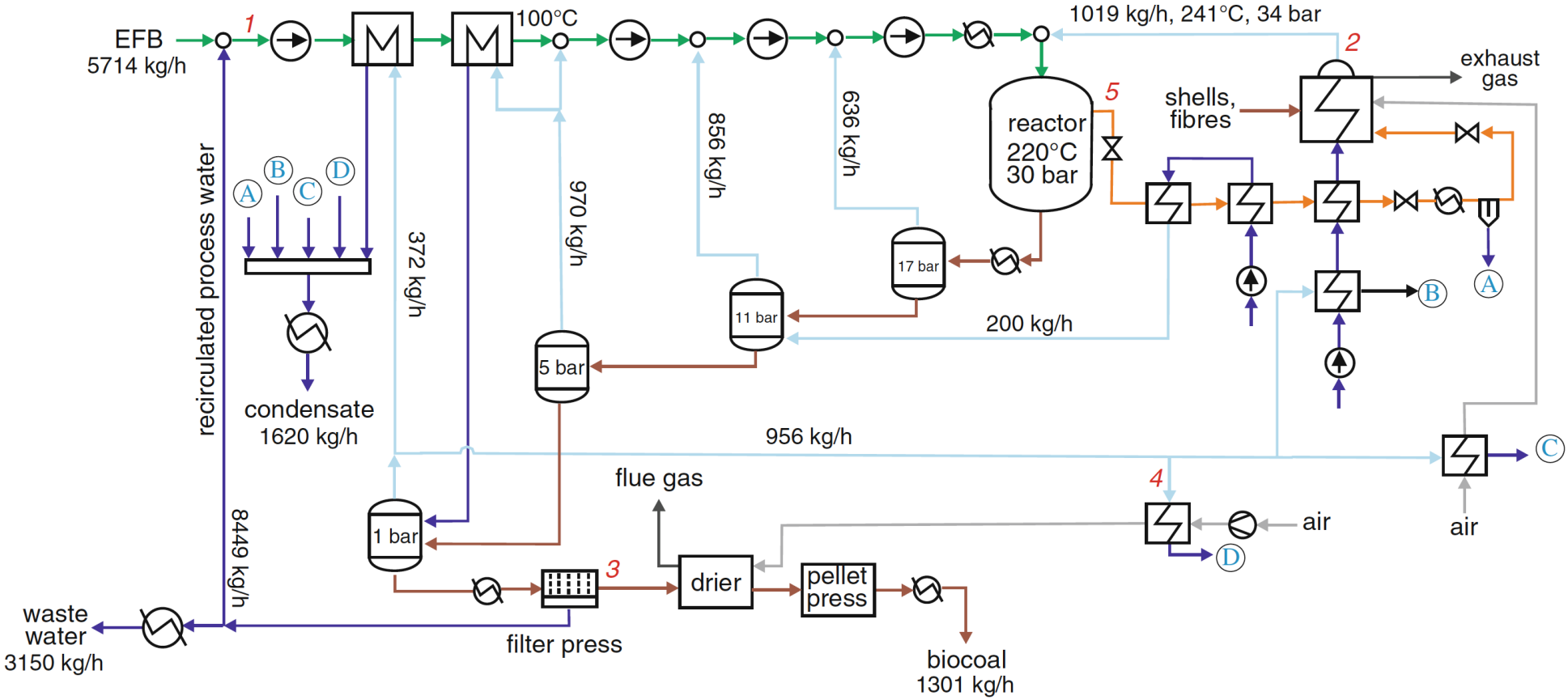

Figure 2.17 A PFD used for simulation of HTC of palm oil fruit bunches (Stemann, Erlach, et al., 2013)

A PFD used to model HTC of off-specification compost (OSC) and grape marc (GM) (separately) is shown in Figure 2.18. The process model was self-developed using the C# programming language (Lucian & Fiori, 2017) and the simulations were run using the parameters detailed in Table 2.14. The model was specified with an operating time of 8000 hours per year, and a plant capacity of 20,000 tons per year on an as-received basis (Lucian & Fiori, 2017). Heat loss in this simulation was simplified, represented in the PFD as 2 heat exchangers (R1 and R2 in Figure 2.18). All equipment was considered to be stationary and adiabatic; no material losses were considered, and pressure drops were considered to be concentrated in equipment. The pelletizing of the biocoal was also included in the simulation (Lucian & Fiori, 2017).

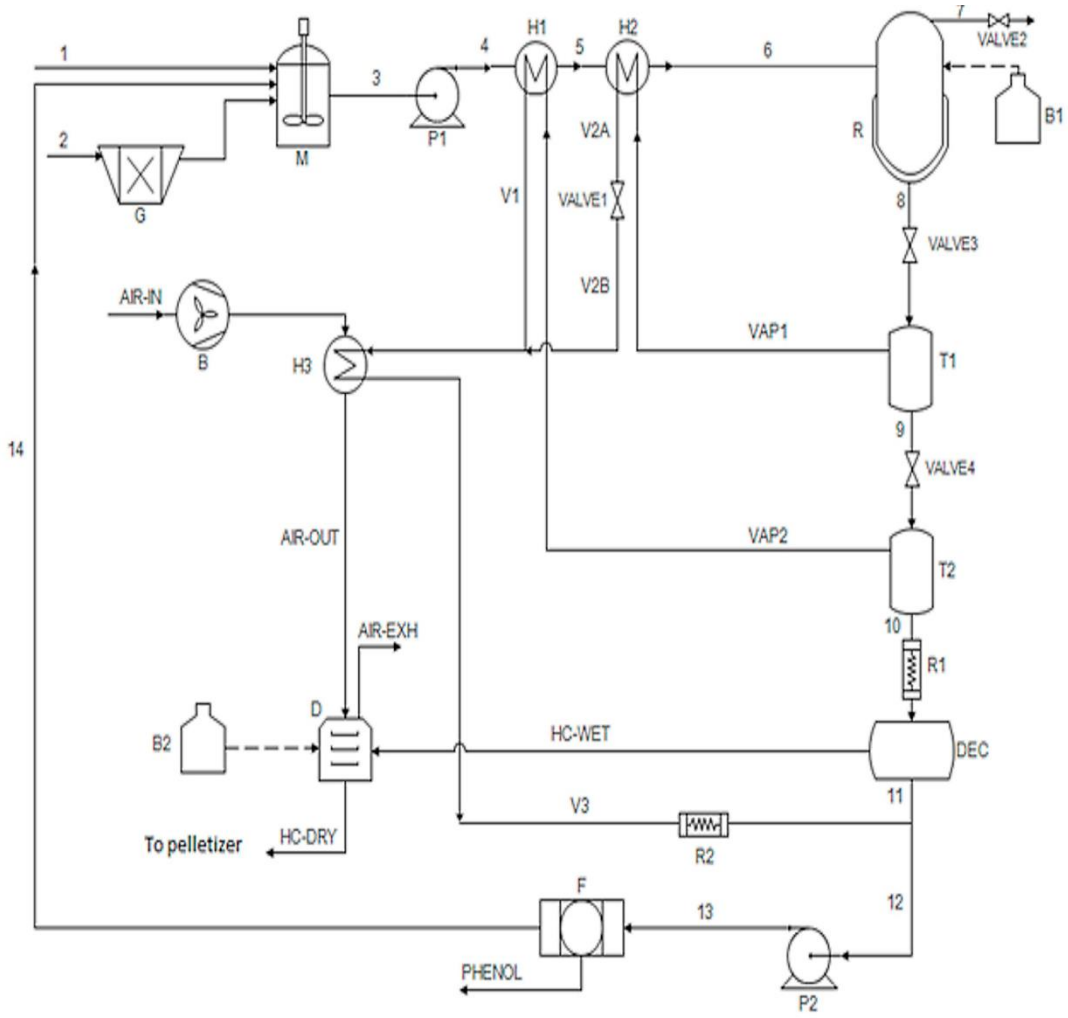

Figure 2.18 A PFD used for simulation of HTC of off-specification compost and grape marc (Lucian & Fiori, 2017)

Table 2.14 Process parameters used in HTC plant simulation (Lucian & Fiori, 2017)

Temperature (°C)	Time (hours)	Moisture content (%)
180	1	30% (OSC)
220	3	65% (GM)
250	8	-

The thermal efficiency of the process was found to be lower when using OSC rather than GM due to the higher moisture content, resulting in a greater

volume of water per unit of dry feedstock (Lucian & Fiori, 2017). The plant efficiency was found to decrease with increasing temperature, although in the case of GM the plant efficiency of HTC at 180°C and 220°C were similar. The plant efficiency was significantly higher for GM than OSC. The difference in HHV between to the two feedstocks contributes to this in addition to the greater volume of water processed per unit of dry feedstock (Lucian & Fiori, 2017).

The most favourable results came from processing grape marc at 220°C for one hour (Lucian & Fiori, 2017). Under these conditions the plant efficiency was 78%. An economic evaluation was performed on the plant operating under these conditions. The reactor volume was 8 m^3, the density of the slurry was 920 kg/m^3, and the reactor was 75% filled. The pressure in the reactor was 50 bar, taking the vapour pressure of water into account (approximately 23 bar at 220°C), the overpressure due to gas production was 10 bar, and the factor of safety was 1.5 (Lucian & Fiori, 2017). The total capital investment was estimated at 1,773,881 €, and the annual operating costs at 832,984 €. An average loan interest rate of 5% and a repayment time of 10 years were assumed, resulting in an annual repayment of 229,717 € for the capital investment (Lucian & Fiori, 2017). With reference to these numbers, a break-even selling price for the biocoal produced was calculated to be 200 €/ton, which equates to 8.3 €/GJ_{HHV} assuming a biocoal HHV of 25.64 GJ/ton is produced under these conditions (Lucian & Fiori, 2017). This HHV value was derived from previous experimental work (Basso et al., 2016; Lucian & Fiori,

2017). This biocoal price is within the range reported in the study described previously (Lucian & Fiori, 2017; Stemann, Erlach, et al., 2013). This matches the market price of biocoal by Ingelia S.L (170 €/ton) (Ingelia, n.d.). At this price, biocoal would be competitive with wood pellets (typically 150-200 €/ton), but not yet with coal (43 €/ton in 2016) (Lucian & Fiori, 2017).

2.7 Current status of HTC

One of the earliest commercial scale continuous process HTC plants was built by Ingelia. The plant is modular, and therefore up-scaling is facile (Ingelia, n.d.). As was stated in section 2.6, Ingelia currently advertise a market value of (170 €/ton) (Ingelia, n.d.). The company claims to be able to work with any type of organic waste, and advertised input materials such as food waste, municipal solid waste, agricultural waste, green waste, and sewage sludge (Ingelia, n.d.). The biocoal produced is in line with international standards for biofuels as well as biofertilizers, and the liquor can be used for fertilisation/irrigation of agricultural fields after desalination and concentration (Ingelia, n.d.).

Other HTC technologies that have been developed include CarboREN® by SunCoal (Suncoal, n.d.-a). SunCoal operate a HTC pilot plant which is operated for customer purposes in weekly runs. This allows for the possibility to scale up and validate production processes determined in a laboratory setting, as well as the capacity to produce samples on the ton scale. The facility can run the process under batch or continuous operation (Suncoal, n.d.-b). Antaco also provide a patented HTC process to turn organic waste into biocoal, aiming to replace fossil coal for energy generation (Antaco, n.d.). Terra Nova offers an HTC technology as a wastewater treatment option, proposing utilisation of sewage sludge rather than disposal. The technology produces some solid fuel as well as recovering phosphorous (TerraNova, n.d.-a). The fuel has proposed uses in generating energy in lignite power plants or lowering the energy

requirements in cement or waste incineration plants (TerraNova, n.d.-b). HTCycle GmbH are developing a HTC process to produce biocoal from sewage sludge and other wet residues (HTCycle, n.d.-b). The biocoal product is proposed to have use in thermal processes, as well as a feedstock for the production of activated carbon for use in wastewater treatment and bio-based carbon black for utilisation in the rubber industry (HTCycle, n.d.-a). AVA-CO2 put an industrial-sized HTC plant into operation in 2010 in Karlsruhe, Germany. The plant had a capacity of 14400 litres, and an annual capacity of 8400 tonnes of biomass (BusinessWire, 2010).

Chapter 3 Materials and Methods

3.1 Sample preparation

3.1.1 Fuel feedstocks

The biomass feedstocks used in this study were utilised on an as-received basis, with as little prior preparation as possible. This was to reduce the amount of energy-expending processing utilised, as using minimal processing would be useful in ensuring the sustainability and economic viability of HTC. In addition to this, over preparation of the biomass prior to treatment would reduce the advantageous impact of HTC, for example grinding biomass prior to treatment would mean that the enhanced friability of biocoal would not be utilised.

Commercially sourced softwood pellets (Brites) were used to represent a high-quality biomass currently in use as a fuel. This is due to the biomass having a relatively low moisture content and low ash (therefore alkali and alkaline earth metal) content.

Miscanthus was studied due to its interest as an energy crop. The miscanthus pellets used in this study was obtained from E.ON UK plc (Williams et al., 2015).

Jatropha was also investigated in this study as an energy crop. Jatropha seeds were provided from Malaysia by ACGT sdn. bhd. (Madanayake, Gan, Eastwick, & Ng, 2016)

Olive cake was studied as a waste biomass feedstock with high levels of alkali and alkaline earth metal composition. The olive cake studied was sourced from EDF Energy plc (Williams et al., 2017).

Bagasse was utilised in this study due to interest in it as a waste biomass feedstock. Shredded bagasse was acquired from AB sugar, originating from Zambia, Africa (Williams, 2016).

Sunflower shells were studied as a potential waste biomass feedstock for HTC. The shells were sourced from Russia by EDF Energy plc (Williams et al., 2015).

Sewage sludge was investigated as a waste biomass stream. The primary sewage sludge was obtained from Severn Trent wastewater treatment.

Digestate produced from anaerobic digestion of rye was studied as a potential bountiful source of waste biomass fuel.

A food waste anaerobic digestate was also studied. The digestate was provided by Biogen UK ltd, and was mixed with clothes fibres sourced from John Lewis. The ratio of digestate to fibres was 4:1.

Minced beef (10% fat), raw carrot, and dried rice were used to represent food waste. The minced beef was boiled before use, to remove as much fat as possible (in initial tests the considerable fat content resulted in difficulty recovering the biocoal). These foodstuffs were purchased from Sainsbury's.

A bituminous coal was also studied for comparison with the biomass-derived fuels studied. The coal used was sourced from the Cerrejón mine in Colombia.

3.1.2 HTC

The HTC experiments were performed in a 75 ml Parr reactor, which can be seen in Figure 3.1. Biomass and deionised water were added to the reactor so that it was at least 1/3 filled (as to ensure water vapour pressure is reached), and the desired W/B ratio was satisfied. The moisture content of the biomass was taken into account when calculating the required volume of distilled water. The reactor was then sealed using the cap, washer, sleeve, and pressure gauge. The cap was sealed onto the reactor using bolts on the sleeve, and were tightened to 15 Nm using a torque wrench.

Once assembled, the air was purged from the vessel and a 1 bar (gauge) nitrogen atmosphere established using a compressed nitrogen line, monitored with an external pressure gauge. The reactor was then fastened to a clamp above a sand bath contained within a jack. The sand bath was then raised using the jack so that the reactor was completely immersed. The sand bath was pre-heated to the desired reaction temperature, so the heating is isothermal. There was a small drop in temperature when the reactor is introduced, but the reaction temperature is reached again within five minutes. An external thermocouple was used in the sand bath to ensure that the temperature readings from the control panel were correct. The full set-up can be seen in Figure 3.2. The gauge pressure was noted when the reactor had reached reaction temperature, to confirm water vapour pressure was reached. The pressures reached in the HTC experiments typically were in the range of 10-50 bar.

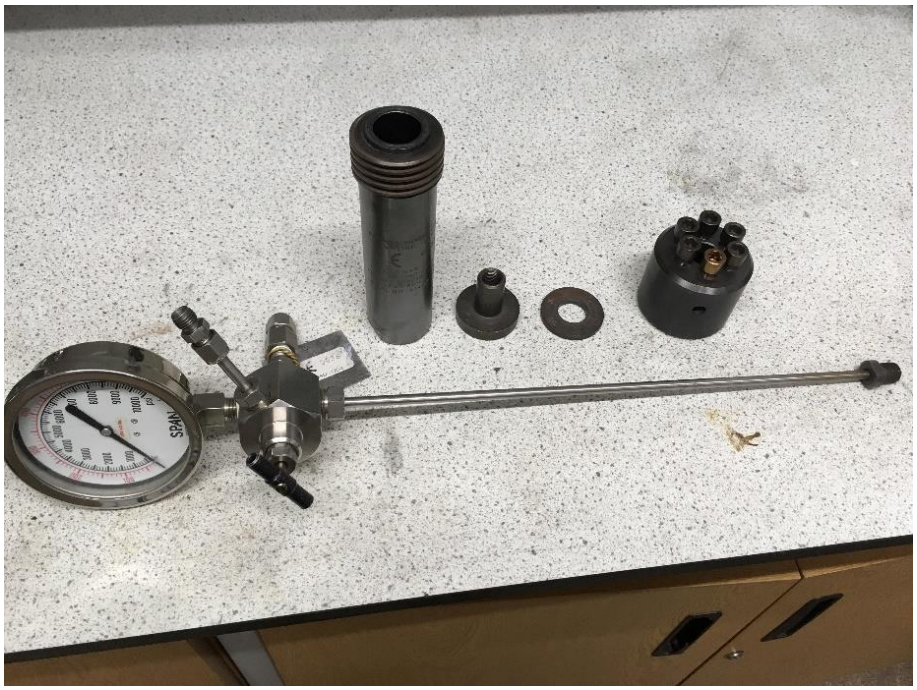


SPAN

Figure 3.1 75 ml parr reactor used in HTC experiments, disassembled (top) and assembled (bottom)

Figure 3.2 HTC experiment set-up

Once the desired experiment duration had passed, the reactor was removed from the sand bath and cooled by allowing compressed are to flow through the

head of the reactor (through the hole in the sleeve) using a compressed air line. Compressed air cooling was used so that the reaction could be quenched as soon as possible once the reactor had been removed from the sand bath. Once cooled to ambient temperature, the gas was collected using a glass gas syringe and stored in a gas bag for GC analysis. This was performed by attaching an adapter to the pressure gauge, which in turn connected to the gas syringe using some plastic tubing. The reactor was then depressurised by opening the valve, which forced the gas into the syringe. The reactor was then disassembled and the process liquor separated using vacuum filtration through a Buchner funnel. Care was taken not to use any deionised water in this stage so the process liquor was not diluted. The process liquor was then removed from the Buchner flask, stored in a sealed glass vial and refrigerated. The reactor was then rinsed out into the funnel with deionised water to collect as much biocoal as possible. The biocoal was then washed with deionised water, and subsequently dried at 105˚C for at least 8 hours. The biocoal was then allowed to cool to room temperature and reach equilibrium moisture content before the mass was recorded. The biocoal was then transferred to a sealed glass vial and stored in a freezer. All equipment was then washed with 50:50 methanol:DCM, followed by soap and hot water, followed by deionised water. The reactor was then fully dried at 105˚C.

Safety measures used when performing HTC experiments included a gasket in the pressure gauge that would rupture if the reactor was being subjected to

pressures that are not considered to be within the safe working range. In addition to this, the sand bath used to heat the reactor is raised on a jack, so that if there is any malfunction in the reactor, the lever for the jack can be released and the heat source for the reactor can be immediately and safely removed. Protective gloves were used at all times when handling equipment during use of the sand bath.

3.1.3 Torrefaction (Horizontal tube furnace)

Torrefied biomass was produced as a biomass derived fuel to compare to biocoal and leached biomass in terms of fuel properties. This process was chosen as it one that uses comparative conditions to HTC to produce a comparable fuel, but is not effective at alkali and alkaline earth removal (Hidayat et al., 2017). This makes the process a useful comparison to HTC.

Torrefaction was performed using a horizontal tube furnace (HTF), shown in Figure 3.3. Biomass was weighed out and placed in a ceramic boat. The biomass was then inserted into the glass tube of the HTF using a metal hook inserted into the hole on the edge of the boat. The furnace was then purged of air by passing a 2000 cm^3/min flow of nitrogen through the tube for 15 minutes, as determined by a flow meter attached to a tube inserted into the stopper sealing one end of the HTF. The gas left the HTF through another tube attached to a stopper on the other end, and the air was bubbled through water to capture any particulates evolved from the HTF.

Once purged of air, the furnace was heated to the process temperature at a heating rate of 10˚C/min while the flow of nitrogen was maintained. Once the desired temperature was reached, the furnace was held isothermally for the desired residence time, after which the heating elements were turned off and the furnace was allowed to cool to room temperature while maintaining the flow of nitrogen. The temperature in the HTF was determined by the value displayed on the control module. Once cooled, the ceramic boat was removed from the furnace using a metal hook and the torrefied wood was left uncovered in a fume hood for at least three hours to allow the moisture content equilibrate prior to weighing and storage in a sealed glass vial in a freezer.

For safe operation of the HTF, there was an automatic switch on the side of the furnace, where a metal key was inserted when the furnace is closed. If the furnace was opened while operating, the key would be pulled out of the socket through the action of opening the furnace, and the electrical feed to the furnace would be cut off.

Figure 3.3 Horizontal tube furnace used in torrefaction experiments

3.1.4 Torrefaction (Parr reactor)

So that the role of water in HTC reaction pathways can be studied, a biomass fuel was to be produced using the same equipment as in the HTC experiments. Although torrefaction is normally conducted in an open system with a flow of nitrogen flowing through the reactor, the closed system of the Parr reactor utilised in the HTC experiments (described in section 3.1.2, and shown in Figure 3.1) is used in this case. This was to minimise the differences between the experiments, so that a direct comparison could be made.

The procedure outlined in section 3.1.1 was followed to perform the closed-system torrefaction experiment with a couple of minor changes:

- The sample was fully dried in an oven at 105˚C for at least 8 hours prior to processing
- No water was added to the reactor

3.1.5 Acid leaching

As was detailed in section 2.5, leaching can remove significant quantities of alkali and alkaline earth metals, but does little to advance other fuel properties of biomass. This makes the process a useful comparison to HTC and torrefaction, as comparing the two could allow for assessment of the impact of alkali and alkaline earth metal content on the combustion properties of biomass, in comparison to other factors such as composition and surface area

changes. To maximise the removal of alkali and alkaline earth removal, acid leaching was used.

The acid leached olive cake was produced by immersing milled olive cake (0-75 µm) in 1M hydrochloric acid in a glass beaker, and stirring at 60°C for 8 hours, using a stirrer hotplate. Olive cake was chosen due to the large concentrations of alkali and alkaline metals present in the biomass, so that the impact of these elements on the combustion properties of the biomass can be seen clearly. The temperature was measured using a thermocouple. After 8 hours, the mixture was cooled with stirring and was then filtered under vacuum using a Buchner funnel. The biomass was washed with DI water until the pH approached neutral. The pH was determined using litmus paper. The biomass was then dried in an oven at 105°C and then allowed to cool to room temperature.

3.1.6 Chemical activation

As was stated in sections 1.3.5 and 2.3.6, biomass and hydrochar both could be used as a coal alternative in producing activated carbon. Activation of both untreated biomass and hydrochar was performed to investigate the impact of HTC on the outcomes of activation.

The biomass and biocoal samples were activated in a horizontal tube furnace (HTF). The samples were physically mixed with potassium hydroxide before

being placed into a ceramic boat, which was then inserted into the HTF using a metal hook. The tube was purged for 15 minutes with nitrogen (flow rate 1000 cm^3/min), introduced via a tube inserted into the stopper at one end of the glass tube. The gas was removed through a tube attached to the stopper at the other end of the glass tube, and was bubbled through water to remove any particulates from the purged gas. The flow was determined using a flow meter attached to the input tube. After the furnace is purged of oxygen, the temperature was raised to 700°C at a heating rate of 5°C/min. The temperature was maintained isothermally for one hour before turning off the furnace and allowing the sample to cool to room temperature, maintaining the flow of nitrogen. The ceramic boat was then removed from the furnace using a metal hook, and the samples were then washed thoroughly with distilled water until pH of water was neutral. The pH was measured using litmus paper. The washed char was then dried at 105°C for at least 8 hours. The samples were then allowed to cool to room temperature before weighing.

3.1.7 Grinding and sieving

In order to ensure that the intrinsic char reactivity was being studied in TGA char reactivity experiments, the samples were ground to 0-75 μ m particle size. To investigate the role of particle size on the measure char reactivity of the sample, 75-150 μ m particle size fractions were also produced.

The samples were ground by a Retsch PM 100 ball mill, seen in Figure 3.4. A filling factor of approximately 2/3 was maintained to ensure optimal operation of the mill. After each interval of grinding, additional sample was added to adjust the filling factor back to 2/3. The samples were ground at a frequency of 450 rpm in multiple two-minute segments. These segments were repeated until sufficient sample was produced, and the vast majority of the sample was in the desired particle size range to minimise fractioning of the sample. The balls were then removed from the mill, before transferring the sample to the sieves.

When the quantity of sample was insufficient for use of the ball mill, a pestle and mortar was used. The sample was crushed in the ball mill in small batches to avoid any spillages through over-filling of the mortar. After grinding, the sample was transferred onto the sieves.

To ensure the safe operation of the ball mill, the clamp that keeps the mill in place in the apparatus is fitted with a lock. When tightening the clamp, this is held open using the head of a lever, which also ensures that the clamp is tightened to a sufficient degree. When the lever is removed after sufficient tightening, the lock is tripped. The lock needs to be levered open using the tightening lever to remove the clamp and free the vessel. Additionally, the mill does not operate if the lid of the apparatus is not securely closed. A switch tripped by closing the lid of the apparatus ensures this.

Figure 3.4 Ground bagasse in ball mill (top) and fully assembled ball mill (bottom)

The feedstock was sieved using Retsch sieves and a Retsch AS 200 sieve shaker, shown in Figure 3.5. The sieves were stacked from largest mesh size to lowest mesh size, with a collection tray at the bottom of the stack. The sample to be sieved was placed on the topmost sieve, and the stack was secured onto the shaker by placing the sieves on the shaker and lowering and locking the lid using the levers. The sieve shaker was then operated using an amplitude of 1.5 mm over an interval of 5 minutes. The samples were then removed from the sieves onto paper sheets, first by tipping the sieve onto the paper and then by thoroughly brushing the sieves. The samples were then transferred from the sheets into glass vials for storage in a freezer. The sieves were then cleaned using brushes and compressed air. Use of water was avoided when cleaning the sieves as to avoid swelling of the biomass leaving sample stuck in the mesh or breaking of the sieve mesh.

Figure 3.5 Assembled sieves and sieve shaker

To ensure that minimal fractioning of the samples was occurring, the proximate analysis of the two fractions received were determined and compared. An illustrative example of this can be seen in Table 3.1. It can be seen that the composition of the two fractions are very similar. In addition to this, all of the analysis of the samples that would be relevant to char reactivity apart from

proximate analysis were performed on the 0-75 μm fraction rather than on the whole unground biocoal, so any assertions made on the char reactivity of the samples is relevant to this fraction.

Table 3.1 Proximate analysis of the 0-75 µm and 75-150 µm fraction of wood biocoals

Temperature (˚C)	Residence time (min)	W/B ratio	Biocoal particle size (μ m)	Proximate analysis			
				Moisture	Volatile matter	Fixed Carbon	Ash
200	60	4	0-75	0.3	81.8	18.0	1.0
200	60	4	75-150	0.2	81.1	18.0	0.7
225	60	4	0-75	0.3	74.6	23.9	1.1
225	60	4	75-150	2.6	71.7	25.1	0.7

3.1.8 Drop tube furnace devolatilisation

Temperature, residence time, heating rate, and particle phase all have an impact on char morphology, and can have a significant influence on the carbon burnout of coal (Le Manquais, Snape, McRobbie, & Barker, 2011). Pulverised fuel (PF) boilers operate with short residence times, high temperatures, high heating rates, and dilute particle phases, which are quite different to the conditions used in thermogravimetric analysis (Le Manquais et al., 2011). Therefore, in studying the combustion properties of fuels, it is important to study the combustion of chars produced in a DTF simulating PF conditions. This is especially true when studying coal, as it is very difficult to observe the intrinsic char reactivity of coal using solely TGA (Le Manquais, Snape, McRobbie, Barker, & Pellegrin, 2009). The high surface areas of coal chars produced in a DTF reduces the influence of diffusion control on char combustion, so the observed char reactivity is closer to the intrinsic char reactivity than what would be found in chars produced using a TGA of HTF (Le Manquais et al., 2009). As the biomass fuels studied in this thesis are compared to coal, it is important to study the combustion properties of drop tube chars produced from these fuels.

A diagram of a DTF can be seen in Figure 3.6, and images of the DTF used can be seen in Figure 3.7. The internal diameter of the feed probe and work tube were 3 mm and 50 mm, respectively. Before the experiment was run, the height

of the probe was adjusted so that the residence time for the particles in the DTF would be 600ms. Then, before heating the DTF to the desired temperature, the cooling water for the feeding probe and collector probe were turned on. The DTF was then programmed to heat up to the desired operating temperature of 1300°C in specific intervals which required different heating rates to avoid damage. First the DTF was heated from room temperature to 300°C at a heating rate of 1°C/min; then secondly from 300°C to 600°C at a rate of 3°C/min; and then finally from 600°C to 1300°C at a rate of 5°C/min. The DTF was then isothermal until the run was complete. Nitrogen with 1% oxygen (to discourage tar formation by burning off evolved volatile matter (Le Manquais et al., 2009)) was then allowed to flow through the DTF at a total flow rate of 12100 cm^3/min. Pulverised sample (a small particle size of 0-75 µm was used to avoid blockage) was slowly fed through a glass funnel into the feeder tube of the furnace, being pre-heated in the feeder tube before being subjected to the main heating section. The devolatilised sample was then collected from the collector probe, weighed, and stored in a sealed glass vial in a freezer.

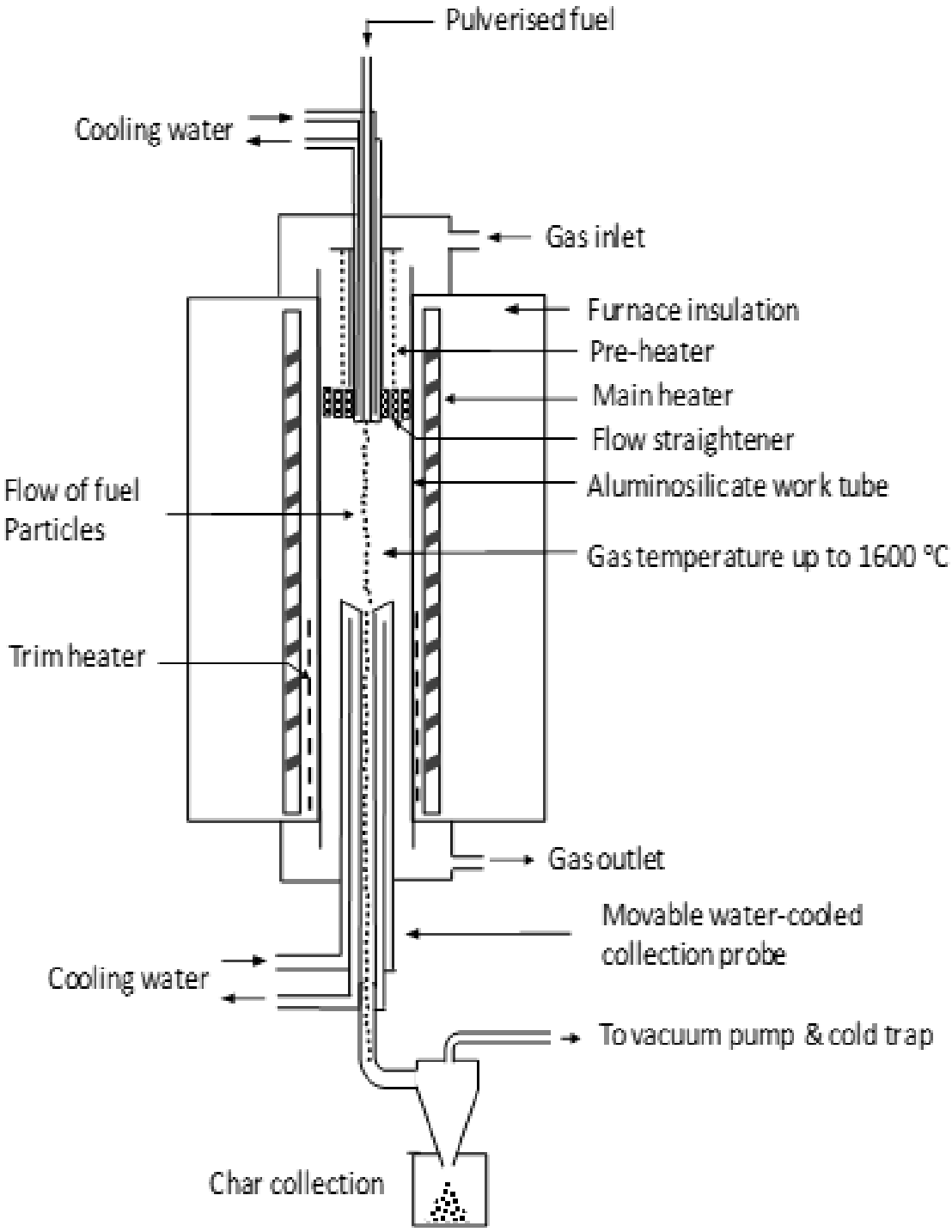

Figure 3.6 Diagram of devolatilisation of fuel particles in a drop tube furnace

Figure 3.7 Drop tube furnace used for high heating rate devolatilisation

3.2 Analysis

3.2.1 Thermogravimetric analysis

Thermogravimetric analysis (TGA) was used to give the proximate analysis of the samples generated. The proximate analysis is useful for comparing fuels, and can give an indication of the degree to which HTC is making biomass more coal-like. In addition to this, there is a wide array of proximate analysis data available in literature, which means that comparisons can be made to a wide variety of biomass feedstocks and HTC conditions, and the HTC results can be verified. TGA was used as it provides quick results, and can process multiple samples in sequence. TGA was also used to perform char reactivity analysis of samples. Again, this was used due to the speed and ease of analysis, allowing for multiple repeats to be performed in quick succession.

The thermogravimetric analysis was performed using a TA Q500 thermogravimetric analyser, shown in Figure 3.8. Before the analysis procedure was started, the platinum pans were tared in the TGA. After this the sample was loaded onto the pan so that it fully covered the bottom. 10-40 mg of the sample was typically used. The pans were then placed in the auto-sampler tray and the sequence was run. After completion, the pans were cleaned using a wire brush, deionised water, and acetone. An ultrasonic bath filled with soap and water was used to clean the pans on the event of initial washing being

insufficient. The results were processed using TA Universal Analysis 2000 software.

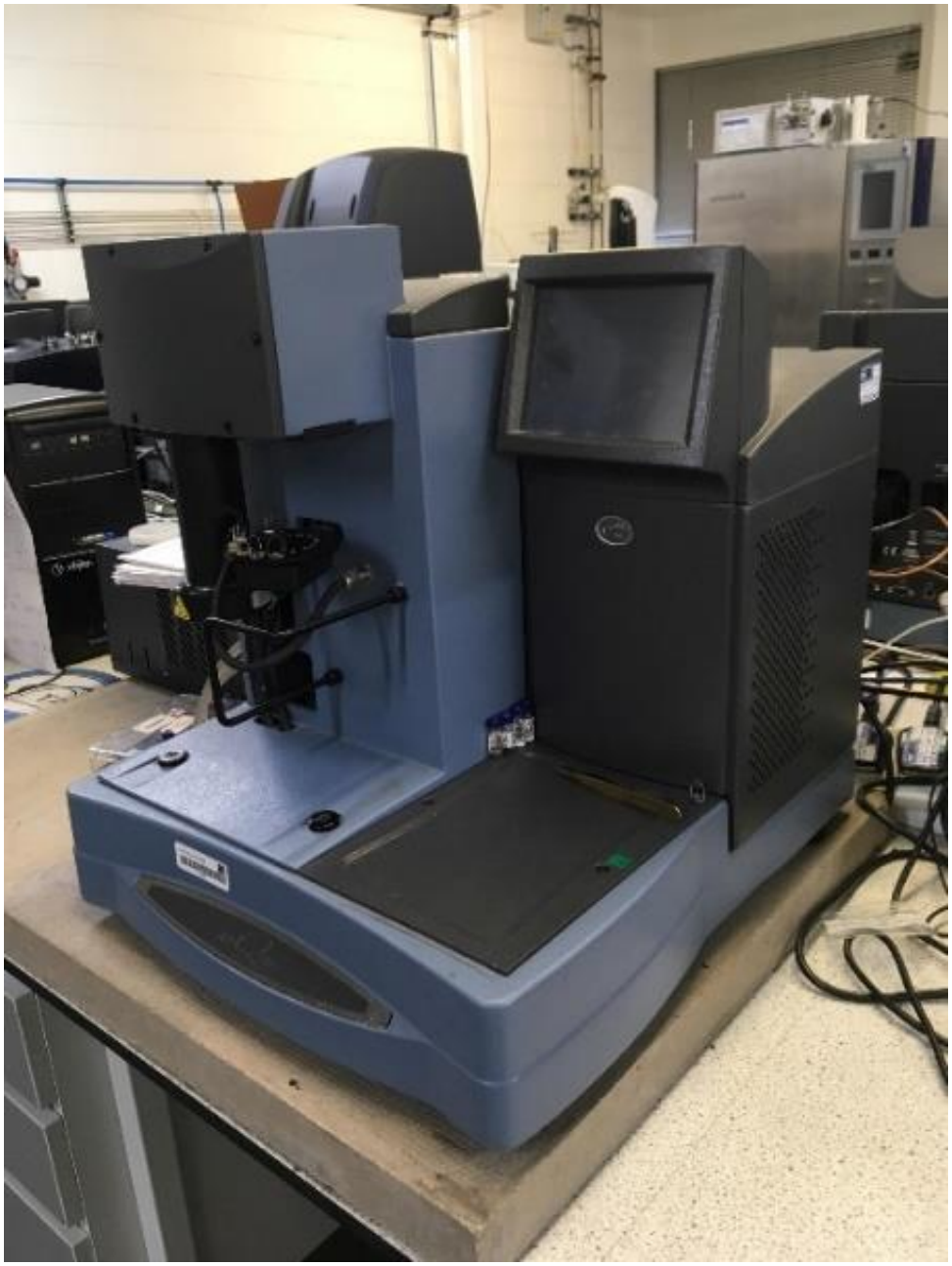

Figure 3.8 TA Q500 TGA analyser

3.2.1.1 Proximate analysis

Proximate analysis is a basic fuel analysis where the moisture, volatile matter, fixed carbon, and ash content of a fuel are ascertained. The TGA procedure used to obtain the proximate analysis was as follows:

- Establish a nitrogen atmosphere
- Increase temperature to 105˚C at 50˚C/minute
- Isothermal for 10 minutes to remove the moisture content
- Increase temperature to 700˚C at 50˚C/minute
- Isothermal for 10 minutes to remove volatile matter
- Introduce air
- Isothermal for 10 minutes to burn the fixed carbon and leave the ash behind
- Cool to room temperature

An example proximate analysis, where the different fractions of the fuel are labelled, can be seen in Figure 3.9. A devolatilisation temperature of 700˚C was used, as this was the temperature used for devolatilisation prior to char reactivity analysis, and the proximate analysis was to match this procedure.

There is a small collection of samples where the proximate analysis used a devolatilisation temperature of 850˚C, rather than 700˚C. These were the

sewage sludge and sewage sludge biocoals, and were performed by an understudy student group. The slightly raised devolatilisation temperature does not significantly effect the volatile matter content determination of the biocoal, and the samples are only referenced briefly in this thesis. The values are labelled as using the higher devolatilisation temperature where they are included in Appendix 2.

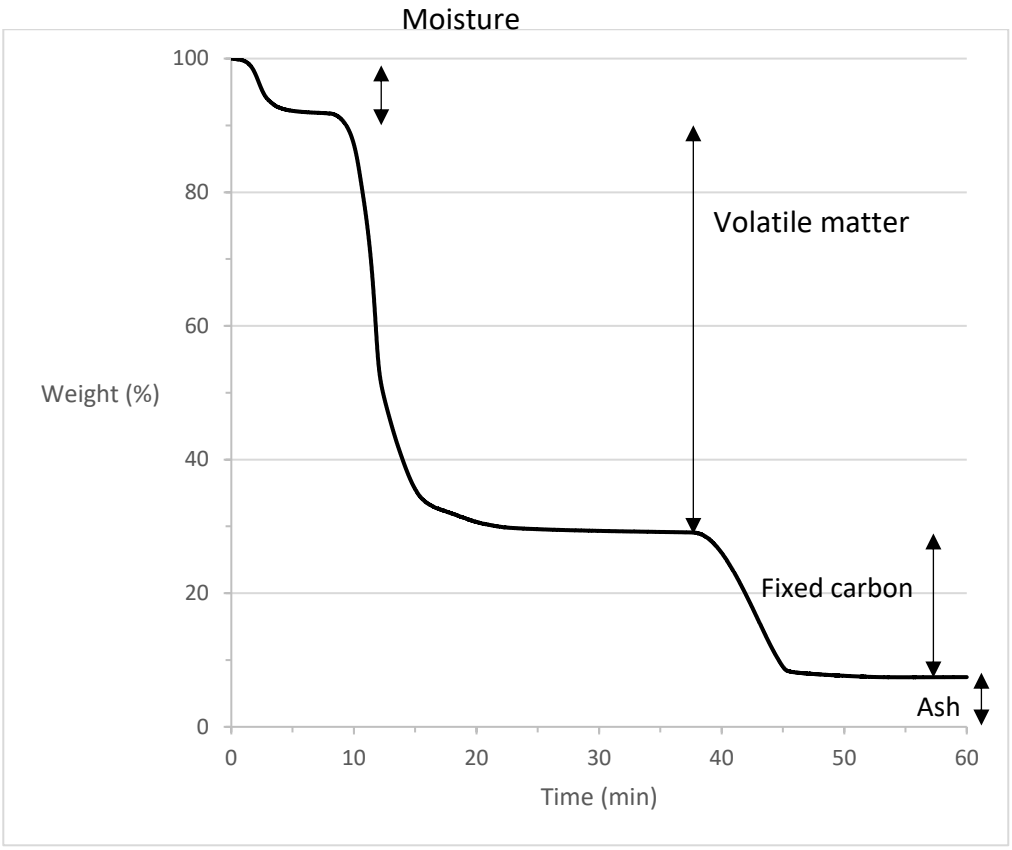

Figure 3.9 Example proximate analysis decomposition curve

Some of the samples had proximate analysis performed using TGA data supplemented by gravimetric determination of moisture and ash. This was done because TGA alone is not particularly accurate in determining fractions which small percentage of the total analysis, such as the small moisture and ash

content found in some biocoals. The TGA proximate analysis was performed following the International Organisation for Standardisation method for coal (ISO 17246:2010), where the moisture content is determined at 105°C; the volatile matter content at 900°C; the ash content after burning at 500°C and then 815°C; and the fixed carbon content from the subtraction of the other three fractions from 100% (Sermyagina, Saari, Kaikko, & Vakkilainen, 2015). The heating rate used was 50°C/min. The only alteration to this was that the ash content determination was performed solely at 550°C as to avoid the loss of alkali and alkaline earth metals (Oliveira et al., 2013), which would inhibit further analysis of the ash. The moisture and ash content of the samples were determined gravimetrically on an as-received basis by heating the samples in ceramic crucibles, using a muffle furnace. The volatile matter was determined through TGA for ease of analysis, as the volatile matter content was large enough that the TGA values would be well within the error of detection of TGA. When determining moisture and ash content gravimetrically, the ISO standard methods were followed. Firstly, the crucibles were conditioned prior to use by heating at the determination temperature for at least 60min. The crucibles were then cooled, weighed, and then the sample was then placed evenly in the bottom of the crucible. The crucible was weighed again before the crucible was placed in the furnace at room temperature. Once the sample had been loaded in the furnace, a flow of compressed air was introduced via a gas line attached to the furnace through the door. In moisture determination, the temperature was raised to 105˚C and temperature was held stable for at least 120 min (Zhu,

2014). In ash determination the furnace was heated to 250˚C and then held at temperature for 60 minutes. Afterwards, the temperature was raised to 550˚C and the temperature was held for at least 120 min. If there was any doubt that the incineration reached completion, the crucible was reloaded and heated in the furnace at 550 ˚C for 30 min intervals until the change in mass was lower than 0.5 mg (BSI, 2015). After the desired residence time had been completed, the muffle furnace and compressed air flow was turned off, and allowed to cool to room temperature. Once fully cooled, the crucible containing the samples was weighed, and the sample was decanted into glass vials, which were sealed then stored in a freezer.

3.2.1.2 Char reactivity analysis

Two size fractions were investigated for the char reactivity study, the 0-75 µm and 75-150 µm fractions. Small particle sizes were studied to limit the risk of observing Regime II (chemical and diffusion control) or Regime III (diffusion-dominated) control, rather than Regime I control (pure kinetic control) (Jenkinson, 2015; Manquais, Snape, Mcrobbie, Barker, & Pellegrini, 2009). The full analysis was performed on the 0-75 µm fraction, while the 75-150 µm fraction was studied to assess the role of particle size on the observed char reactivity of the samples. Before determining the char reactivity, the sample was devolatilised in the TGA by heating at 700˚C under nitrogen for 10 minutes. After this, the temperature was reduced to the desired combustion temperature before air was introduced to induce combustion. The heating rate

used was 50°C/min. The devolatilisation temperature was chosen to combine speed of analysis with avoiding annealing of char and minimising the volatilisation of alkali and alkaline earth metals (as these elements were the key factors investigated in the study). The temperature profile of the char reactivity experiments, and a typical decomposition curve of a sample of wood biocoal (generated at 225°C over a residence time of 60 minutes with a water to biomass ratio of 4:1) at 475°C can be seen in Figure 3.10.

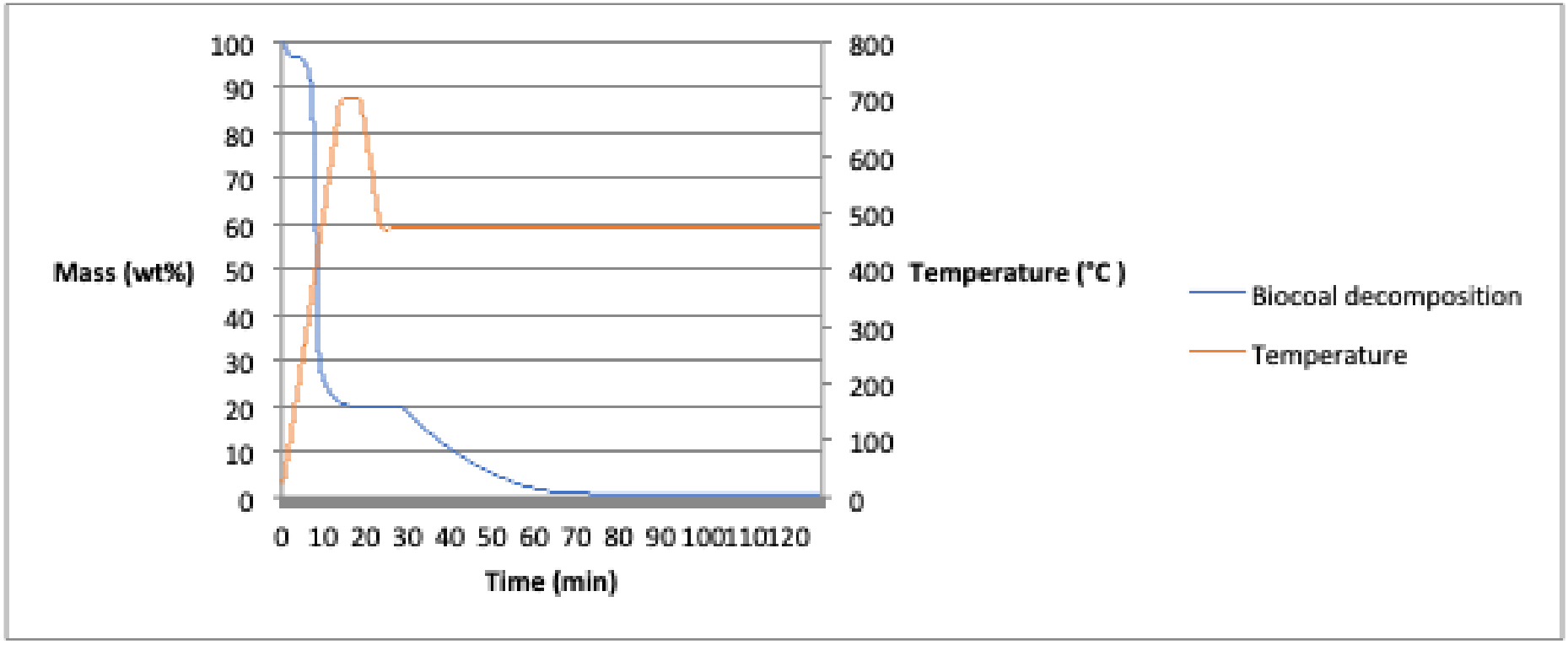

Figure 3.10 Temperature profile and decomposition curve generated in char reactivity determination of a biocoal using an isothermal combustion temperature of 475°C (Air is introduced once temperature has equilibrated at 475°C)

There char reactivity was determined as the time required for combustion to consume 90% of the char (t_{90}). The values were determined from 5% to 95% char burnout as to avoid the slight temperature increase due to ignition impacting the evaluation. The t_{90} values determined at 475˚C were used to compare the fuels as it was considered to be low enough to ensure Regime I control in the higher reactivity samples, while being high enough to ensure that the lower reactivity samples can combust completely over a reasonable timeframe for efficient analysis.

The activation energy (E_a) and the pre-exponential factor (A) of char combustion were determined using the isothermal combustion of the fuels at multiple combustion temperatures. The temperature ranges used to determine E_a and A were tailored to the sample studied to account for differing reactivity. The temperature ranges used in the analysis can be seen in Table 3.2. These precautions were taken to ensure that combustion was being investigated under Regime I control, rather then Regime II or Regime III control (Jenkinson, 2015; Manquais et al., 2009). Only two temperatures were used for E_a and A determination in olive cake as the sample did not ignite at lower temperatures, and temperatures above those used would likely have shown Regime II or Regime III control.

Table 3.2 Temperature ranges used for the determination of activation energy and pre-exponential factor of various fuels

Fuel	Temperatures used (°C)
Wood	375, 400, 425, 450, 475
Torrefied wood	425, 450, 475, 500
Wood biocoal (200°C)	425, 450, 475, 500, 525
Wood biocoal (225°C)	425, 450, 475, 500, 525
Olive cake	475, 525
Acid leached olive cake	400, 425, 450, 475, 500,
Olive cake biocoal (200°C)	375, 400, 425, 450, 475
Olive cake biocoal (225°C)	425, 450, 475, 500, 525
Bituminous coal	475, 500, 525, 550, 575

The first order rate constant, k_a, was determined for combustion at each of these temperatures, before being inputted into the Arrhenius rate equation to determine E_a and A. K_a was determined graphically by determining the gradient of the straight line plot of –ln(1-α) vs. time (between 5 and 95% char burnout), satisfying Equation 3.1. The value α is the proportion of mass converted at any point displayed as a fraction.

Equation 3.1 Equation used to derive rate constant

$$-\ln(1-\alpha) = k_a t$$

Legend: α – fractional mass conversion
k_a – first order rate constant
t - time

Once the k_a values were determined for char burnout at the different temperatures, a plot of $\ln K_a$ vs. 1000/T was produced, which then using the Arrhenius equation described in Equation 3.1 gives E_a and A as the gradient and intercept of the plot, respectively. 1000/T was used as the reciprocal temperature to adjust the range to one that is easier to manipulate. This does not have an affect on the gradient and intercept of the plot, so does not affect the value of E_a and A. The Arrhenius rate equation is as follows:

Equation 3.2 Arrhenius rate equation

$$lnk_a = lnA - \frac{E_a}{RT}$$

Legend: k_a – first order rate constant
A – pre-exponential factor
E_a – activation energy
R – gas constant (8.314 $JK^{-1}mol^{-1}$)
T - temperature

A worked example of the calculation of E_a and A can be seen in section 3.3.8.

3.2.2 Elemental analysis

Elemental analysis is a useful tool for comparing the composition of biomass, pre-treated biomass, and coal in the assessment of HTC. Additionally, there is a wide variety of elemental analysis data in literature, spanning numerous feedstocks and HTC conditions. This makes performing elemental analysis useful in verifying the HTC experiments through comparison with the literature.

Elemental analysis was conducted using a LECO CHN 628 elemental analyser, which is shown in Figure 3.11. Solid samples were required to be in the mass range of 0.075-0.01g for analysis. The analyser was calibrated by performing the analysis numerous times without a sample loaded, until the values generated by the analyser approached zero. Subsequently, 5 samples of 2,5-(Bis(5-tert-butyl-2-benzo-oxazol-2-yl) thiophene (BBOT) were weighed into aluminium foil cups. These cups were then folded so that the sample was sealed within the cup before insertion into the auto-sampler for the analyser. These calibration samples were then each designated as 'drift standard', and the analysis was performed. Once the standards had been analysed, the operation 'drift calibrate' was performed to calibrate the analyser. The samples to be analysed were processed in the same manner as the BBOT, but were designated as 'unknown' rather than 'drift standard'. Liquid samples were processed in aluminium capsules rather than cups.

Figure 3.11 LECO CHN analyser

3.2.3 Ion chromatography

Ion chromatography was used to determine the concentration of specific inorganic elements (alkali and alkaline earth metals) in HTC process liquor. This analytical technique was used as the process liquor would need little processing

prior to analysis (solely filtration and in some cases dilution with ultrapure water). This allows analysis to be completed efficiently.

The samples were filtered under vacuum into a conical flask using a Buchner funnel and electrical pump prior to analysis to ensure no particulates were present, as these would block the column if present. Analysis was performed immediately after filtration, as carbonaceous material was seen to precipitate out of the process liquor over time in storage.

The analysis was performed using a Thermo-Fisher Scientific ICS5000+ system, shown in Figure 3.12. For cation analysis, a Dionne IonPac^{TM} CS17 column was used with Dionex EGC 500 methanesulfonic acid eluent. Before calibration, a sample of ultrapure water (used for diluting of standards and samples) was passed through the system to confirm the purity of the water. The system was calibrated before the runs by injecting 5 standard solutions containing the ions to be analysed (sodium, potassium, magnesium and calcium). The standard solutions were prepared by measuring the required volume of the standard solutions for the target ions into separate 50 ml volumetric flasks using a volumetric pipette and syringe. Ultrapure water was then added to the volumetric flask until the meniscus of the solution was level with the mark on the neck of the flask. The flask was then capped before inversion numerous times to ensure proper mixing of the solutions. The concentrations used in the calibration of the system were 10, 20, 30, 40, and 50 ppm. When inputting the sample details into the software, the concentration of the sample was noted

and the sample was designated as ‘standard’. The calibration was then run. The samples were then analysed one by one, labelled ‘unknown’ in the software. If the samples were seen to be far outside the calibration range, the samples were diluted using the same method outlined for the preparation of the calibration standards. Once completed, a report was constructed on the Chromeleon ion chromatography software so the results can be analysed.

Figure 3.12 Thermo-Fisher Scientific ICS5000+ system

3.2.4 Gas composition determination using gas chromatography

Determining the composition of the gas produced by HTC is important for completing the mass and carbon balances, as well as providing information that can be used to consider the chemical reactions occurring during the

experiment. Gas chromatography was used to determine this, and the sample was processed immediately upon collection from the reactor.

Gas chromatography was conducted using a Perkin Elmer Clarus 580 GC system, fitted with flame ionisation and thermal conductivity detectors. The apparatus is shown in Figure 3.15. Two standard gases were analysed. The hydrocarbon standard gas was methane, and a non-hydrocarbon standard was a gaseous mixture consisting of 10% hydrogen, 10% carbon dioxide, and 40% carbon monoxide by volume. These standards were stored in gas cylinders, and were extracted using a 100 µl glass gas syringe (with needle attached) trough a diaphragm. The gases were then injected into the analyser through a diaphragm in the injection line.

The samples to be analysed were collected from the reactor once cooled using a glass syringe and an adapter attached to the pressure gauge, as described in section 3.1.2. The samples were then transferred from the gas bag to the analyser using the 100 µl glass gas syringe through the diaphragm on the gas bag. The 100 µl of sample gas was injected with a split ratio of 10:1, at a temperature of 250°C. Separation was performed on an alumina plot fused silica column, using helium as the carrier gas. The oven temperature was ramped from 60°C (13 min hold time) to 180°C (10 min hold time) at a rate of 10°C/min.

The concentration of CO_2, CO and H_2 was determined through direct comparison of the signal values for the unknown sample and the non-hydrocarbon standard gas (injected separately). Individual hydrocarbon gas yields were determined with reference to methane as the external standard gas (injected separately). To calculate the yield of C_2-C_5 hydrocarbon gases using the methane standard, relative response factors were used as multipliers for the calculated gas yield. These were predetermined from a standard mixture of C_1-C_5 gases (Uguna, Carr, Snape, & Meredith, 2015), and can be seen in Table 3.3.

Figure 3.13 Perkin Elmer Clarus 580 GC system

Table 3.3 Response factors used to calculate different hydrocarbon concentrations with reference to a methane standard

Compound	Response factor
CH_4	1.00
C_2H_4	1.88
C_2H_6	1.94
C_3H_6	2.44
C_2H_8	2.75
C_4 alkanes	3.16
C_4 alkenes	3.31
C_5 alkanes	3.25
C_5 alkenes	3.32

3.2.5 Bomb calorimetry

Bomb calorimetry was used to determine the gross calorific value of some samples. The heating value is a key fuel property for comparison between untreated biomass, pre-treated biomass, and coal.

The analysis was conducted using an IKA C5000 bomb calorimeter. The sample pelletized for analysis using a Graney Specac manual hydraulic press. The sample was placed between the two metal disks in the die, and the pressing rod was inserted on top. After this, the die was secured to the press using a

clamp, and 2 tonnes of pressure was achieved through pulling the lever multiple times. After this, the clamp was released. The pellet was then collected by pushing the disks out of the mould. The pelletized sample was the placed in the crucible, resting on top of a cotton thread that is tied to the ignition wire on the crucible holder. The crucible is suspended on the crucible holder, and the crucible holder was carefully placed inside the decomposition vessel. The cover was then secured using the cap screw, and the decomposition vessel was inserted into the calorimeter. The decomposition vessel was then filled with oxygen (99.95%) to a pressure of 30 bar, and the analysis was run. Before analysing the unknown samples, the calorimeter is calibrated by combusting benzoic acid as a reference material. The gross calorific value is then calculated using the temperature change in the water surrounding the decomposition chamber during combustion of the sample.

3.2.6 Textural characterisation

Surface area was identified as an important variable to study when determining the contributing factors for the char reactivity of a fuel. Additionally, surface area is an important factor in activated carbon performance.

Textural characterisation was performed using a Micromeritics 2420 accelerated surface area and porosity (ASAP) system. This was used to record the nitrogen adsorption and desorption isotherms of the samples at -196°C. The analyser can be seen in Figure 3.14. Approximately 300 mg of the samples were

weighed into the specialised flasks supplied for the analyser. These flasks were then fastened into the analyser, the heating elements were attached and the samples were degassed under dynamic vacuum conditions for hours at 300˚C. The heating elements were then removed and the flasks were allowed to cool to room temperature before weighing to determine the mass of degassed sample. The cooling sleeves of the analyser were then filled with liquid nitrogen and were raised so that the flasks were submerged. The adsorption and desorption isotherms were then determined. The cooling sleeves were then lowered, and the flasks were removed once equilibrated to room temperature. The samples were then transferred to glass vials, which were sealed before storing in a freezer.

The Brunauer-Emmett-Teller (BET) model was used to determine specific surface areas of the samples. Density functional theory (DFT) was employed to determine Total pore volume (VT), Micropore volume (V_{mic}) and the pore size distribution.

Figure 3.14 Micromeritics 2420 accelerated surface area and porosity (ASAP) system

3.2.7 X-ray fluorescence spectroscopy

X-ray fluorescence (XRF) analysis was performed on the low-temperature ash generated from the fuels to determine the concentration of alkali and alkaline earth metals. XRF was chosen as it is a fast analysis which can process a number

of samples quickly and the ash samples did not need to be processed before determination of the inorganic content.

The XRF analysis was performed using two separate instruments due to unforeseen circumstances resulting in access issues. The majority of XRF analysis was performed using a Bruker S8 TIGER spectrometer running the semi-quantitative program 'Quantexpress', for a run time of 7 minutes. The ash was analysed as a loose powder behind Mylar film in a PTFE sample cup, and a 8mm mask was used.

To ensure that the results being given by the Bruker S8 TIGER spectrometer were reliable, olive cake ash was analysed 5 times and the variation was recorded. The results of the runs and the variation in detection can be seen in Table 3.3. It can be seen that the results are reliable for the elements studied. It was not possible to assess the variability in sodium detection, as the olive cake ash contained very little sodium. The concentration of sodium was too low to be detected in all but one of the runs. The assumption was made that the sodium detection was reliable for other samples due to the accuracy of detection for the other elements.

Table 3.4 Variation in XRF analysis using Bruker S8 TIGER spectrometer

Element detected	Run					Average	Error (95%)
	1	2	3	4	5		
Na	0.47	0.00	0.00	0.00	0.00	N/A	N/A
Mg	2.94	2.95	2.90	2.95	2.90	2.93	0.05
Si	3.75	3.88	4.18	3.63	3.88	3.86	0.41
K	35.19	35.11	34.85	34.6	35.50	35.05	0.68
Ca	11.76	11.09	11.76	11.12	11.90	11.53	0.78
Fe	1.07	1.16	1.09	1.06	1.11	1.10	0.08

Additional XRF analysis was performed using a Panalytical Epsilon 3 XL XRF spectrometer. The run time was 18 minutes, and the samples were analysed as a loose powder behind Mylar film in a PTFE sample cup.

As the majority of the samples were analysed using the Bruker spectrometer and the XRF studies performed were comparative, the values given by the Panalytical spectrometer were adjusted to match the values found using the Bruker spectrometer. The olive cake ash used in the repeatability study was also used in this case, and the adjustment factors determined can be seen in Table 3.5.

Table 3.5 Comparison between Bruker S8 TIGER and Panalytical Epsilon 3 XL XRF spectrometers including adjustment factor for XRF studies

XRF spectromoter	Observed concentration and adjustment (%)					
	Na	**Mg**	**Si**	**K**	**Ca**	**Fe**
Bruker	0.00	3.10	3.57	26.04	10.03	0.89
Panalytical	0.47	2.94	3.75	35.19	11.76	1.07
Adjustment	*N/A*	*-5.56*	*4.78*	*26.00*	*14.67*	*17.25*

3.2.8 NMR

Nuclear magnetic resonance (NMR) spectroscopy was used to track the reaction pathways of HTC by tracking the decomposition of the components of biomass, and identifying the degradation products that were in the process liquor. Knowledge of these allows for discussion on the chemical reactions occurring during the experiments.

Solid-state carbon-13 NMR was performed using a Bruker MSL 300 spectrometer, shown in Figure 3.15. A 200 MHz two-channel (proton/heteroatom) probe was used. The Solid sample was packed into a 7 mm zirconia rotor with Kel-F cap a using a metal press. Tetrakis(trimethylsilyl)silane (TKS) was used as a reference material and was pressed on top of the sample in the rotor before capping. The rotor was then inserted into the probe and spun at a rate of 5000 Hz using compressed air. The signal from the spectrometer was then tuned and matched before running the data acquisition to ensure the spectrometer is calibrated. The tuning and

matching were performed using the dials on the probe, and they were tuned until the signal was central and the peak reached the bottom of the screen. The acquisition was then run for 2500 scans running a cross polarisation pulse program. Cross polarisation was used to speed up the analysis. The contact time used was 0.03 s and the dwell time was 16.8 µs. After acquisition the spectra were obtained and the peaks assigned and integrated using Bruker Topspin 3.5 software.

Liquid state proton NMR was preformed using a Bruker 400 MHz NMR spectrometer with a multinuclear auto tune broad-band observe probe. The HTC process liquor samples were dried in an oven at 70°C to before dissolving in D_2O in a concentration of at least 1.5% by mass for analysis. The drying temperature of 70°C was used to minimise loss of volatile matter from the sample. The samples were then transferred into NMR tubes that were then analysed in the spectrometer. The spin rate used was 8224Hz, and the number of scans was 16. The overall acquisition time was 4 seconds.

Figure 3.15 Bruker MSL 300 NMR spectrometer

3.3 Calculations

3.3.1 Mass yield on a dry, ash free basis

The mas yield on a dry, ash free (DAF) basis was calculated so that the fate of the organic content of biomass could be studied. This is important because the organic content of biomass provides the energy of the fuel, to the DAF yield can act as a proxy for the energy yield of the process. This was calculated firstly by determining the mass of the DAF fraction of both the biomass feedstock and biocoal. This was calculated by multiplying the mass of the samples on an as-received basis by their respective DAF fraction. The DAF fraction of the sample is determined using proximate analysis, where moisture and ash content of the sample (on a per cent basis) is taken away from 100%. This value is then divided by 100 to give the decimal fraction representing the DAF content of the sample, and then multiplied by the as-received mass of the sample to give the DAF mass. The DAF yield is then given by the ratio of the DAF mass of the biocoal and the DAF mass of the feedstock. An example of the calculation of the DAF yield for HTC of miscanthus at 200°C, with a W/B ratio and residence time of 4:1 and 60 minutes respectively, using the data shown in Table 3.6, is shown below.

Table 3.6 Data used in calculation of DAF mass yield

Description	Value
Mass biomass (as received)	8.00 g
Mass biocoal (as received)	5.32 g
Mass yield (as received)	66.5 %
Untreated biomass moisture content	6.4 %
Untreated biomass ash content	2.7 %
Biocoal moisture content	3.1%
Untreated biomass ash content	2.2 %

Calculation of DAF fraction for biomass:

$$DAF\ fraction_{(Biomass)} = \frac{100 - (6.4 + 4.7)}{100}$$

$$DAF\ fraction_{(Biomass)} = 0.889$$

Calculation of DAF fraction for biocoal:

$$DAF\ fraction_{(Biocoal)} = \frac{100 - (3.1 + 2.2)}{100}$$

$$DAF\ fraction_{(Biocoal)} = 0.947$$

Calculation of DAF mass of biomass:

$$Mass_{Biomass,DAF} = 8.00\ \times\ 0.889$$

$$Mass_{Biomass,DAF} = 7.11\ g$$

Calculation of DAF mass of biocoal:

$$Mass_{Biocoal,DAF} = 5.32\ \times\ 0.947$$

$$Mass_{Biocoal,DAF} = 5.04\ g$$

Calculation of DAF yield:

$$Yield_{DAF} = \frac{5.04}{7.11} \times 100$$

$$\underline{Yield_{DAF} = 70.9\ \%}$$

3.3.2 Carbon yield

The carbon basis was calculated using the mass of the feedstock biomass and biocoal product in addition to the elemental analysis, so that the fate of carbon during HTC could be easily assessed. This is important because carbon is the main source of energy in biomass, shown by the lower carbon density of biomass resulting in biomass having a lower energy density than coal (Demirbaş, 2001; Aidan Mark Smith et al., 2018). The carbon yield was calculated by first multiplying the mass of both the biomass feedstock and biocoal product by their carbon content, determined by elemental analysis. This gives the mass of carbon in the feedstock biomass and biocoal. The ratio of the mass of carbon in the biocoal and the mass of carbon in the biomass is the carbon yield. An example of the calculation of the carbon yield for HTC of Brites wood pellets at 200°C, with a W/B ratio and residence time of 4:1 and 60 minutes respectively, using the data shown in Table 3.7, is shown below.

Table 3.7 Data used in calculation of carbon yield

Description	Value
Mass biomass (as received)	8.00 g
Mass biocoal (as received)	5.32 g
Mass yield (as received)	66.5 %
Untreated biomass carbon content	48.0 %
Biocoal carbon content	50.4 %

Calculation of mass of carbon in biomass:

$$Mass_{Biomass,C} = \frac{8.00 \times 48.0}{100}$$

$$Mass_{Biomass,C} = 3.84\ g$$

Calculation of mass of carbon in biocoal:

$$Mass_{Biocoal,C} = \frac{5.32 \times 50.4}{100}$$

$$Mass_{Biocoal,C} = 2.68\ g$$

Calculation of carbon yield:

$$Yield_C = \frac{2.68}{3.84} \times 100$$

$$\underline{Yield_C = 69.8\%}$$

3.3.3 Energy yield

The energy yield of HTC was calculated as the ratio between the total energy content of the biocoal produced and the biomass feedstock. This was calculated by first multiplying the HHV of the biocoal by the yield of HTC, and then dividing by the HHV of the feedstock biomass. An example of this is given below, using data from the HTC of miscanthus at 200°C with a W/B ratio and residence time of 4:1 and 60 minutes, respectively. The data used in the calculation is displayed in Table 3.8.

Table 3.8 Data used in calculation of energy yield

Description	Value
Mass yield (as received)	66.5 %
Calculated HHV of biomass (MJ/kg)	19.3
Calculated HHV of biocoal (MJ/kg)	20.4

$$Energy_{Biocoal} = \frac{20.4 \times 66.5}{100}$$

$$Energy_{Biocoal} = 13.6\ MJ$$

$$Yield_E = \frac{13.6}{19.3} \times 100$$

$$Yield_E = 70.4\%$$

3.3.4 Normalised proximate analysis of biocoals

For the design of experiments (DoE) study of miscanthus HTC, the proximate analysis of the biocoals produced was normalised with respect to the mass yield and proximate analysis of the feedstock biomass (miscanthus). This was so that the composition of the biocoals could be directly compared to the composition of the feedstock on an absolute basis using one value (a percentage comparison to the original moisture, volatile matter, fixed carbon, or ash content). The calculation for the relative fixed carbon content of miscanthus biocoal produced at 200°C, with a W/B ratio and residence time of 4:1 and 60 minutes respectively is used here as an illustrative example. The calculation uses data shown in Table 3.9, and is shown below.

Table 3.9 Data used in calculation of normalised fixed carbon content of biocoal

Description	Value
Mass biomass (as received)	8.00 g
Mass biocoal (as received)	5.32 g
Mass yield (as received)	66.5%
Fixed carbon of biomass (%)	21.7%
Fixed carbon of biocoal (%)	20.0%

Calculation of mass of fixed carbon in biomass:

$$Mass_{FC,biomass} = \frac{8.00 \times 21.7}{100}$$

$$Mass_{FC,biomass} = 1.74\ g$$

Calculation of mass of fixed carbon in biocoal:

$$Mass_{FC,biocoal} = \frac{5.32 \times 20.0}{100}$$

$$Mass_{FC,biocoal} = 1.06\ g$$

Calculation of normalised fixed carbon of biocoal:

$$\%FC_{initial} = \frac{1.06}{1.74} \times 100$$

$$\underline{\%FC_{initial} = 60.9\%}$$

$\%FC_{initial}$ – fixed carbon content of biocoal as a percentage of the fixed carbon content of the untreated biomass on an absolute basis

3.3.5 Calculation HHV using carbon content

So that the higher heating value (HHV) of biocoals could be determined quickly, a calculation using the elemental analysis of the biocoal (determined using the method described in section 3.2.2) was utilised. This was calculated using a calculation proposed by David A. Tillman in his book *Wood as an Energy Resource* (Tillman, 1978), described in Equation 3.3. This value was found to be more accurate for the samples than the Dulong formula in this case, as shown in Table 3.10. where the calculated values were compared with experimentally determined values for a selection of biocoals. The experimentally determined values were acquired using bomb calorimetry (method described in section 3.2.6).

Equation 3.3 Equation used to derive higher heating value from carbon content

$$HHV = 0.4373C - 1.6701 \quad \text{(Tillman, 1978)}$$

Table 3.10 Comparison of calculated and experimentally determined HHV of selected miscanthus biocoals

Fuel	HTC temperature (°C)	HHV (MJ/kg)				
		Actual	Calculated (Tillman)	Difference	Calculated (Dulong)	Difference
Miscanthus biocoal	200	19.7	20.4	+3.6%	17.5	-11.2%
Miscanthus biocoal	225	23.6	23.7	+0.4%	22.0	-6.8%
Miscanthus biocoal	250	26.5	26.4	-0.4%	25.3	-4.5%

3.3.6 Calculating theoretical biomethane potential for anaerobic digestion of HTC process liquor

The theoretical biomethane potential (BMP) for anaerobic digestion of HTC process liquor was determined using the Buswell equation (equation 3.4) and the Boyle equation (Equation 3.5).

Equation 3.4 Theoretical biomethane potential (Buswell equation)

$$BMP_{thBW} = \frac{22400\left(\frac{n}{2}+\frac{a}{8}-\frac{b}{4}\right)}{12n+a+16b}$$

Legend: n – carbon content (%), a – hydrogen content (%), b – oxygen content (%)

Equation 3.5 Theoretical biomethane potential (Buswell equation)

$$BMP_{thBO} = \frac{22400\left(\frac{n}{2}+\frac{a}{8}-\frac{b}{4}-\frac{3c}{8}\right)}{12n+a+16b+14c}$$

Legend: n – carbon content (%), a – hydrogen content (%), b – oxygen content (%), c – nitrogen content

3.3.7 Calculating energy production from anaerobic digestion of HTC process liquor

To investigate the potential of using anaerobic digestion of HTC process liquor to augment the energy yield of HTC, the HHV of potential methane produced was calculated using the theoretical BMP of the process liquor. This was calculated by multiplying the BMP by the volatile solids (VS) content of the process liquor and the water to biomass ratio to ascertain the volume of methane produced per kilogram of biomass feedstock. The VS content was calculated using This was multiplied by the HHV of methane (energy produced by anaerobic digestion per kg of biomass feedstock. An example of this for the anaerobic digestion of process liquor produced from HTC of rice at 180°C, with a W/B ratio and residence time of 2:1 and 60 minutes respectively can be seen below. The data used in the calculation can be seen in .

Data used in calculation of energy production from anaerobic digestion of HTC process liquor

Description	Value
BMP_{thBO} (ml CH_4/g_{VS})	88.7
Carbon content (%)	10.7
Mass of water (kg)	2
HHV of methane (MJ/m^3)	39.8

$$VS\ content = 10.7 \times 1.8$$

$$VS\ content = 19.3\%$$

$$Mass\ VS = 19.3\ \times\ 2$$

$$Mass\ VS = 38.6\ g$$

$$Volume\ CH_4 = 88.7\ \times\ 38.6$$

$$Volume\ CH_4 = 3424\ cm^3$$

$$Energy_{CH4}\ = \frac{3424\ \times\ 39.8}{1000000}$$

$$Energy\ _{CH4} = 0.14\ MJ_{CH4}/kg_{biomass}$$

3.3.8 Example calculation for activation energy and pre-exponential factor of char combustion

An illustrative example for the calculation of activation energy and pre-exponential factor is shown below, where these values are determined for isothermal combustion of soft wood biocoal produced at 200°C over 60 minutes with a W/B ratio of 4:1. The k_a values for isothermal combustion of the biocoal at the five temperatures chosen for the analysis can be seen in Table 3.11, and the straight line fit of $\ln k_a$ vs. 1/T can be seen in Figure 3.16.

Table 3.11 k_a values for isothermal combustion of soft wood biocoal (200°C, 60 minutes, 4:1 W/B) at multiple temperatures

Isothermal combustion temperature (K)	k_a	lnK_a
698	0.02	-3.96
723	0.04	-3.25
748	0.08	-2.47
773	0.17	-1.75
798	0.36	-1.02

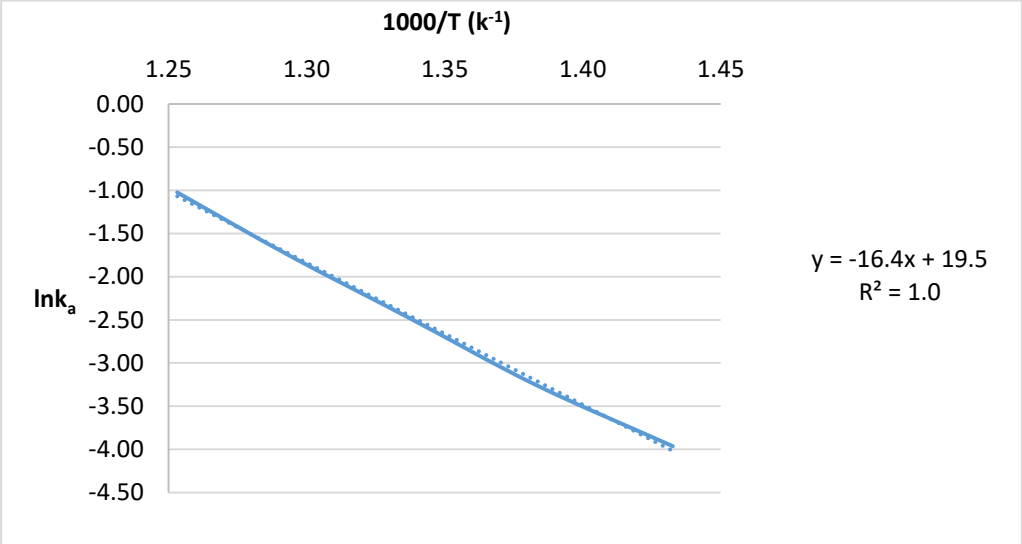

Figure 3.16 Plot of lnka vs. 1000/T for isothermal combustion of soft wood biocoal (200°C, 60 minutes, 4:1 W/B) at multiple temperatures

The calculation to determine E_a is as follows:

$$lnk_a = lnA - \frac{E_a}{RT}$$

$$y = mx + C$$

$$m = \frac{-E_a}{R}$$

$$E_a = -mR$$

$$m = -16.427$$

$$R = 8.31\, JK^{-1}mol^{-1}$$

$$E_a = -(-16.427) \times 8.31$$

$$\underline{E_a = 136.5}$$

The calculation to determine A is as follows:

$$lnk_a = lnA - \frac{E_a}{RT}$$

$$y = mx + C$$

$$lnA = C$$

$$A = e^C$$

$$C = 19.517$$

$$A = e^{19.517}$$

$$\underline{A = 2.99 \times 10^8}$$

3.3.9 Henry's law calculations

To show the total carbon dioxide yield of HTC, the amount of CO_2 that would be dissolved in the process liquor of HTC under ambient conditions (which were the conditions at which the gas was collected) was to be accounted for. To calculate this, the Henry's Law formula (Equation 3.6) was used.

Equation 3.6 Henry's law formula

$$K_H = \frac{P}{C}$$

Legend: K_H – Henry's constant, P – partial pressure, C – solubility of gas

3.3.10 Relative aromatic carbon content

The relative aromatic content of the biocoals in comparison to the untreated feedstock was calculated using the same procedure as described in section 3.3.3, with the concentration of aromatic moieties in the samples being used instead of the components described by proximate analysis.

4

Chapter 4 Impact of HTC parameters and feedstock on product distribution, composition, and properties

Before any in-depth analysis can be performed on the impact of HTC on specific chemical properties of biomass, it is essential to understand how the process parameters and feedstock variation can affect the basic outputs – the yield of HTC and the composition of the biocoal produced. The basic composition of biomass fuels can be displayed through proximate and ultimate analysis, the former detailing the composition of the fuel in terms of the major fuel components (moisture, volatile matter, fixed carbon, and ash), and the latter through the elemental composition of the fuel. This is required both to give an understanding of the basic process and results of HTC, and to ensure that the method in which the lab-scale HTC experiments were carried out produces a biocoal that conforms to literature values, ensuring that any further investigations into the behaviour of the biocoal produced are made in confidence. This chapter will focus on how the yield and composition of biocoal varies with HTC parameters and changing feedstock.

4.1 Materials and methods

The HTC experiments were carried out as described in section 3.1.2. All of the values described are for single HTC experiments, with the exception of the data showing the repeatability of HTC yield. The main factors studied were temperature, residence time, and W/B ratio.

A Design of Experiments (DoE) statistical study of HTC of miscanthus was carried out, and the factorial design used is shown in Table 4.1. Yield and composition data were recorded for every HTC experiment. and will be used to supplement and verify the findings of the DoE study. This will also be used to show the effect of varying feedstock on the yield and properties of biocoal. Proximate analysis, elemental analysis, gas composition analysis, and testing were performed as described in sections 3.2.1.1, 3.2.2, and 3.2.4 respectively.

Table 4.1 Miscanthus HTC DoE factorial design

Factorial label	Temperature (°C)	Residence time (min)	W/B ratio
---	200	60	4
--+	200	60	6
-+-	200	240	4
-++	200	240	6
000	225	150	5
+--	250	60	4
+-+	250	60	6
++-	250	240	4
+++	250	240	6

Statistical analysis for the DoE data set was performed using an analysis of variance (ANOVA) general linear model using Minitab software. This produced the p-value for the impact of the different factors in the outcome variable. If this value is below 0.05, then the impact of the factor is statistically significant,

meaning that is distinguishable from random variance. 'Main effects' plots generated using Minitab software were used to show the broad impact of the three variables on the outcomes of HTC. These gave the mean values for the levels for each variable compared in three panes side-by-side. For the extremes of the levels (signified by '-' and '+' in Table 4.1), this is the mean of 4 experiments, for the mid point ('000' in Table 4.1), the value used is from the single experiment.

4.2 Mass balance of HTC experiments

To confirm the validity of the HTC experiments, and to ensure that as much of the HTC products as possible are being accounted for and analysed after HTC, a mass balance was performed on HTC of Brites wood pellets at temperatures of 200, 225, and 250. The W/B ratio was 4, and the residence time was 60 minutes for each of these experiments. The mass balances produced can be seen in Table 4.2. The solid yield on a DAF basis was determined by the mass and proximate analysis of the feedstock and biocoals (calculated as shown in section 3.3.1); the liquid yield was determined from the elemental analysis of the liquor; and the gas yield was determined from the gas chromatography of the product gas normalised to 100% to disregard the nitrogen used to produce an inert atmosphere in the Parr reactor.

Table 4.2 Mass balance of HTC of wood

Sample	Solid yield (DAF[1]) (%)	Liquid yield (DAF[1]) (%)	Gas yield (DAF[1]) (%)	Total mass recovered (%)
200°C biocoal	72.4	12.0	1.5	85.9
225°C biocoal	69.7	11.3	3.4	84.4
250°C biocoal	56.7	11.3	7.8	75.8

[1]DAF – dry, ash free basis

In the case of HTC at 200 and 225°C, the mass balance is between 84-86%, with the vast majority of the mass being recovered. At the higher temperature of 250°C, only around 76% of the mass is accounted for at the end of the experiment. This could be explained by the mass of water generated by HTC not being accounted for; more water will be generated at higher temperatures due to increased decomposition of the biomass, which can be seen in the total solid mass accounted for decreasing. In addition to this, some organic matter is lost through volatile mater evaporating and solid matter precipitating from the process liquor.

4.3 Repeatability of experiments and analysis

4.3.1 Mass yield

To assess the repeatability of the HTC experiments, HTC experiments involving two feedstocks under two sets of conditions each were repeated in triplicate. The average yield of HTC experiments and the error (to 95% certainty in terms

of mass yield) can be seen in Table 4.3. The maximum variance is seen in HTC of soft wood at 200°C, where an error of 3.0 percentage points (4.5% of the yield value) is seen. This means that any change in yield within 5% of one another cannot be separated from random variance. In both cases, higher temperature HTC had a lesser variance in yield with HTC of soft wood and olive cake at 225°C having error values of 1.3% and 1.7% (0.9 and 0.8 yield percentage points), respectively.

Table 4.3 Variability of yield of HTC experiments

Feedstock	Temperature (°C)	Time (min)	W/B ratio	Mass Yield (%) (ar basis[1])
Soft wood	200	60	4	66.3 ± 3.0
Soft wood	225	60	4	65.7 ± 0.9
Olive cake	200	60	6	51.3 ± 2.0
Olive cake	225	60	6	47.1 ± 0.8

[1]ar basis – as received basis

4.3.2 Proximate analysis

The variance of the proximate analysis of biocoals can be seen in Appendix 2, and the proximate analysis of the miscanthus biocoals used in the DoE are included in Table 4.4 as an example. The proximate analyses were run in triplicate. Proximate analysis is generally accurate in describing the volatile matter content and the fixed carbon content of the samples, but is not as accurate in determining the moisture content or ash content. The error in measurement for volatile matter and fixed carbon is under 5%, which is much lower than the changes in composition seen when process parameters change. In the case of moisture determination, the error in determination was mostly under 5%, but there are some cases where the error is much larger, up to 80%.

This is due to the low moisture content of biocoals resulting in a very small mass of moisture in the sample to be measured. In addition to this, the humidity of the laboratory or storage space can result in a fluctuation in the moisture content of the sample. The samples also have low ash contents, which results in a large variance in ash determined, shown by an error of 8-41%.

Table 4.4 Variability of proximate analysis of HTC experiments

Temperature (°C)	Time (min)	W/B ratio	Moisture (%)	Volatile matter (%)	Fixed carbon (%)	Ash (%)
Untreated miscanthus			6.4 ± 0.1	67.2 ± 0.8	21.7 ± 0.4	4.7 ± 0.5
200	60	4	3.1 ± 0.1	74.5 ± 0.5	20.0 ± 0.4	2.4 ± 0.2
200	60	6	2.4 ± 1.9	77.5 ± 1.8	18.0 ± 0.3	2.1 ± 0.2
200	240	4	2.9 ± 0.1	74.3 ± 1.2	20.0 ± 0.7	2.7 ± 0.5
200	240	6	2.1 ± 1.1	75.8 ± 1.2	19.6 ± 0.1	2.5 ± 0.9
225	150	5	2.1 ± 0.1	68.4 ± 0.7	27.2 ± 0.8	2.3 ± 0.2
250	60	4	1.6 ± 0.6	60.4 ± 1.9	33.9 ± 0.5	4.1 ± 1.7
250	60	6	1.2 ± 0.0	61.7 ± 0.4	33.6 ± 0.3	3.5 ± 0.2
250	240	4	1.0 ± 0.8	52.3 ± 1.9	41.4 ± 2.2	5.3 ± 0.4
250	240	6	1.4 ± 0.1	51.6 ± 2.7	43.2 ± 2.6	3.8 ± 0.3

4.4 The impact of process parameters on yield of miscanthus HTC

Biocoal yield data from the HTC experiments carried out can be seen in Appendix 1. The yield on a dry, ash free (DAF) basis; and on a carbon basis were calculated as described in sections 3.3.1 and 3.3.2, respectively. The dry, ash free yield of HTC of non-waste biomass ranged from 34 to 84% (carbon yield 46-81%), and for waste biomass the range observed was 2 to 74 % (carbon yield 4-91%). These values conform to literature values (Kambo & Dutta, 2014; Kang, Li, Fan, & Chang, 2012; Nizamuddin et al., 2017; Oliveira et al., 2013; Sermyagina et al., 2015; Aidan Mark Smith et al., 2018). The significantly lower limit for waste biomass is due to some waste biomass feedstocks decomposing significantly under HTC conditions. HTC of beef mince yields little solid product, due to being composed mostly of fats (lipids) and proteins, which degrade easily under HTC conditions and do not lead to solid products (Kruse et al., 2016; Yue et al., 2017). HTC of sewage sludge can also experience high solubilisation of the organic content (which results in low DAF yields) (Aidan M. Smith et al., 2016). In the case of lignocellulosic biomass (which comprises all of the non-waste biomass and a selection of the waste biomass studied), the presence of high levels of lignin, cellulose, and hemicellulose result in a consistently higher solid yield, due to lignin being mostly unaffected by HTC (Liu et al., 2013), alongside cellulose forming an aromatic solid product (Falco et al., 2011) and hemicellulose degradation products repolymerising into solid products (Titirici et al., 2008).

The p-values for the impact of temperature, residence time, and W/B ratio on the carbon yield of HTC of miscanthus can be seen in Table 4.5, and the main effects plots can be seen in Figure 4.1. The only factor that is statistically significant in this study is temperature, indicating that temperature has the primary influence on the yield of HTC under the range of conditions studied. As temperature increases, the carbon yield decreases sharply. This matches similar work, with a study of HTC of miscanthus at 190, 225, and 260°C over a residence time of 5 minutes produces biocoal in mass yields of 83.5, 66.9, and 47.8% respectively (Kambo & Dutta, 2015b). The significant decrease in yield with increasing temperature has also been reported in a study of HTC of loblolly pine (Lynam et al., 2015).

Table 4.5 P-values for the impact of temperature, time and water: biomass on the carbon yield of miscanthus HTC (ANOVA general linear model).

Variable	P-value
Temperature	0.002
Residence time	0.141
Water: biomass	0.464

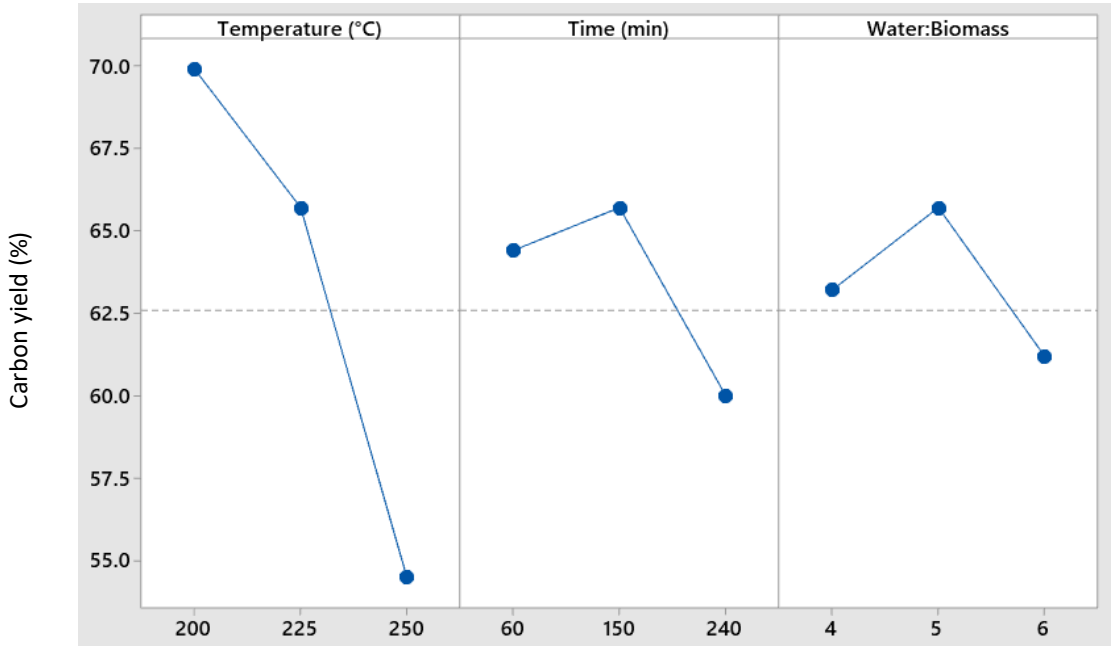

Figure 4.1 'Main effects' plots of carbon yield of miscanthus HTC

The decrease in yield is accompanied by a visual change in the biocoal. The further hydrothermal decomposition of the biomass at high temperatures results in a biocoal that is darker in colour, has a smaller particle size, and is more homogenous. The visual difference between miscanthus biocoal produced at 200 and 250°C can be seen in Figure 4.2.

Figure 4.2 Miscanthus biocoal produced at 200°C (left) and 250°C (right)

Although this study did not show a statistically significant impact for residence time on carbon yield, a study of HTC of paper mill sludge residue found that residence time was statistically significant. The impact was 3-7 lower than that of temperature (Mäkelä, Benavente, & Fullana, 2015), which matches what is seen in Figure 4.1. Further repeats of the HTC experiments would need to be conducted to attempt to find the statistically significant effect of residence time on the HTC of miscanthus in this study.

In the range used for this study, W/B ratio has an insignificant effect on the carbon yield of HTC. This is also seen in another study that used low W/B ratios (Mäkelä et al., 2015). The range used in this study may have been too narrow and the values studied too low to show the true impact of W/B ratio on the yield of HTC. Further experiments conducted indicated that extremely high

W/B ratios have a large detrimental effect on carbon yield. The carbon yield of HTC of rye anaerobic digestate at 215°C with increasing W/B ratio is shown in Figure 4.3. The carbon yield declines steadily with increasing W/B ratio, and although these values are only through a single determination, the large change in carbon yield is likely to be statistically significant. The impact of high W/B ratios on the yield of HTC described has also been reported in the literature for HTC of pine wood, with increasing the W/B ratio from 5 to 10 decreasing the energy yield in all cases (Lynam et al., 2015). This effect was seen in be greater at higher temperatures (Lynam et al., 2015). These effects can be explained by a greater impact of hydrolysis reactions through more water being present (Sermyagina et al., 2015).

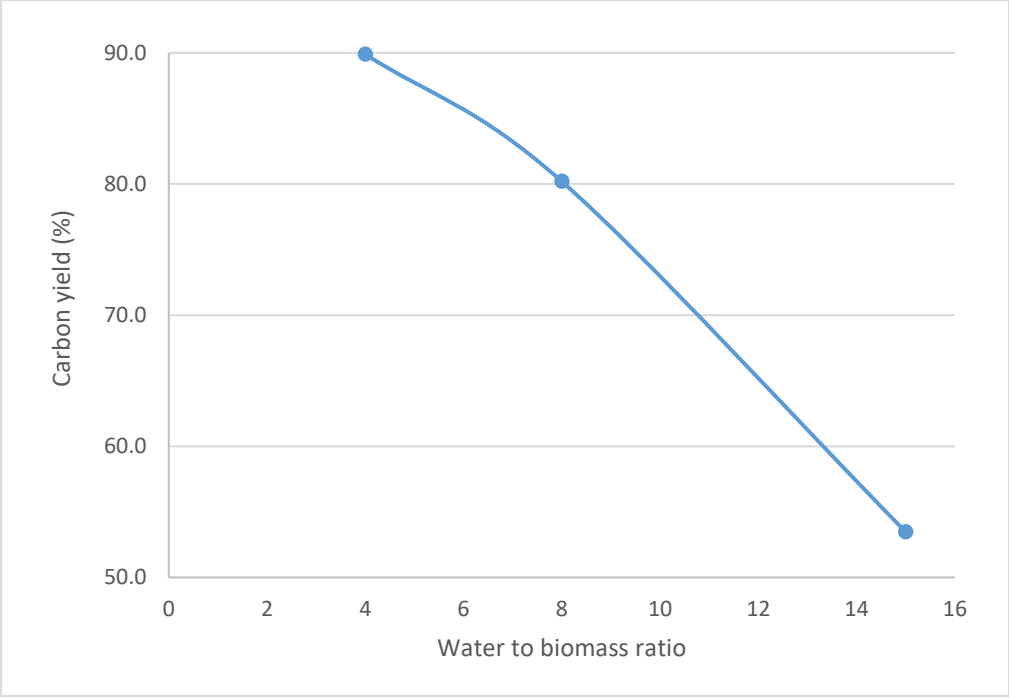

Figure 4.3 Impact of W/B ratio on carbon yield of HTC (215°C) of rye anaerobic digestate (single determination)

The influence of particle size was investigated using a small number of miscanthus HTC experiments outside of the test matrix, as well as in some soft wood HTC experiments. This data can be seen in Appendix 1. Decreasing particle size was shown to slightly increase carbon yield at low HTC temperatures. As was the case with residence time, this effect was larger at higher HTC temperatures. These findings are in opposition to some literature findings, with one study finding that increasing particle size increases the mass yield. It was hypothesised that mass transfer effects were limiting the rate of the HTC reaction (Reza, Yan, et al., 2013). The opposite trend seen in the HTC experiments conducted for this study are likely due to the much longer residence time – the timescale in the literature study from seconds to a few minutes, rather than hours (Reza, Yan, et al., 2013). The HTC reaction would be mostly completed in the hour timescale, meaning that mass transfer effects are not an issue in the experiments performed for this study. The increase in yield with decreasing particle size seen at longer residence times could be do to efficient mixing, having a larger surface area of biomass exposed to water allowing for large initial carbon concentrations in the process liquor, some of which will react crash out as solids after further reaction under HTC conditions.

4.5 The impact of HTC parameters on miscanthus biocoal composition

4.5.1 Proximate analysis

The proximate analysis of the miscanthus feedstock and biocoals can be seen in Table 4.4 (section 4.3.2), and further proximate analysis data for biocoals produced from other feedstocks can be seen in Appendix 2. The composition of the biocoals are consistent with literature values (He et al., 2013; Kambo & Dutta, 2014; Liu, Quek, & Balasubramanian, 2014; Aidan Mark Smith et al., 2018). In general, biocoal has a lower moisture and volatile matter content than biomass, and a higher fixed carbon content. The lower moisture content is the result of HTC removing moisture during the thermal treatment, alongside the process rendering the biocoal product hydrophobic (Acharya et al., 2015; He et al., 2013). The lower volatile matter and higher fixed carbon content of biocoals is a result of decomposition and removal of the volatile matter (for example hemicellulose, cellulose and extractives) during HTC, in addition to some of the degradation products repolymerising to form aromatic solid carbon joining the remaining lignin as fixed carbon (Aidan M. Smith & Ross, 2019). The fixed carbon content is closely tied to lignin content (Aidan M. Smith & Ross, 2019), which is mostly unaffected my HTC (Liu et al., 2013) so the removal of other components of biomass increases the concentration of lignin and hence fixed carbon generating material. The ash content of a biocoal can be lower or higher than that of its feedstock biomass, determined by the inorganic elements present (Aidan M. Smith et al., 2016). In general, the data from this study

showed that biocoals produced at high HTC temperatures (above 230°C) had a higher ash content than biocoals produced at lower temperatures. This is due to increased decomposition of organic material (for example cellulose (Coronella et al., 2014)), coupled with the lower polarity of water at higher temperatures (Aidan M. Smith et al., 2016). An outlier in these general trends in proximate composition is HTC of miscanthus, where the biocoal produced at 200°C has a similar fixed carbon content to the untreated miscanthus, and a slightly higher volatile matter content. This indicates that the decomposition and loss of biomass components that generate fixed carbon is occurring at the same levels as loss of volatile matter, moisture, and ash.

In terms of proximate composition on a dry, ash-free basis, non-waste biomass produced biocoal has a volatile matter content between 54 and 87% and a fixed carbon content between 13 and 46%. Waste biomass produced biocoal with volatile matter content between 50 and 95% and fixed carbon content between 50 and 5%. As was described for the lower carbon yield, the higher volatile matter and lower fixed carbon content in some (non-lignocellulosic) waste biomass feedstocks can be attributed to the biochemical composition. Biomass feedstocks like sewage and foodstuffs contain components that are easily degraded by HTC, and do not recombine to become fixed carbon, for example proteins and lipids (Kruse et al., 2016; Yue et al., 2017). This, in combination with low lignin content (Aidan M. Smith & Ross, 2019), results in the biocoal produced from sewage and protein-based foodstuff having a high volatile matter content and low fixed carbon content.

To properly assess the decomposition of the components of biomass that generate volatile matter and fixed carbon in proximate analysis, the composition of the miscanthus biocoal produced in the DoE test matrix was normalised using the mass yield and the proximate analysis of the untreated miscanthus feedstock (calculation shown in section 3.3.4). This also allows for the absolute amount of moisture and ash removed by HTC to be shown.

The p-values for the impact of temperature, time and W/B ratio on the relative moisture content of the biocoals in comparison to the feedstock biomass (on an absolute basis), and the 'main effects' plots for these, are shown in Table 4.6 and Figure 4.4, respectively. As was the case with carbon yield, only temperature was found to be statistically significant using the general linear model. The vast majority of the moisture was removed under all HTC conditions studied, with all biocoals having significantly less moisture than the feedstock biomass. As temperature increased, the amount of moisture in the biocoal in comparison to the feedstock biomass drastically decreased, reducing from approximately 25% to 5% of the original moisture content of the biomass. It can be seen in the 'main effects' plots that the impact of time and W/B ratio are much smaller than that of temperature, and the mean values do not vary significantly. The p-values for these factors are above 0.05, so the trends cannot be separated from random variance. In addition to this, the variation in TGA determination of water content is significant and the HTC experiments were run without repeats, meaning that small changes such as what is seen in the

case of varying time and W/B ratio cannot be described accurately using this data set.

Table 4.6 P-values for the impact of temperature, time and W/B ratio on the relative moisture content of miscanthus biocoal (ANOVA general linear model)

Variable	P-value
Temperature	0.000
Residence time	0.129
Water: biomass	0.133

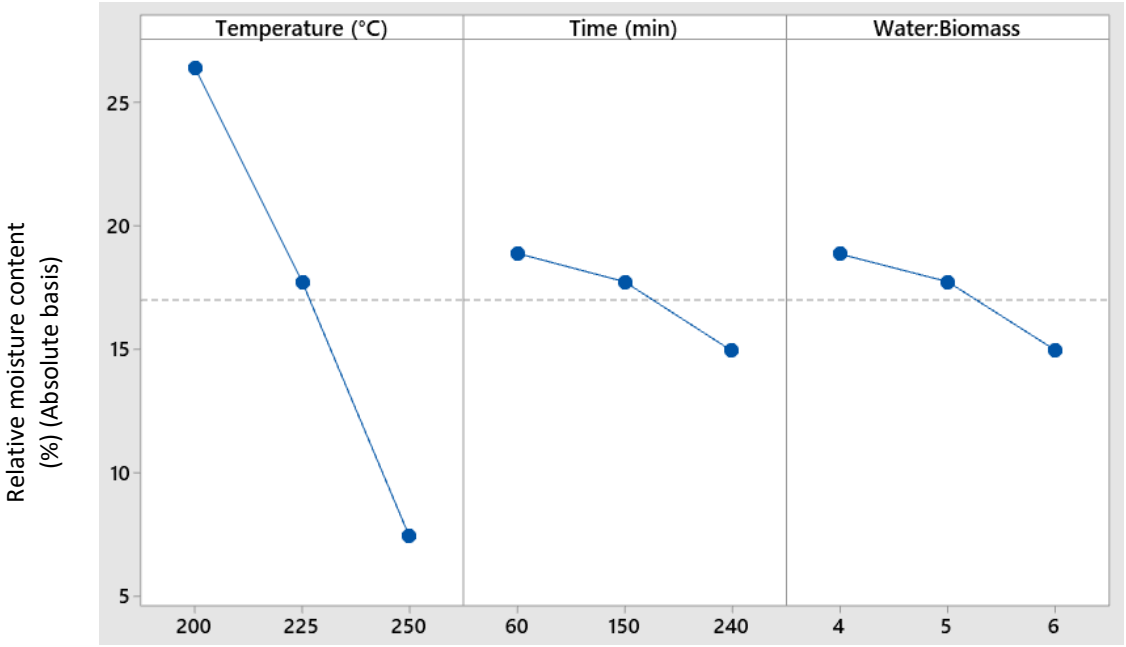

Figure 4.4 'Main effects' plot for the relative moisture content of miscanthus biocoals in comparison to untreated miscanthus

The p-values for the impact of temperature, time and W/B ratio on the relative volatile matter content of the biocoals in comparison to the feedstock biomass (on an absolute basis), and the 'main effects' plots for these, are shown in Table

4.7 and Figure 4.5, respectively. In the case of volatile matter, both temperature and residence time have a statistically significant effect on the relative volatile matter content of the biocoal. Both increasing temperature and increasing residence time results in a decrease in the relative amount of volatile matter in the biocoal, with temperature having a much larger impact than residence time. The impact of temperature on the volatile matter content of the biocoal will be due to the increased decomposition of cellulose at higher HTC temperatures (Coronella et al., 2014). Cellulose decomposes under the conditions used to determine volatile matter, so if there is a lower cellulose content in the biocoal as a result of higher temperature HTC, the volatile matter of the biocoal will be lower. The relative volatile matter content decreasing with increasing residence time could also be due to increased decomposition, with some decomposition reactions requiring longer residence times to complete.

Table 4.7 P-values for the impact of temperature, time and W/B ratio on the relative volatile matter content of miscanthus biocoal (ANOVA general linear model)

Variable	P-value
Temperature	0.000
Residence Time	0.020
Water: biomass	0.911

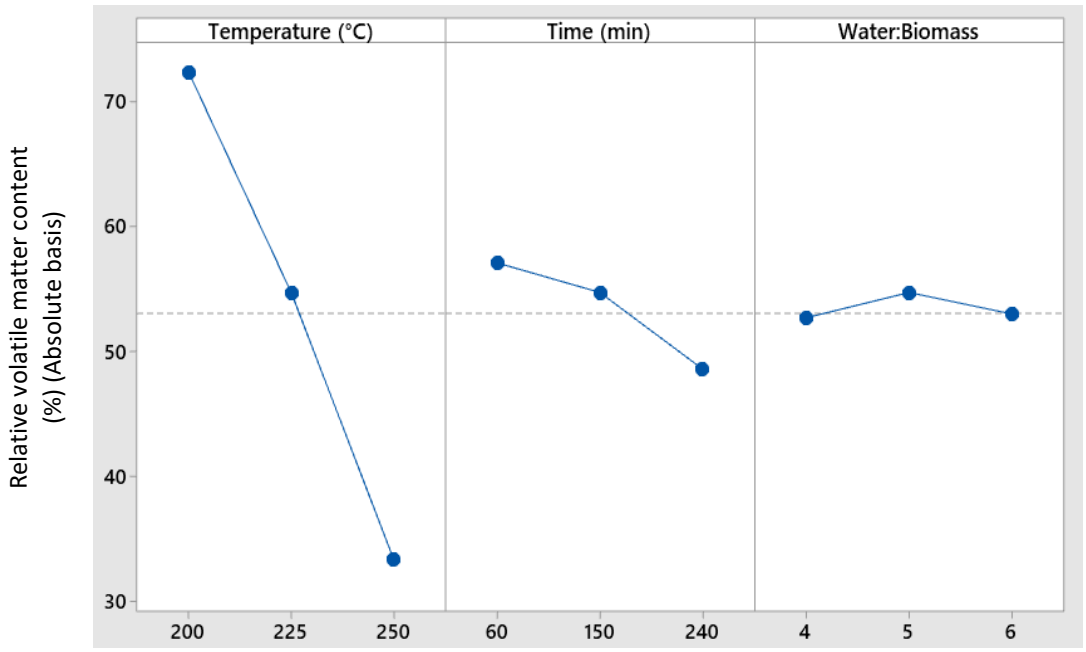

Figure 4.5 'Main effects' plot for the relative volatile matter content of miscanthus biocoals in comparison to untreated miscanthus

The p-values for the impact of temperature, time and W/B ratio on the relative fixed carbon content of the biocoals in comparison to the feedstock biomass (on an absolute basis), and the 'main effects' plots for these, are shown in Table 4.8 and Figure 4.6, respectively. Although lignin is mostly unaffected by HTC, some decomposition occurs (Yue et al., 2018), and this is shown by the amount of material that generates fixed carbon in the biocoal being smaller than that of the untreated biocoal, resulting in a percentage under 100%. At 200°C there is significant decomposition, meaning that the loss of lignin through decomposition is larger than the generation of aromatic carbon through repolymerisation and aromatisation of hemicellulose and cellulose degradation products. The relative fixed carbon content of the biocoals is seen to increase with increasing temperatures, indicating that there are higher levels of aromatisation occurring at higher HTC temperatures. The initial jump seen

between 200°C and 225°C could indicate that the increase in aromatisation is mostly be due to cellulose decomposition. The relative fixed carbon content is similar at 225°C and 250°C, which could be due to the increased lignin decomposition at 250°C being similar to any increase in aromatisation. The relative fixed carbon content appears to vary significantly with changing residence time and W/B ratio, although the variation is less than what is seen in changing temperature. Additionally, the general linear model cannot separate the variation from random variance. The values shown at the mid points of these plots represent only a single experiment in comparison to the points at either extreme representing the mean of 4 experiments, so this value may be an outlier. If the mid point is disregarded, it can be seen that the trend is very close to the mean line. Further experiments around the mid point would have to be performed, and repeats of the original HTC experiments would be necessary to distinguish any statistically significant trends.

Table 4.8 P-values for the impact of temperature, time and W/B ratio on the relative fixed carbon content of miscanthus biocoal (ANOVA general linear model)

Variable	P-value
Temperature	0.010
Time	0.621
Water: biomass	0.346

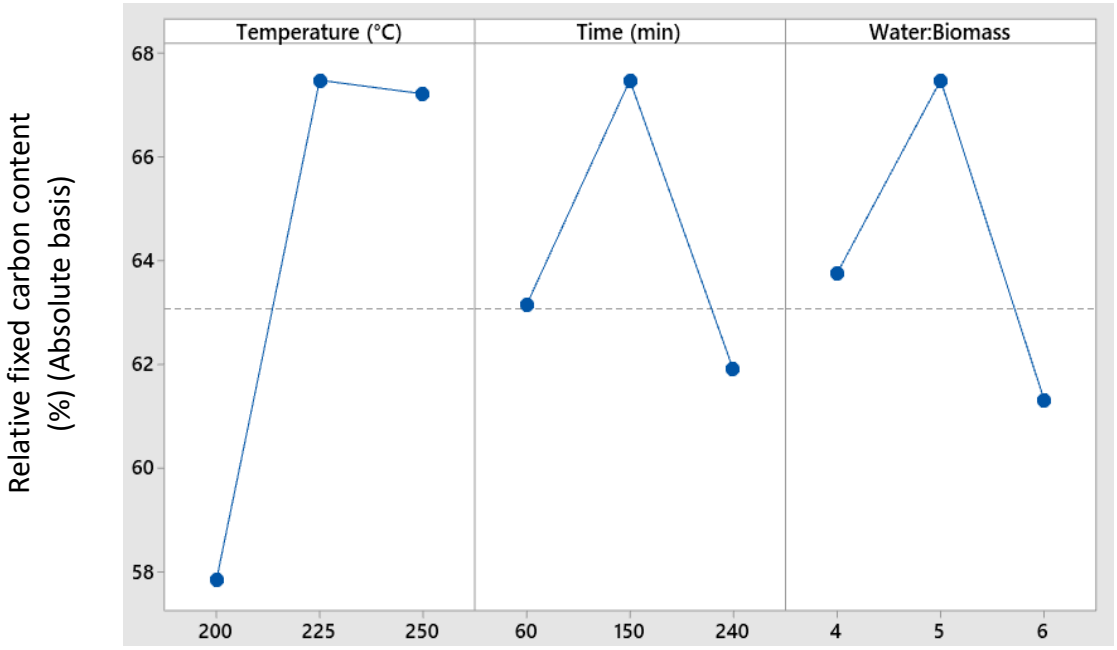

Figure 4.6 'Main effects' plot for the relative fixed carbon content of miscanthus biocoals in comparison to untreated miscanthus

The p-values for the impact of temperature, time and W/B ratio on the relative ash content of the biocoals in comparison to the feedstock biomass, and the main effects plots for these, are shown in Table 4.9 and Figure 4.7, respectively. Although the ash content of the biocoals were all significantly lower than that of the untreated biomass (with approximately 27-34% relative ash content on an absolute basis) showing that in general HTC reduce the ash content, the general linear model shows that the impact of all three variables cannot be seperated from random variance and are therefore statistically insignificant. This is due to the error of determination of ash content through TGA being significant (as described in section 4.3.2) in comparison to the impact of temperature, residence time, and W/B ratio. The limitations of TGA in determining ash content of biomass means that reliable trends for the impact

of HTC means that these trends have to be determined using gravimetric methods of ash determination. This is covered in section 5.3.

Table 4.9 P-values for the impact of temperature, time and W/B ratio on the relative ash content of miscanthus biocoal (ANOVA general linear model)

Variable	P-value
Temperature	0.836
Time	0.966
Water: biomass	0.109

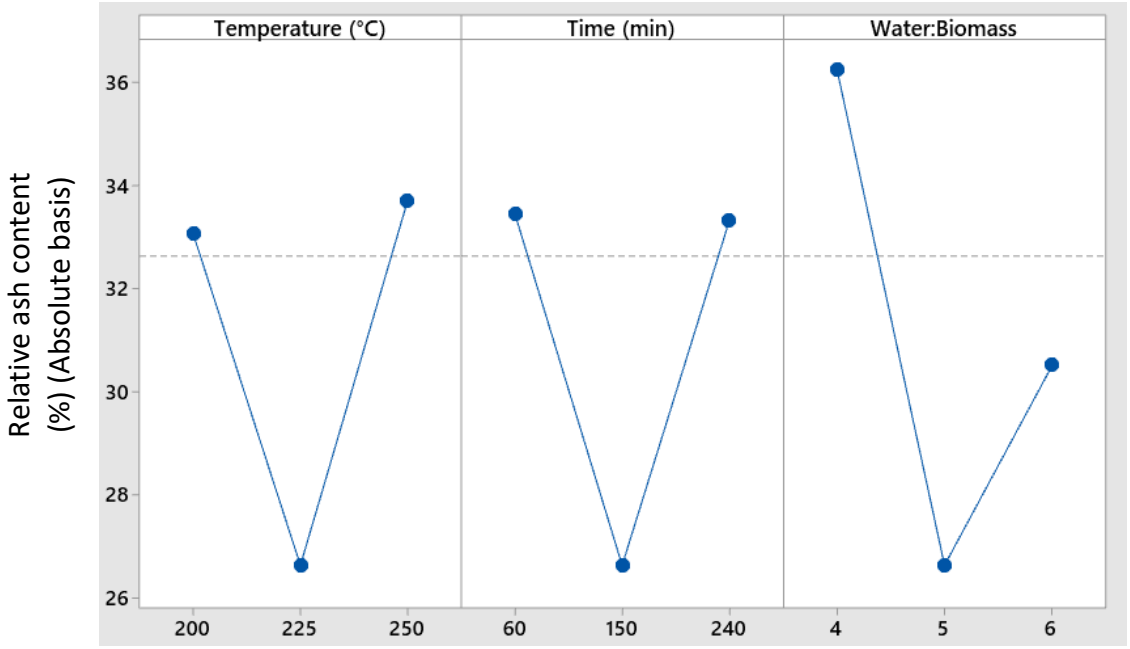

Figure 4.7 'Main effects' plot for the relative ash content of miscanthus biocoals in comparison to untreated miscanthus

4.5.2 Elemental analysis

The elemental analysis of various biocoals and their respective feedstock can be seen in Appendix 3. Non-waste biomass produced biocoal with a carbon content in the range of 50 to 75%, whereas waste biomass produced biocoal with a carbon content in the range of 34 to 73%. These values are consistent with the literature (He et al., 2013; Kambo & Dutta, 2014; Yan et al., 2014). The lower limit of the range in carbon content of waste biocoals is due to sewage sludge exhibiting significant solubilisation of organic content, which has been reported previously (Aidan M. Smith et al., 2016).

HTC increases the carbon content of biomass, while decreasing the hydrogen content in most cases, and increasing HTC temperature increases this effect. This effect is consistent with what is described in the literature, with HTC removing hydrogen and oxygen through dehydration and decarboxylation reactions (Mumme et al., 2011; Aidan Mark Smith et al., 2018). The concentration of nitrogen in biocoal is less predictable, but is generally very low. Nitrogen is mostly present in proteins, which degrade easily under HTC conditions, and could recombine with the biocoal through Maillard reactions (Kruse et al., 2016).

A Van Krevelen diagram of untreated miscanthus and miscanthus biocoals can be seen in , and a comparison diagram showing the biomass, lignite, coal, and anthracite regions can be seen in Figure 4.8. The oxygen content used to

produce the atomic O:C ratio in was calculated by difference – subtracting the carbon, hydrogen and nitrogen content from 100%. Miscanthus biocoal follows a similar trend to the digestate biocoal shown in Figure 4.9. Temperature had the largest impact on the elemental composition of the biocoal, with increasing temperature decreasing both the H/C and O/C ratios, bringing the biocoal closer to the left-bottom corner of the Van Krevelen Diagram, with the biocoals produced at 250°C having H/C and O/C ratios in the range of lignite (as described by the literature Van Krevelen diagram in Figure 4.9). Residence time has a similar effect as temperature, but the effect is smaller in magnitude. The impact of residence time on the elemental composition of miscanthus biocoal is greater at higher temperatures, with the biocoals produced at low temperature (200°C) being clustered together and the biocoals produced at the high temperature (250°C) forming two distinct groups based on the residence time. These will be due to harsher conditions (higher temperatures and longer residence times) resulting in increased decomposition of the biomass. W/B ratio has a negligible effect on the elemental composition of biocoal in the range studied, and the effect could be solely a result of experimental variance.

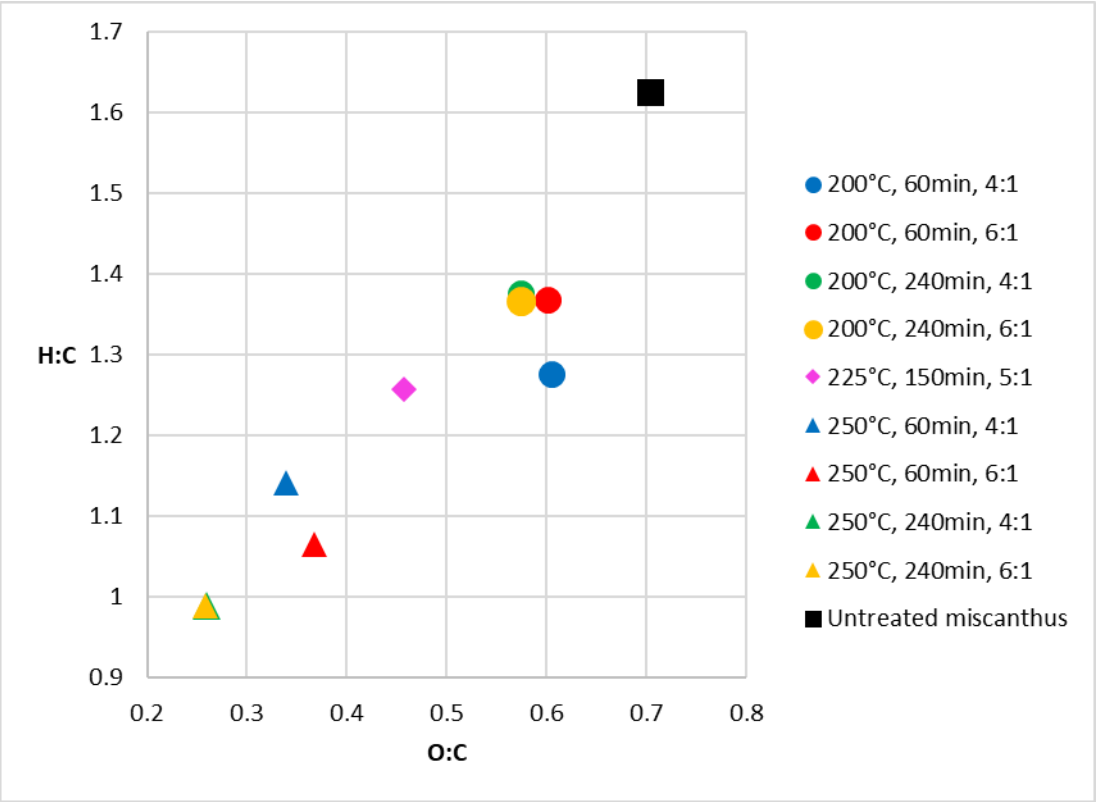

Figure 4.8 Van Krevelen diagram showing H:C vs. O:C (DAF basis) for miscanthus biocoals

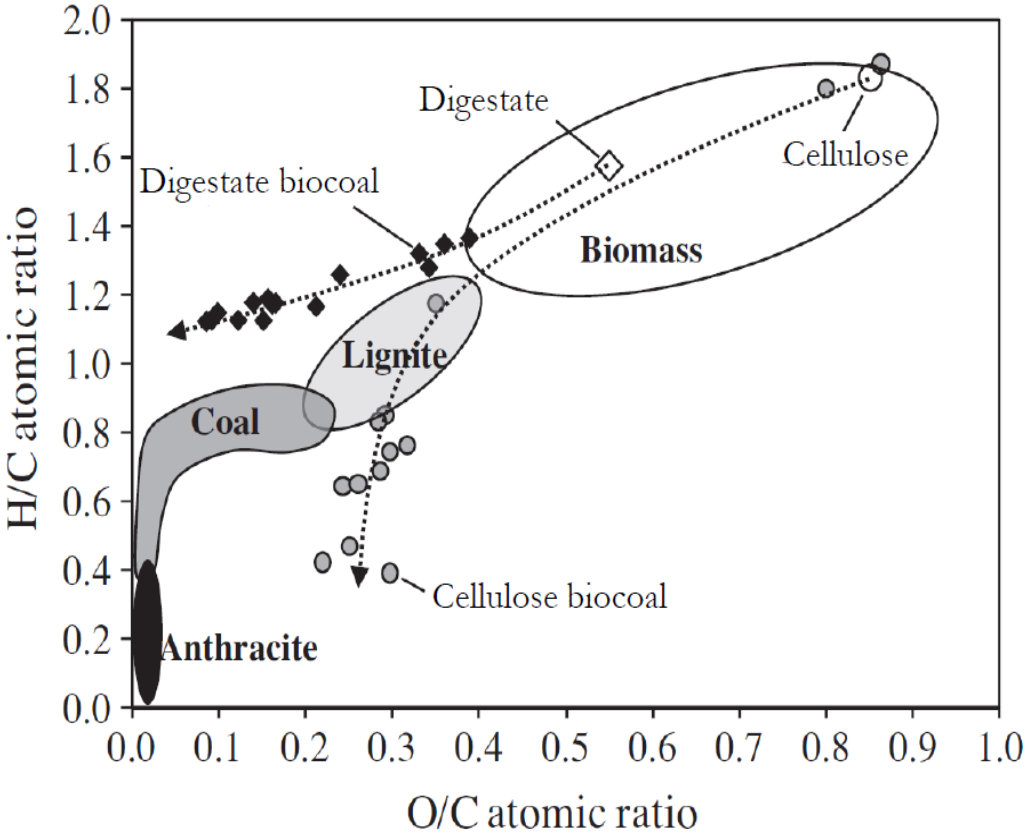

Figure 4.9 Van Krevelen diagram comparing cellulose, maize silage anaerobic digestate, and their respective biocoals (Mumme et al., 2011)

4.5.3 Energetic analysis of miscanthus HTC

The impact of HTC process parameters on the energy yield and densification of miscanthus is shown in Table 4.10. The energy yield is the ratio of the energy contents of the biocoal produced and the biomass feedstock on an absolute basis, as described in section 3.3.3.

Temperature has the primary impact on the energy densification of miscanthus, with very little densification occurring under HTC at 200°C, increasing to a 50% increase in energy density when HTC is performed at 250°C.

This is due to very little decomposition of biomass occurring at 200°C with only hemicellulose decomposing significantly, and limited aromatisation occurring. As temperature increases more cellulose decomposition occurs (Yue et al., 2018), and more hydrogen and oxygen are removed through dehydration and decarboxylation reactions (Mumme et al., 2011; Aidan Mark Smith et al., 2018) so the energy densification increases.

Although there is significant energy densification seen at 250°C, there is a trade off in terms of overall energy yield. When HTC was performed at 200°C, 69-71% of the original energy of the biomass was retained, and this dropped to 48-60%. A similar energy yield to what is seen at 200 and 225°C has been reported for HTC of empty palm fruit bunches. HTC of empty fruit bunches at 220°C was reported to have an energy yield of 72.7% (Stemann, Erlach, et al., 2013). There appears to be a drop in energy yield after 225°C, suggesting that there is significant decomposition of the biomass above this temperature, and significant quantities of carbon are lost in addition to hydrogen and oxygen. This could be indicating the onset of significant cellulose decomposition. A large drop in energy yield is also seen in HTC of loblolly pine, with HTC at 200°C and 260°C resulting in energy yields of between 88.1-95.5% and 61.9-81.8% respectively (Lynam et al., 2015). The higher energy yields seen in the study of HTC of loblolly pine could be due to the significantly shorter residence time (5-20 minutes (Lynam et al., 2015)) or due to the difference in biochemical composition of the feedstock. In this study, the ideal compromise between energy densification and retention of energy was at the mid point temperature

of 225°C, as this gave over double the energy densification of HTC at 200°C, while showing very similar energy yield.

W/B ratio appears to have a significant effect to on the energy yield at high temperatures, where increasing W/B ratio lowers the energy yield. Increasing W/B ratio decreasing the energy yield has been reported previously (Román et al., 2012). This was attributed to the larger volume of water increasing the prevalence of hydrolysis reactions (Román et al., 2012). In the case of miscanthus HTC in this study, W/B ratio does not seem to have a significant effect at the lower temperature of 200°C, which could be due to hydrolysis reactions being limited at this temperature.

Table 4.10 Influence of HTC parameters on HHV and energy yield and densification

HTC conditions			Mass yield (%)	HHV (calculated) (MJ/kg)	Energy yield (%)	Energy densification
Temperature (°C)	Time (min)	W/B ratio				
Untreated miscanthus			-	19.3	-	-
200	60	4	67	20.7	70	1.07
200	240	4	63	21.8	71	1.13
200	60	6	65	20.5	69	1.06
200	240	6	63	21.4	70	1.11
225	150	5	54	24.0	67	1.24
250	60	4	45	27.1	60	1.40
250	240	4	36	29.0	54	1.50
250	60	6	45	26.0	61	1.35
250	240	6	32	29.4	48	1.52

4.6 The impact of feedstock on the carbon yield of HTC

Due to differences in biochemical composition, the feedstock used could have an effect on the value of HTC yield. As was discussed in section 4.4, the range of yields are different in HTC of waste and non-waste biomass due to the non-waste biomass typically being lignocellulosic and some of the waste biomass having high concentrations of easily hydrolysable components such as lipids and proteins. The biochemical composition of different biomass feedstocks can also have an impact on how the carbon yield changes with temperature. The effect of temperature on the carbon yield of HTC of a selection of feedstocks can be seen in Figure 4.10. HTC experiments where there were more than two temperatures studied with comparable W/B ratios and residence times were included in Figure 4.10 to get a clear trend of the effect of temperature in each case. As has been shown in section 4.4, the effect of W/B ratio and residence time is negligible in comparison to the effect of temperature, so any minor differences in these factors will not significantly affect the trends seen.

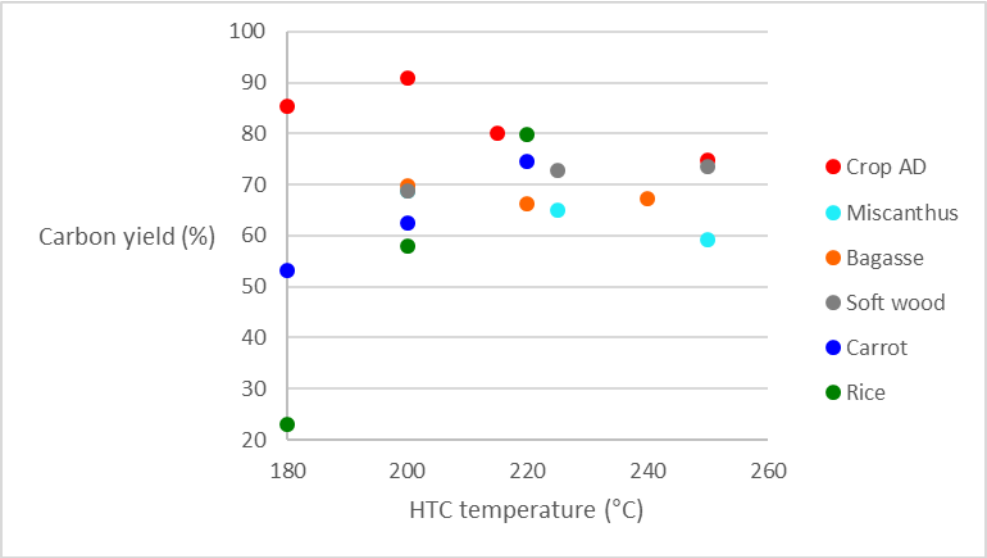

Figure 4.10 Impact of temperature on carbon yield for various biomass feedstocks

Soft wood, bagasse, and miscanthus all have very similar carbon yields at 200°C, being superimposed on one another. This is due to these feedstocks having very similar composition. All three feedstocks have been reported as having similar concentration of hemicellulose (22-26%) (Nizamuddin et al., 2017; Yoshida et al., 2008)), which is the main component of lignocellulosic biomass to decompose under HTC at 200°C . The carbon yield of HTC of these feedstocks stays similar as temperature increases, again due to similar composition. Carbon yield of soft wood and bagasse HTC remains fairly consistent as the HTC temperature increases between 200°C and 250°C and miscanthus carbon yield slightly decreases. This indicates that the harsher conditions are not driving significantly more carbon into the liquid and gaseous phases; and the degradation pathways of the biomacromolecules are likely predominantly aromatisation based, resulting in solid carbon.

HTC of rye anaerobic digestate at 200°C results in a very high carbon yield in comparison to HTC of other feedstocks. The yield sharply decreases above this temperature, producing similar results to the other feedstocks at HTC temperatures between 215-250°C. This is due to the anaerobic digestate having lower holocellulose concentration and a higher lignin concentration than the non-digested lignocellulosic feedstocks. This is due to the labile fraction of the crops (carbohydrate-like molecules like holocellulose) being consumed in digestion, leaving the recalcitrant material (lignin) behind (Tambone et al., 2009). As lignin does not decompose greatly under HTC conditions (Liu et al., 2013), the carbon yield is high. The lignin will begin to react as the HTC temperature increases, resulting in a lower carbon yield.

The carbon yield of HTC of carbohydrate-based food waste (rice and carrot were used as proxies) is low at 180°C, and increases as HTC temperature increased. This is due to a large portion of the organic matter being brought into the aqueous phase in HTC, and at low temperatures there is limited repolymerisation. As HTC temperature increases, more polymerisation occurs, more carbon precipitates out as biocoal, and therefore the carbon yield increases. In the case of rice, this trend is very strong, likely down to the high level of easily hydrolysable organic matter in rice such as carbohydrates, proteins, and lipids (Abdul-Hamid, Raja Sulaiman, Osman, & Saari, 2007).

4.7 The impact of feedstock on biocoal composition

4.7.1 Proximate analysis

As was the case with HTC yield, the feedstock used in HTC has an influence on how the composition of biocoal changes with temperature. The overall trends are the same as seen in HTC of miscanthus, but the magnitude and sensitivity of the changes vary between feedstock. As was seen with the carbon yield of HTC of waste biomass, the higher volatile matter and lower fixed carbon content in some waste biomass feedstocks like sewage and foodstuffs contain proteins and lipids which decompose under HTC conditions and do not significantly recombine in to aromatic carbon material that would generate fixed carbon (Kruse et al., 2016; Yue et al., 2017). This, in combination with low lignin content (Aidan M. Smith & Ross, 2019), results in the biocoal produced from these feedstocks having a high volatile matter content and low fixed carbon content. The effect of HTC temperature on the fixed carbon (on a dry, ash free basis) of HTC of various feedstocks can be seen in Figure 4.11. The effect of HTC temperature on the volatile matter will mirror this, as the two fractions will combine to make 100%. Only feedstocks where there were more than two HTC temperatures studied with the similar W/B ratios and residence times were used in Figure 4.11 so that a clear trend for the effect of temperature could be seen in each case. As has been shown in section 4.2.1, the effect of W/B ratio and residence time is negligible in comparison to the

effect of temperature, so any minor differences in these factors will not significantly effect the trends seen.

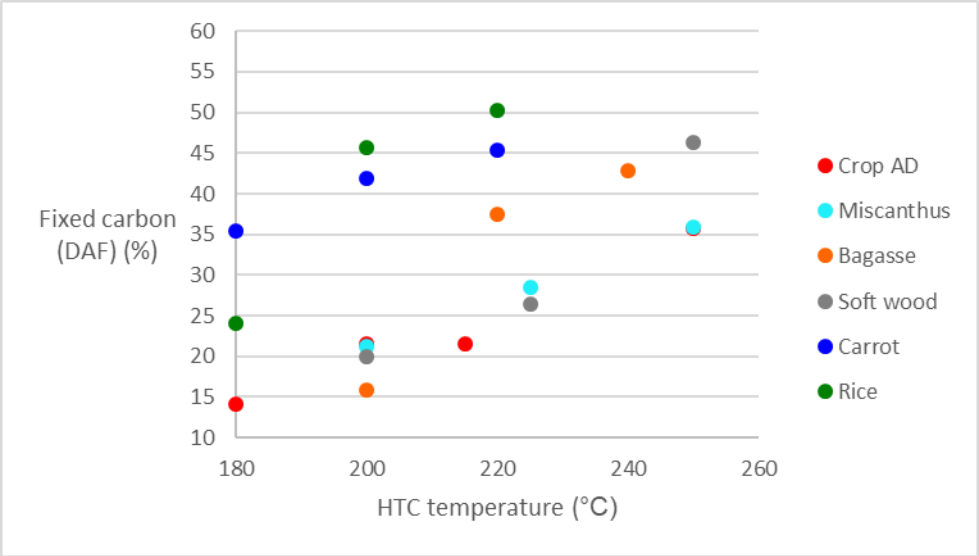

Figure 4.11 Impact of temperature on DAF fixed carbon content for various biomass feedstocks

There is a lesser variation in response to HTC temperature between feedstocks for fixed carbon content as was seen in carbon yield, with fixed carbon content increasing with increasing temperature independent of feedstock. The general increase in fixed carbon content can be attributed to increasing levels of aromatisation at harsher process conditions. Soft wood and rye anaerobic digestate biocoals have a small increase in fixed carbon with increasing temperature at low temperature HTC before increasing exponentially at higher temperatures. In the case of HTC of wood, this is likely due of cellulose decomposition initiating at higher temperature, as this does not occur significantly in low temperature HTC and cellulose degradation under HTC conditions involves significant levels of aromatisation (Falco et al., 2011). In HTC of rye anaerobic digestate this is likely also due to the labile organic content

being removed in digestion (Tambone et al., 2009), resulting in a biomass feedstock that does not react particularly strongly under low temperature HTC conditions. Both the biocoals generated from rye anaerobic digestate at 200 and 225°C have a DAF fixed carbon similar to that of untreated digestate, which provides further evidence to this explanation. The 180°C digestate has a DAF fixed carbon content below that of untreated digestate, which would indicate a balance between degradation of biomass and polymerisation; and at 180°C there is insufficient polymerisation to counteract the impact of decomposition.

HTC of rice and carrot results in biocoals with high fixed carbon contents, especially at temperatures above 200°C. At low HTC temperatures, this is the result of the large loss in reactive carbon (which forms volatile matter in proximate analysis), shown by a low carbon yield in Figure 4.10. This leaves behind a significant concentration of organic matter that forms fixed carbon in proximate analysis. As HTC temperature increases, the large concentration of organic matter in the process liquor begins to repolymerise and aromatize, resulting in a solid comprised of aromatic carbon. This results in the biocoal have a higher fixed carbon content. The sharp increase in rice HTC could be due to there being large volumes of organic matter in the liquor, which may polymerise at higher temperature HTC and precipitate as solid aromatic carbon.

As was stated in section 4.2.1, the ash content of biocoal can be higher or lower than that of the precursor biomass depending on the composition of the biomass ash. If a biocoal is made from biomass feedstocks with high silicon

content, like sewage sludge, the ash content of the biocoal can be significantly higher than that of the precursor (He et al., 2013; Aidan M. Smith et al., 2016). Biomass feedstocks like wood, miscanthus, and olive cake have appreciable concentrations of soluble alkali and alkaline earth metals in its ash (Reza, Lynam, et al., 2013), so biocoals produced from these will have a lower ash content.

4.7.2 Elemental analysis

The elemental analysis of various biocoals and their respective feedstock can be seen in Appendix 3. The trends in elemental composition with HTC temperature, residence time, and W/B ratio seen in HTC of miscanthus are consistent with other feedstocks. The elemental composition of the biocoal varies with feedstock. Carbon content of non-waste biocoal falls in the range between 50-75%, and the range for waste biomass is larger, between 34-73%. These ranges generally follow the initial carbon content of the feedstock biomass.

4.8 The impact of HTC parameters on liquid and gaseous products

4.8.1 Liquid products

4.8.1.1 Carbon content

HTC results in some carbon content of biomass being released as aqueous-soluble organic compounds, such as fatty acids, furans, phenols, furfural and HMF (Becker, Dorgerloh, Paulke, Mumme, & Nehls, 2014). The elemental analysis of various HTC process liquors can be seen in Table 4.11. There was not any variation in the W/B ratio or residence time, so the impact of these factors on the carbon content of the process liquor cannot be made. Although this is the case, temperature is likely to be the dominant factor, as has been seen previous results.

In the case of HTC of soft wood, the elemental composition of the process liquors are largely the same, partly due to the vast majority of the liquor being water. Other studies in literature have shown similar results, with process liquor total organic carbon (TOC) from pine (a softwood like that used in Brites wood pellets) remaining relatively stable with increasing HTC temperature, with the product distribution varying with process severity (Becker et al., 2014). This study also showed that with numerous other feedstocks, TOC increased between 190°C and 230°C, then decreased with increasing temperature above

230°C (Becker et al., 2014). Other studies have shown that TOC of HTC process liquor decreases with increasing HTC temperature (Erdogan et al., 2015b). The decrease in carbon content of the HTC liquor with increasing temperature would indicate that increasing HTC temperature results in the production of more solid carbon through repolymerisation, and more gaseous carbon as CO_2 from decomposition of organics (Fang et al., 2018; Libra et al., 2011; Stemann & Ziegler, 2011). The initial increase in TOC reported between 190 and 230°C (Becker et al., 2014) could be attributed to increased hemicellulose degradation and the cellulose degrading at the higher temperature, bringing much more carbon to the aqueous phase than what is released as solid carbon compounds or as CO_2. The carbon content of process liquor decreasing with increasing temperature can be seen in this study in the case of food HTC. This effect is more pronounced than what was seen in HTC of soft wood due to significantly more organic content being released by the food into the liquor due to the feedstocks being comprised of easily hydrolysable components (such as proteins and lipids). This is shown by the overall lower biocoal carbon yield in HTC of food at lower temperature.

Table 4.11 Elemental composition of HTC process liquor

Biomass	Temperature (°C)	W/B	Elemental composition of liquor (%)		
			C	H	N
Softwood	200	4	1.48	9.08	0.05
Softwood	225	4	1.40	9.77	0.05
Softwood	250	4	1.40	9.67	0.05
Rice (dried)	180	2	10.7	9.61	0.55
Rice (dried)	200	2	6.15	9.15	0.45
Rice (dried)	220	2	1.51	9.11	0.48
Rice (dried)	220	2	1.67	9.56	0.48
Mince (boiled)	180	2	7.2	10.5	2.86
Mince (boiled)	200	2	6.67	10.2	2.49
Carrot (dried)	180	6	2.62	10.3	0.52
Carrot (dried)	200	6	1.33	10.2	0.47
Carrot (dried)	220	6	0.94	10.2	0.57

The significant carbon content in the process liquor of food provides an intriguing oppurtunity for anaerobic digestion of HTC process liquor to recover the carbon content lost in the form of methane. For anaerobic digestion, the carbon to nitrogen ratio has to be 10:1 to 30:1 with the optimum being between 15:1 and 25:1 (Routeledge, 2013). The carbon content and carbon to nitrogen ratio of the process liquor from HTC of food can be seen in Table 4.12. The only instance of the carbon to nitrogen ratio being suitable for anaerobic digestion was in HTC of rice at low temperatures (180°C and 200°C). HTC of mixtures of foodstuffs could result in favourable ratios as well as well as an appreciable carbon content for anaerobic digestion.

Table 4.12 Carbon content and carbon to nitrogen ratio of HTC process liquor

Biomass	Temperature (°C)	Time (min)	W/B ratio	Carbon content (%)	Carbon: nitrogen
Rice (dried)	180	60	2	10.7	22.7
Rice (dried)	200	60	2	6.15	15.9
Rice (dried)	220	60	2	1.51	3.67
Rice (dried)	220	60	2	1.67	4.05
Mince (boiled)	180	60	2	7.2	3.15
Mince (boiled)	200	60	2	6.67	3.13
Carrot (dried)	180	60	6	2.62	5.88
Carrot (dried)	200	60	6	1.33	3.3
Carrot (dried)	220	60	6	0.94	1.92

To assess the potential for augmenting the overall energy yield of HTC through anaerobic digestion of the process liquor, the biomethane potential (BMP_{th}) was calculated for the process liquors from HTC of rice at 180°C and 200°C, as these possessed the required carbon to nitrogen ratio for anaerobic digestion. The BMP_{th} was calculated using both the Buswell equation (Tarvin & Buswell, 1934) (BMP_{thBW}) and Boyle equation (Boyle, 1976) (BMP_{thBO}). These equations are described in section 3.3.6, and the elemental analysis used for the calculations can be seen in Table 4.11. While the BMP represents a theoretical maximum, it is likely that this actual yield of methane would be high due to the organic material in the process liquor of HTC comprising of simple organic acids and sugars (Aidan M. Smith & Ross, 2016). The amount of energy generated (in the form of methane) from anaerobic digestion per kg of biomass fed into HTC was calculated using the $BMPth_{BO}$ as shown in section 3.3.8. The $BMPth_{BO}$ was used as this factored in nitrogen content. The results of these calculations can be seen in Table 4.13.

Table 4.13 Theoretical BMP of HTC process liquor and contribution of anaerobic digestion to the energy yield of HTC

Feedstock	Particle size	Temperature (°C)	Time (min)	W/B	BMP_{thBW} (ml CH_4/gVS)	BMP_{thBO} (ml CH_4/gVS)	Energy produced ($MJ/kg_{biomass}$)		Proportion of original energy content (BMP_{thBO}) (%)		Total energy yield (%)
							Methane	Biocoal	Methane	Biocoal	
Rice (dried)	Grains	180	60	2	92.5	88.7	0.14	3.5	0.9	23.5	24.4%
Rice (dried)	Grains	200	60	2	18.8	16.0	0.02	9.4	0.1	61.7	61.8%

Anaerobic digestion of the process liquor from HTC of rice at 180°C has a larger BMP_{th}, primarily due to the liquor having a significantly higher carbon content than the liquor produced at 200°C. This, in addition to a poor energy yield for the biocoal, results in methane production significantly enhancing the energy yield. Employing anaerobic digestion in this case was calculated to increase the energy yield by 3.7%. In HTC of rice at 200°C, methane production does not add much in terms of energy yield enhancement (0.2%) due to poorer BMP and a much higher energy yield in the biocoal. The combined energy yield of the two are lower than what has been reported previously in the literature. Augmenting HTC of seaweed with anaerobic digestion of the process liquor has been reported to have the potential to retain 80% of the original energy content of the seaweed (Aidan M. Smith & Ross, 2016). The discrepancy with this may be due to the anaerobic digestion calculation being performed on evaporated process water (which has a higher carbon content)(Aidan M. Smith & Ross, 2016), or composition differences between seaweed and rice.

4.8.1.2 Inorganic content

The concentration of inorganic elements in HTC process liquor of various HTC experiments can be seen in Table 4.14, and the ash composition of the feedstocks are shown in Table 4.15. There are significant concentrations of alkali and alkaline earth metals in the liquor, showing that HTC is effective in removal of these elements from biomass. Similar trends are shown here as were discussed in section 4.2.1 in terms of overall removal of inorganic

elements. The concentration of each inorganic element recovered depends on the feedstock processed, due to the composition of the feedstock ash (Aidan M. Smith et al., 2016). The majority elements removed in HTC of softwood, miscanthus, and olive cake are calcium, sodium, and potassium respectively as these are the major components of their ash. The degree of removal of selected alkali/alkaline earth metals is further discussed in section 5.3.

Table 4.14 Alkali metal concentration in HTC process liquors

Biomass	Temperature (°C)	Residence time (min)	W/B	Mass of element in process liquor (mg/L)			
				Na	K	Mg	Ca
Softwood	250	60	6	149	162	0	921
Miscanthus	200	60	6	1725	808	77	206
Miscanthus	200	60	4	1461	603	58	220
Miscanthus	200	240	4	2102	1220	45	398
Miscanthus	200	240	6	1517	896	72	1126
Miscanthus	225	150	5	2125	1340	40	963
Miscanthus	250	60	4	1461	603	58	220
Miscanthus	250	240	4	2434	1430	35	391
Miscanthus	250	60	6	1141	578	30	1008
Miscanthus	250	240	6	1615	980	67	1271
Olive cake	200	60	6	204	3796	239	326

Table 4.15 Ash composition of biomass feedstocks

Biomass	Ash content (%)	Concentration of inorganic element in biomass (mg/kg)					
		Na	Mg	Si	K	Ca	Fe
Soft wood	0.6	68.3	110	60.4	923	1700	100
Miscanthus	7.86	12600[1]	582	10700	5790	4130	802
Olive cake	9.5	N/A[2]	2510	3570	32000	10000	867

[1]Value could not be adjusted as the UoN XRF analyser detected no sodium in the olive cake ash used as the reference ash, see section 3.2.9
[2]Concentration of sodium was too low to be detected

4.8.2 Gaseous products

The gas produced in selected HTC experiments, on a nitrogen free basis, can be seen in Table 4.16. The vast majority all of the gas generated by HTC is CO_2, due to the relatively mild conditions. The volume of gas generated increases exponentially with increasing HTC temperature, as does the concentration of hydrogen, carbon monoxide, and hydrocarbon gas in the product. This matches the trend seen in carbon content of process liquor decreasing with increasing HTC temperature, as more carbon is driven into the gaseous and solid phases.

The volume and composition of gas produced varies with varying feedstock. HTC of miscanthus produces more total gas as well as higher concentrations of carbon monoxide and lower concentrations of hydrocarbons than HTC of soft wood. The presence of carbon monoxide in the product gas of miscanthus HTC suggests the presence of the water gas shift reaction.

Table 4.16 Gas production and composition of HTC of various feedstocks (N_2-free basis)

Biomass	Temperature (°C)	Generated gas (ml)	Gas composition (%)			
			H_2	CO_2	CO	Hydrocarbon
Soft wood	200	49	0.2	99.4	0.2	0.3
Soft wood	225	112	0.2	99.5	0.0	0.3
Soft wood	250	301	2.3	96.5	0.4	0.7
Miscanthus	200	107	0.2	96.9	2.8	0.1
Miscanthus	225	180	0.2	95.6	4.1	0.1
Miscanthus	250	444	0.9	90.6	8.3	0.6
Sewage	200	72	0.0	98.9	0.8	0.3

4.9 Conclusions

1. HTC temperature has the primary impact on the yield of biocoal. Increasing HTC temperature decreased the yield. Particle size of biomass had a small effect on the carbon yield of biomass, with decreasing particle size increasing the yield.

2. Temperature also has the largest impact on the composition of biocoal. Increasing HTC temperature lowered the moisture content and volatile matter content, while increasing the fixed carbon content of biomass. The ash content of the biocoal was higher or lower than that of the feedstock dependent on the composition on the ash.

3. Residence time and W/B ratio had much weaker effects on the yield and composition of biocoal, and in most cases were found to be statistically insignificant within the DoE data set. Residence time had a statistically significant effect on the degradation of volatile matter from biomass, with increasing residence time resulting in a biocoal with less volatile matter on an absolute basis.

4. W/B ratio did not have any statistically significant effect in the range studied in the DoE. When W/B was increased to extremely high ratios, a detrimental effect on the yield was seen.

5. Increasing HTC temperature resulting in a biocoal with lower O:C and H:C atomic ratios, as more hydrogen and oxygen are lost through dehydration and decarboxylation reactions. Increasing residence time had the a similar but lesser effect when the HTC temperature was high. HTC at high temperatures produced a biocoal with similar elemental composition to lignite.

6. HTC temperature was also found to be the key factor in energy yield and energy densification of biomass. Increasing HTC temperature resulted in a lower energy yield but a more energy dense biocoal. The HTC temperature of 225°C provided a good compromise of these two factors, with energy yield decreasing significantly beyond this temperature. Increasing W/B ratio was seen to have a detrimental effect on the energy yield at high HTC temperature.

7. The yield of HTC and composition of the feedstock has a significant effect on the results of HTC. Waste biomasses have a wider variation in carbon yield than non-waste biomass. This is due to the biochemical composition of the feedstocks. This also impacts how the yield of HTC changes with varying HTC temperature. Although the composition of the biocoals vary between feedstock, the trends were generally consistent with respect to varying the process conditions.

8. HTC of some feedstocks results in a liquor that has an appreciable carbon content. In general, increasing HTC temperature decreases the carbon content in the liquor, but some cases were seen where the carbon content was unchanged by increasing HTC temperature. The decrease in carbon content is hypothesised to be due to increased repolymerisation of soluble organic compounds at higher HTC temperatures resulting in carbon joining the solid phase.

9. Anaerobic digestion of the process liquor of HTC could have significant potential to augment the energy yield of HTC. Anaerobic digestion of process liquor generated from HTC of rice at 180°C was calculated to have the potential to increase the energy yield by 3.7%. At higher HTC temperature where more energy was retained in the biocoal, the relative contribution of anaerobic digestion was much weaker.

10. The gas generated by HTC mostly consists of carbon dioxide, with negligible concentrations of carbon monoxide, hydrogen, methane, and other hydrocarbons. The volume of gas generated increases exponentially with increasing HTC temperature, as does the concentration of hydrogen, carbon monoxide, and hydrocarbon gas in the product. The volume and composition of gas produced varies with varying feedstock.

Chapter 5 The impact of HTC on char reactivity of biomass, generating a coal-equivalent fuel

As was discussed in Chapter 2, biocoal has potential application as a coal replacement in power generation, with many of the current institutions who produce biocoal as a process for turning waste biomass into fuel for power generation (Antaco, n.d.) and in industrial applications such as lowering the energy requirement for cement production or waste incineration (TerraNova, n.d.-b). In order for biomass to be an efficient coal replacement in both combustion and industrial applications, it must have similar properties to coal, which is not the case with untreated biomass (Nunes, Matias, & Catalão, 2014). Biomass is much more reactive than coal (Vassilev et al., 2015). The char reactivity of a fuel is a large factor in determining the heat release and flame stability during combustion (alongside volatile matter content), which results in biomass combusting in a much different manner to coal (Lu, Kong, Sahajwalla, & Harris, 2002). This is described in section 2.3.5, where it was shown that untreated miscanthus showed a two-stage combustion profile, with a lower char initiation temperature than that seen in coal (Aidan Mark Smith et al., 2018).

This study was conceived due to the known catalytic effect of alkali and alkaline earth metals on combustion (Jones, Darvell, Bridgeman, Pourkashanian, & Williams, 2007), and the significant removal of these elements by HTC. Therefore, if it was found that alkali and alkaline earth metal content is the key property influencing char reactivity, this would provide HTC with another

advantage over pre-treatments that do little to remove these elements, such as torrefaction. Particular attention was to be made to the concentration of potassium, sodium, calcium, and magnesium in the fuels investigated, as these have been shown to catalyse combustion (Jones et al., 2007; Yi et al., 2018). Char surface area and fuel composition were two further properties that were identified as having the potential to influence the char reactivity of a fuel. As such, these were also investigated to develop a full understanding on the mechanism on the effect of HTC on the char reactivity of biomass.

In this chapter, the entirety of data needed to discuss the char burnout of TGA and DTF chars will be laid out before in-depth discussion of the trends. This is so that the full data set can be effectively discussed allowing for identification of the over-arching trends.

5.1 Materials and methods

Biocoals were produced according to the procedure described in section 3.1.2. The process parameters used are displayed in Table 5.1. Various biomass feedstocks were used to provide different initial concentrations alkali/alkaline earth metal content, so that different difficulties of feedstock would be investigated. In particular, the removal of sodium, potassium, magnesium, and calcium was studied. Soft wood pellets were used as a biomass feedstock with extremely low alkali and alkaline earth metal content, and olive cake was selected as a biomass containing extremely high levels of these elements.

Table 5.1 HTC process parameters used to produce the four biocoals

Biomass	Temperature (°C)	W/B ratio	Residence time (min)
Bagasse	200	4.1	60
Miscanthus	200	4:1	60
Olive cake	200	6:1	60
Olive cake	225	6:1	60
Soft wood	200	4:1	60
Soft wood	225	4:1	60
Soft wood	250	4:1	60

Torrefaction was chosen as a comparison for HTC as does little to affect the alkali/alkaline earth metal content of biomass (Hidayat et al., 2017), and is utilised to create a solid fuel for thermal applications (Acharya et al., 2015). Torrefaction was performed in a horizontal tube furnace as described in section 3.1.3, at a temperature of 300°C and a residence time of 1 hour. The torrefaction was performed under a temperature near the maximum of the torrefaction range so that a large change in biomass composition through torrefaction, so this factor could be investigated effectively.

Acid leaching was employed to remove as much of the alkali and alkaline earth metal content as possible. The method used for acid leaching is described in 3.1.4.

Wood pellets were used as the feedstock for torrefaction and olive cake was used for acid leaching. The wood pellets were chosen for torrefaction so that the best-case biomass (in terms of alkali and alkaline earth metal content) would be compared between HTC and torrefaction. Olive cake was chosen for acid leaching so that a large difference in alkali and alkaline earth metal concentration could be investigated using the same feedstock.

A high-volatile bituminous coal was acquired for comparison with the biomass derived fuels, originating from the Cerrejón mine in Colombia.

High heating rate chars were generated from all the samples using a drop tube furnace (DTF), the method of which is detailed in section 3.1.8. This simulates the first stage of combustion, devolatilisation under high heating rates. The particle size of the feedstock was <75 µm, the furnace temperature was 1300°C, and the residence time was 600ms.

All of the samples were ground so that they could pass through a 75 µm mesh sieve. This was done to ensure that the intrinsic char reactivity of the fuels was being studied, as it has been shown that particle size has a significant impact on the control regime and observed activation energy of coal burnout (Le Manquais et al., 2009). The larger surface area of samples with smaller particle size means that a large portion of the sample is in contact with air, meaning that diffusion control is absent. The samples which were sufficient in quantity

were ground using a ball mill, those which were not were ground using a pestle and mortar.

The proximate analysis and char reactivity of the samples were analysed using TGA, as described in section 3.2.1.

5.2 Yield and proximate analysis

The yield of the HTC experiments on an as received (AR) and dry-ash-free (DAF) basis are listed in Table 5.2. These values and are close to those found in the literature. The wood HTC yields at 200°C and 225°C match in a study of the effects of process parameters on the HTC of coniferous wood chips, where HTC at 200°C and 220°C for 3 hours with a W/B ratio of 6 gave mass yields of approximately 68 and 63%, respectively (Sermyagina et al., 2015). In addition to this, the yield for HTC of low- and high-quality wood chips at an initial temperature of 220°C, followed by a 4 hour residence time at 180°C, was reported as 60.5% and 64.4%, respectively (Oliveira et al., 2013). Another study states the yield range for HTC of poplar wood and olive residues between 180-230°C being 51.9-89.9% and 49.0-75.4%, respectively (Nizamuddin et al., 2017). This matches what is seen in Table 5.2, with the yield values being within the stated range, and with HTC of olive cake having a lower yield than wood. The yield of miscanthus HTC on an dry basis has been reported as between 73-76%, which is slightly higher than what is reported in this study, but is fairly close (Aidan Mark Smith et al., 2018). The decrease in mass yield seen with increasing

HTC temperature is also consistent with the literature (Kang et al., 2012; Nizamuddin et al., 2017; Sermyagina et al., 2015).

Table 5.2 Mass yield of HTC experiments producing biocoals for char reactivity analysis (AR and DAF basis)

Biomass	Process	Temperature (°C)	Mass yield (AR[2]) (%)	Mass yield (DAF[3]) (%)
Bagasse	HTC	200	68.3[1]	67.0
Miscanthus	HTC	200	63.4[1]	70.4
Olive cake	HTC	200	51.3 ± 2.0	56.8
Olive cake	HTC	225	47.1 ± 0.8	51.7
Soft wood	HTC	200	66.3 ± 3.0	68.5
Soft wood	HTC	225	65.7 ± 0.9	68.7
Soft wood	HTC	250	53.6[1]	56.7
Soft wood	Torrefaction	300	35.8[1]	37.5

[1]Experiment was not run in triplicate so error could not be established

[2]AR – As received basis

[3]DAF – Dry, ash free basis

Torrefaction of soft wood at 300°C has a much lower yield than the HTC experiments. This mass yield of 35.8% found in the torrefaction experiment was lower than expected, with torrefaction of waste wood using similar method producing a mass yield of 44.42% at a temperature of 300°C over a residence time of 50 minutes (Poudel, Karki, & Oh, 2018). This indicates that the conditions used in the torrefaction were harsher than expected. This could be due to the temperature overshooting before settling at the desired isothermal

temperature of 300°C. This could also be due to a longer residence time being used in the torrefaction than in the experiment described above. The torrefaction used for this study was 60 minutes (10 minutes longer than in the study described in the literature), and the heating and cooling rates could be lower. This would result in the biomass being exposed to high temperatures for much longer in the torrefaction experiment performed for this study. The heating and cooling rates were not published for the experiment used for comparison (Poudel et al., 2018), so this cannot be validated. The residence time can have a significant influence on the mass yield of torrefaction at high temperatures. A large drop in mass yield in torrefaction of beech wood at 300°C from 30 minutes to 150 minutes has been reported, with the yield dropping from slightly under 60% to just above 35% (Gucho, Shahzad, Bramer, Akhtar, & Brem, 2015). This is a result of increasing cellulose decomposition at high temperature torrefaction with increasing residence time (Gucho et al., 2015). The mass yield shown at torrefaction at 300°C over 150 minutes is similar to that seen in the torrefaction experiment performed here. This further indicates that the conditions in the experiment performed may have been harsher than expected. This result will not have a significant impact on the comparison to HTC and acid leaching, as the torrefied biomass sample used still represents torrefaction, albeit torrefaction under conditions slightly harsher than the traditional range (200-300°C) (Libra et al., 2011). One of the aims of the study was to compare HTC to high temperature torrefaction (to maximise the change in composition of the biomass), therefore the comparisons made in this study will still be valid.

The proximate analysis of the fuels is shown in. As was described in section 4.4, the moisture and volatile matter of biocoal is lower than that of the biomass feedstock, and the fixed carbon content is higher, which results in an increase in the higher heating value (HHV) of the biomass (Nhuchhen & Afzal, 2017).

In this study, HTC is extremely effective in removing inorganic material from the biomass, with all of the biocoals having ash contents significantly lower than their respective untreated biomass feedstock. At lower temperatures, increasing the HTC temperature decreased the ash content, but at high HTC temperatures the ash content increases with increasing temperature. This is due to a combination of the polarity of water decreasing with increasing temperature (Aidan M. Smith et al., 2016), and increased decomposition of the organic compounds in the biomass. Torrefaction does not remove inorganic content from the biomass significantly, resulting in a higher ash content in the torrefied wood than in the untreated wood.

Table 5.3 Proximate analysis of the fuels

Sample	Moisture (AR[2]) (%)	Volatile matter (DAF[3]) (%)	Fixed carbon (DAF[3]) (%)	Ash (AR[2]) (%)
Soft wood	5.4	86.1	13.9	0.61
Torrefied soft wood	3.3	39.2	60.8	1.2
Soft wood biocoal (200°C)	2.6	82.1	17.9	0.22
Soft wood biocoal (225°C)	1.5	75.1	24.9	0.12
Soft wood biocoal (250°C)	2.0[1]	53.7	46.3	0.33
Olive cake	6.3	81.6	18.4	9.5
Acid leached olive cake	1.8	79.6	20.4	3.0
Olive cake biocoal (200°C)	1.3	75.1	24.9	5.5
Olive cake biocoal (225°C)	1.7	73.3	26.7	5.0
Bagasse	2.8[1]	87.5	12.5	10.7
Bagasse biocoal	2.3[1]	84.2	15.8	5.3
Miscanthus	5.1[1]	76.5	23.5	7.9
Miscanthus biocoal	2.1[1]	82.8	17.2	2.0
Bituminous coal	3.4[1]	40.8	59.2	5.2

[1]Determined by TGA and not gravimetrically

[2]AR – As received basis

[3]DAF – Dry, ash free basis

The biocoals have compositions between that of their respective untreated biomass feedstock and the bituminous coal investigated, but are not particularly close to the coal in terms of volatile matter and fixed carbon content. The torrefied wood is much more similar to the bituminous coal in this

regard. This is due to the harsher conditions used in the torrefaction degrading more of the volatile matter.

The volatile matter and fixed carbon content of the torrefied wood do not match what was expected, being lower and higher than expected values respectively. This, alongside the yield data described above, indicates that the conditions may have been harsher than what was set out in the methodology (section 3.1.3). Torrefaction of beech wood at 300 for 30 minutes has been shown to produced torrefied wood with a volatile matter content of approximately 60% on a dry basis (61% on a DAF basis, with an ash content of 1.5% (dry basis)) (Gucho et al., 2015). Slightly harsher conditions were used in the torrefaction performed for char reactivity analysis, as the residence time was one hour. It was shown that longer residence times result in a lower torrefaction yield (Gucho et al., 2015), so it would follow that the volatile matter of the torrefied wood here would be less, but the degree to which this is the case was not expected, and indicates that there may have been a spike in temperature in the HTF after ramping to the desired process temperature. As was stated before, one of the aims of the study was to use high temperature torrefaction as the comparison to HTC (to maximise the change in composition of the biomass), therefore the comparisons made in this study will still be valid.

The composition of the acid leached olive cake is similar to olive cake in terms of volatile matter and fixed carbon, indicating that acid leaching has not greatly effected the composition of the olive cake in terms of the major components

of the biomass. Acid leaching removed much of the inorganic content of the olive cake, proving to be more effective at this than HTC at both 200°C and 225°C.

5.3 XRF analysis

The effect of HTC temperature on the extent of removal of total ash and alkali/alkaline earth metals is shown in Table 5.4. It can be seen that HTC is very effective in removing potassium, with over 95% removal in all cases apart from HTC of bagasse. The majority of sodium was also removed in all cases. The ease of removal of these elements by HTC has been reported previously (Aidan M. Smith et al., 2016). In HTC of soft wood, sodium removal was seen to increase when the HTC temperature was increased from 200°C to 225°C, and then decrease when the temperature was further increased to 250°C. This could be due to the further lowering polarity of water, or could be due to sodium being adsorbed into the biocoal surface due to surface functionality increasing with increasing temperature (Aidan M. Smith et al., 2016).

Calcium and magnesium removal was also effective in HTC of soft wood, miscanthus, and bagasse. The extent of calcium and magnesium removal from miscanthus in these experiments (86% and 96%, respectively) is also seen in the literature, with another study showing very similar magnesium and calcium removal from miscanthus, showing approximately 90% removal of these elements through HTC at 200°C (Reza, Lynam, et al., 2013). The efficacy of removal of these elements from these feedstocks indicates that they are present in the feedstocks primarily in the form of ionic salts, which are easily removed (Aidan M. Smith et al., 2016). In the case of HTC of olive cake, less effective calcium and magnesium removal is seen. This could be due to higher

proportions of these elements being incorporated with the biomacromolecules in the biomass (Aidan M. Smith et al., 2016). The increased removal of these elements at the higher HTC temperature of 225°C also points to this, as further degradation of the biomacromolecules would release higher proportions of these elements to the process liquor.

Table 5.4 Extent of total ash and alkali/alkaline earth metal removal by HTC

Sample	HTC temperature (°C)	Total ash removal (%)	Alkali/alkaline earth metal removal (wt%)			
			Na	Mg	K	Ca
Soft wood	200	76	81	82	95	81
Soft wood	225	87	89	93	97	92
Soft wood	250	71	84	95	97	98
Olive cake	200	70	N/A[1]	54	98	34
Olive cake	225	75	N/A[1]	66	98	41
Bagasse	200	66	N/A[1]	86	86	87
Miscanthus	200	84	99	96	99	86

[1]Concentration of sodium was too low to be detected by XRF

The concentration of selected inorganic elements in the sample ashes is shown in Table 5.5. The concentration of the inorganic elements is displayed as milligrams of ash per kilogram of sample, so that the absolute values of alkali and alkaline earth metal concentration with respect to the mass of the sample combusted could be used when discussing the char reactivity of the samples.

Table 5.5 Total ash content and concentration of selected inorganic elements in the fuel ash

Sample	Total ash content (%)	Concentration of inorganic elements in sample (mg/kg)					
		Na	Mg	Si	K	Ca	Fe
Wood	0.6	68.3	110	60.4	923	1700	100
Torrefied wood	1.2	156	213	128	3630	2210	117
Wood biocoal (200°C)	0.2	20.0	29.3	153	70.6	496	80.8
Wood biocoal (225°C)	0.1	11.2	12.0	50.3	42.2	209	27.8
Wood biocoal (250°C)	0.3	21	9.9	93.6	59.7	68.7	20.1
Olive cake	9.5	N/A[1]	2510	3570	32000	10000	867
Acid leached olive cake	3.0	135	1880	6840	471	207	531
Olive cake biocoal (200°C)	5.5	N/A[1]	2220	5610	1370	13000	1360
Olive cake biocoal (225°C)	5.0	N/A[1]	1810	4030	1570	12600	1230
Bagasse	10.7	0.00[2]	856	25400	3200	2600	5170
Bagasse biocoal (200°C)	5.25	131[2]	179	14700	672	504	919
Miscanthus	7.86	12600[2]	582	10700	5790	4130	802

Miscanthus biocoal (200°C)	2.04	149[2]	40.8	4670	124	920	1660
Bituminous coal	5.2	414	367	10200	1040	1090	3600

[1]Concentration of sodium was too low to be detected

[2]Value could not be adjusted as the UoN XRF analyser detected no sodium in the olive cake ash used as the reference ash, see section 3.2.9

Wood biocoal has significantly lower concentrations of alkali and alkaline earth metals in comparison to all the other biocoals produced. This is due to the low initial concentration of alkali and alkaline earth metals in the biomass feedstock coupled with the effectiveness of HTC in removing alkali and alkaline earth metals. The significant differences in ash composition between these biocoals will allow for detailed discussion on the impact of the concentration of alkali and alkaline earth metal concentration on the reactivity of biocoals.

The wood biocoal produced at 225°C has a lower concentration of alkali and alkaline earth metals than the wood biocoal produced at 200°C as a result of the increased removal of these species being greater than the increased degradation of organic matter. The wood biocoal produced at 250°C has a higher concentration of sodium and potassium than wood biocoal produced at 225°C. This is due to there being further degradation of the organic fraction at 250°C, without any increase in the removal of these inorganic elements. This is exacerbated in the case of sodium by the removal of this element being less effective at 250°C. Calcium and magnesium concentrations were seen to be lower in the wood biocoal produced at 250°C, as the removal of these elements was greater at this temperature.

In the case of olive cake biocoal, both the 200°C and 225°C biocoals have similar concentration of alkali and alkaline earth elements, despite the removal of these species being greater at the higher temperature. This is due to the

significant increase in decomposition of organic matter from the olive cake at 225°C, shown by the sharp decrease in DAF yield seen in Table 5.2.

Torrefaction is not particularly effective in removing alkali and alkaline earth metals (Hidayat et al., 2017). In the torrefaction performed for this study, all of the inorganic elements investigated were seen to increase in concentration. This results in significant concentrations of alkali and alkaline earth metals in the torrefied wood.

Acid leaching was very effective in reducing the alkali and alkaline earth metal content of the olive cake. Acid leached olive cake had much lower potassium and calcium concentrations than the olive cake biocoals, alongside a comparable magnesium concentration.

5.4 Textural characterisation

The textural characterisation of the drop tube chars generated from the soft wood and olive cake fuels is shown in Table 5.6. These chars are generated under an extremely high temperature and heating rate, which results in chars with very high surface area (Le Manquais et al., 2009). The surface area of the DTF chars are similar to previously reported data, with DTF chars of eucalyptus, willow, and their torrefied analogues showing surfaces area in the same order of magnitude as those reported in Table 5.6 (McNamee, Darvell, Jones, & Williams, 2015). The surface areas of the DTF chars produced in this study are

slightly higher, possibly due to the higher devolatilisation temperature used (the DTF devolatilisation from the literature was performed at a temperature of 1100°C, rather than 1300°C) (McNamee et al., 2015).

Table 5.6 Textural characterisation of the DTF chars

Sample	BET surface area (m^2/g)	Micropore surface area (m^2/g)	Micropore volume (cm^3/g)
Wood DTF char	125 ± 8	91	0.036 ± 0.001
Torrefied wood DTF char	335 ± 1	475	0.19 ± 0.00
Wood biocoal (200°C) DTF char	150 ± 2	189	0.075 ± 0.000
Wood biocoal (225°C) DTF char	219 ± 2	268	0.11 ± 0.00
Olive cake DTF char	78 ± 1	91	0.037 ± 0.001
Acid leached olive cake DTF char	172 ± 1	230	0.092 ± 0.001
Olive cake biocoal (200°C) DTF char	97 ± 1	110	0.044 ± 0.000
Olive cake biocoal (225°C) DTF char	113 ± 0	145	0.058 ± 0.001
Coal DTF char	104 ± 7	61	0.025 ± 0.000

The DTF chars generated from the untreated wood and wood biocoals have higher surface areas than their olive cake analogues. This is likely due to the olive cake being compressed during processing, resulting in a dense feedstock with a low surface area. The wood pellets were not compressed to the same extent in pelleting, so retain much of the natural structure and spacing of wood biomass.

Torrefaction, acid leaching, and HTC result in higher surface area DTF chars. This could be due to processing altering the porosity of the samples, through decomposition of some of the organic content. This is pointed to by the DTF chars made from pre-treated samples all showing a larger micropore volume than their respective untreated feedstock.

A similar increase in surface area of biomass through torrefaction has been reported in torrefaction of poplar particles at 300°C over 9.6 minutes (Granados, Basu, Chejne, & Nhuchhen, 2017), and when miscanthus was torrefied at 250°C and 270°C for 30 minutes (Xue et al., 2014). This was attributed to the increased expulsion of gaseous products producing pores in the biomass (Xue et al., 2014). Although examples of increased surface area in torrefied biomass have been reported, torrefaction has also been shown to produce a sample with a smaller surface area than the untreated feedstock. Torrefaction of poplar particles at torrefaction temperatures of 280°C and at

300°C for short residence times exhibited a decrease in surface area was seen (Granados et al., 2017). This was hypothesised to be due to blockage of pores through melted biomass components which did not decompose under the less harsh conditions (Granados et al., 2017). Torrefied willow and eucalyptus produced at 270-290°C over 30 minutes were also reported to have a smaller surface area than their untreated analogues (McNamee et al., 2015). Any components of biomass that would melt to block pores under torrefaction conditions would fully decompose under the harsh conditions of DTF devolatilisation, so any blockages by these components would be completely removed, and the underlying porosity of the biomass material would be evident. Torrefaction develops porosity in biomass (Xue et al., 2014), which would result in an increase in surface area. This is what is shown in Table 5.6.

Biocoals have been reported previously as having a higher surface area than their respective untreated biomass. HTC was seen to greatly increase the surface area of palm shell (Nizamuddin et al., 2016). Increasing HTC temperature increasing the surface area of biocoal has also been reported (Parshetti, Kent Hoekman, & Balasubramanian, 2013), although there have also been cases where the opposite effect was seen (Nizamuddin et al., 2016). Blockage of pores could be the cause of the reduction in surface area. This phenomenon has been reported in the production of activated carbon from biocoal (Román et al., 2013). DTF devolatilisation conditions would decompose any organic matter causing a blockage, showing the underlying porosity of the biocoal.

Water-leaching and acid-leaching of rice husk has also been shown to increase the surface area of the sample. (W. Xu et al., 2018) Hydrolysis of biomass in these treatments was considered the cause of this (W. Xu et al., 2018).

Torrefaction of the wood pellets increased the surface area significantly more than HTC. The harsher conditions of the torrefaction treatment in comparison to the HTC experiments is a likely contributor to this, producing a greater porosity and therefore a greater surface area. DTF chars produced from high-temperature biocoals possessing a higher surface area than those produced from low-temperature biocoals also points to this.

The coal DTF char has a surface area lower than that of wood DTF char, so HTC and torrefaction of wood makes this difference much larger. Olive cake DTF char has a lower surface area than that of the coal DTF char; with HTC resulting in olive cake biocoal DTF chars having similar surface areas to the coal DTF char.

5.5 Char reactivity analysis

5.5.1 Char burnout analysis of TGA and DTF chars

The TGA chars were produced by devolatilisation at 700°C, resulting in the reactive fractions of these samples (hemicellulose, cellulose, lipids, and

proteins) degrading (X. Wang, Sheng, & Yang, 2017; Yang et al., 2007). The carbonaceous material remaining will consist mainly of remaining lignin content (as lignin degrades between 160–900°C under pyrolysis conditions (Yang et al., 2007)), as well as any solid aromatic carbon generated from the reactive (volatile) fractions that had reacted to join the solid phase through processing (for example repolymerisation in HTC (Aidan M. Smith & Ross, 2019)).

The burnout of the TGA chars produced from untreated wood, torrefied wood, wood biocoals (produced at 200°C, 225°C, and 250°C), and the bituminous coal are compared in Figure 5.1. The t_{90} values for their combustion can be seen in Table 5.7. It can be seen that HTC greatly lowers the reactivity of the soft wood. Increasing HTC temperature to 225°C further decreases the reactivity of the wood biocoal, but increasing the temperature further to 250°C does not have the same magnitude of change. The soft wood biocoal produced at 250°C is similar in reactivity to the soft wood biocoal produced at 225°C (the averaged burnout curves are nearly completely superimposed on one another), although the error in the burnout of the 250°C biocoal means that significant conclusions cannot be drawn. The soft wood biocoals had char reactivity similar to that of the high volatile bituminous coal. Biocoals have been reported previously to have lower reactivity than untreated biomass. HTC of miscanthus being shown to increase the temperature at which the volatile burn peak was found (with the effect being greater at higher HTC temperatures) (Aidan Mark Smith et al.,

2018), and coconut fibre biocoal was found to have a lower reactivity to untreated coconut fibre (Liu et al., 2013).

Torrefaction of wood slightly lowers the reactivity of soft wood, but the effect is much smaller than what is seen in HTC. Torrefaction has been reported previously to reduce the char reactivity of willow and eucalyptus, with increasing torrefaction temperature further decreasing the reactivity (McNamee et al., 2015).

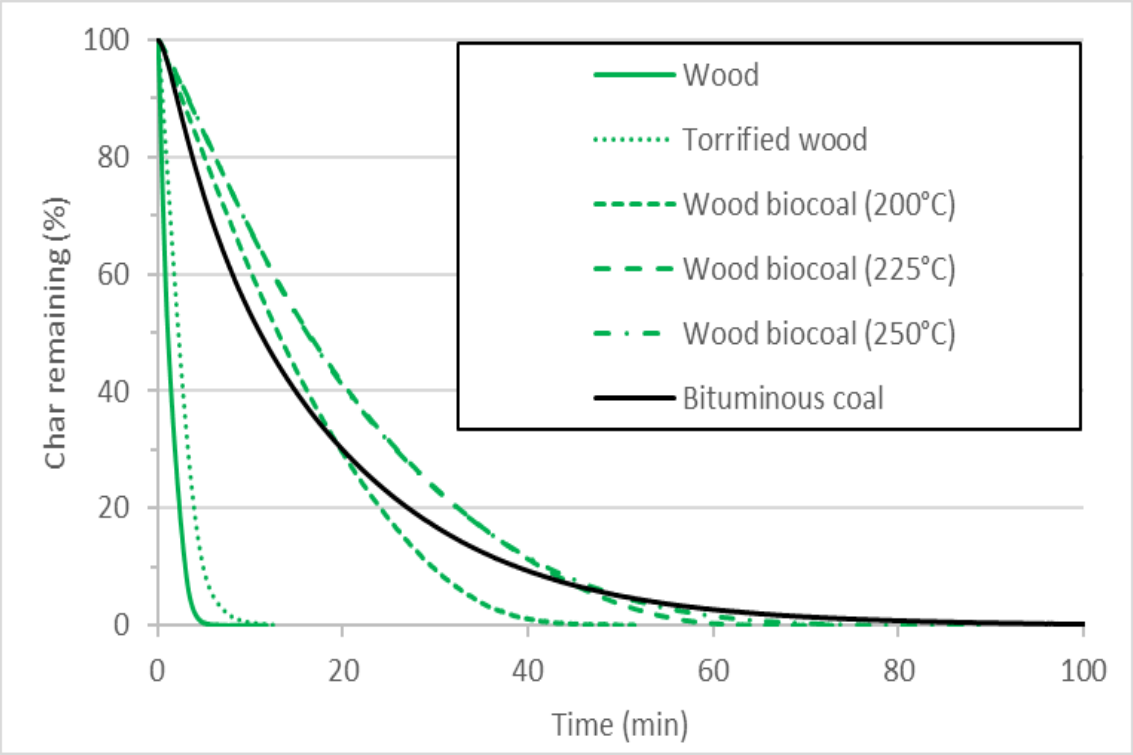

Figure 5.1 Char burnout comparison of wood, torrefied wood, wood biocoals, and bituminous coal (0-75 μ m particle size)

Table 5.7 90% char burnout times (t_{90}) (between 5-95% char consumption) for wood, torrefied wood, wood biocoals, and bituminous coal (0-75 μ m particle size)

Sample	t_{90} (95-5%) (min)
Wood	3.2 ± 1.1
Torrefied wood	5.6 ± 0.8
Wood biocoal (200°C)	32.2 ± 1.1
Wood biocoal (225°C)	45.7 ± 3.0
Wood biocoal (250°C)	46.7 ± 11.2
Bituminous coal	44.4 ± 3.0

The burnout of the TGA chars produced from untreated olive cake, acid leached olive cake, olive cake biocoals (produced at 200°C and 225°C), and the bituminous coal studied are compared in Figure 5.2. The t_{90} values for their combustion in Table 5.8. The char reactivity of olive cake biocoal is lower than that of untreated olive cake, but the reduction is not as great as what was seen in HTC of wood in Figure 5.1. The resultant biocoals have a reactivity that is in between that of the untreated olive cake and the bituminous coal. As with HTC of wood, increasing the HTC temperature results in a less reactive boicoal. Acid leaching of the olive cake results in a fuel which is less reactive than the coal.

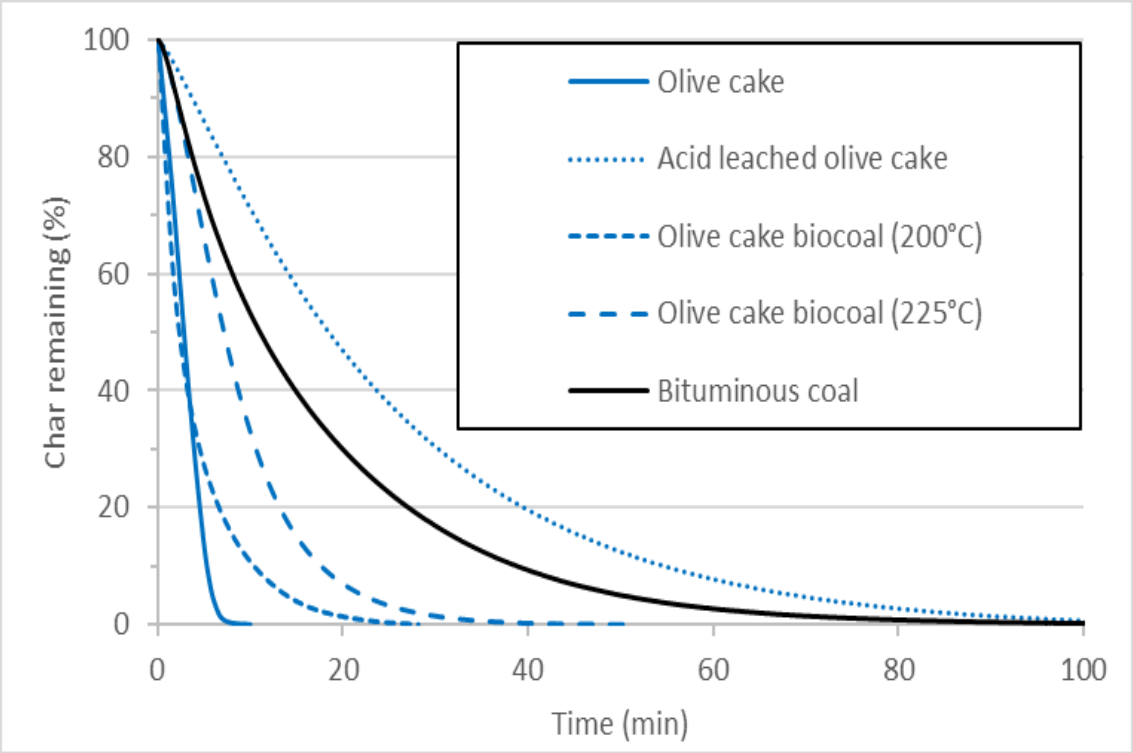

Figure 5.2 Char burnout comparison of olive cake, acid leached olive cake, olive cake biocoals, and bituminous coal (0-75 µm particle size)

Table 5.8 90% char burnout times (t_{90}) (between 5-95% char consumption) of olive cake, acid leached olive cake, olive cake biocoals, and bituminous coal (0-75 µm particle size)

Sample	t_{90} (95-5%) (min)
Olive cake	5.3 ± 1.6
Acid leached olive cake	66.5 ± 5.5
Olive cake biocoal (200°C)	13.5 ± 5.1
Olive cake biocoal (225°C)	20.9 ± 0.9
Bituminous coal	44.4 ± 3.0

The burnout of TGA chars produced from bagasse, bagasse biocoal (produced at 200°C), and the bituminous coal are compared in Figure 5.3; and those produced from miscanthus, miscanthus biocoal (produced at 200°C), and the

bituminous coal in Figure 5.4. The t_{90} values for the combustion of these can be seen in Table 5.9 and Table 5.10, respectively. As with HTC of olive cake, HTC of bagasse and miscanthus results in a biocoal with a char reactivity that is intermediate between that of the untreated biomass feedstock and coal. The reduction in char reactivity is significantly less than what is seen in wood HTC. The olive cake, bagasse, and miscanthus biocoals all have similar burnout times.

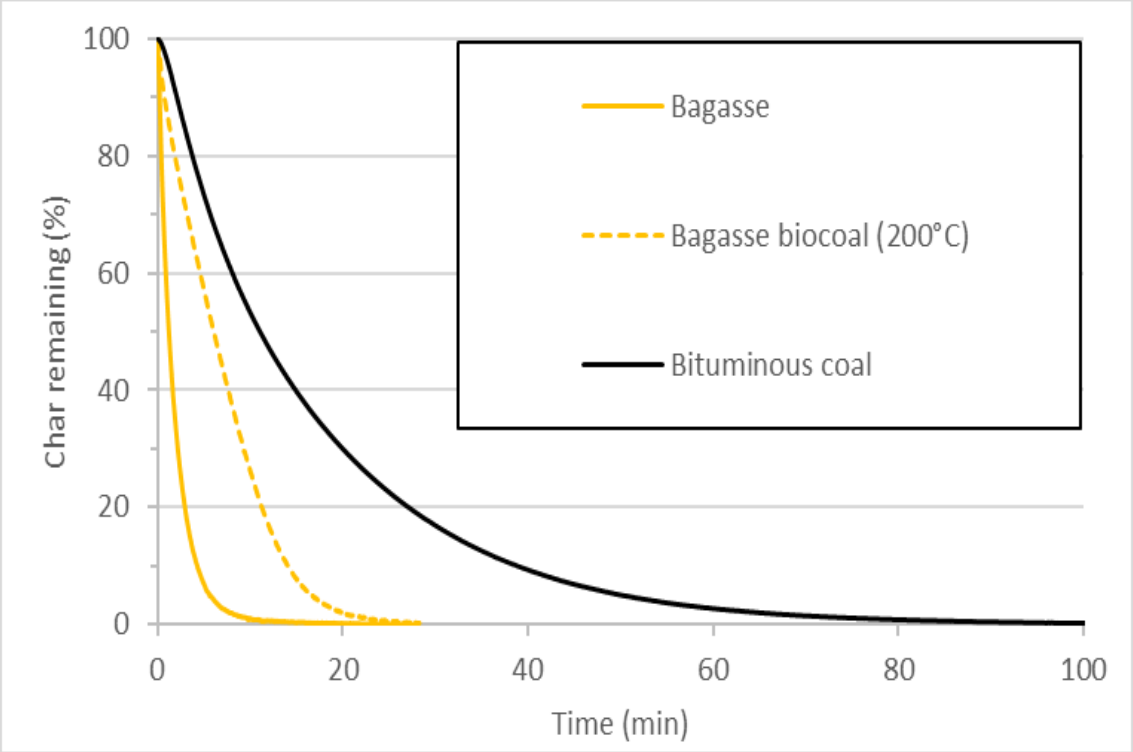

Figure 5.3 Char burnout comparison of bagasse, bagasse biocoal, and bituminous coal (0-75 µm particle size)

Table 5.9 90% char burnout times (t_{90}) (between 5-95% char consumption) of bagasse, bagasse biocoal, and bituminous coal (0-75 µm particle size)

Sample	**t_{90} (95-5%) (min)**
Bagasse	5.53 ± 1.17
Bagasse biocoal (200°C)	15.95 ± 2.56
Bituminous coal	44.4 ± 3.0

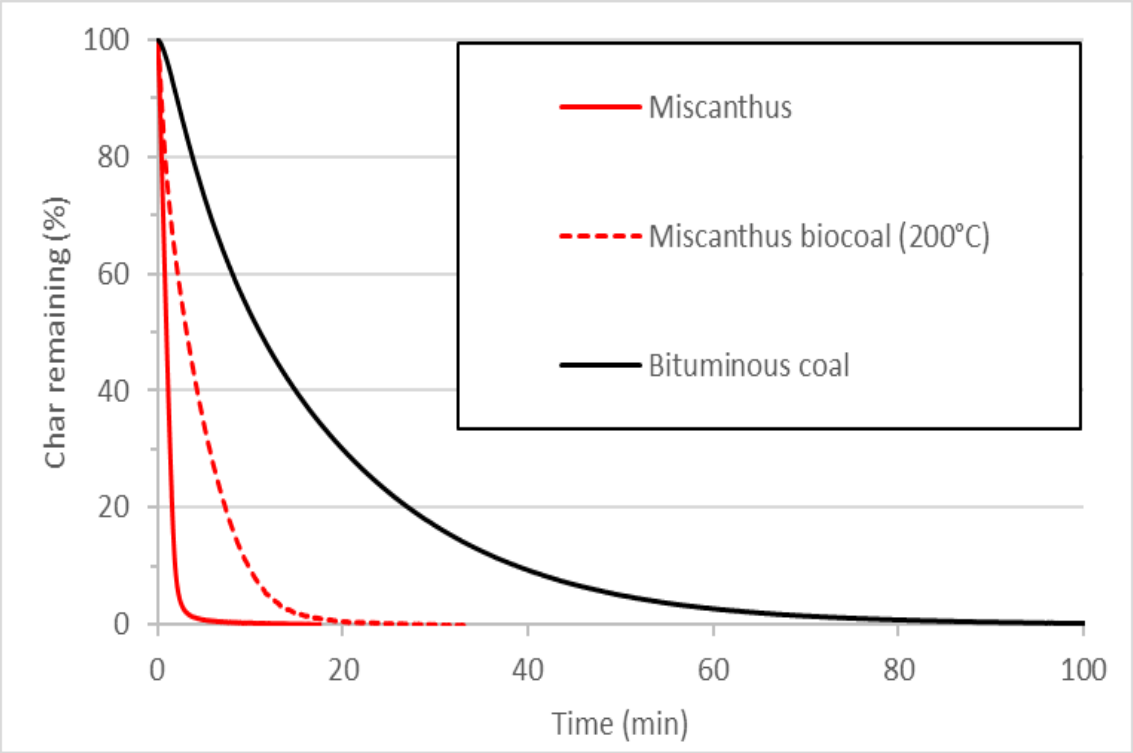

Figure 5.4 Char burnout comparison of miscanthus, miscanthus biocoal, and bituminous coal (0-75 µm particle size)

Table 5.10 90% char burnout times (t_{90}) (between 5-95% char consumption) of miscanthus, miscanthus biocoal, and bituminous coal (0-75 µm particle size)

Sample	t_{90} (95-5%) (min)
Miscanthus	2.14 ± 0.06
Miscanthus biocoal (200°C)	11.41 ± 4.25
Bituminous coal	44.4 ± 3.0

The char burnout of the biocoals produced from each biomass studied using HTC at 200°C as well as the bituminous coal are compared in Figure 5.4 and the t_{90} values for the combustion of these can be seen in Table 5.11. As has been described earlier, wood biocoal is the least reactive, and is similar in reactivity to the bituminous coal. The biocoals produced from miscanthus,

bagasse, and olive cake are more reactive than wood biocoal, and all possess similar reactivity.

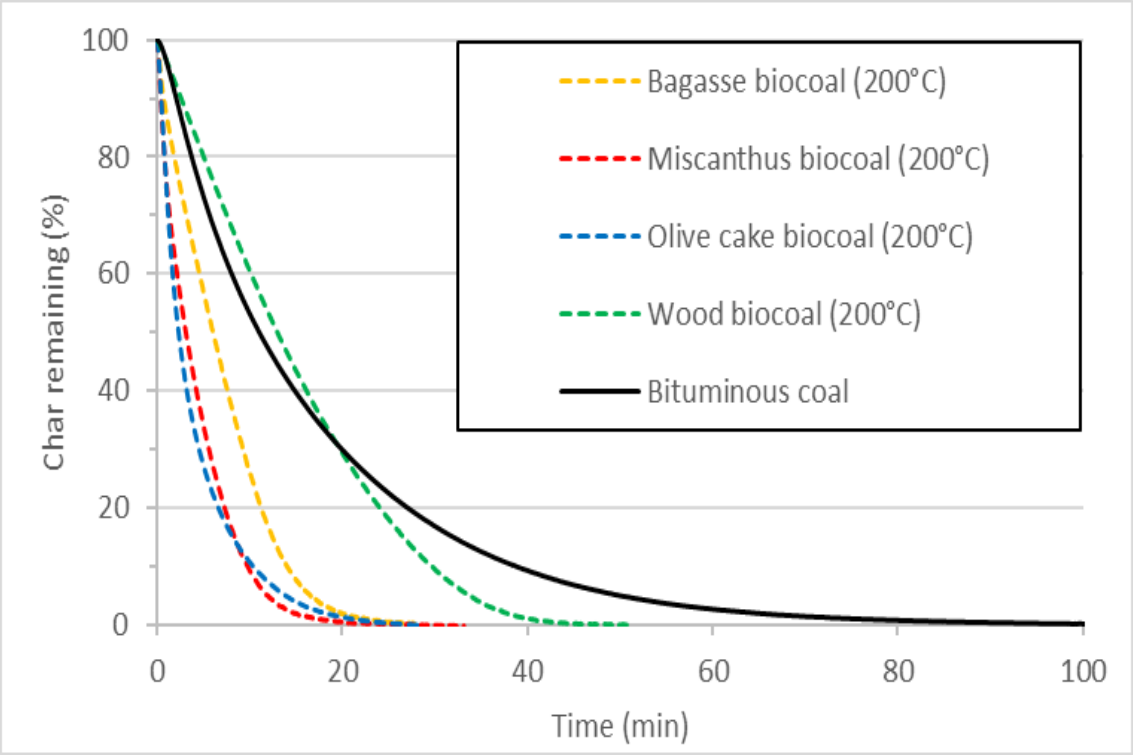

Figure 5.5 Char burnout comparison of bagasse, miscanthus, wood, and olive cake biocoals produced at 200°C and bituminous coal (0-75 µm particle size)

Table 5.11 90% char burnout times (t_{90}) (between 5-95% char consumption) of bagasse, miscanthus, wood, and olive cake biocoals produced at 200°C and bituminous coal (0-75 µm particle size)

Sample	t_{90} (95-5%) (min)
Wood biocoal (200°C)	32.2 ± 1.1
Olive cake biocoal (200°C)	13.5 ± 5.1
Bagasse biocoal (200°C)	15.95 ± 2.56
Miscanthus biocoal (200°C)	11.41 ± 4.25
Bituminous coal	44.4 ± 3.0

The extent of alkali metal extraction by HTC shown in Table 5.4, coupled with the known catalytic effect of of alkali and alkaline earth metals on combustion (Jones et al., 2007; Yi et al., 2018) points towards catalysis by alkaline and alkaline earth metals being a primary contributer to the char reactivity. This case is clearly shown by the wood biocoals, with the extent of alkali/alkalkine earth metal removal with HTC temperature matching the trends in char reactivity closely. The 200°C soft wood biocoal has a higher alkali/alkaline earth metal content than the 225°C biocoal, which has a very similar alkali/alkaline earth metal contents to the 250°C biocoal. Therefore it would follow that if alkali/alkaline earth metal content had a significant impact on the char reactivity of biocoal, then the 200°C biocoal would be the most reactive, and the 225°C and 250°C biocoals would be similar in reactivity. This is the case shown in Figure 5.6. The intermediate char reactivity of olive cake, bagasse, and miscanthus biocoals also indicates that the alkali and alkaline earth metal concentration is a significant contributer to char reactivity, as there are significant levels of alkali and alkaline earth metals in these biocoals, resulting in them being more reactive than the soft wood biocoals.

Changes to the composition and surface area of the fuels appear to have a secondary effect on their char reactivity of TGA chars. This can be seen in the char reactivity of olive cake being reduced considerably more by acid leaching than the char reactivity of the wood through torrefaction. The proximate composition of the olive cake was not greatly changed by the leaching process,

and the leached olive cake had a higher surface area than the untreated olive cake (which would be expected to increase the char reactivity). This means that the primary contributor to the reduction of char reactivity would be the removal of alkali and alkaline earth metals. Although there is no data on the surface area of the slow heating rate chars, torrefied biomass has been shown in the literature to have a smaller surface area than untreated biomass, presumably due to components melting and blocking pores (Granados et al., 2017). The reduction of the char reactivity of wood by torrefaction would likely be mainly due to changes in composition and surface area as torrefaction does not significantly remove the alkaline and alkaline earth metal content of biomass (Hidayat et al., 2017). The decrease in char reactivity of TGA chars through torrefaction is much smaller than what is seen through HTC and acid leaching, indicating that the impact of surface area and composition changes is much less than that of alkali/alkaline earth metal removal.

The effect of composition and surface area changes on the reactivity of the biocoals can also be seen in the case of olive cake biocoal TGA chars. As the concentration of alkali and alkaline earth metals are similar in both biocoals, the lower reactivity of the higher HTC temperature biocoal would likely be the result of more aggressive conditions further altering the composition, or through surface area decreasing through deposition of organics clogging pores. Chars that are representative of those found in pulverised fuel combustion were generated using a drop tube furnace (DTF) at 1300°C. At this temperature, hemicellulose, cellulose, and lignin will all decompose (X. Wang et al., 2017;

Yang et al., 2007), leaving behind a solid comprised of the aromatic degradation products. This was shown in section 2.3.7, where biochar made using the Advanced Gasification Technology (AGT) process at 1200°C resulted in a biochar that was comprised of 100% aromatic carbon (Wiedner et al., 2013). The chars generated have a considerably larger surface area than those made using TGA (Le Manquais et al., 2009). The DTF chars are generally more reactive than their respective TGA chars. This matches what is described in the literature, with a study of bituminous coal TGA and DTF chars showing that DTF chars were more easily combusted than analogous TGA chars (Manquais et al., 2009). An example of this can be seen in Figure 5.6, where TGA and DTF chars produced from wood biocoals are compared.

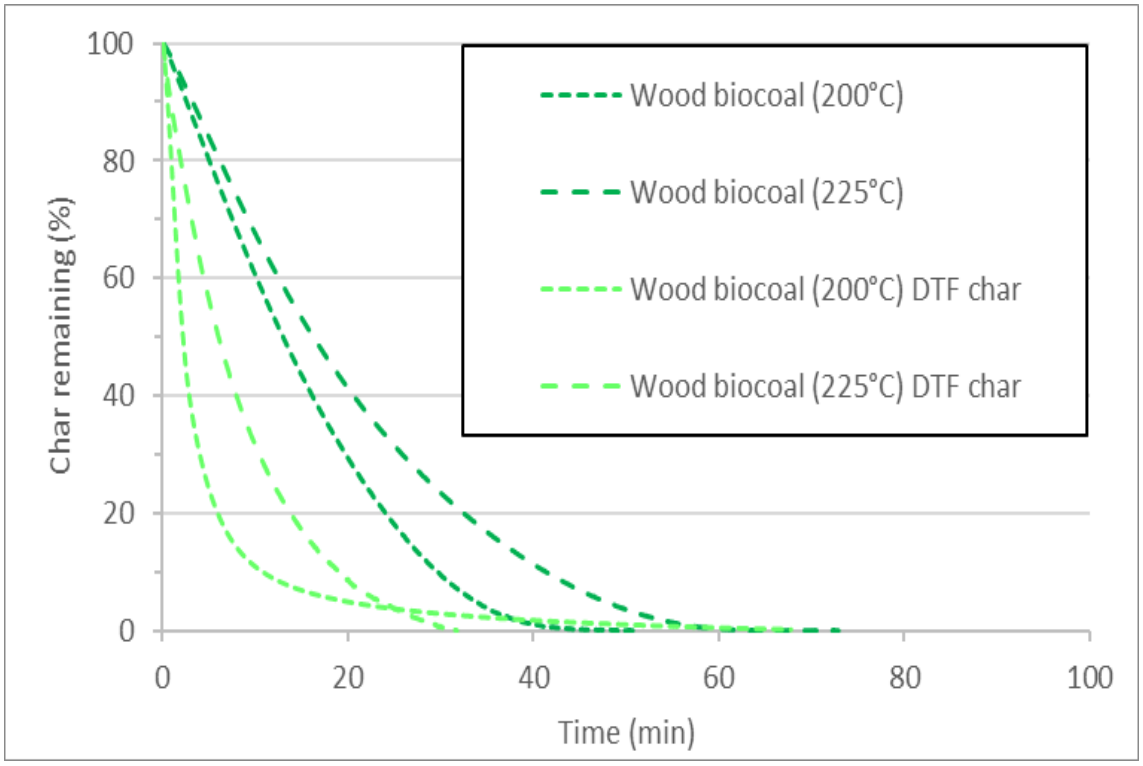

Figure 5.6 Char burnout comparison of TGA and DTF chars generated from wood biocoals (0-75 µm particle size)

The char burnout curves of the DTF chars made from the wood, olive cake, and coal fuels are shown in Figure 5.7, Figure 5.8, and Figure 5.9. The t_{90} values are displayed in Table 5.12. The one clear exception to the trend of DTF devolatilisation reducing the char reactivity of the samples was acid leached olive cake. The reactivity of acid leached olive cake was left largely unchanged by DTF devolatilisation, resulting in a DTF char with similar reactivity to the analogous TGA char.

In the case of the effect of DTF devolatilisation on the char reactivity of untreated wood, the extremely fast burnout at these burnout temperatures mean that there is a high associated error. This causes the error values of the two burnout curves to overlap considerably meaning that significant conclusions cannot be drawn.

The biocoal and coal DTF chars having similar burnout profiles to their respective TGA chars; and the impact of feedstock, pre-treatment, and pre-treatment conditions are also similar. This shows that the trends seen in the char burnout of the TGA chars are still true when the fuels are devolatilised under high heating rates representative of PF combustion. The only exception to this is the effect of HTC temperature on the char reactivity of olive cake biocoal DTF chars, where the char produced from the higher HTC temperature biocoal is more reactive than its lower HTC temperature counterpart. This is the reverse of what is seen in the olive cake biocoals that have not been devolatilised in the DTF.

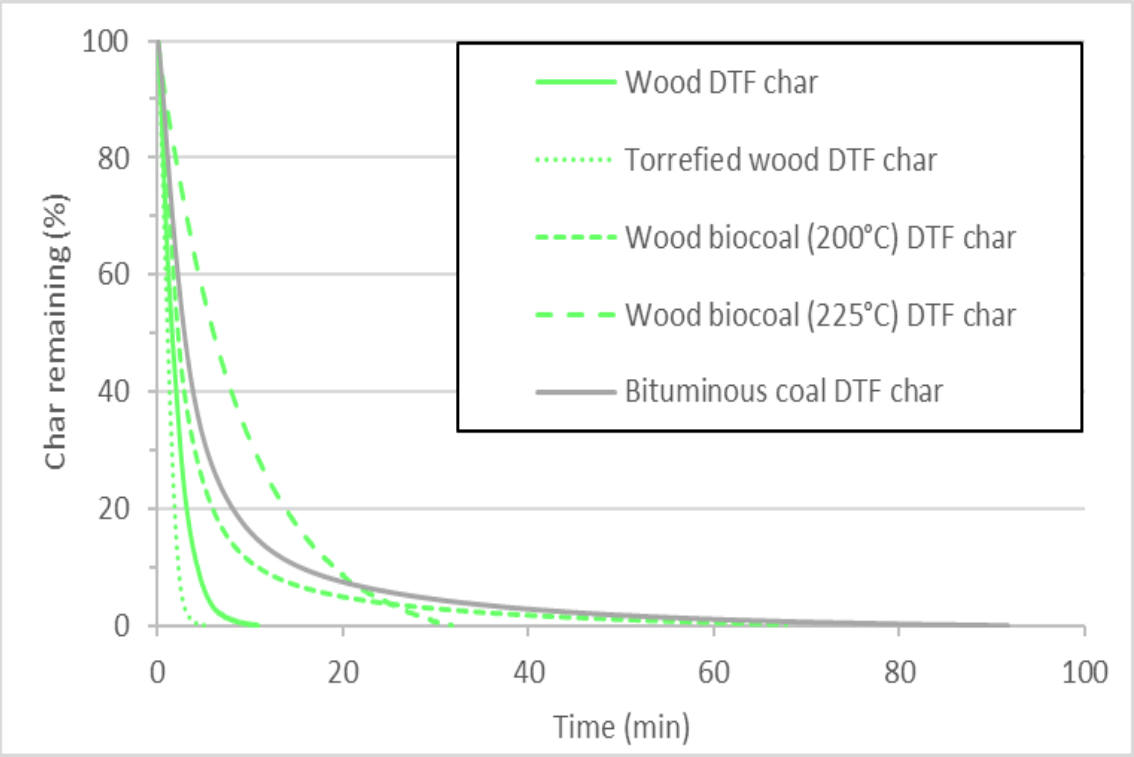

Figure 5.7 Char burnout comparison of DTF chars generated from wood derived fuels and bituminous coal (0-75 µm particle size)

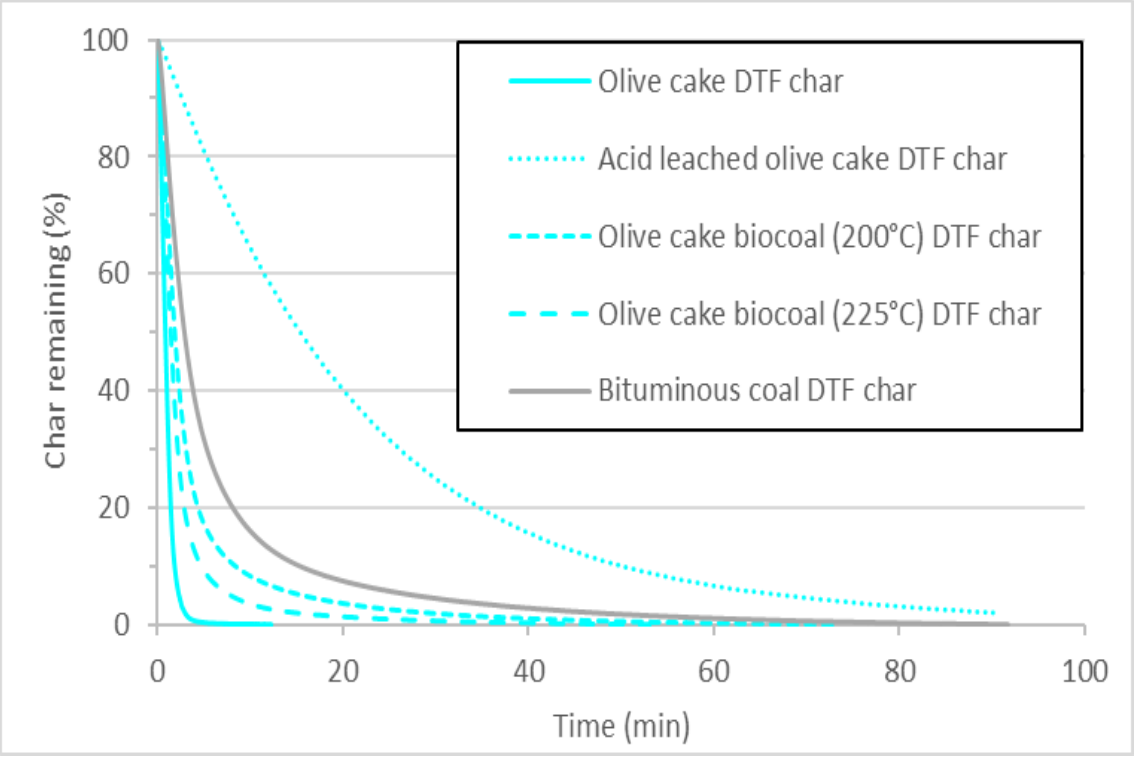

Figure 5.8 Char burnout comparison DTF chars generated from olive cake derived fuels and bituminous coal (0-75 µm particle size)

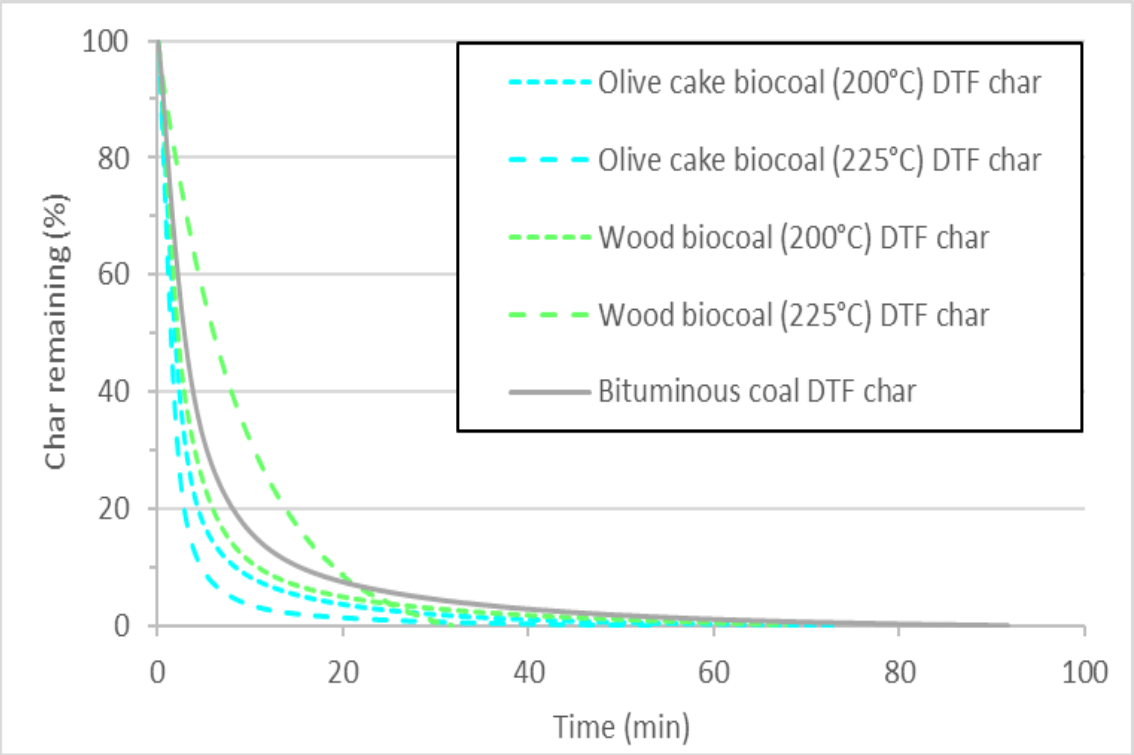

Figure 5.9 Char burnout comparison of DTF chars generated from the biocoals and bituminous coal (0-75 µm particle size)

Table 5.12 t_{90} values of DTF chars (0-75 µm particle size)

Sample	t_{90} (95-5%) (min)
Wood DTF char	4.6 ± 2.2
Torrefied wood DTF char	2.4 ± 0.4
Wood biocoal (200°C) DTF char	19.2 ± 3.3
Wood biocoal (225°C) DTF char	22.5 ± 5.0
Olive cake DTF char	2.2 ± 0.3
Acid leached olive cake DTF char	65.8 ± 7.6
Olive cake biocoal (200°C) DTF char	15.4 ± 3.4
Olive cake biocoal (225°C) DTF char	7.4 ± 3.2
Bituminous coal DTF char	27.3 ± 3.4

Devolatilisation of the samples in the DTF will result in the composition of the samples becoming very similar. This is seen with AGT chars produced at a similar temperature – 1200°C. AGT Chars produced from wood chips, poplar, wheat straw, sorghum, and olive cake were all shown to exhibit 100% aromatic carbon in carbon NMR spectra (Wiedner et al., 2013). This means that the impact of composition will not be seen in the DTF chars, with surface areas and alkali/alkaline earth metal concentration dominating the char reactivity.

Further evidence of alkali/alkaline earth metal content providing a primary influence on char reactivity can bee seen in the biocoal DTF chars. These have a higher surface area than their untreated biomass analogues, which would be expected to increase the reactivity. All of the biocoal DTF chars are considerably less reactive than the untreated biomass DTF chars, indicating that the effect of removing of alkali and alkaline earth metals is much larger than the effect of increasing surface area. In addition to this, the effect of HTC temperature on the char reactivity wood biocoal DTF chars is the same as what is seen in the low heating rate chars. The further loss of alkali and alkaline earth metals is further reducing the char reactivity in competition with the surface area increasing with increasing HTC temperature.

As was seen in the case of composition changes affecting the char reactivity of olive cake biocoal TGA chars, the similar alkali and alkaline earth metal content of the two biocoals allows for the effect of surface area to become significant

in determining the char reactivity of the olive cake biocoal DTF chars. This is seen in the olive cake biocoal DTF char derived from the higher HTC temperature biocoal being more reactive than its lower HTC temperature counterpart. This is the reverse of the trend seen when the olive cake biocoal char reactivity was studied without DTF devolatilisation. This could be due to DTF chars having a considerably larger surface area than their slow heating rate analogues (Le Manquais et al., 2009; McNamee et al., 2015) and the extremely harsh devolatilisation conditions greatly altering the composition of the fuels. This would emphasise the effect of surface area and reduce the effect of composition seen at lower heating rates. This would suggest that the effect of fuel composition on char reactivity becomes even less significant when the fuel is subjected to high heating rates representative of PF combustion. There might be some volatilisation of alkali and alkaline earth metals under the conditions used in DTF devolatilisation. This would reduce the catalytic affect, which coupled with the large increase in surface area brought about by high heating rate devolatilisation in the DTF (Le Manquais et al., 2009; McNamee et al., 2015) would result in the impact of surface area becoming more prominent.

It has been shown that alkali and alkaline earth metals are a primary factor in determining the char reactivity of biomass. The significantly higher alkali and alkaline earth metal content of all the biocoals produced from feedstocks other than wood pose a potential issue – the olive cake biocoals have an alkali/alkaline earth metal content over an order of magnitude higher than that of wood biocoals, while the baggase and miscanthus biocoals have

alkali/alkaline earth metal contents of approximately an order of magnitude higher than the wood biocoals. Significantly greater alkali and alkaline earth removal may be necessary to create a biocoal with similar reactivity to the bituminous coal studied from olive cake, bagasse, or miscanthus. As was shown in section 4.3.1, there could be the an ideal set of HTC conditions to maximise alkali/alkaline earth removal, but whether or not HTC has the ability to reduce the alkali/alkaline earth metal content of these biocoals so that they are close to that of the wood biocoals has not been fully investigated at this time. An alternative measure would be to leach the biomass prior to HTC, either with water or acids. The main disadvantage of leaching (producing a wet fuel product) would be mitigated by HTC due to biocoal being hydrophobic (Acharya et al., 2015), and acid leaching prior to HTC (with retention of the leaching solution into the HTC process) could be beneficial to the biocoal produced, as acids can catalyse HTC and produce a higher HHV (Lynam et al., 2011).

5.5.2 Determining the activation energy and pre-exponential factor of fuels

To further understand how HTC affects the reactivity of biomass, the activation and pre-exponential factor associated with the char burnout of some of the wood and olive cake biocoal TGA chars were determined and compared to that of their untreated biomass feedstock, torrefied wood, acid leached olive cake, and bituminous coal TGA chars. The method used to determine these values is described in section 3.2.1.2. The values were determined through char burnout

at 5 temperatures, and the temperature range used was dependent on the reactivity of the sample. The $\ln K_a$ vs 1/T trends used to determine activation energy and pre-exponential factor for the fuels can be seen in Figure 5.10, and the activation energy and pre-exponential factor values determined can can be seen in Table 5.13. The temperature ranges used for each fuel in the study are listed in section 3.2.1.2. In the case of olive cake combustion ignition did not occur at low combustion temperatures, so the first two temperatures where ignition occurred were used. Higher temperatures than this were not used in an attempt to ensure that Regime I combustion (true kinetic control (Manquais et al., 2009)) was occuring, as the combustion proceeded quickly upon ignition at lower combustion temperatures.

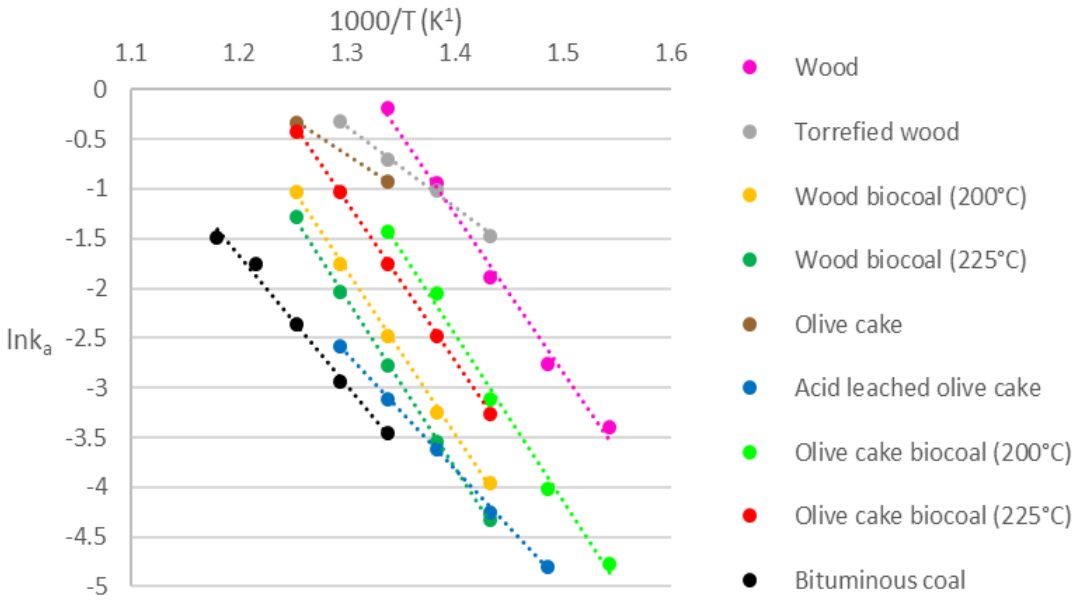

Figure 5.10 $\ln K_a$ vs. 1/T trends used to determine activation energy and pre-exponential factor for the fuels

Table 5.13 Activation energy and pre-exponential factor for soft wood fuels, olive cake fuels, and bituminous coal

Sample	Activation energy (kJ/mol)	Pre-exponential factor (min^{-1})
Wood	133	1.43×10^{9}
Torrefied wood	68	2.82×10^{4}
Wood biocoal (200°C)	137	2.99×10^{8}
Wood biocoal (225°C)	141	4.48×10^{8}
Olive cake[1]	59	5.09×10^{3}
Acid leached olive cake	97	2.49×10^{5}
Olive cake biocoal (200°C)	139	1.31×10^{9}
Olive cake biocoal (225°C)	132	2.98×10^{8}
Bituminous coal	108	1.12×10^{6}

[1]Values determined using only two burnout temperatures due to ignition difficulties

The trends shown in Figure 5.10 match what has been previously described in section 5.2.4.1. The biomass fuels and torrefied wood are the most reactive, with the olive cake biocoals having reactivities in between that of the untreated biomass fuels and the bituminous coal studied. The wood biocoals and acid leached olive cake have reactivities approching that of the bituminous coal studied.

The values for activation energy and pre-exponential factor for the soft wood biomass and olive cake biocoals are similar to those in the literature (Bach & Tran, 2015; Rollinson & Williams, 2016). The significant dependence of rate constant on combustion temperature indicates that pure kinetic control is being observed in the wood, wood biocoal, olive cake biocoal, and acid leached olive cake combustion analysis (Jenkinson, 2015). The $\ln k_a$ vs. 1/T trend for coal, torrefied biomass, and olive cake are not as steep as the other fuels, which indicates that there may be some diffusion control present in the combustion

of these samples (Regime II control). This is also seen in the case of coal combustion, as the t_{90} seen for coal combustion at 475°C in this study being significantly larger than the char burnout comparison displayed previously in Section 5.2.4.1 (88.6 minutes compared to 44.4 ± 3.0 min). The t_{90} value shown in this study is close to the 75-150 µm fraction burnout (99.3 min). This indicated that agglomeration of the coal particles may have occurred, either though moisture absorption prior to analysis or swelling of the coal during plastic softening in devolatilisation (Manquais et al., 2009). It was expected that determining the intrinsic reactivity of coal would be problematic, as it has been seen in a previous study comparing TGA and DTF coal chars that the intrinsic reactivity of the coal could not be determined using TGA char with a particle size of <20 µm (Manquais et al., 2009). The <20 µm sample studied exhibited Regime II control (Manquais et al., 2009). The char reactivity of coal shown in the burnout analysis in section 5.4.2.1 should be considered as being close to the intrinsic reactivity of the coal as the relative reactivity between this sample and the the other fuels was consistent between both the TGA and DTF chars. In addition to this, the DTF chars have a much larger surface area than their slow-heating rate TGA analogues, so the DTF chars are less likely to encounter diffusion control, and are therefore more likely to represent Regime I control and therefore the intrinsic chemical reactivity of the fuel (Manquais et al., 2009).

In the case of olive cake, the lowest temperatures needed to ignite the sample were too high to display Regime I control, and in the case of torrefaction, a

lower temperature range is needed to show Regime I control. As both exhibit Regime II control at the low temperature ranges used in this study, they are very reactive, therefore the observations made in section 5.2.4.1 are valid.

All of the biocoals exhibit Regime I combustion at 475°C, confirming that intrinsic char reactivity of these fuels is being observed.

As the combustion of olive cake was shown to exhibit Regime II control, the comparison between biocoals and their respective biomass feedstock will be limited to the soft wood biocoals. Combustion of the soft wood biocoals has a higher activation energy and lower pre-exponenetial factor than the combustion of untreated soft wood. This indicates that combustion of the char is more difficult to achieve, and that the combustion is slower when it is triggered. The increase in activation energy could be explained by removal of alkali/alkaline earth metals reducing catalysis. The activation energy of both soft wood biocoals have a similar value to that of demineralised pine wood chips (Jenkinson, 2015), which adds further evidence to this hypothesis. It has been shown that in coals activation energy also correlates with ordering of carbon structure, with more ordered carbon structures having a higher activation energy (B. Wang et al., 2012). Biocoal has been shown to exhibit higher ordered structure characteristics than untreated biomass due to removal of amorphous fractions (Guo, Dong, Liu, Yu, & Zhu, 2015), so it would follow that biocoal would have a higher activation energy. The degree to which this has influenced the results in this study has not been investigated, but the previous analysis

conducted earlier in section 5.2.4 suggested that composition changes did not have as significant an effect on the burnout.

The acitvation energy and pre-exponential for the drop tube chars were not determined in this study due to the irregular shape of their burnout curves. An example of this is shown in Figure 5.11. The rate of combustion of the DTF char is much higher earlier in combustion, indicating a change in the combustion kinetics near to completion of burnout. This means that the gradient of the straight-line plot (the rate constant) is not indicative of the overall combustion, so any further analysis using the rate constant would be inaccurate. Further investigation into the rate of combustion of DTF chars is recommended.

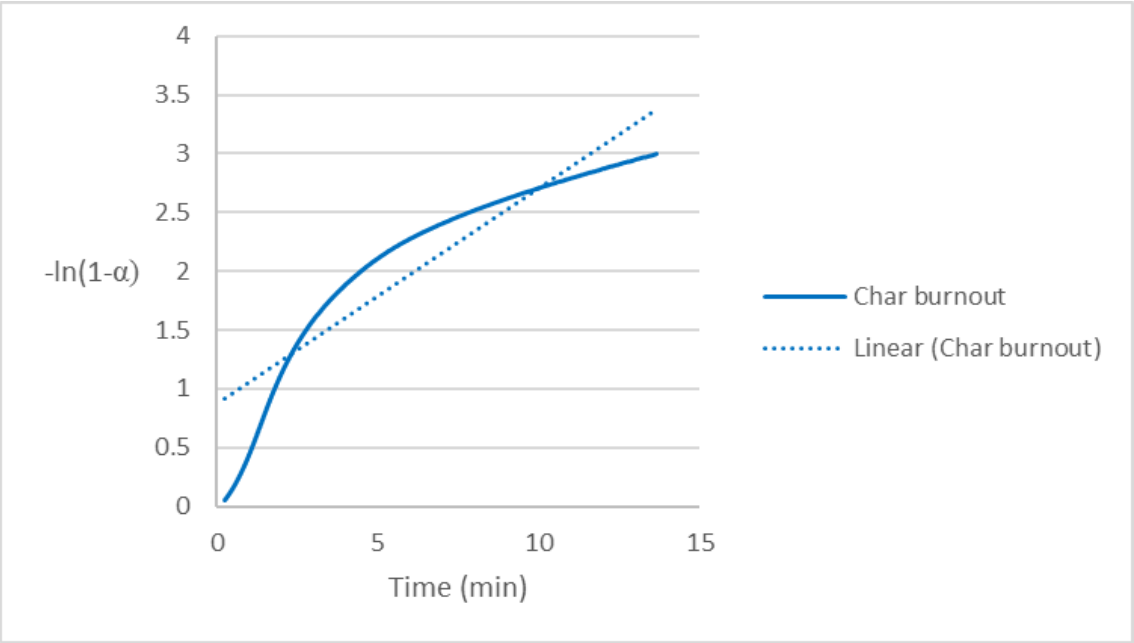

Figure 5.11 Irregular char burnout of wood biocoal (200°C) DTF char (at 500°C)

5.5.3 The impact of particle size on char burnout of biocoal

Previous work has shown that particle size has a negligible effect on the char burnout of biomass at particle sizes below 250 µm (Farrow, 2013). This indicates that mass transfer is not determining the rate of combustion, and the intrinsic char reactivity is being displayed by the biomass char burnout curves displayed in this chapter. To ensure that this is the case, char burnout curves of the 0-75 µm and 75-150 µm particle size fractions of all the fuels apart from the miscanthus and bagasse fuels were recorded. The burnout of both particle size fractions of the biocoal produced from soft wood at 225°C was performed in triplicate, to determine the variability of the burnout to ensure that the ranges matched. The 75-150 µm fractions of all the other fractions were only determined once, due to time constraints. The burnout of the two soft wood

biocoal fractions produced at 225°C can be seen in Figure 5.12 and the t_{90} values for the two fractions for all the fuels where two particle size fractions were studied can be seen in Table 5.14. The mean burnout curves are superimposed on one another, showing that the two particle sizes burn out at very similar rates in this case. This is also shown in the t_{90} values where the two have almost identical values. The other biomass fuels all had 75-150 µm particle size fraction t_{90} values that were close to the range shown in their 0-75 µm analogues. Producing the burnout curves in triplicate could bring the values closer similar to what was seen in the case of the soft wood biocoal produced at 225°C. This shows that the particle size does not have a significant effect on the burnout of biocoal and untreated biomass, so the burnout should not be under mass transfer control and the intrinsic char reactivity is being seen. Torrefied wood and coal both displayed a significant dependence on particle size in char burnout, with the char burnout time almost doubling in both cases. This is another indicator that the combustion of these fuels is under Regime II control.

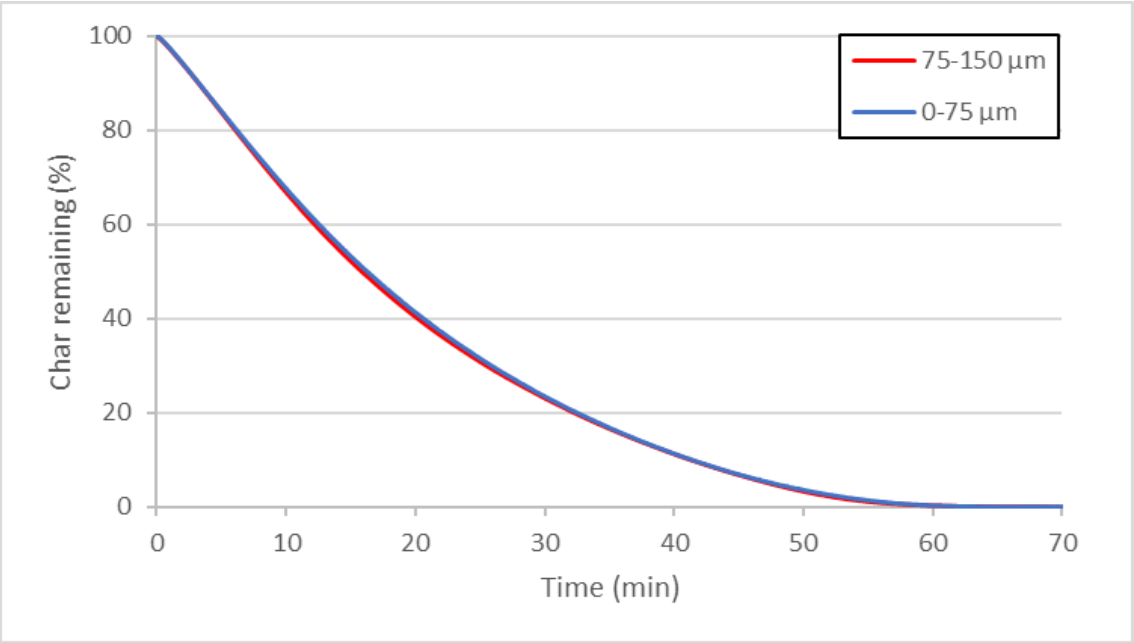

Figure 5.12 Char burnout curves for the 0-75 and 75-150 µm particle size fraction of soft wood biocoal produced at 225°C

Table 5.14 t90 values for the 0-75 and 75-150 µm particle size fractions of various fuels

Sample	Particle size fraction (µm)	t_{90} (95-5%) (min)
Wood	0-75	3.2 ± 1.1
	75-150	4.6[1]
Olive cake	0-75	5.3 ± 1.6
	75-150	5.3[1]
Torrefied wood	0-75	5.6 ± 0.8
	75-150	10.8[1]
Acid leached olive cake	0-75	66.5 ± 5.5
	75-150	60.0[1]
Wood biocoal (200°C)	0-75	32.2 ± 1.1
	75-150	38.8[1]
Wood biocoal (225°C)	0-75	45.7 ± 3.0
	75-150	45.7 ± 3.1
Olive cake biocoal (200°C)	0-75	13.5 ± 5.1
	75-150	11.4[1]
Olive cake biocoal (225°C)	0-75	20.9 ± 0.9
	75-150	17.8[1]
Bituminous coal	0-75	44.4 ± 3.0
	75-150	99.2[1]

[1] t_{90} value only determined by a single run

5.6 Generation of biocoal with similar volatile matter content and char reactivity to coals

As shown in Table 5.3, the biocoals produced have a much higher volatile matter content than that of the bituminous coal studied. For biocoal to be an efficient coal replacement it must also match the composition of coal. As the wood biocoals had similar char reactivity to the bituminous coal studied, they were subjected to torrefaction to lower their volatile matter content to produce a coal-equivalent fuel. Torrefaction was shown in Figure 5.1 to have a minor effect on the char reactivity of biomass, so it was thought that the reactivity of the biocoals would remain in the region of the bituminous coal studied if they were torrefied. The torrefaction temperature required to achieve a volatile matter in the region of high volatile bituminous coal was determined by stepwise devolatilisation by TGA. The biocoal produced at 200°C was torrefied at a temperature of 370°C, and the biocoal produced at 225°C was torrefied at 290°C. The proximate analysis of the torrefied biocoals in comparison to the bituminous coal is shown in Table 5.15. The torrefied biocoals have a DAF volatile matter content in the range of sub-bituminous and high-volatile bituminous coals, with the torrefied biocoal generated from the 225°C biocoal having a volatile matter content similar to that of the bituminous coal studied. Both torrefied biocoals have a significantly lower ash content than the coal, which mean that ash deposition would be a more minor issue.

Table 5.15 Proximate analysis of coal and torrefied wood biocoals

Sample	Moisture (AR) (%)	Volatile matter (DAF) (%)	Fixed carbon (DAF) (%)	Ash (AR) (%)
Bituminous coal	3.4	40.8	59.2	5.2
Torrefied wood biocoal (200°C)	4.5	28.9	71.1	0.2
Torrefied wood biocoal (225°C)	1.9	45.9	54.1	0.4

The char reactivity of the torrefied wood biocoals was compared to that of the non-torrefied wood biocoals and the coal to ensure that it had not been altered significantly by torrefaction. The char burnout curves of the torrefied biocoals, non-torrefied biocoals, and bituminous coal are compared in Figure 5.13, and the t_{90} values are listed in Table 5.16. In the case of the biocoal produced at 200°C, torrefaction results in a small decrease in reactivity; similar to what is seen when the wood pellets were torrefied. This would likely be due to changes to the composition of the fuel due to the harsh torrefaction conditions. This brought the char reactivity of this biocoal closer to that of the bituminous coal studied.

The biocoal produced at 225°C saw virtually no change in char reactivity, with the char burnout curves of the biocoal and torrefied biocoal being almost superimposed on one another. This could be due to both the higher HTC temperature biocoal having already undergone greater composition change than the lower HTC temperature biocoal, and the torrefaction temperature

being lower. In both cases, the resultant torrefied biocoal had a char reactivity similar to that of the bituminous coal studied.

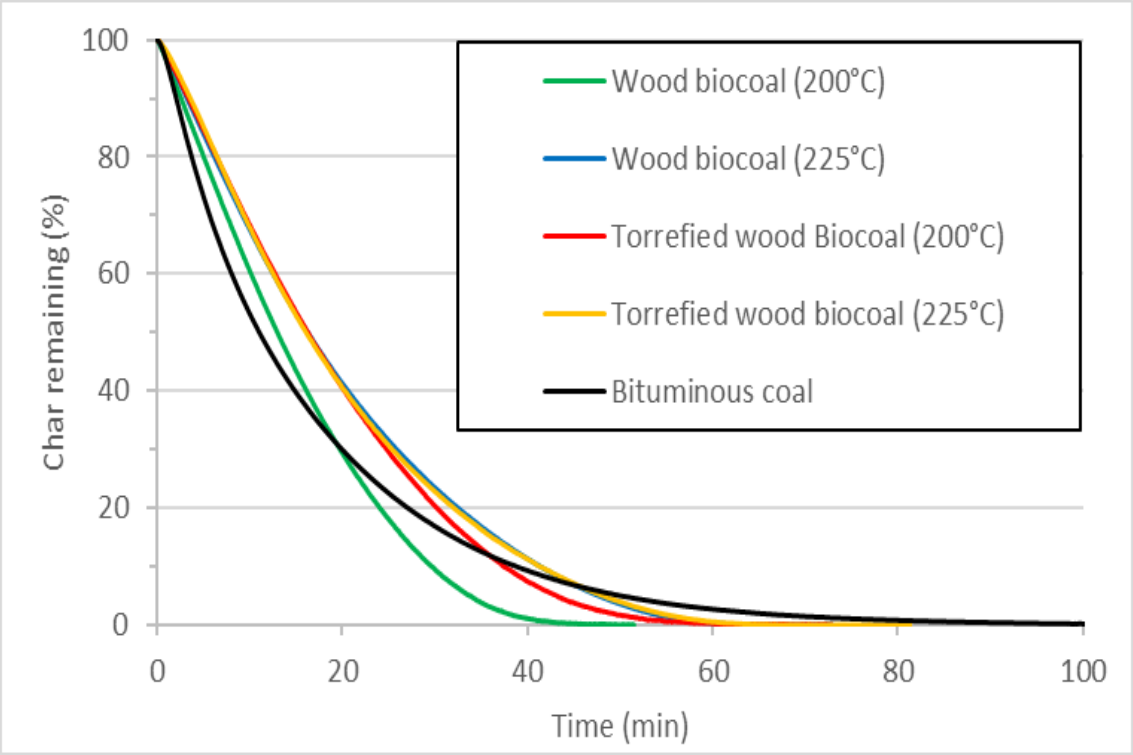

Figure 5.13 Char burnout comparison of wood biocoals and torrefied wood biocoals

Table 5.16 t90 values for wood biocoals, torrefied wood biocoals, and coal

Sample	**t_{90} (95-5%) (min)**
Wood biocoal (200°C)	32.2 ± 1.1
Wood biocoal (225°C)	45.7 ± 3.0
Torrefied wood biocoal (200°C)	40.5 ± 1.9
Torrefied wood biocoal (225°C)	46.1 ± 3.1
Bituminous coal	44.4 ± 3.0

5.7 Conclusions

1. HTC of reduces the char reactivity of biomass. The removal of alkali and alkaline earth metals from the biomass is a primary factor in this. The surface area and composition provide secondary impact to the char reactivity.

2. HTC increases the activation energy and lowers the pre-exponential factor of combustion of soft wood biomass, indicating that combustion of biocoal is more difficult to initiate, and progresses at a slower rate than untreated biomass.

3. HTC of biomass with low alkali and alkaline earth metal content results in a fuel with a similar reactivity to that of high-volatile bituminous coal.

4. HTC of biomass with higher alkaline and alkaline earth metal content results in a biocoal with a reactivity between that of its untreated biomass feedstock and coal, as significant levels of these species remain in the fuel.

5. The trends described are seen both in combustion of TGA chars and DTF chars, indicating that the observations made are true under realistic PF combustion conditions.

6. Coal-equivalent fuels were produced by torrefaction of soft wood biocoals. The torrefied biocoal had a DAF volatile matter content in the range of sub bituminous and high-volatile bituminous coal, with similar reactivity to high-volatile bituminous coal, and a very low ash content.

Chapter 6 The impact of water on HTC chemical reactions

The chemistry of torrefaction has been more thoroughly researched in comparison to HTC, and is well established. It is dominated by the thermal degradation of hemicellulose. At the temperature range of torrefaction, hemicellulose undergoes dehydration, deacetylation, and depolymerisation. Other proposed reactions include decarboxylation, de-carbonylation, de-methoxylation, intermolecular derangement, condensation and aromatization (Kambo & Dutta, 2015b). It is a two-step degradation, with hemicellulose breaking down to produce 'reactive hemicellulose' which in turn decomposes and recombines creating various products, the composition and quantity of which has not been closely studied as of yet. Degradation of cellulose can also occur in high-temperature torrefaction (in some cases seen at >270°C) (Ciolkosz & Wallace, 2011). Lignin will soften during torrefaction but will not undergo significant chemical changes (Ciolkosz & Wallace, 2011).

The chemistry involved in HTC has been studied, and reaction mechanisms have been conceived which explain it. The primary difference between the chemistry of torrefaction and hydrothermal carbonisation is that water is involved in the reaction pathways. Under HTC conditions, hydrogen bonding is weakened, allowing water to autoionize into hydronium (H_3O^+) and hydroxide (OH^-) ions (Ruiz et al., 2013). This results in a increase in the occurrence of acid- and base-catalysed reactions (Katritzky, Nichols, Siskin, Murugan, & Balasubramanian, 2001). HTC reaction pathways begin with hydrolysis (Libra et al., 2011), with the

resulting fragments initiating the other principle reactions, namely dehydration, condensation, aromatization, and decarboxylation (Hoekman et al., 2017; Libra et al., 2011; Oliveira et al., 2013). These reactions do not occur in succession but rather happen simultaneously in competition (Fang et al., 2018). The hydrolysis occurs first due to having the lowest activation energy (Fang et al., 2018).

The different components of biomass degrade to form a variety of products. Extractives such as proteins and lipids generally decompose into compounds that typically remain in the liquid, aqueous, or gaseous phase. Proteins generate amino acids which then decompose to produce ammonia (Kruse et al., 2016), and lipids form organic compounds that stay in the liquid phase likely through hydrolysis of triglyceride (Yue et al., 2018). Degradation of hemicellulose and cellulose in biomass typically involves aromatisation and recombination reactions that result in some the degradation products returning to the solid phase as hydrochar. HTC of hemicellulose first produces sugar monomers, which then further react to form furfurals among other organic compounds (Reza, Lynam, et al., 2013). The furfurals then combine and aromatize to form hydrochar (Reza, Lynam, et al., 2013). HTC of cellulose forms some glucose, which then produces a number of organic molecules (5-HMF, levulinic acid, dihydroxyacetone, and formic acid), but the majority of the degradation is through dry thermal degradation as the oligomers formed in the degradation form envelopes to minimise surface area in contact with water (Falco et al., 2011).

Water is involved in HTC reactions, and could donate hydrogen to the degradation products of biomass in competing reactions to aromatisation. For example, the furfural produced in hemicellulose and cellulose decomposition polymerise before aromatization to produce hydrochar, but furfurals can also react with superheated water to produce other organic compounds. For example 2-methylfuran as been shown to convert to 5-methylfurfuryldimethylamine with a 48% yield when treated with Me_2-NH/ aqueous HCHO at 165°C for 1.4 minutes; 2,5-Dimethylfuran has been shown to produce 2,5-hexanedione in superheated D_2O (250°C) over 30 minutes; and 2,3-Dihydrobenzofuran has been shown to produce phenol with yields of 87% and 60% when heated in water at 250°C in the presence of aqueous sulphite and phosphoric acid, respectively (Katritzky et al., 2001).

In reactions where hydrogen is donated from water, production of CO_2 or H_2O could be sinks for the oxygen in the reacting water molecule. This means that increased CO_2 yields in HTC could indicate hydrogen donation. Decarboxylation reactions will also result in loss of CO_2.

6.1 Materials and methods

Three hydrochars were produced using Brites soft wood pellets a feedstock. HTC was carried out at 200, 225, and 250°C. The HTC procedure is described in section 3.1.2.

Torrefied wood was produced in the same Parr reactor that was used for HTC. This procedure is described in section 3.1.3. Torrefaction was performed at the mid-point HTC temperature of 225°C for a residence time of 60 minutes. Only the mid-point temperature of those used in the HTC experiments was used for torrefaction as the aromatisation of biomass by torrefaction is already well established and only one torrefaction reference point was necessary for comparison to HTC.

Analysis for this study was performed using elemental analysis (both of solid phase and liquid phase products), gas chromatography, and NMR spectroscopy. The methods used to conduct these analyses can be seen in sections 3.2.2, 3.2.4, and 3.2.8 respectively.

6.2 Mass balance and product composition

The mass balance of the HTC and torrefaction experiments can be seen in Table 6.1.. The solid yield was determined by the mass and proximate analysis of the biochar and hydrochars; the liquid yield was determined from the

elemental analysis of the liquor; and the gas yield was determined from the gas chromatography of the product gas normalised to 100% to disregard the nitrogen used to produce an inert atmosphere in the Parr reaction.

Table 6.1 Mass balance of HTC and torrefaction of wood

Sample	Solid yield (DAF[1]) (%)	Liquid yield (DAF[1]) (%)	Gas yield (DAF[1]) (%)	Total mass recovered (%)
200°C hydrochar	72.4	12.0	1.5	85.9
225°C hydrochar	69.7	11.3	3.4	84.4
250°C hydrochar	56.7	11.3	7.8	75.8
225°C biochar	90.8	N/A	1.7	92.5

[1]DAF – dry, ash free basis

HTC has a much lower solid yield than torrefaction under the conditions studied. This is mainly due to cellulose decomposing in HTC, while being relatively unaffected in torrefaction under the conditions studied. In HTC, cellulose reacts at around 200°C (Reza, Lynam, et al., 2013), whereas under torrefaction conditions a temperature of between 315-400°C is typically required (Yang et al., 2007), although some reactions have been seen at 270°C (Ciolkosz & Wallace, 2011). Hemicellulose decomposes both in HTC and torrefaction under the conditions studied (Reza, Lynam, et al., 2013; Yang et al., 2007). Increasing HTC temperature resulted in a lower solid yield, which is also reported in the literature (Álvarez-Murillo, Román, Ledesma, & Sabio, 2015b).

Less of the original mass was accounted for from the HTC experiments than that from torrefaction, and the amount of mass accounted for decreased as

HTC temperature increased. This could be due to a number of factors. A major factor in this is the production of water in HTC, as described in section 4.2, which has not been accounted for. Additionally, some hydrochar was seen precipitating from the liquor after filtration. More precipitate was seen in process liquors produced at higher temperatures. If there were oils produced during HTC, they could have been entrained in the char, and lost in the washing and drying stages. There was no oil observed in the hydrochar or liquor, so this effect would be small if present. Highly volatile matter could have been lost from the process liquor prior to elemental analysis, and some gaseous products could have been lost during handling prior to analysis. Solid biochar constituted the vast majority of the torrefaction products, representing nearly 91% of the mass balance. Assembling a mass balance was significantly easier in this case.

The elemental analysis of the solid products can be seen in Table 6.2. It shows that HTC increases the carbon content of biomass while decreasing the hydrogen and oxygen content. This is due to dehydration and decarboxylation reactions (He et al., 2013; Aidan M. Smith et al., 2016). The effect of HTC on the nitrogen content at 200°C and 225°C is marginal but increasing the temperature of HTC slightly increases the nitrogen content of the biomass, resulting in the 250°C hydrochar having a nitrogen content 40% larger than that of untreated wood. This indicates that nitrogen is staying in the solid phase, with a potential mechanism for this being through Maillard reactions (Kruse et al., 2016).

Torrefaction has a similar effect as HTC on the elemental composition of wood but does not have as large an effect as HTC at the same temperature. HTC at 225°C increases the carbon content of wood by 20%, whereas torrefaction at 225°C only increases it by 8%, having a similar effect on the carbon content as at HTC at 200°C. This is due to the decomposition of cellulose in HTC (Reza, Lynam, et al., 2013), and the significant removal of oxygen and hydrogen through dehydration and decarboxylation reactions (He et al., 2013; Aidan M. Smith et al., 2016).

Table 6.2 Elemental analysis of untreated wood, hydrochar, and biochar

Sample	Elemental composition (%)			
	C	H	N	O[1]
Wood	48.0 ± 0.2	6.6 ± 0.2	0.23 ± 0.04	45.2
200°C hydrochar	52.8 ± 0.8	5.9 ± 0.5	0.21 ± 0.06	41.1
225°C hydrochar	57.4 ± 0.1	5.8 ± 0.0	0.25 ± 0.02	36.6
250°C hydrochar	69.4 ± 0.4	5.2 ± 0.1	0.32 ± 0.03	25.1
225°C biochar	51.7 ± 1.0	6.1±0.4	0.18 ± 0.06	42.1

[1]Oxygen content calculated by difference

The elemental analysis of the HTC liquors can be seen in Table 6.3. As was described in section 4.8.8.1, in this case the carbon content of the liquor does not change significantly with HTC temperature, which is broadly in opposition with what is reported in the literature.

Table 6.3 Elemental composition of HTC process liquor

Sample	Elemental composition (%)			
	C	H	N	O[1]
200°C liquor	1.48±0.05	9.08±0.18	0.05±0.01	89.4
225°C liquor	1.40±0.11	9.77±0.11	0.05±0.01	88.8
250°C liquor	1.40±0.12	9.67±0.45	0.05±0.02	88.9

[1]Oxygen content calculated by difference

The composition of the HTC and torrefaction product gas (normalised to account for any air ingress) can be seen in Table 6.4. The gas generated includes any dissolved carbon dioxide, which was determined using Henry's law

calculations, the working of which can be seen in Table 6.5. An example of Henry's law calculations can be seen in section 3.3.9. The vast majority of gas produced by both HTC and torrefaction is CO_2. The gas produced by the low-temperature HTC experiments was over 99%, and conducting HTC under harsher conditions slightly increased the production of hydrogen and hydrocarbons. HTC at 250°C still produced over 96% CO_2. HTC generates more H_2, CO, and hydrocarbons than torrefaction. In all cases, the vast majority of hydrocarbon gas is methane. HTC produced double the volume of CO_2 than torrefaction at the same temperature., Increased CO_2 production could indicate the presence of water hydrogen donation in HTC reactions.

Table 6.4 Normalised gas composition of HTC and torrefaction product gas

Process	Gas yield (AR) (%)[1]	Gas yield (DAF) (%)[1]	Gas composition (detected) (%)			
			H_2	CO_2	CO	HC
200°C HTC	1.4	1.5	0.19	99.40	0.16	0.25
225°C HTC	3.2	3.4	0.23	99.48	0.03	0.26
250°C HTC	7.1	7.8	2.33	96.53	0.42	0.72
225°C Torrefaction	1.5	1.7	0.00	99.82	0.00	0.18

[1]Includes dissolved CO_2

Table 6.5 Dissolved carbon dioxide in process liquor

Volume of water (l)	H (mol/L.atm)	Partial pressure (atm)	Dissolved CO_2			
			Concentration (Mol/l)	Moles	Mass (g)	% of CO_2 generated
0.0296	0.034	0.464	0.0158	0.000467	0.0205	18.7
0.0296	0.034	0.686	0.0233	0.000690	0.0304	12.0
0.0296	0.034	0.807	0.0274	0.000812	0.0358	6.3

6.3 Carbon balance

A carbon balance of the experiments is shown in Table 6.6. The carbon balance is needed to ensure that all of the original carbon can be accounted for and therefore any assertions on the impact of the processes on the carbon content of the biomass could be made with confidence. The mass of solid and liquid carbon was calculated using the elemental analysis combined with the solid yield and mass of the total water present in the system, respectively. The mass of the gaseous product was calculated from the composition and yield of the gas, alongside the molar masses of the gaseous products. The vast majority of the original carbon in the untreated wood can be accounted for in all cases. Virtually all of the original carbon can be found after torrefaction, but less carbon was accounted for in the HTC experiments. The potential pathways for carbon to be unaccounted for are the same as was described in section 6.2.1.

The carbon balance for the HTC experiments accounts for a higher percentage of the original material than the mass balance, due to the generation of water not having an impact on the carbon balance. A further difference between the carbon balance is how it is affected by HTC temperature. More of the original carbon can be accounted for in higher temperature HTC, which is the inverse of what was seen in the mass balances. This could be due to the process liquor carbon content decreasing with increasing temperature. This means that there is less carbon that could potentially be lost through volatilisation.

Table 6.6 Carbon balance of HTC and torrefaction of wood

Sample	Mass carbon in products (g)				% Carbon accounted
	Solid	Liquid	Gaseous	Total	
Soft wood	3.84	N/A	N/A	3.84	100
200°C hydrochar	2.89	0.45	0.02	3.36	88
225°C hydrochar	3.02	0.43	0.06	3.51	91
250°C hydrochar	2.98	0.43	0.15	3.56	93
225°C biochar	3.64	N/A	0.03	3.76	98

6.4 NMR study of aromatisation by HTC and torrefaction

The ^{13}C NMR spectra of the untreated wood and torrefied wood are displayed in Figure 6.1; and the ^{13}C NMR spectra of the wood hydrochars can be seen in Figure 6.2, and the legend used for peaks assignment can be seen in Table 6.7. The peaks between 160-100 ppm represent the aromatic carbon, those between 100-50 ppm represent cellulose and hemicellulose, and those between 60-50 ppm represent the methoxy carbon in lignin. The hydrochar spectra are similar to those seen in the literature, shown in Figure 6.3. The hydrochars represented by the literature spectra were produced at maximum temperature of 230°C from a variety of feedstocks (maize silage, greenery, digestate, and sewage sludge)(Wiedner et al., 2013). The hydrochar spectra shown in Figure 6.2 are most similar to the lignocellulosic hydrochars, sharing the large, distinctive lignin methoxy peak. This peak is prominent as lignin is a significant component of lignocellulosic biomass (Gani & Naruse, 2007; Tekin et al., 2014), and does not decompose significantly under HTC conditions (Reza,

Lynam, et al., 2013; Yue et al., 2018). This peak is much less prominent in the case of sewage and digestate hydrochar. Sewage sludge typically does not have significant quantities of lignin (He et al., 2013; Huang et al., 2013), but the composition of the biogas feedstock was not published (Wiedner et al., 2013) so observations cannot be made.

The decomposition of cellulose and hemicellulose in HTC is shown by the reduction in the large peak between 100-50 ppm. This reduction is larger when HTC temperature is increased, indicating increased decomposition. Lignin is shown to be largely unaffected, seen by the methoxy peak becoming more prominent after processing.

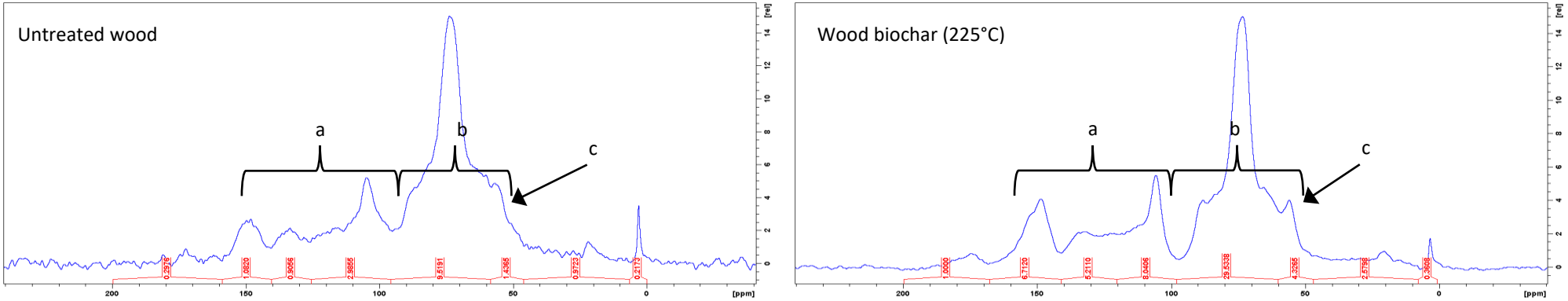

Figure 6.1 ^{13}C NMR spectra of untreated wood and wood biochar

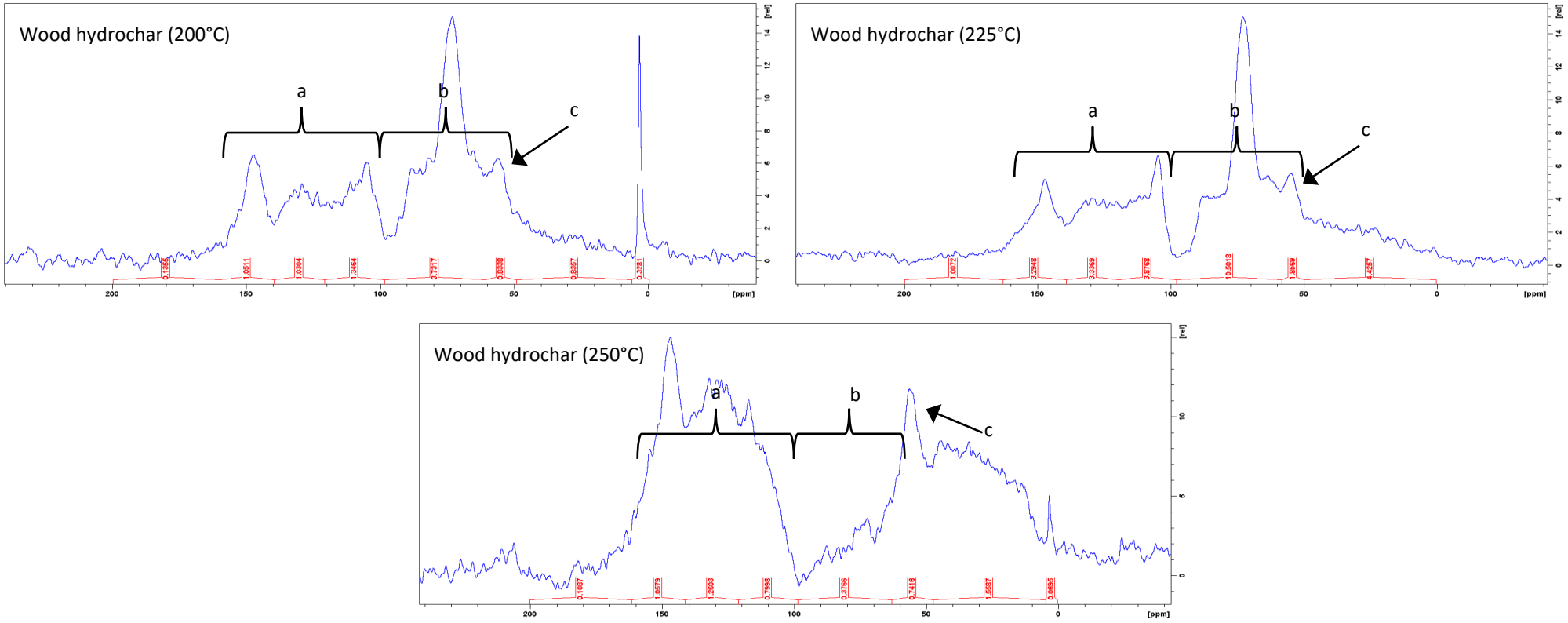

Figure 6.2 ^{13}C NMR spectra of wood hydrochars

Table 6.7 Peak assignment of ^{13}C NMR spectra

Label	Assignment
a	Aromatic carbon
b	Cellulose/ hemicellulose
c	Lignin (methoxy carbon)

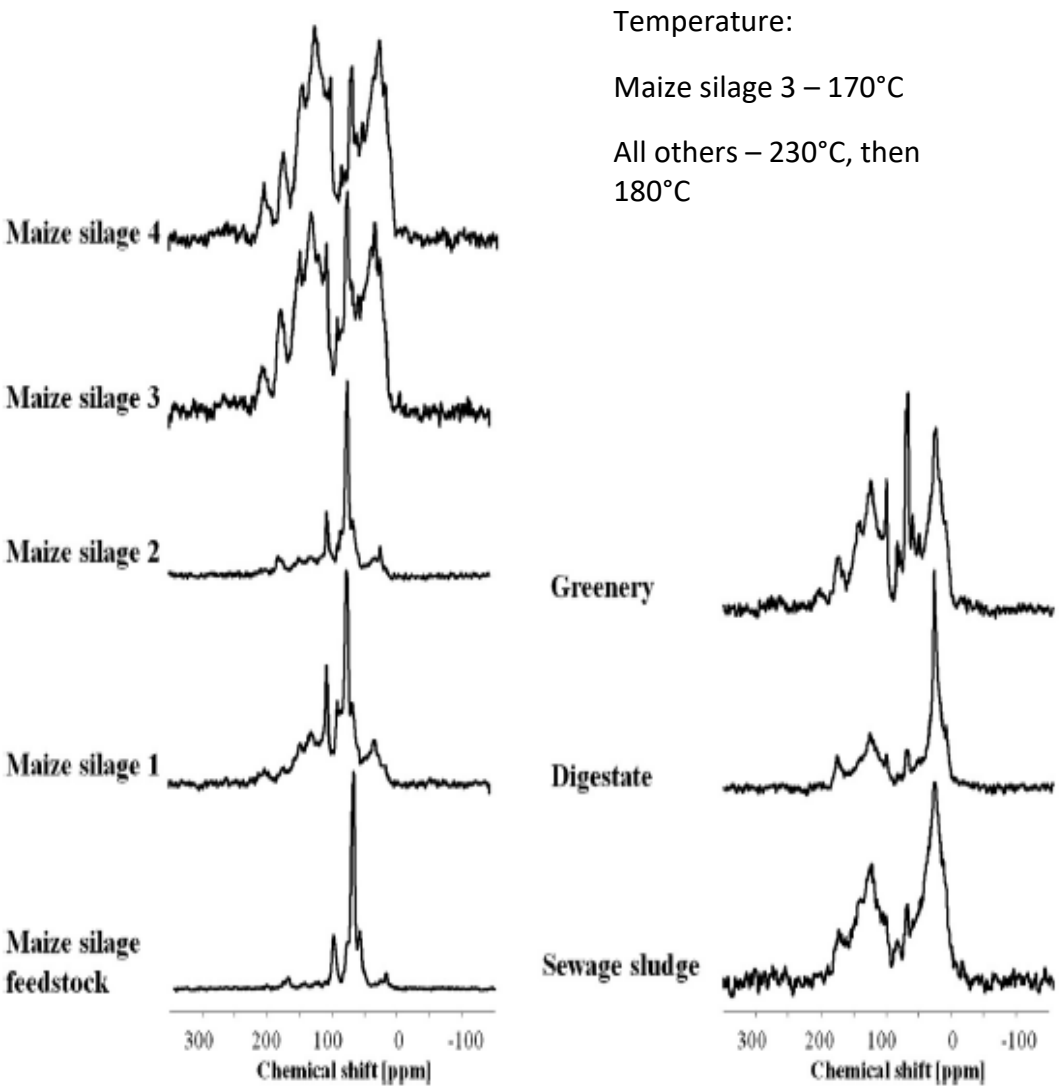

Figure 6.3 ^{13}C NMR spectra for a selection of hydrochars (Wiedner et al., 2013)

Table 6.8 HTC conditions used in hydrochar production (Wiedner et al., 2013)

Hydrochar	Feedstock	Temperature (°C)		Time (min)		Pressure (MPa)	
		Stage 1	Stage 2	Stage 1	Stage 2	Stage 1	Stage 2
Maize silage 1	Maize silage	230	180	15	75	2.8	1
Maize silage 2	Maize silage	230	180	15	75	2.8	1
Maize silage 3	Maize silage	170	N/A	90	N/A	0.79	N/A
Maize silage 4	Maize silage 3	230	180	15	75	2.8	1
Leftover food	Leftover food	230	180	15	75	2.8	1
Biogas digestate	Biogas digestate	230	180	15	75	2.8	1
Greenery	Greenery	230	180	15	75	2.8	1

The aromatic carbon content of samples (determined using the peaks between the chemical shifts of 160-100 ppm), in addition to the proportion of original aromatic carbon in the samples as compared to that in the feedstock wood (which shows the amount of aromatic carbon that has been generated) can be seen in Table 6.9. The calculation of the proportion of original aromatic carbon is described in section 3.3.10.

Table 6.9 Degree of aromatisation of biomass by HTC and torrefaction

Sample	Aromatic carbon (%)	Proportion of original aromatic carbon (%)
Wood	28.6	N/A
200°C hydrochar	36.9	97.4
225°C hydrochar	37.1	102.43
250°C hydrochar	52.2	108.1
225°C biochar	34.6	117.7

It can be seen that although HTC vastly increases the percentage of aromatic carbon in the solid fuel, torrefaction generates significantly more aromatic carbon on an absolute basis. The higher aromatic carbon content of the wood hydrochars in comparison to torrefied wood, despite a lesser degree of aromatisation, will be due to the significantly higher degradation of non-aromatic organic components (such as hemicellulose and cellulose) in HTC. This is alluded to by the data shown in Table 6.1, which shows that HTC has a much lower solid mass yield than torrefaction. During HTC, the vast majority of the hemicellulose content of the biomass decomposes, and cellulose decomposes at higher temperatures (Reza, Lynam, et al., 2013). This leaves behind the lignin content of the biomass (which is fairly unaffected by HTC (Liu et al., 2013; Reza, Lynam, et al., 2013)), which has significant levels of aromatic carbon. This would be the main mechanism for the increase in aromatic carbon content of hydrochars. In torrefaction, hemicellulose is removed (Kambo & Dutta, 2015b), but cellulose degrades at 315–400°C (Yang et al., 2006), so will not be removed in the torrefaction conditions used.

The lesser generation of absolute aromatic carbon in HTC could be due to the presence of water resulting in a number of reactions that compete with aromatisation reactions. These would include reactions where hydrogen from the water molecules are donated to the organic molecules involved in the reaction, which would result in the remaining oxygen from water being released as carbon dioxide or more water. The significantly higher CO_2 yield of HTC in comparison to torrefaction at the same temperature, as seen in Table 6.4, could indicate that these reactions are occurring to a significant extent, and as a result are reducing the degree of aromatisation in the feedstock through competition with aromatisation reactions.

In the case of HTC at 200°C, loss of non-aromatic carbon appears to be the sole factor in increasing aromatic carbon concentration, as there is no increase in absolute aromatic carbon in comparison to the feedstock untreated wood. Aromatisation reactions in HTC begin at higher HTC temperatures, with the proportion of absolute aromatic carbon in comparison to the feedstock biomass increasing steadily with temperature. This matches the known chemistry of HTC, described in section 2.3.3. Cellulose begins to degrade a HTC temperatures above 200°C (Reza, Lynam, et al., 2013), and the mechanism in which it degrades produces aromatic carbon, as the cellulose oligomers produced in the degradation form envelopes to minimise the surface area exposed to water. The resulting dry, homogenous heating regime experienced

by the majority of the oligomers results in reactions that produce aromatic carbon (Falco et al., 2011). Additionally, in HTC of furfural residue, the concentration of 5-HMF in the process liquor has been shown to drop above the HTC temperatures of 220°C, being undetectable in the process liquor of HTC at 240°C (Yue et al., 2018). This indicates that 5-HMF is undergoing self-condensation (including aromatisation) and rehydration reactions, producing some solid hydrochar (Yue et al., 2018). The hydrochar produces would contain aromatic carbon, increasing the absolute aromatic carbon content of the hydrochar. Aromatic carbon is also produced by polymerisation and aromatisation of carbohydrates produced by degradation of hemicellulose (Aidan M. Smith et al., 2016), which would progress faster under higher HTC temperatures like what was described for 5-HMF.

^{1}H NMR of the HTC liquors can be seen in Figure 6.4, and the peak assignment can be seen in Table 6.10. The strong signal at 4.6 ppm is the solvent peak (HDO). This peak is so large in comparison to the others due to limitations in the feasible organic concentration in comparison to the 99.9% purity of D_2O. Additionally, some residual water may have been present in the organic sample as gentle heating was used to dry the samples as to avoid losing volatile organic matter.

HTC reactions are complex and produce a wide variety of organic compounds, but some of the peaks seen in the ^{1}H NMR of the process liquor can be matched

to degradation products of hemicellulose and cellulose generated in HTC that have been described in section 2.3.3. Potential degradation products identified include 5-HMF, levulinic acid, glycerol, hydroxyacetone, and acetaldehyde. The assignment of peaks to degradation products can be seen in **Table** 6.10. As the process liquor of HTC is a complicated mixture of organic compounds, there are some peaks that have multiple potential assignments. For example, the close cluster of peaks between 3.0 and 4.0 ppm could be due to glycerol (formed from the decomposition of residual lipids), or could be due to anhydroxylose originating from hemicellulose (Sun, Sun, Sun, & Su, 2004; Yue et al., 2018). The presence of these degradation products in the process liquor confirms the reaction mechanisms of HTC laid out in section 2.3.3, and also points to a significant portion of the degradation products remaining in the liquor rather than recombining to join the hydrochar.

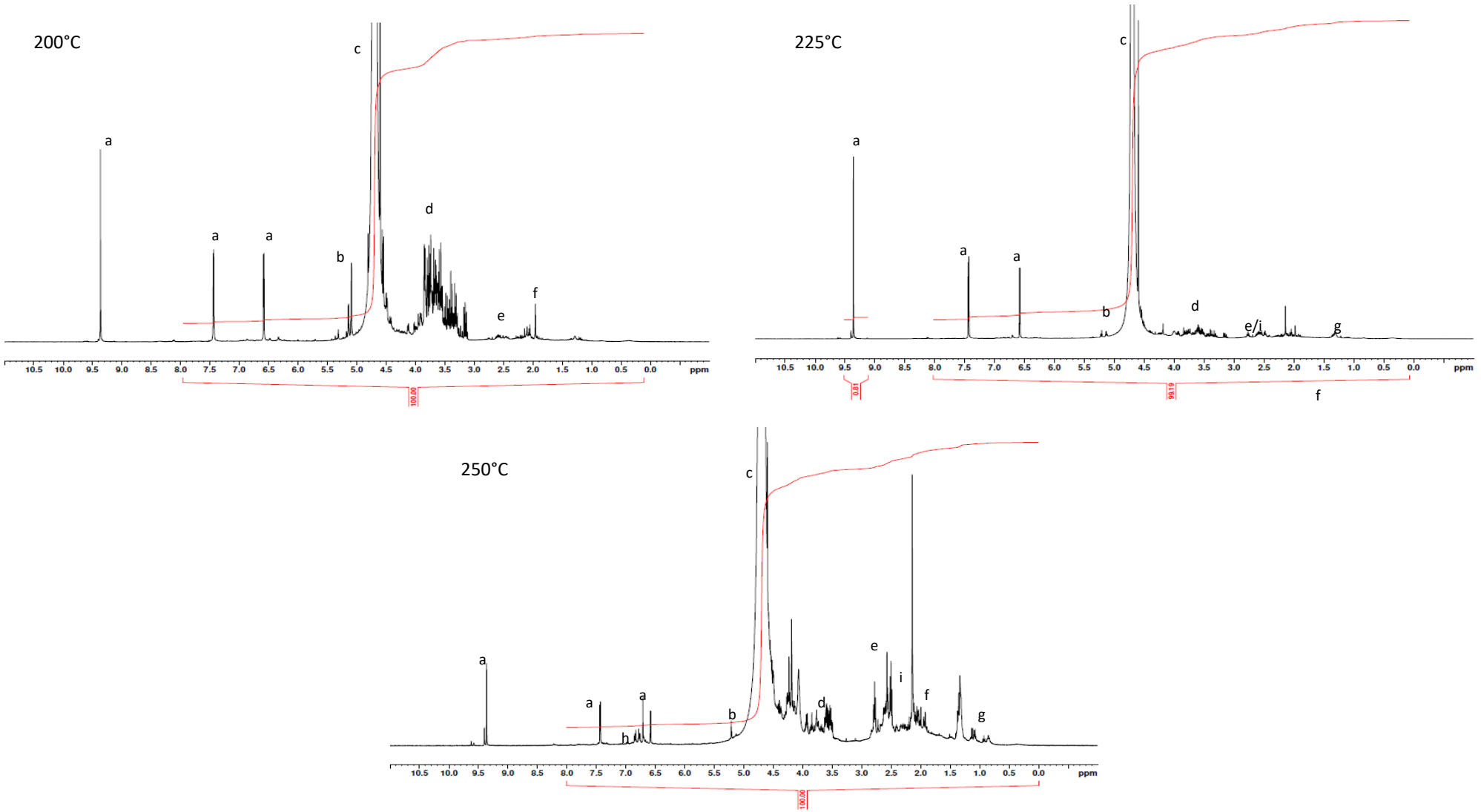

Figure 6.4 ^{1}H NMR spectra of HTC process liquor

Table 6.10 Peak assignment of ^{1}H NMR spectra

Label	Assignment	Reference
a	5-HMF	(Yue et al., 2017)
b	D-arabinofuranosyl	(Sun et al., 2004)
c	Solvent peak (HDO)	-
d	Anydroxylose/glycerol	(Sun et al., 2004; Yue et al., 2018)
e	Levulinic acid	(Yue et al., 2018)
f	Acetaldehyde	(Yue et al., 2018)
g	Aliphatic carbon	(Yue et al., 2018)
h	Aromatic carbon	(Yue et al., 2018)
i	Benzylic	-

Peaks begin to appear in the process liquor NMR at shifts of 6.5-7.0 ppm, and the relative signal strength of peaks around 2.3 is seen to increase with increasing HTC temperature. These could be representative of aromatic protons or benzylic protons, which would show that some aromatic carbon is being lost to the liquor in HTC. There appears to be little to no aromatic content in the 200°C liquor, with the main carbon content being generated from decomposition of hemicellulose and cellulose. This further indicates that there is no significant aromatisation reactions occurring in low-temperature HTC in this case, as nearly 100% of the original aromatic carbon is retained in the hydrochar, and little to no aromatic carbon is lost to the liquid phase. In the case of HTC at 250°C, the liquor has significant concentrations of aromatic carbon. This aromatic carbon could originate either from loss of newly generated aromatic carbon, or from partial decomposition of lignin. An increase in aromatic carbon content in HTC liquor with increasing HTC

temperature has also been seen in HTC of furfural residue, and this was attributed to decomposition of lignin (Yue et al., 2018). The majority of lignin degradation products will condense easily to form solid products, some lignin fragments could remain in the aqueous phase trough stabilisation by hemicellulose degradation products (Fang et al., 2018). The continued increase in aromatisation with increasing HTC temperature coupled with the increasing loss of aromatic carbon into the liquor could indicate that the degree of aromatisation is increasing exponentially with temperature.

6.5 Conclusions

1. A carbon balance of HTC of wood pellets at 200, 225, and 250°C; as well at torrefaction of wood pellets at 225°C was performed. Over 88% of the original carbon was accounted for in all cases

2. HTC and torrefaction were both found to increase the aromatic carbon content of the wood pellets, although torrefaction increases the absolute aromatic carbon of the feedstock to a much higher degree than HTC at the same temperature.

3. In HTC at 200°C, the increase in aromatic carbon content was solely due to the decomposition of hemicellulose and cellulose from the biomass, and subsequent loss of non-aromatic carbon.

4. Aromatisation reactions were observed in HTC at 225°C, with the hydrochar containing a higher amount of absolute aromatic carbon that the feedstock wood. Aromatisation was seen to increase with increasing HTC temperature. At high HTC temperatures some aromatic carbon was found in the process liquor, either from loss of newly generated aromatic carbon, or from partial decomposition of lignin.

5. Increased CO_2 yields suggest that the suppression of aromatisation could be due to hydrogen donation in competing reactions.

Chapter 7 The impact of HTC on chemical activation of olive cake

Biomass is seen as a potential cheap and sustainable source of activated carbon, and HTC has been proposed as a pre-treatment which could improve the results of activation (Jain, Balasubramanian, & Srinivasan, 2016b; Tay, Ucar, & Karagöz, 2009). In this study, the effect of HTC on the yield of activation and the porosity of activated carbon is investigated. The surface area of activated carbon is important, as a high surface area is key to the performance of the material in adsorption applications. Olive cake hydrochar (produced at 240°C for 2 hours with a 1:1 W/B ratio) and raw olive cake were chemically activated with KOH at a temperature of 700°C. KOH to feedstock ratios of 0.5, 1 and 2 were studied. The labelling of the samples can be seen in Table 7.1.

Table 7.1 Summary of olive cake and olive cake hydrochar activation ratios

Feedstock	KOH:Biomass	Label
Olive cake	0.5:1	OC(0.5)
	1:1	OC(1)
	2:1	OC(2)
Olive cake hydrochar	0.5:1	HC(0.5)
	1:1	HC(1)
	2:1	HC(2)

7.1 Activation yield and proximate analysis

The yield of the activation of olive cake and olive cake hydrochar is displayed in Table 7.2. The overall yield takes into account the yield of HTC by comparing the mass of final product to that of the original untreated biomass feedstock.

Activation of hydrochar has a much higher yield than the activation of untreated biomass, but when the yield of HTC is taken into account, there is very little difference. The 1:1 ratio of KOH and feedstock is a slight exception to this, as use of hydrochar resulted in a lower overall yield. Use of higher ratios of KOH to feedstock resulted in a decrease in overall yield both when using biomass or hydrochar. A decrease in activation yield with increasing activating agent has been previously reported in the activation of grape seeds (Okman, Karagöz, Tay, & Erdem, 2014).

Table 7.2 Activation yield of olive cake and olive cake hydrochar

Sample	Activation yield (%)	Overall yield (%)
OC(0.5)	27.6	27.6
OC(1)	27.3	27.3
OC(2)	22.3	22.3
HC(0.5)	56.0	27.5
HC(1)	53.2	22.3
HC(2)	50.8	21.3

The proximate analysis of the untreated olive cake, olive cake hydrochar, and the activated carbon samples are shown in Table 7.3. The activated carbon

samples have a higher moisture content than their feedstock, which could be due to a higher porosity in the activated carbon (Rengaraj, Moon, Sivabalan, Arabindoo, & Murugesan, 2002). They also have a lower volatile matter and higher fixed carbon content than their precursor, which can be attributed to the harsh conditions involved in the activation resulting in decomposition of hemicellulose, cellulose, and lignin from biomass (Guillot, Py, Stoeckli, Chambat, & Cagnon, 2008). The higher ash fraction of activated carbon is mainly due to the loss of volatile matter and moisture during activation.

The use of hydrochar instead of untreated biomass does not appear to have a significant effect on the dry, ash-free (DAF) volatile matter and fixed carbon content of the activated carbon char. There might be a larger fixed carbon content produced by activation with high ratios of KOH to feedstock, but this difference is negligible. This indicates that HTC does not impact the activation significantly in terms of the proximate analysis of the final product.

Table 7.3 Proximate analysis of olive cake, olive cake hydrochar, and their respective activated carbon

Sample	Moisture (%)	Volatile matter (AR) (%)	Volatile matter (DAF) (%)	Fixed carbon (AR) (%)	Fixed carbon (DAF) (%)	Ash (%)
Olive Cake	6.2	63.1	73.5	22.9	26.5	7.9
OC(0.5)	9.9	9.1	12.3	64.9	87.7	16.1
OC(1)	8.7	11.1	14.3	66.3	85.7	13.9
OC(2)	6.9	9.2	11.9	68.0	88.1	16.0
Olive cake Hydrochar	0.4	55.8	60.4	36.6	39.6	7.2
HC(0.5)	8.6	9.5	13.6	60.1	86.4	21.8
HC(1)	8.8	10.7	13.9	66.2	86.1	14.3
HC(2)	4.6	6.2	8.0	70.9	92.0	18.2

7.2 Textural analysis

N_2 adsorption/desorption isotherms along with Density functional theory (DFT) pore size distribution of the activated carbon samples can be seen in Figure 7.1. The isotherms broadly match the IUPAC classification of type I isotherms throughout, showing rapid saturation at lower relative pressure before reaching a plateau (Alothman, 2012). This shows that the structures are significantly microporous. Increasing the activating agent to feedstock ratio slightly increased the size of the pores.

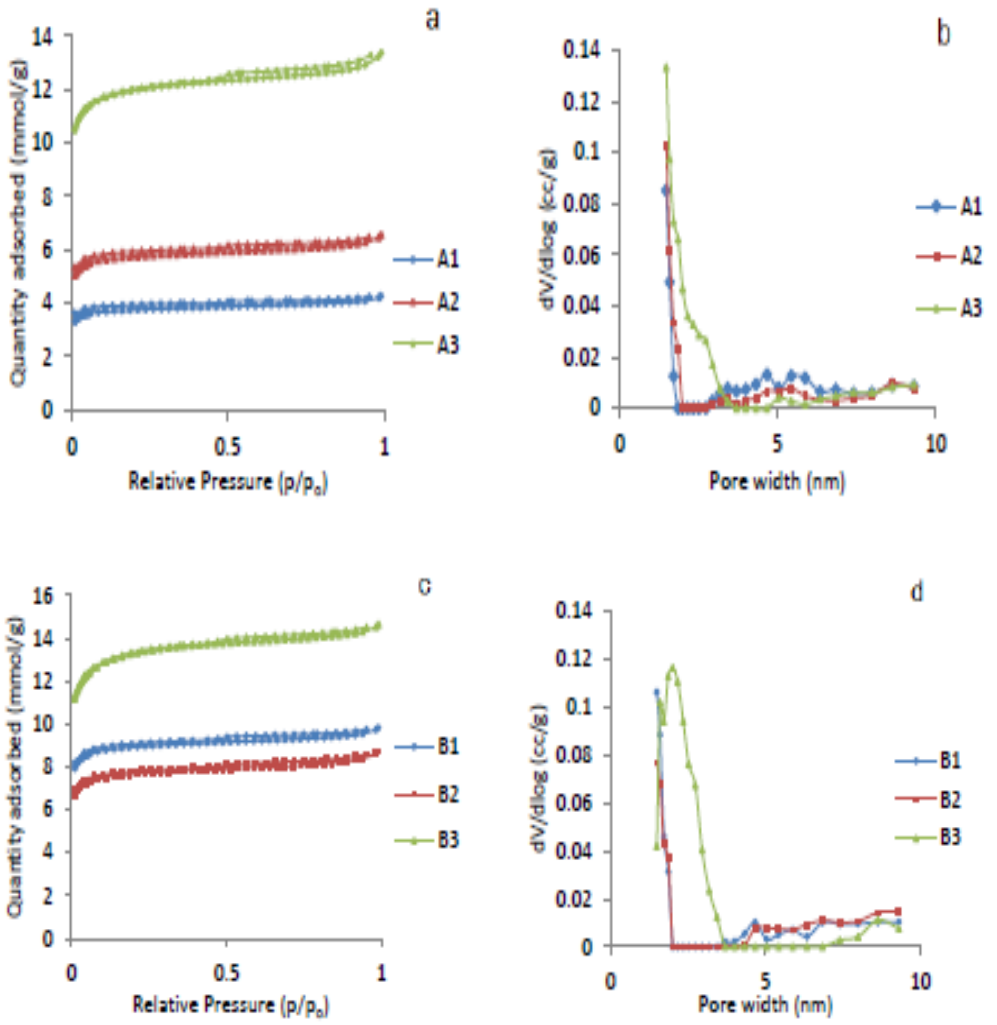

Figure 7.1 N_2 Adsorption isotherms and DFT Pore Width Data of Olive Cake Hydrochar (a,b) and untreated Olive Cake (c,d) Activated Carbon

A summary of some of the textural properties of the activated carbon samples are shown in Table 7.4. The pore size of all the samples were similar, as was seen in Figure 7.1. The surface area of the samples broadly increased with increasing activating agent to feedstock ratio. This has been reported previously in the chemical activation of anthracite with KOH (Lillo-Ródenas, Lozano-Castelló, Cazorla-Amorós, & Linares-Solano, 2001), although in a study

of activation of grape seed, the influence of activatiing agent to feedstock ratio is more complicated, with the influence of activation temperature having a stronger, more direct influence. Increasing activation temperature was found to increase the surface area of the activated carbon (Okman et al., 2014).

The surface areas of the untreated olive cake activated carbon samples were all larger than that of their hydrochar counterparts, with the most pronounced difference being with the activated carbon made using 0.5:1 KOH:biomass. This is due to pore blockage through the deposition of organic matter from the aqueous phase in the process liquor to the hydrochar (Román et al., 2013). Increasing the activating agent to feedstock ratio quickly increases the surface area of the hydrochar derived activated carbon, with the activated carbon produced using a 2:1 ratio possessing a micropore surface area similar to that of the activated carbon produced from untreated olive cake under the same conditions. This could indicate that increasing the amoount of KOH in the system results in the deposited organic compounds produced in HTC decomposing, exposing the pores and increasing the surface area of the activated carbon.

Table 7.4 Summary of relevant textural properties of olive cake hydrochar and untreated olive cake activated carbon

Sample	Pore Size (nm)	Surface Area(m^2/g)	Micropore Surface Area (m^2/g)	Total Pore Volume (VT), (cc/g)	Micropore Volume (Vmic), (cc/g)	Micropore Volume fraction
OC(0.5)	1.69	806.01	789.51	0.27	0.25	92.60
OC(1)	1.76	687.53	667.56	0.23	0.22	95.65
OC(2)	1.75	1158.08	1134.63	0.40	0.38	95.00
HC(0.5)	1.74	339.19	328.86	0.12	0.10	83.33
HC(1)	1.77	515.37	501.05	0.17	0.16	94.11
HC(2)	1.74	1064.10	1041.45	0.36	0.34	94.44

Scanning electron microscopy (SEM) images of required samples were recorded and presented in Figure 7.2. They clearly show the generation of pores in activation, and that activation of untreated olive cake generates more micropores than activation of olive cake hydrochar. It also shows that HTC does not drastically change the morphology of olive cake.

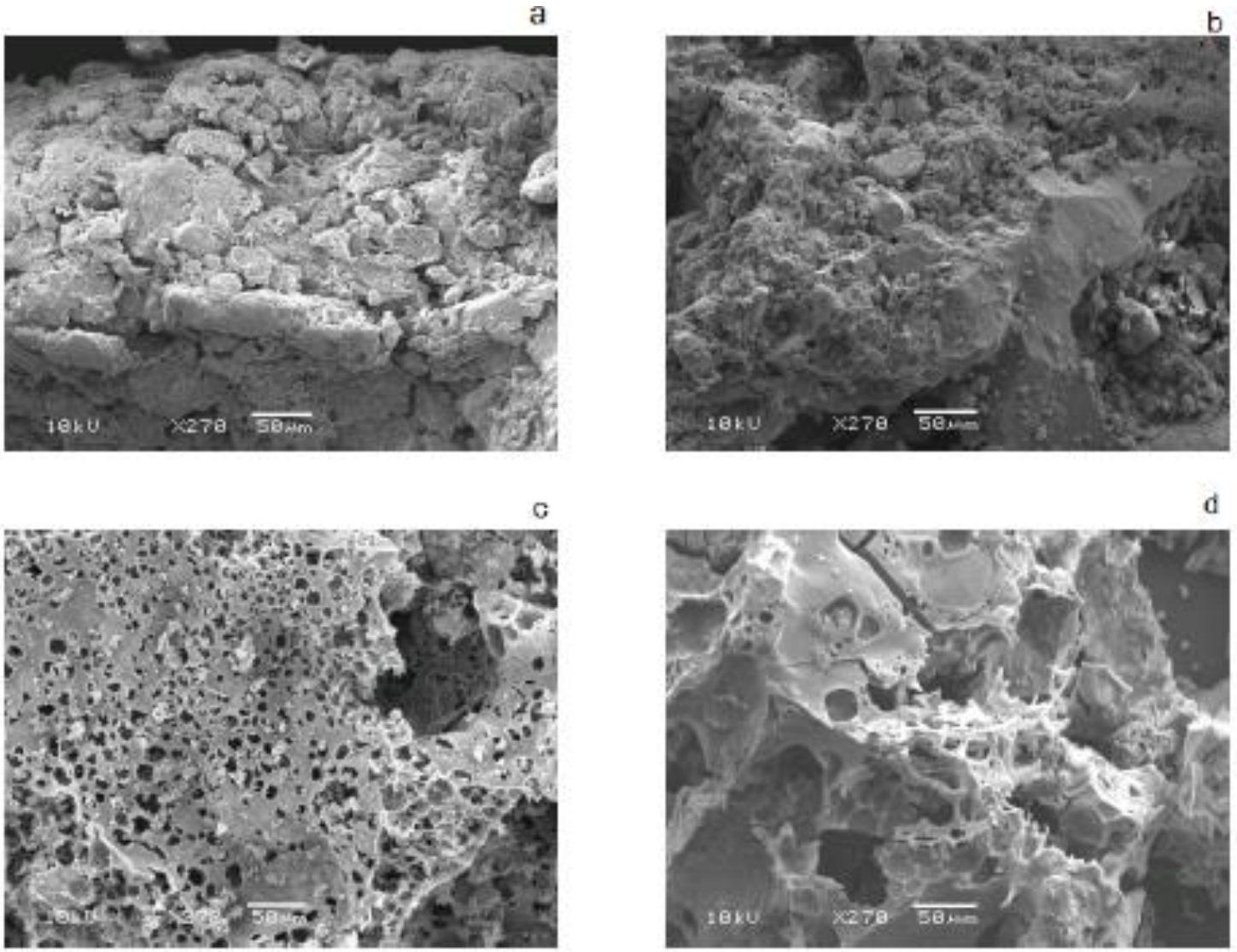

Figure 7.2 SEM images of (a) olive cake (b) olive cake hydrochar (c) activated carbon OC(2) (d) activated carbon HC(2)

7.3 Conclusions

1. Activation of hydrochar results in a greater yield in comparison to untreated biomass, although the overall yield of HTC and activation is similar to that of activation of untreated biomass.

2. Hydrochar-derived activated carbon has similar pore distribution to biomass-derived activated carbon

3. Hydrochar-derived activated carbon has a lower surface area and micropore volume is less, likely due to depositing of organics on the surface of the hydrochar during HTC blocking pores. The use of higher ratios of activating agent to feedstock lessens this deficiency.

8

Chapter 8 Conclusions and recommended future work

8.1 Conclusions

A parametric study into the impact of temperature, residence time, and W/B ratio on the HTC of miscanthus has been conducted, and was supplemented with additional HTC data to provide knowledge on how the outcomes of HTC vary with both reaction parameters and feedstock. In addition to this, the impact of HTC on the combustion properties of biomass has been investigated, the role of water in degradation reactions in HTC have been described, and the impact of HTC on the production of activated carbon has been studied. The outcomes of the investigation are as follows:

1. Temperature had the largest effect on yield of HTC and composition of biocoal. The HTC yield increased as temperature increased, with the biocoal having lower moisture and volatile matter content, alongside higher fixed carbon content. The ash content of biocoal was higher or lower than that of the feedstock biomass, dependent on the composition of the ash. Residence time and W/B ratio had a much weaker impact on HTC than temperature in the ranges studied, in many cases being found statistically insignificant.

2. Particle size of biomass had a small effect on the carbon yield of biomass. In separate HTC experiments on miscanthus and soft wood, it

was seen that decreasing particle size was shown to slightly increase carbon yield, with this effect being magnified at higher HTC temperatures.

3. The biochemical composition of the feedstock has a significant effect on the results of HTC. The presence of large quantities of easily hydrolysable organic compounds in some biomass feedstocks resulted in low yields, and the absence of reactive organic matter in some resulted in very high yields. In some cases, for example HTC of rice, increasing the HTC temperature vastly increases the carbon yield due to repolymerisation of degradation products.

4. HTC increases the carbon content of biomass and decreases the hydrogen and oxygen content. This effect is increased by increasing HTC temperature, with HTC of miscanthus at 250°C producing a biocoal with a similar atomic H:C and O:C ratio to lignite. Residence time and W/B ratio had a much weaker impact on the elemental composition, especially at low temperature.

5. The elemental composition of biocoals was variable between feedstock, and the composition was closely linked to the composition of the feedstock biomass. The trends in biocoal composition with temperature, residence time, and W/B ratio were generally consistent between feedstocks..

6. HTC of some feedstocks results in a liquor which has a significant carbon content. Anaerobic digestion of the process liquor was calculated to have a significant potential to augment the energy yield of HTC, especially when the energy yield in biocoal is low.

7. HTC lowers the char reactivity of biomass. This seems to be caused primarily by removal of catalytic alkali and alkaline earth metals from the biomass, with the surface area and composition providing secondary effects. This trend is also seen in combustion of chars produced using high heating rates representative of pulverised fuel (PF) combustion. HTC increases the activation energy and lowers the pre-exponential factor of combustion of soft wood biomass.

8. HTC of biomass with low alkali and alkaline earth metal content results in a fuel with a similar reactivity to that of high-volatile bituminous coal, whereas in the case of biomass with higher alkaline and alkaline earth metal content the resulting biocoal has a reactivity between that of its untreated biomass feedstock and coal.

9. Coal-equivalent fuels were produced by torrefaction of soft wood biocoals. The torrefied biocoal had a DAF volatile matter content in the range of sub bituminous and high-volatile bituminous coal, with similar reactivity to high-volatile bituminous coal, and a very low ash content.

10. HTC and torrefaction were both found to increase the aromatic carbon content of the wood pellets. In low-temperature HTC this was solely due to removal of non-aromatic organic compounds from the biomass, whereas at higher-temperature HTC and in torrefaction aromatisation of the feedstock occurred. The extent of aromatisation reactions in torrefaction was significantly greater than in HTC, indicating that the presence of water suppressed aromatisation during HTC.

11. HTC was found to have little effect on the overall yield of production for activated carbon. The activated carbon produced from hydrochars had a similar pore distribution to that produced from untreated olive cake, but possessed a much lower surface area due to deposition of organic matter clogging the pores. Increasing the ratio vastly improved the surface area of the hydrochar-derived activated carbon.

8.2 Recommended future work

This study further illustrated that HTC is an intriguing biomass pre-treatment with exciting potential. As such, more research should be conducted to deepen our knowledge of the process fundamentals and potential applications. Future HTC research that should be considered includes:

1. Further investigation into the impact of residence time and W:B ratio on the yield and composition of HTC. This study showed that these factors are mostly statistically insignificant in the range studied in the DoE and are much less impactful than HTC temperature, but repeat experiments would provide more accuracy. Additionally, there are numerous process conditions both inside and outside the limits of the test matrix that could provide useful information on the impact of these parameters.

2. Conducting further tests examining the role of alkali/alkaline earth metal content on the char reactivity of biomass fuels. Firstly, further tests should be conducted to verify the results laid out in Chapter 5. The particle size experiments shown in section 5.2.4.3 showed that there was little difference between burnout of biocoal in the 0-75 µm range and that of biocoal in the 75-150 µm range, and any variations shown were insignificant in comparison to the char burnout changes described, but there was enough variation between samples to warrant further

study. Both 0-75 µm and 75-150 µm represent very small particle sizes, which are in the range seen in PF combustion. A full particle size study would include particle size ranges up to 500 µm.

3. It could be worthwhile investigating the potential of acid leaching prior to HTC as a means to produce biocoal with similar reactivity to bituminous coal from biomass with high alkali/alkaline earth metal contents. Acid leaching of olive cake proved that olive cake could become as unreactive as coal, and combining this with the advanced fuel properties of biocoal would have the potential to produce a coal-equivalent fuel from waste biomass.

4. This study initiated some research into the behaviour of biocoal chars produced at high heating rate in a drop tube furnace (DTF), representative of char produced under pulverised fuel conditions. Further investigation of the combustion behaviour of these chars in comparison to coal and biomass DTF chars would be very useful for assessing the potential of biocoal as a coal replacement. Further work that could be investigated well as determination of the activation energy and pre-exponential factor of DTF char combustion of various biocoal feedstocks, as well as investigating the ignition behaviour of the chars. The former would involve further study of the irregular DTF char burnout curves which were displayed in section 5.2.4.2. This could be done by determining the rate constant for each stage of combustion.

5. This study investigated the role of water in the aromatisation reactions in HTC. Further fundamental studied into the chemistry of HTC is recommended as to further understand how HTC affects biomass, so that the process can be better understood and optimisation can be carried out easier.

References

Abdul-Hamid, A., Raja Sulaiman, R. R., Osman, A., & Saari, N. (2007). Preliminary study of the chemical composition of rice milling fractions stabilized by microwave heating. *Journal of Food Composition and Analysis*, *20*(7), 627–637. https://doi.org/10.1016/j.jfca.2007.01.005

Acharya, B., Dutta, A., & Minaret, J. (2015). Review on comparative study of dry and wet torrefaction. *Sustainable Energy Technologies and Assessments*, *12*, 26–37. https://doi.org/10.1016/j.seta.2015.08.003

Adams, R. C., MacLean, F. S., Dixon, J. K., Bennett, F. M., Martin, G. I., & Lough, R. . (1951). *The utilization of organic wastes in N.Z.: Second interim report of the inter-departmental committee.*

Agbor, E., Zhang, X., & Kumar, A. (2014). A review of biomass co-firing in North America. *Renewable and Sustainable Energy Reviews*, *40*, 930–943. https://doi.org/10.1016/j.rser.2014.07.195

Ail, S. S., & Dasappa, S. (2016). Biomass to liquid transportation fuel via Fischer Tropsch synthesis - Technology review and current scenario. *Renewable and Sustainable Energy Reviews*, *58*, 267–286. https://doi.org/10.1016/j.rser.2015.12.143

Alothman, Z. A. (2012). A review: Fundamental aspects of silicate mesoporous materials. *Materials*, *5*(12), 2874–2902. https://doi.org/10.3390/ma5122874

Álvarez-Murillo, A., Román, S., Ledesma, B., & Sabio, E. (2015a). Study of variables in energy densification of olive stone by hydrothermal carbonization. *Journal of Analytical and Applied Pyrolysis*, *113*. https://doi.org/10.1016/j.jaap.2015.01.031

Álvarez-Murillo, A., Román, S., Ledesma, B., & Sabio, E. (2015b). Study of variables in energy densification of olive stone by hydrothermal carbonization. *Journal of Analytical and Applied Pyrolysis*, *113*, 307–314. https://doi.org/10.1016/j.jaap.2015.01.031

Antaco. (n.d.). Biocoal. Retrieved April 11, 2019, from http://www.antaco.co.uk/biocoal/

Baccar, R., Bouzid, J., Feki, M., & Montiel, A. (2009). Preparation of activated carbon from Tunisian olive-waste cakes and its application for adsorption of heavy metal ions. *Journal of Hazardous Materials*, *162*(2–3), 1522–1529. https://doi.org/10.1016/j.jhazmat.2008.06.041

Bach, Q. V., & Skreiberg, O. (2016). Upgrading biomass fuels via wet torrefaction: A review and comparison with dry torrefaction. *Renewable and Sustainable Energy Reviews*, *54*, 665–677.

https://doi.org/10.1016/j.rser.2015.10.014

Bach, Q. V., & Tran, K. Q. (2015). Dry and Wet Torrefaction of Woody Biomass-A Comparative Studyon Combustion Kinetics. *Energy Procedia*, *75*(1876), 150–155. https://doi.org/10.1016/j.egypro.2015.07.270

Baruya, P. (2015). World forest and agricultural crop residue resources for cofiring, (April). IEA Clean Coal Centre. Retrieved from http://www.usea.org/sites/default/files/042015_World Forest and agricultural crop residue resources for cofiring_ccc249.pdf

Basso, D., Patuzzi, F., Castello, D., Baratieri, M., Rada, E. C., Weiss-Hortala, E., & Fiori, L. (2016). Agro-industrial waste to solid biofuel through hydrothermal carbonization. *Waste Management*, *47*, 114–121. https://doi.org/10.1016/j.wasman.2015.05.013

Becker, R., Dorgerloh, U., Paulke, E., Mumme, J., & Nehls, I. (2014). Hydrothermal carbonization of biomass: Major organic components of the aqueous phase. *Chemical Engineering and Technology*, *37*(3). https://doi.org/10.1002/ceat.201300401

Bhuiyan, A. A., Blicblau, A. S., & Naser, J. (2017). Co-firing of biomass and slagging in industrial furnace: A review on modelling approach. *Journal of the Energy Institute*, *90*(6), 838–854. https://doi.org/10.1016/j.joei.2016.08.010

Biller, P., Ross, A. B., Skill, S. C., Lea-Langton, A., Balasundaram, B., Hall, C., … Llewellyn, C. A. (2012). Nutrient recycling of aqueous phase for microalgae cultivation from the hydrothermal liquefaction process. *Algal Research*, *1*(1), 70–76. https://doi.org/10.1016/j.algal.2012.02.002

Borrero-lópez, A. M., Masson, E., Celzard, A., & Fierro, V. (2018). Industrial Crops & Products Modelling the reactions of cellulose , hemicellulose and lignin submitted to hydrothermal treatment. *Industrial Crops & Products*, *124*(July), 919–930. https://doi.org/10.1016/j.indcrop.2018.08.045

Boyle, W. C. (1976). Energy recovery from sanitary landfills - a review. In *Microbial Energy Conversion* (pp. 119–138). Oxford: Elsevier. https://doi.org/10.1016/B978-0-08-021791-8.50019-6

British Petroleum. (2017). BP Statistical Review of World Energy 2017. *British Petroleum*, (66), 1–52. https://doi.org/http://www.bp.com/content/dam/bp/en/corporate/pdf/energy-economics/statistical-review-2017/bp-statistical-review-of-world-energy-2017-full-report.pdf

BSI. (2015). *BSI Standards Publication Solid biofuels — Determination of the content of volatile matter*.

Bui, M., Fajardy, M., & Mac Dowell, N. (2017). Bio-Energy with CCS (BECCS) performance evaluation: Efficiency enhancement and emissions

reduction. *Applied Energy*, *195*, 289–302. https://doi.org/10.1016/j.apenergy.2017.03.063

Burns, W., & Nicholson, S. (2017). Bioenergy and carbon capture with storage (BECCS): the prospects and challenges of an emerging climate policy response. *Journal of Environmental Studies and Sciences*, *7*(4), 527–534. https://doi.org/10.1007/s13412-017-0445-6

BusinessWire. (2010). AVA-CO2 Introduces the First Industrial-Size Hydrothermal Carbonisation (HTC) Plant in the World. Retrieved April 11, 2019, from https://www.businesswire.com/news/home/20101026006679/en/AVA-CO2-Introduces-Industrial-Size-Hydrothermal-Carbonisation-HTC-Plant

Calzavara, Y., Joussot-Dubien, C., Boissonnet, G., & Sarrade, S. (2005). Evaluation of biomass gasification in supercritical water process for hydrogen production. *Energy Conversion and Management*, *46*(4), 615–631. https://doi.org/10.1016/j.enconman.2004.04.003

Chen, D., Gao, A., Cen, K., Zhang, J., Cao, X., & Ma, Z. (2018). Investigation of biomass torrefaction based on three major components: Hemicellulose, cellulose, and lignin. *Energy Conversion and Management*, *169*(May), 228–237. https://doi.org/10.1016/j.enconman.2018.05.063

Chen, J., Li, C., Ristovski, Z., Milic, A., Gu, Y., Islam, M. S., … Dumka, U. C. (2017). A review of biomass burning: Emissions and impacts on air quality, health and climate in China. *Science of the Total Environment*, *579*(November 2016), 1000–1034. https://doi.org/10.1016/j.scitotenv.2016.11.025

Chen, Xinfei, Ma, X., Peng, X., Lin, Y., Wang, J., & Zheng, C. (2018). Effects of aqueous phase recirculation in hydrothermal carbonization of sweet potato waste. *Bioresource Technology*, *267*(381), 167–174. https://doi.org/10.1016/j.biortech.2018.07.032

Chen, Xuejiao, Lin, Q., He, R., Zhao, X., & Li, G. (2017). Hydrochar production from watermelon peel by hydrothermal carbonization. *Bioresource Technology*, *241*. https://doi.org/10.1016/j.biortech.2017.04.012

Chew, J. J., & Doshi, V. (2011). Recent advances in biomass pretreatment - Torrefaction fundamentals and technology. *Renewable and Sustainable Energy Reviews*, *15*(8), 4212–4222. https://doi.org/10.1016/j.rser.2011.09.017

Ciolkosz, D., & Wallace, R. (2011). A review of torrefaction for bioenergy feedstock production. *Biofuels, Bioproducts and Biorefining*, *5*, 317–329. https://doi.org/10.1002/bbb

Committee on Climate Change (CCC). (2017). *2017 Report to Parliament – Meeting Carbon Budgets: Closing the policy gap*. Retrieved from

https://www.theccc.org.uk/wp-content/uploads/2017/06/2017-Report-to-Parliament-Meeting-Carbon-Budgets-Closing-the-policy-gap.pdf

Coronella, C. J., Lynam, J. G., Reza, M. ., & Uddin, M. . (2014). Hydrothermal Carbonization of Lignocellulosic Biomass. In F. Jin (Ed.), *Application of Hydrothermal Reactions to Biomass Conversion* (1st ed., pp. 275–311). Berlin: Springer-Verlag Berlin Heidelberg.

Czernik, S., & Bridgwater, A. V. (2004). Overview of Applications of Biomass Fast Pyrolysis Oil, *Energy & Fuels* (12), 590–598.

DEFRA. (2007). *UK Biomass Strategy*. London.

Demirbaş, A. (2001). Relationships between lignin contents and heating values of biomass. *Energy Conversion and Management*, *42*(2), 183–188. https://doi.org/10.1016/S0196-8904(00)00050-9

Drax. (2017). A positive negative. Retrieved July 16, 2018, from https://www.drax.com/energy-policy/a-positive-negative/

E&T. (2019). Drax becomes the first power station to capture carbon from biomass.

Erdogan, E., Atila, B., Mumme, J., Reza, M. T., Toptas, A., Elibol, M., & Yanik, J. (2015a). Characterization of products from hydrothermal carbonization of orange pomace including anaerobic digestibility of process liquor. *Bioresource Technology*, *196*, 35–42. https://doi.org/10.1016/j.biortech.2015.06.115

Erdogan, E., Atila, B., Mumme, J., Reza, M. T., Toptas, A., Elibol, M., & Yanik, J. (2015b). Characterization of products from hydrothermal carbonization of orange pomace including anaerobic digestibility of process liquor. *Bioresource Technology*, *196*, 35–42. https://doi.org/10.1016/j.biortech.2015.06.115

Erlach, B., Harder, B., & Tsatsaronis, G. (2012). Combined hydrothermal carbonization and gasification of biomass with carbon capture. *Energy*, *45*(1), 329–338. https://doi.org/10.1016/j.energy.2012.01.057

Erlach, Berit, Wirth, B., & Tsatsaronis, G. (2011). Co-Production of Electricity, Heat and Biocoal Pellets from Biomass: A Techno-Economic Comparison with Wood Pelletizing, *World Renewable Energy Conngress,* May 2011, 508–515. https://doi.org/10.3384/ecp11057508

Falco, C., Baccile, N., & Titirici, M. M. (2011). Morphological and structural differences between glucose, cellulose and lignocellulosic biomass derived hydrothermal carbons. *Green Chemistry*, *13*(11), 3273–3281. https://doi.org/10.1039/c1gc15742f

Fang, J., Zhan, L., Ok, Y. S., & Gao, B. (2018). Minireview of potential applications of hydrochar derived from hydrothermal carbonization of

biomass. *Journal of Industrial and Engineering Chemistry*, *57*, 15–21. https://doi.org/10.1016/j.jiec.2017.08.026

Farrow, T. S. (2013). *A Fundamental Study of Biomass Oxy-fuel Combustion and Co-combustion*. University of Nottingham.

Fick, G., Mirgaux, O., Neau, P., & Patisson, F. (2014). Using biomass for pig iron production: A technical, environmental and economical assessment. *Waste and Biomass Valorization*, *5*(1), 43–55. https://doi.org/10.1007/s12649-013-9223-1

Freiberg, A., Scharfe, J., Murta, V. C., & Seidler, A. (2018). The use of biomass for electricity generation: A scoping review of health effects on humans in residential and occupational settings. *International Journal of Environmental Research and Public Health*, *15*(2). https://doi.org/10.3390/ijerph15020354

Funke, A., & Ziegler, F. (2011). Heat of reaction measurements for hydrothermal carbonization of biomass. *Bioresource Technology*, *102*(16), 7595–7598. https://doi.org/10.1016/j.biortech.2011.05.016

Gai, C., Zhang, F., Lang, Q., Liu, T., Peng, N., & Liu, Z. (2017). Facile one-pot synthesis of iron nanoparticles immobilized into the porous hydrochar for catalytic decomposition of phenol. *Applied Catalysis B: Environmental*, *204*, 566–576. https://doi.org/10.1016/j.apcatb.2016.12.005

Gani, A., & Naruse, I. (2007). Effect of cellulose and lignin content on pyrolysis and combustion characteristics for several types of biomass. *Renewable Energy*, *32*(4), 649–661. https://doi.org/10.1016/j.renene.2006.02.017

Gheewala, S. H., Berndes, G., & Jewitt, G. (2011). *The bioenergy and water nexus*. *Biofuels, Bioproducts and Biorefining* (Vol. 5). https://doi.org/10.1002/bbb.295

Granados, D. A., Basu, P., Chejne, F., & Nhuchhen, D. R. (2017). Detailed investigation into torrefaction of wood in a two-stage inclined rotary torrefier. *Energy and Fuels*, *31*(1), 647–658. https://doi.org/10.1021/acs.energyfuels.6b02524

Gucho, E. M., Shahzad, K., Bramer, E. A., Akhtar, N. A., & Brem, G. (2015). Experimental study on dry torrefaction of beech wood and miscanthus. *Energies*, *8*(5), 3903–3923. https://doi.org/10.3390/en8053903

Guillot, A., Py, X., Stoeckli, F., Chambat, G., & Cagnon, B. (2008). Contributions of hemicellulose, cellulose and lignin to the mass and the porous properties of chars and steam activated carbons from various lignocellulosic precursors. *Bioresource Technology*, *100*(1), 292–298. https://doi.org/10.1016/j.biortech.2008.06.009

Guo, S., Dong, X., Liu, K., Yu, H., & Zhu, C. (2015). Chemical, energetic, and

structural characteristics of hydrothermal carbonization solid products for lawn grass. *BioResources*, *10*(3), 4613–4625. https://doi.org/10.15376/biores.10.3.4613-4625

He, C., Giannis, A., & Wang, J. Y. (2013). Conversion of sewage sludge to clean solid fuel using hydrothermal carbonization: Hydrochar fuel characteristics and combustion behavior. *Applied Energy*, *111*, 257–266. https://doi.org/10.1016/j.apenergy.2013.04.084

Heidenreich, S., & Foscolo, P. U. (2015). New concepts in biomass gasification. *Progress in Energy and Combustion Science*, *46*, 72–95. https://doi.org/10.1016/j.pecs.2014.06.002

Hernandez, M., Salimbeni, A., Hitzl, M., Zhang, J., Wang, G., Wang, K., & Wang, C. (2018). Evaluation of utilising ingelia hydrochar produced from organic residues for blast furnaces injection comparison with anthracite and bituminous coal. In *European Biomass Conference and Exhibition Proceedings* (Vol. 2018, pp. 1560–1568). https://doi.org/10.5071/26thEUBCE2018-ICO.8.5

Hidayat, S., Fauzan, R. F. S., Jeong, S., Chun, D., Yoo, J., Kim, S., … Choi, H. (2017). Use of Torrefaction and Solvent Extraction to Produce Ash-less Biomass as a Solid Fuel Feedstock for Co-firing. *Energy and Fuels*, *31*(6), 6056–6064. https://doi.org/10.1021/acs.energyfuels.6b03165

Hoekman, S. K., Broch, A., Felix, L., & Farthing, W. (2017). Hydrothermal carbonization (HTC) of loblolly pine using a continuous, reactive twin-screw extruder. *Energy Conversion and Management*, *134*, 247–259. https://doi.org/10.1016/j.enconman.2016.12.035

Hoekman, S. K., Broch, A., & Robbins, C. (2011). Hydrothermal Carbonization (HTC) of Lignocellulosic Biomass. *Energy & Fuels*, *25*(4), 1802–1810. https://doi.org/10.1021/ef101745n

Hosseini, S. E., & Wahid, M. A. (2014). Development of biogas combustion in combined heat and power generation. *Renewable and Sustainable Energy Reviews*, *40*, 868–875. https://doi.org/10.1016/j.rser.2014.07.204

HTCycle. (n.d.-a). High performance carbon. Retrieved April 11, 2019, from https://htcycle.ag/en/high-performance-carbon_17

HTCycle. (n.d.-b). HTCycle Technology - best solution for waste disposal. Retrieved April 11, 2019, from https://htcycle.ag/en/technology_7

Huang, H. jun, Yuan, X. zhong, Zhu, H. na, Li, H., Liu, Y., Wang, X. li, & Zeng, G. ming. (2013). Comparative studies of thermochemical liquefaction characteristics of microalgae, lignocellulosic biomass and sewage sludge. *Energy*, *56*, 52–60. https://doi.org/10.1016/j.energy.2013.04.065

Iakovou, E., Karagiannidis, A., Vlachos, D., Toka, A., & Malamakis, A. (2010). Waste biomass-to-energy supply chain management: A critical synthesis.

Waste Management, *30*(10), 1860–1870. https://doi.org/10.1016/j.wasman.2010.02.030

IEA. (2017a). *CO2 emissions from fuel combustion*.

IEA. (2017b). *Key world energy statistics*.

IEA. (2018). *World energy balances: Overview*.

Ingelia. (n.d.). Ingelia Model. Retrieved April 11, 2019, from https://ingelia.com/index.php/negocio-sostenible/modelo-ingelia/?lang=en

Jain, A., Balasubramanian, R., & Srinivasan, M. P. (2016a). Hydrothermal conversion of biomass waste to activated carbon with high porosity: A review. *Chemical Engineering Journal*, *283*, 789–805. https://doi.org/10.1016/j.cej.2015.08.014

Jain, A., Balasubramanian, R., & Srinivasan, M. P. (2016b). Hydrothermal conversion of biomass waste to activated carbon with high porosity: A review. *Chemical Engineering Journal*, *283*(December 2017), 789–805. https://doi.org/10.1016/j.cej.2015.08.014

Jenkinson, P. (2015). *A New Classification System for Biomass and Waste Materials for their use in Combustion*. University of Nottingham.

Jiang, L., Hu, S., Sun, L., Su, S., Xu, K., He, L., & Xiang, J. (2013). Influence of different demineralization treatments on physicochemical structure and thermal degradation of biomass, *Bioresource Technology*, *146*, 254–260. https://doi.org/10.1016/j.biortech.2013.07.063

Jones, J. M., Darvell, L. I., Bridgeman, T. G., Pourkashanian, M., & Williams, A. (2007). An investigation of the thermal and catalytic behaviour of potassium in biomass combustion. *Proceedings of the Combustion Institute*, *31 II*, 1955–1963. https://doi.org/10.1016/j.proci.2006.07.093

Kambo, H. S., & Dutta, A. (2014). Strength, storage, and combustion characteristics of densified lignocellulosic biomass produced via torrefaction and hydrothermal carbonization. *Applied Energy*, *135*, 182–191. https://doi.org/10.1016/j.apenergy.2014.08.094

Kambo, H. S., & Dutta, A. (2015a). A comparative review of biochar and hydrochar in terms of production, physico-chemical properties and applications. *Renewable and Sustainable Energy Reviews*, *45*, 359–378. https://doi.org/10.1016/j.rser.2015.01.050

Kambo, H. S., & Dutta, A. (2015b). Comparative evaluation of torrefaction and hydrothermal carbonization of lignocellulosic biomass for the production of solid biofuel. *Energy Conversion and Management*, *105*, 746–755. https://doi.org/10.1016/j.enconman.2015.08.031

Kambo, H. S., Minaret, J., & Dutta, A. (2018). Process Water from the Hydrothermal Carbonization of Biomass: A Waste or a Valuable Product? *Waste and Biomass Valorization*, *9*(7), 1181–1189. https://doi.org/10.1007/s12649-017-9914-0

Kang, S., Li, X., Fan, J., & Chang, J. (2012). Characterization of hydrochars produced by hydrothermal carbonization of lignin, cellulose, d-xylose, and wood meal. *Industrial and Engineering Chemistry Research*, *51*(26), 9023–9031. https://doi.org/10.1021/ie300565d

Kang, S., Ye, J., Zhang, Y., & Chang, J. (2013). Preparation of biomass hydrochar derived sulfonated catalysts and their catalytic effects for 5-hydroxymethylfurfural production. *RSC Advances*, *3*(20), 7360–7366. https://doi.org/10.1039/c3ra23314f

Kashaninejad, M. (2011). Biomass Feedstock Pre-Processing - Part 1: Pre-Treatment. In M. Aurelio dos Santos Bernardes (Ed.), *Biofuel's Engineering Process Technology*. InTech.

Kathirvale, S., Muhd Yunus, M. N., Sopian, K., & Samsuddin, A. H. (2004). Energy potential from municipal solid waste in Malaysia. *Renewable Energy*, *29*(4), 559–567. https://doi.org/10.1016/j.renene.2003.09.003

Katritzky, A. R., Nichols, D. A., Siskin, M., Murugan, R., & Balasubramanian, M. (2001). Reactions in high-temperature aqueous media. *Chemical Reviews*, *101*(4), 837–892. https://doi.org/10.1021/cr960103t

Kröger, M., & Müller-Langer, F. (2012). Review on possible algal-biofuel production processes. *Biofuels*, *3*(3), 333–349. https://doi.org/10.4155/bfs.12.14

Kruger, C., Kicherer, A., Kormann, C., & Raupp, N. (2018). Biomass Balance: An Innovative and Complementary Method for Using Biomass as Feedstock in the Chemical Industry. In E. Benetto, K. Gericke, & M. Guiton (Eds.), *Designing Sustainable Technologies, Products and Policies*. Cham: Springer.

Kruse, A., & Dahmen, N. (2015). Water - A magic solvent for biomass conversion. *Journal of Supercritical Fluids*, *96*, 36–45. https://doi.org/10.1016/j.supflu.2014.09.038

Kruse, A., Koch, F., Stelzl, K., & Zeller, M. (2016). Fate of Nitrogen during Hydrothermal Carbonization, *Energy & Fuels,* 6–11. https://doi.org/10.1021/acs.energyfuels.6b01312

Kummamuru Venkata, B., Lang, A., Bradley, D., Koljonen, T., Andersson, K., Hammes, K., & Sidiki Uyar, T. (2016). *World Energy Resources: Bioenergy 2016*. https://doi.org/10.1016/0165-232X(80)90063-4

Ladanai, S., & Vinterbäck, J. (2009). Global Potential of Sustainable Biomass for Energy Technology. Swedish University of Agricultural Sciences.

Le Manquais, K., Snape, C. E., McRobbie, I., & Barker, J. (2011). Evaluating the combustion reactivity of drop tube furnace and thermogravimetric analysis coal chars with a selection of metal additives. *Energy and Fuels*, *25*(3), 981–989. https://doi.org/10.1021/ef101577z

Le Manquais, K., Snape, C., McRobbie, I., Barker, J., & Pellegrin, V. (2009). Comparison of the combustion reactivity of TGA and drop tube furnace chars from a bituminous coal. *Energy and Fuels*, *23*(9), 4269–4277. https://doi.org/10.1021/ef900205d

Li, Jiebing, Gellerstedt, G., & Toven, K. (2009). Steam explosion lignins; their extraction, structure and potential as feedstock for biodiesel and chemicals. *Bioresource Technology*, *100*(9), 2556–2561. https://doi.org/10.1016/j.biortech.2008.12.004

Li, Jun, Brzdekiewicz, A., Yang, W., & Blasiak, W. (2012). Co-firing based on biomass torrefaction in a pulverized coal boiler with aim of 100% fuel switching. *Applied Energy*, *99*, 344–354. https://doi.org/10.1016/j.apenergy.2012.05.046

Libra, J. A., Ro, K. S., Kammann, C., Funke, A., Berge, N. D., Neubauer, Y., … Emmerich, K.-H. (2011). Hydrothermal carbonization of biomass residuals: a comparative review of the chemistry, processes and applications of wet and dry pyrolysis. *Biofuels*, *2*(1), 71–106. https://doi.org/10.4155/bfs.10.81

Lillo-Ródenas, M. A., Lozano-Castelló, D., Cazorla-Amorós, D., & Linares-Solano, A. (2001). Preparation of activated carbons from Spanish anthracite - II. Activation by NaOH. *Carbon*, *39*(5), 751–759. https://doi.org/10.1016/S0008-6223(00)00186-X

Liu, Z., Quek, A., & Balasubramanian, R. (2014). Preparation and characterization of fuel pellets from woody biomass, agro-residues and their corresponding hydrochars. *Applied Energy*, *113*, 1315–1322. https://doi.org/10.1016/j.apenergy.2013.08.087

Liu, Z., Quek, A., Kent Hoekman, S., & Balasubramanian, R. (2013). Production of solid biochar fuel from waste biomass by hydrothermal carbonization. *Fuel*, *103*, 943–949. https://doi.org/10.1016/j.fuel.2012.07.069

Liu, Z., Quek, A., Kent Hoekman, S., Srinivasan, M. P., & Balasubramanian, R. (2012). Thermogravimetric investigation of hydrochar-lignite co-combustion. *Bioresource Technology*, *123*, 646–652. https://doi.org/10.1016/j.biortech.2012.06.063

Liu, Z., Zhang, F., Hoekman, S. K., Liu, T., Gai, C., & Peng, N. (2016). Homogeneously Dispersed Zerovalent Iron Nanoparticles Supported on Hydrochar-Derived Porous Carbon: Simple, in Situ Synthesis and Use for Dechlorination of PCBs. *ACS Sustainable Chemistry and Engineering*, *4*(6), 3261–3267. https://doi.org/10.1021/acssuschemeng.6b00306

Lockwood, M. (2013). The political sustainability of climate policy: The case of the UK Climate Change Act. *Global Environmental Change*, *23*(5), 1339–1348. https://doi.org/10.1016/j.gloenvcha.2013.07.001

Lu, L., Kong, C., Sahajwalla, V., & Harris, D. (2002). Char structural ordering during pyrolysis and combustion and its influence on char reactivity. *Fuel*, *81*(9), 1215–1225. https://doi.org/10.1016/S0016-2361(02)00035-2

Lucian, M., & Fiori, L. (2017). Hydrothermal carbonization of waste biomass: Process design, modeling, energy efficiency and cost analysis. *Energies*, *10*(2). https://doi.org/10.3390/en10020211

Lynam, J. G., Coronella, C. J., Yan, W., Reza, M. T., & Vasquez, V. R. (2011). Acetic acid and lithium chloride effects on hydrothermal carbonization of lignocellulosic biomass. *Bioresource Technology*, *102*(10), 6192–6199. https://doi.org/10.1016/j.biortech.2011.02.035

Lynam, J. G., Reza, M. T., Yan, W., Vásquez, V. R., & Coronella, C. J. (2015). Hydrothermal carbonization of various lignocellulosic biomass. *Biomass Conversion and Biorefinery*, *5*(2), 173–181. https://doi.org/10.1007/s13399-014-0137-3

Madanayake, B. N., Gan, S., Eastwick, C., & Ng, H. K. (2016). Thermochemical and structural changes in Jatropha curcas seed cake during torrefaction for its use as coal co-firing feedstock. *Energy*, *100*, 262–272. https://doi.org/10.1016/j.energy.2016.01.097

Maddi, B., Viamajala, S., & Varanasi, S. (2011). Comparative study of pyrolysis of algal biomass from natural lake blooms with lignocellulosic biomass. *Bioresource Technology*, *102*(23), 11018–11026. https://doi.org/10.1016/j.biortech.2011.09.055

Mäkelä, M., Benavente, V., & Fullana, A. (2015). Hydrothermal carbonization of lignocellulosic biomass: Effect of process conditions on hydrochar properties. *Applied Energy*, *155*, 576–584. https://doi.org/10.1016/j.apenergy.2015.06.022

Manquais, K. Le, Snape, C., Mcrobbie, I., Barker, J., & Pellegrini, V. (2009). Comparison of the Combustion Reactivity of TGA and Drop Tube Furnace Chars from a Bituminous Coal. *Energy and Fuels*, *25*(9), 4269–4277. https://doi.org/10.1021/ef900205d

Mathieson, J., Rogers, H., Somerville, M., Ridgeway, P., & Jahanshahi, S. (2011). Use of biomass in the iron and steel industry - An Australian perspective. *1st International Conference on Energy Efficiency and CO2 Reduction in the Steel Industry (EECR Steel 2011) - Incorporated in METEC InSteelCon 2011*, (July), 1–10. Retrieved from https://publications.csiro.au/rpr/pub?list=BRO&pid=csiro:EP115427&sb=RECENT&n=10&rpp=50&page=53&tr=5047&dr=all&dc4.browseYear=2011

Matsumura, Y., Minowa, T., Potic, B., Kersten, S. R. A., Prins, W., Van Swaaij, W. P. M., … Antal, M. J. (2005). Biomass gasification in near- and super-critical water: Status and prospects. *Biomass and Bioenergy*, *29*(4), 269–292. https://doi.org/10.1016/j.biombioe.2005.04.006

Mauro, C., Rentizelas, A. A., & Chinese, D. (2018). International vs. domestic bioenergy supply chains for co-firing plants: The role of pre-treatment technologies. *Renewable Energy*, *119*, 712–730. https://doi.org/10.1016/j.renene.2017.12.034

McKendry, P. (2002). Energy production from biomass (part 1): overview of biomass. *Bioresource Technology*, *83*(1), 37–46. https://doi.org/10.1016/S0960-8524(01)00118-3

McManus, M. C. (2010). Life cycle impacts of waste wood biomass heating systems: A case study of three UK based systems. *Energy*, *35*(10), 4064–4070. https://doi.org/10.1016/j.energy.2010.06.014

McNamee, P., Darvell, L. I., Jones, J. M., & Williams, A. (2015). The combustion characteristics of high-heating-rate chars from untreated and torrefied biomass fuels. *Biomass and Bioenergy*, *82*, 63–72. https://doi.org/10.1016/j.biombioe.2015.05.016

Miedema, J. H., Benders, R. M. J., Moll, H. C., & Pierie, F. (2017). Renew, reduce or become more efficient? The climate contribution of biomass co-combustion in a coal-fired power plant. *Applied Energy*, *187*, 873–885. https://doi.org/10.1016/j.apenergy.2016.11.033

Milbrandt, A., & Overend, R. (2009). Assessment of biomass resources from marginal lands in APEC economies. APEC Energy Working Group. https://doi.org/10.2172/968464

Ming, J., Wu, Y., Liang, G., Park, J.-B., Zhao, F., & Sun, Y.-K. (2013). Sodium salt effect on hydrothermal carbonization of biomass: a catalyst for carbon-based nanostructured materials for lithium-ion battery applications. *Green Chemistry*, *15*(10), 2722. https://doi.org/10.1039/c3gc40480c

Mohamad Nor, N., Lau, L. C., Lee, K. T., & Mohamed, A. R. (2013). Synthesis of activated carbon from lignocellulosic biomass and its applications in air pollution control - A review. *Journal of Environmental Chemical Engineering*, *1*(4), 658–666. https://doi.org/10.1016/j.jece.2013.09.017

Mumme, J., Eckervogt, L., Pielert, J., Diakité, M., Rupp, F., & Kern, J. (2011). Hydrothermal carbonization of anaerobically digested maize silage. *Bioresource Technology*, *102*(19), 9255–9260. https://doi.org/10.1016/j.biortech.2011.06.099

Muri, H. (2018). The role of large — scale BECCS in the pursuit of the 1 . 5 ° C target : an Earth system model perspective OPEN ACCESS The role of large — scale BECCS in the pursuit of the 1 . 5 ◦ C target : an Earth system

model perspective. *Environmental Research Letters*, *13*(044010).

Nanda, S., Azargohar, R., Dalai, A. K., & Kozinski, J. A. (2015). An assessment on the sustainability of lignocellulosic biomass for biorefining. *Renewable and Sustainable Energy Reviews*, *50*, 925–941. https://doi.org/10.1016/j.rser.2015.05.058

Ng, K. W., MacPhee, J. A., Giroux, L., & Todoschuk, T. (2011). Reactivity of bio-coke with CO2. *Fuel Processing Technology*, *92*(4), 801–804. https://doi.org/10.1016/j.fuproc.2010.08.005

Nhuchhen, D., & Afzal, M. (2017). HHV Predicting Correlations for Torrefied Biomass Using Proximate and Ultimate Analyses. *Bioengineering*, *4*(1), 7. https://doi.org/10.3390/bioengineering4010007

Nizamuddin, S., Baloch, H. A., Griffin, G. J., Mubarak, N. M., Bhutto, A. W., Abro, R., … Ali, B. S. (2017). An overview of effect of process parameters on hydrothermal carbonization of biomass. *Renewable and Sustainable Energy Reviews*. https://doi.org/10.1016/j.rser.2016.12.122

Nizamuddin, S., Mubarak, N. M., Tiripathi, M., Jayakumar, N. S., Sahu, J. N., & Ganesan, P. (2016). Chemical, dielectric and structural characterization of optimized hydrochar produced from hydrothermal carbonization of palm shell. *Fuel*, *163*, 88–97. https://doi.org/10.1016/j.fuel.2015.08.057

Novianti, S., Nurdiawati, A., Zaini, I. N., Prawisudha, P., Sumida, H., & Yoshikawa, K. (2015). Low-potassium Fuel Production from Empty Fruit Bunches by Hydrothermal Treatment Processing and Water Leaching. *Energy Procedia*, *75*, 584–589. https://doi.org/10.1016/j.egypro.2015.07.460

Nunes, L. J. R., Matias, J. C. O., & Catalão, J. P. S. (2014). A review on torrefied biomass pellets as a sustainable alternative to coal in power generation. *Renewable and Sustainable Energy Reviews*, *40*, 153–160. https://doi.org/10.1016/j.rser.2014.07.181

Nzihou, A., & Stanmore, B. (2013). The fate of heavy metals during combustion and gasification of contaminated biomass-A brief review. *Journal of Hazardous Materials*, *256–257*, 56–66. https://doi.org/10.1016/j.jhazmat.2013.02.050

Okman, I., Karagöz, S., Tay, T., & Erdem, M. (2014). Activated carbons from grape seeds by chemical activation with potassium carbonate and potassium hydroxide. *Applied Surface Science*, *293*, 138–142. https://doi.org/10.1016/j.apsusc.2013.12.117

Oliveira, I., Blöhse, D., & Ramke, H. G. (2013). Hydrothermal carbonization of agricultural residues. *Bioresource Technology*, *142*, 138–146. https://doi.org/10.1016/j.biortech.2013.04.125

Pantaleo, A., Candelise, C., Bauen, A., & Shah, N. (2014). ESCO business

models for biomass heating and CHP: Profitability of ESCO operations in Italy and key factors assessment. *Renewable and Sustainable Energy Reviews*, *30*, 237–253. https://doi.org/10.1016/j.rser.2013.10.001

Parshetti, G. K., Kent Hoekman, S., & Balasubramanian, R. (2013). Chemical, structural and combustion characteristics of carbonaceous products obtained by hydrothermal carbonization of palm empty fruit bunches. *Bioresource Technology*, *135*, 683–689. https://doi.org/10.1016/j.biortech.2012.09.042

Patrizio, P., Leduc, S., Chinese, D., Dotzauer, E., & Kraxner, F. (2015). Biomethane as transport fuel - A comparison with other biogas utilization pathways in northern Italy. *Applied Energy*, *157*, 25–34. https://doi.org/10.1016/j.apenergy.2015.07.074

Pehnt, M., & Henkel, J. (2009). Life cycle assessment of carbon dioxide capture and storage from lignite power plants. *International Journal of Greenhouse Gas Control*, *3*(1), 49–66. https://doi.org/10.1016/j.ijggc.2008.07.001

Perkins, G., Bhaskar, T., & Konarova, M. (2018). Process development status of fast pyrolysis technologies for the manufacture of renewable transport fuels from biomass. *Renewable and Sustainable Energy Reviews*, *90*(July 2017), 292–315. https://doi.org/10.1016/j.rser.2018.03.048

Peters, J. F., Iribarren, D., & Dufour, J. (2015). Biomass Pyrolysis for Biochar or Energy Applications? A Life Cycle Assessment., *Environmental Science and Technology*, 49 (8), 5195-5202 https://doi.org/10.1021/es5060786

Poudel, J., Karki, S., & Oh, S. C. (2018). Valorization of waste wood as a solid fuel by torrefaction. *Energies*, *11*(7). https://doi.org/10.3390/en11071641

Prawisudha, P., Namioka, T., & Yoshikawa, K. (2012). Coal alternative fuel production from municipal solid wastes employing hydrothermal treatment. *Applied Energy*, *90*(1), 298–304. https://doi.org/10.1016/j.apenergy.2011.03.021

Rabemanolontsoa, H., & Saka, S. (2013). Comparative study on chemical composition of various biomass species. *RSC Advances*, *3*(12), 3946–3956. https://doi.org/10.1039/c3ra22958k

Rahbari, M. (2011). *Feasibility of Improving Biomass Combustion through Extraction of Nutrients*, Cennatak.

Raychaudhuri, A., & Ghosh, S. K. (2016). Biomass Supply Chain in Asian and European Countries. *Procedia Environmental Sciences*, *35*, 914–924. https://doi.org/10.1016/j.proenv.2016.07.062

Rengaraj, S., Moon, S. H., Sivabalan, R., Arabindoo, B., & Murugesan, V. (2002). Agricultural solid waste for the removal of organics: Adsorption

of phenol from water and wastewater by palm seed coat activated carbon. *Waste Management*, *22*(5), 543–548. https://doi.org/10.1016/S0956-053X(01)00016-2

Reza, M. T., Andert, J., Wirth, B., Busch, D., Pielert, J., Lynam, J. G., & Mumme, J. (2014). Hydrothermal Carbonization of Biomass for Energy and Crop Production. *Applied Bioenergy*, *1*(1), 10–29. https://doi.org/10.2478/apbi-2014-0001

Reza, M. T., Lynam, J. G., Uddin, M. H., & Coronella, C. J. (2013). Hydrothermal carbonization: Fate of inorganics. *Biomass and Bioenergy*, *49*, 86–94. https://doi.org/10.1016/j.biombioe.2012.12.004

Reza, M. T., Yan, W., Uddin, M. H., Lynam, J. G., Hoekman, S. K., Coronella, C. J., & Vásquez, V. R. (2013). Reaction kinetics of hydrothermal carbonization of loblolly pine. *Bioresource Technology*, *139*, 161–169. https://doi.org/10.1016/j.biortech.2013.04.028

Rollinson, A. N., & Williams, O. (2016). Experiments on torrefied wood pellet: study by gasification and characterisation for waste biomass to energy applications. *Royal Society Open Science*. https://doi.org/10.1098/rsos.150578

Román, S., Nabais, J. M. V, Laginhas, C., Ledesma, B., & González, J. F. (2012). Hydrothermal carbonization as an effective way of densifying the energy content of biomass. *Fuel Processing Technology*, *103*, 78–83. https://doi.org/10.1016/j.fuproc.2011.11.009

Román, S., Valente Nabais, J. M., Ledesma, B., González, J. F., Laginhas, C., & Titirici, M. M. (2013). Production of low-cost adsorbents with tunable surface chemistry by conjunction of hydrothermal carbonization and activation processes. *Microporous and Mesoporous Materials*, *165*, 127–133. https://doi.org/10.1016/j.micromeso.2012.08.006

Routeledge. (2013). *Bioenergy Production by Anaerobic Digestion*. (N. E. Korres, P. O'Kiely, J. A. H. Benzie, & J. S. West, Eds.). Routledge.

Ruiz, H. A., Rodríguez-Jasso, R. M., Fernandes, B. D., Vicente, A. A., & Teixeira, J. A. (2013). Hydrothermal processing, as an alternative for upgrading agriculture residues and marine biomass according to the biorefinery concept: A review. *Renewable and Sustainable Energy Reviews*, *21*, 35–51. https://doi.org/10.1016/j.rser.2012.11.069

Saari, J., Sermyagina, E., Kaikko, J., Vakkilainen, E., & Sergeev, V. (2016). Integration of hydrothermal carbonization and a CHP plant: Part 2 – operational and economic analysis. *Energy*, *113*, 574–585. https://doi.org/10.1016/j.energy.2016.06.102

Saddawi, A., Jones, J. M., Williams, A., & Le Coeur, C. (2012). Commodity Fuels from Biomass through Pretreatment and Torrefaction: Effects of Mineral

Content on Torrefied Fuel Characteristics and Quality, *Energy and Fuels*, *26*(11), 6466–6474. https://doi.org/10.1021/ef2016649

Sander, K., Waqar Haider, S., & Hyseni, B. (2011). Wood-Based Biomass Energy Development for Sub-Saharan Africa. Africa Renewable Energy Access Program (AFREA)

Schleussner, C. F., Rogelj, J., Schaeffer, M., Lissner, T., Licker, R., Fischer, E. M., … Hare, W. (2016). Science and policy characteristics of the Paris Agreement temperature goal. *Nature Climate Change*, *6*(9), 827–835. https://doi.org/10.1038/nclimate3096

Schlomann, B., Gruber, E., Geiger, B., Kleeberger, H., Wehmhörner, U., Herzog, T., & Konopka, D.-M. (2006). Energy consumption of the tertiary sector (trade , commerce and services) for the years 2004 to 2006. BMWi.

Searcy, E., Flynn, P., Ghafoori, E., & Kumar, A. (2007). The relative cost of biomass energy transport. *Applied Biochemistry and Biotechnology*, *137–140*(1–12), 639–652. https://doi.org/10.1007/s12010-007-9085-8

Sermyagina, E., Saari, J., Kaikko, J., & Vakkilainen, E. (2015). Hydrothermal carbonization of coniferous biomass: Effect of process parameters on mass and energy yields. *Journal of Analytical and Applied Pyrolysis*, *113*, 551–556. https://doi.org/10.1016/j.jaap.2015.03.012

Sharma, A., Pareek, V., & Zhang, D. (2015). Biomass pyrolysis - A review of modelling, process parameters and catalytic studies. *Renewable and Sustainable Energy Reviews*, *50*, 1081–1096. https://doi.org/10.1016/j.rser.2015.04.193

Sheldon, R. A. (2014). Green and sustainable manufacture of chemicals from biomass: State of the art. *Green Chemistry*, *16*(3), 950–963. https://doi.org/10.1039/c3gc41935e

Slade, R. (2011). Energy from biomass : the size of the global resource An assessment of the evidence that biomass can make a major contribution to future global energy supply. UKERC

Smith, Aidan M., & Ross, A. B. (2016). Production of bio-coal, bio-methane and fertilizer from seaweed via hydrothermal carbonisation. *Algal Research*, *16*. https://doi.org/10.1016/j.algal.2016.02.026

Smith, Aidan M., & Ross, A. B. (2019). The Influence of Residence Time during Hydrothermal Carbonisation of Miscanthus on Bio-Coal Combustion Chemistry. *Energies*, *12*(3), 523. https://doi.org/10.3390/en12030523

Smith, Aidan M., Singh, S., & Ross, A. B. (2016). Fate of inorganic material during hydrothermal carbonisation of biomass: Influence of feedstock on combustion behaviour of hydrochar. *Fuel*, *169*, 135–145. https://doi.org/10.1016/j.fuel.2015.12.006

Smith, Aidan Mark, Whittaker, C., Shield, I., & Ross, A. B. (2018). The potential for production of high quality bio-coal from early harvested Miscanthus by hydrothermal carbonisation. *Fuel*, *220*(February), 546–557. https://doi.org/10.1016/j.fuel.2018.01.143

Spitzer, R. Y., Mau, V., & Gross, A. (2018). Using hydrothermal carbonization for sustainable treatment and reuse of human excreta. *Journal of Cleaner Production*, *205*, 955–963. https://doi.org/10.1016/j.jclepro.2018.09.126

Stelte, W. (2013). *Steam explosion for biomass pre-treatment*.

Stemann, J., Erlach, B., & Ziegler, F. (2013). Hydrothermal carbonisation of empty palm oil fruit bunches: Laboratory trials, plant simulation, carbon avoidance, and economic feasibility. *Waste and Biomass Valorization*, *4*(3), 441–454. https://doi.org/10.1007/s12649-012-9190-y

Stemann, J., Putschew, A., & Ziegler, F. (2013). Hydrothermal carbonization: Process water characterization and effects of water recirculation. *Bioresource Technology*, *143*, 139–146. https://doi.org/10.1016/j.biortech.2013.05.098

Stemann, J., & Ziegler, F. (2011). Assessment of the Energetic Efficiency of A Continuously Operating Plant for Hydrothermal Carbonisation of Biomass. *World Renewable Energy Congress 2011 - Sweden*, 125–132. https://doi.org/10.3384/ecp11057125

Sun, J. X., Sun, X. F., Sun, R. C., & Su, Y. Q. (2004). Fractional extraction and structural characterization of sugarcane bagasse hemicelluloses. *Carbohydrate Polymers*, *56*(2), 195–204. https://doi.org/10.1016/j.carbpol.2004.02.002

Suncoal. (n.d.-a). Biofuels - Suncoal. Retrieved April 11, 2019, from https://www.suncoal.com/solutions/biofuels/

Suncoal. (n.d.-b). Facilities - Suncoal. Retrieved April 11, 2019, from https://www.suncoal.com/company/facilities/

SXCoal. (2018). China installed biomass power capacity up 22.6pct in 2017. Retrieved March 7, 2019, from http://www.sxcoal.com/news/4568861/info/en

Tabil, L., Adapa, P., & Kashaninejad, M. (2009). Biomass Feedstock Pre-Processing - Part 1: Pre-Treatment. In M. Aurelio dos Santos Bernardes (Ed.), *Biofuel's Engineering Process Technology*. InTech.

Tambone, F., Genevini, P., D'Imporzano, G., & Adani, F. (2009). Assessing amendment properties of digestate by studying the organic matter composition and the degree of biological stability during the anaerobic digestion of the organic fraction of MSW. *Bioresource Technology*, *100*(12), 3140–3142. https://doi.org/10.1016/j.biortech.2009.02.012

Tarvin, D., & Buswell, A. M. (1934). The Methane Fermentation of Organic Acids and Carbohydrates. *Journal of the American Chemical Society*. https://doi.org/10.1021/ja01323a030

Tay, T., Ucar, S., & Karagöz, S. (2009). Preparation and characterization of activated carbon from waste biomass. *Journal of Hazardous Materials*, *165*(1–3), 481–485. https://doi.org/10.1016/j.jhazmat.2008.10.011

Tekin, K., Karagöz, S., & Bektaş, S. (2014). A review of hydrothermal biomass processing. *Renewable and Sustainable Energy Reviews*, *40*, 673–687. https://doi.org/10.1016/j.rser.2014.07.216

TerraNova. (n.d.-a). Hydrothermal Carbonization. Retrieved April 11, 2019, from http://terranova-energy.com/en/

TerraNova. (n.d.-b). The TerraNova® Ultra -Process. Retrieved April 11, 2019, from http://terranova-energy.com/en/project/process/

Tews, I.J., Zhu, Y., Drennan, C.V., Elliot, D.C., Snowden-Swan, L.J., Onarheim, K., Solantausta, Y., Beckman, D. (2014). Biomass Direct Liquefaction Options : TechnoEconomic and Life Cycle Assessment. U.S. Department of Energy Office of Scientific and Technical Information

Tillman, D. . (1978). *Wood as an Energy Resource*. New York, NY, USA: Academic Press.

Titirici, M.-M., Antonietti, M., & Baccile, N. (2008). Hydrothermal carbon from biomass: a comparison of the local structure from poly- to monosaccharides and pentoses/hexoses. *Green Chemistry*, *10*(11), 1204. https://doi.org/10.1039/b807009a

Titirici, M.-M., Thomas, A., & Antonietti, M. (2007). Back in the black: hydrothermal carbonization of plant material as an efficient chemical process to treat the CO_2 problem? *New Journal of Chemistry*, *31*(6), 787. https://doi.org/10.1039/b616045j

Titirici, M.-M., White, R. J., Falco, C., & Sevilla, M. (2012). Black perspectives for a green future: hydrothermal carbons for environment protection and energy storage. *Energy & Environmental Science*, *5*(5), 6796. https://doi.org/10.1039/c2ee21166a

Uddin, M. H., Reza, M. T., Lynam, J. G., & Coronella, C. J. (2013). Effects of water recycling in hydrothermal carbonization of loblolly pine. *Environmental Progress and Sustainable Energy*. https://doi.org/10.1002/ep.11899

Uguna, C. N., Carr, A. D., Snape, C. E., & Meredith, W. (2015). High pressure water pyrolysis of coal to evaluate the role of pressure on hydrocarbon generation and source rock maturation at high maturities under geological conditions. *Organic Geochemistry*, *78*, 44–51. https://doi.org/10.1016/j.orggeochem.2014.10.013

Vamvuka, D., & Alloimonos, N. (2017). Combustion behaviour of Olive pruning/animal manure blends in a fluidized bed combustor. *Heliyon*, *3*(9), e00385. https://doi.org/10.1016/j.heliyon.2017.e00385

Vassilev, S. V., Baxter, D., Andersen, L. K., & Vassileva, C. G. (2010). An overview of the chemical composition of biomass. *Fuel*, *89*(5), 913–933. https://doi.org/10.1016/j.fuel.2009.10.022

Vassilev, S. V., Vassileva, C. G., & Vassilev, V. S. (2015). Advantages and disadvantages of composition and properties of biomass in comparison with coal: An overview. *Fuel*, *158*, 330–350. https://doi.org/10.1016/j.fuel.2015.05.050

Verma, V. K., Bram, S., & De Ruyck, J. (2009). Small scale biomass heating systems: Standards, quality labelling and market driving factors - An EU outlook. *Biomass and Bioenergy*, *33*(10), 1393–1402. https://doi.org/10.1016/j.biombioe.2009.06.002

Wang, B., Sun, L., Su, S., Xiang, J., Hu, S., & Fei, H. (2012). Char structural evolution during pyrolysis and its influence on combustion reactivity in air and oxy-fuel conditions. *Energy and Fuels*, *26*(3), 1565–1574. https://doi.org/10.1021/ef201723q

Wang, X., Sheng, L., & Yang, X. (2017). Pyrolysis characteristics and pathways of protein, lipid and carbohydrate isolated from microalgae Nannochloropsis sp. *Bioresource Technology*, *229*, 119–125. https://doi.org/10.1016/j.biortech.2017.01.018

Weiner, B., Poerschmann, J., Wedwitschka, H., Koehler, R., & Kopinke, F.-D. (2014). Influence of Process Water Reuse on the Hydrothermal Carbonization of Paper. *ACS Sustainable Chemistry & Engineering*, *2*(9), 2165–2171. https://doi.org/10.1021/sc500348v

Werther, J., & Ogada, T. (1999). Sewage sludge combustion. *Progress in Energy and Combustion Science*, *25*(1), 55–116. https://doi.org/10.1016/S0360-1285(98)00020-3

Wheeldon, I., Christopher, P., & Blanch, H. (2017). Integration of heterogeneous and biochemical catalysis for production of fuels and chemicals from biomass. *Current Opinion in Biotechnology*, *45*(March), 127–135. https://doi.org/10.1016/j.copbio.2017.02.019

Wiedner, K., Rumpel, C., Steiner, C., Pozzi, A., Maas, R., & Glaser, B. (2013). Chemical evaluation of chars produced by thermochemical conversion (gasification, pyrolysis and hydrothermal carbonization) of agro-industrial biomass on a commercial scale. *Biomass and Bioenergy*, *59*, 264–278. https://doi.org/10.1016/j.biombioe.2013.08.026

Williams, O. (2016). *On Biomass Milling for Power Generation*. University of Nottingham.

Williams, O., Eastwick, C., Kingman, S., Giddings, D., Lormor, S., & Lester, E. (2015). Investigation into the applicability of Bond Work Index (BWI) and Hardgrove Grindability Index (HGI) tests for several biomasses compared to Colombian La Loma coal. *Fuel*, *158*, 379–387. https://doi.org/10.1016/j.fuel.2015.05.027

Williams, O., Eastwick, C., Kingman, S., Giddings, D., Lormor, S., & Lester, E. (2017). Overcoming the caking phenomenon in olive mill wastes. *Industrial Crops and Products*, *101*, 92–102. https://doi.org/10.1016/j.indcrop.2017.02.036

Wils, A., Calmano, W., Dettmann, P., Kaltschmitt, M., & Ecke, H. (2012). Reduction of fuel side costs due to biomass co-combustion. *Journal of Hazardous Materials*, *207–208*, 147–151. https://doi.org/10.1016/j.jhazmat.2011.03.082

Xingang, Z., Zhongfu, T., & Pingkuo, L. (2013). Development goal of 30 GW for China's biomass power generation: Will it be achieved? *Renewable and Sustainable Energy Reviews*, *25*, 310–317. https://doi.org/10.1016/j.rser.2013.04.008

Xu, J., Thomsen, M. H., & Thomsen, A. B. (2010). Investigation of acetic acid-catalyzed hydrothermal pretreatment on corn stover. *Applied Microbiology and Biotechnology*, *86*(2), 509–516. https://doi.org/10.1007/s00253-009-2340-x

Xu, W., Wei, J., Chen, J., Zhang, B., Xu, P., Ren, J., & Yu, Q. (2018). Comparative Study of Water-Leaching and Acid-Leaching Pretreatment on the Thermal Stability and Reactivity of Biomass Silica for Viability as a Pozzolanic Additive in Cement. *Materials*, *11*(9), 1697. https://doi.org/10.3390/ma11091697

Xue, G., Kwapinska, M., Kwapinski, W., Czajka, K. M., Kennedy, J., & Leahy, J. J. (2014). Impact of torrefaction on properties of Miscanthus × giganteus relevant to gasification. *Fuel*, *121*, 189–197. https://doi.org/10.1016/j.fuel.2013.12.022

Yakaboylu, O., Harinck, J., Smit, K. G., & de Jong, W. (2015). Supercritical water gasification of biomass: A literature and technology overview. *Energies*, *8*(2), 859–894. https://doi.org/10.3390/en8020859

Yan, W., Hoekman, S. K., Broch, A., & Coronella, C. J. (2014). Effect of hydrothermal carbonization reaction parameters on the properties of hydrochar and pellets. In *Environmental Progress and Sustainable Energy* (Vol. 33, pp. 676–680). https://doi.org/10.1002/ep.11974

Yang, H., Yan, R., Chen, H., Lee, D. H., & Zheng, C. (2007). Characteristics of hemicellulose, cellulose and lignin pyrolysis. *Fuel*, *86*(12–13), 1781–1788. https://doi.org/10.1016/j.fuel.2006.12.013

Yang, H., Yan, R., Chen, H., Zheng, C., Lee, D. H., & Liang, D. T. (2006). In-Depth Investigation of Biomass Pyrolysis Based on Three Major Components: Hemicellulose, Cellulose and Lignin. *Energy and Fuels*, *20*, 388–393.

Yao, Z., & Ma, X. (2018). Effects of hydrothermal treatment on the pyrolysis behavior of Chinese fan palm. *Bioresource Technology*, *247*(381), 504–512. https://doi.org/10.1016/j.biortech.2017.09.142

Yi, B., Yuan, Q., Cao, H., Niu, W., Wang, M., Zhu, Y., & Yan, S. (2018). Effect of alkali and alkaline earth metal species on the combustion characteristics of cattle manures. *RSC Advances*, *8*(21), 11705–11713. https://doi.org/10.1039/c8ra00965a

Yoshida, M., Liu, Y., Uchida, S., Kawadara, K., Ukagami, Y., Ichinose, H., … Fukuda, K. (2008). Effects of Cellulose Crystallinity, Hemicellulose, and Lignin on the Enzymatic Hydrolysis of Miscanthus sinensis to Monosaccharides. *Bioscience, Biotechnology, and Biochemistry*, *72*(3), 805–810. https://doi.org/10.1271/bbb.70689

Young, J. D., Anderson, N. M., Naughton, H. T., & Mullan, K. (2018). Economic and policy factors driving adoption of institutional woody biomass heating systems in the U.S. *Energy Economics*, *69*, 456–470. https://doi.org/10.1016/j.eneco.2017.11.020

Yu, C., Thy, P., Wang, L., Anderson, S. N., Vandergheynst, J. S., Upadhyaya, S. K., & Jenkins, B. M. (2014). Influence of leaching pretreatment on fuel properties of biomass. *Fuel Processing Technology*, *128*, 43–53. https://doi.org/10.1016/j.fuproc.2014.06.030

Yu, M. M., Masnadi, M. S., Grace, J. R., Bi, X. T., Lim, C. J., & Li, Y. (2015). Co-gasification of biosolids with biomass: Thermogravimetric analysis and pilot scale study in a bubbling fluidized bed reactor. *Bioresource Technology*, *175*, 51–58. https://doi.org/10.1016/j.biortech.2014.10.045

Yue, F., Marcus, C., Yan, X., Liu, Y., & Xiang, D. (2018). NMR studies of stock process water and reaction pathways in hydrothermal carbonization of furfural residue. *Green Energy and Environment*, *3*(2), 163–171. https://doi.org/10.1016/j.gee.2017.08.006

Yue, F., Pedersen, C. M., Liu, Y., Qiao, Y., Wang, Y., Qian, G., … Zhao, T. (2017). Valorization of Furfural Residue by Hydrothermal Carbonization: Processing Optimization, Chemical and Structural Characterization. *ChemistrySelect*, *2*(2), 583–590. https://doi.org/10.1002/slct.201602026

Zhao, P., Shen, Y., Ge, S., Chen, Z., & Yoshikawa, K. (2014). Clean solid biofuel production from high moisture content waste biomass employing hydrothermal treatment. *Applied Energy*, *131*, 345–367. https://doi.org/10.1016/j.apenergy.2014.06.038

Zhu, Q. (2014). *Coal sampling and analysis standards standards*. IEA Clean

Coal Centre.

Appendix 1 HTC yield data

Non-waste biomass

Biomass	Particle size	Temperature (°C)	Residence time (min)	Water: biomass	Yield (%)		
					AR	DAF	C
Brites wood	<1mm	200	60	6	78.0	84.1	80.5
Brites Wood	Pellets	200	60	4	65.9	69.5	68.8
Brites Wood	Pellets	225	60	4	64.1	67.8	72.7
Brites wood	<212µm	250	60	2	60.9	62.9	81.0
Brites wood	<1mm	250	60	2	58.4	61.2	77.4
Brites wood	<1mm	250	60	6	52.5	57.0	68.1
Brites wood	pellets	250	60	4	53.6	56.7	73.5
Jatropha	<1mm	200	60	4	53.0	55.7	57.3
Jatropha	<1mm	240	120	6	42.0	43.2	52.5
Jatropha	<1mm	240	120	6	46.3	50.2	52.2
Miscanthus	<1mm	200	60	4	67.1	71.0	70.1
Miscanthus	<1mm	200	60	6	66.0	70.1	69.8
Miscanthus	Pellets	200	60	6	65.0	69.8	68.8
Miscanthus	Pellets	200	60	4	66.5	70.7	69.9
Miscanthus	Pellets	200	240	4	63.3	67.2	69.8
Miscanthus	Pellets	200	240	6	63.0	67.6	69.2
Miscanthus	Pellets	225	150	5	53.8	57.8	64.9
Miscanthus	Pellets	225	30	2	64.7	69.3	74.2
Miscanthus	Pellets	225	30	4	61.9	66.3	68.2
Miscanthus	Pellets	225	30	6	60.4	65.2	66.6
Miscanthus	Pellets	250	60	4	44.9	47.7	60.1
Miscanthus	Pellets	250	240	6	32.0	34.1	46.3

Miscanthus	Pellets	250	60	6	45.2	48.4	59.3
Miscanthus	Pellets	250	240	6	37.5	39.1	52.9
Miscanthus	Pellets	250	240	4	36.1	38.1	52.3

Legend: AR – as received basis, DAF – dry, ash free basis, C – carbon basis

Waste biomass

Biomass	Particle size	Temperature (°C)	Time (min)	W/B	Yield (%)		
					AR	DAF	C
Bagasse	<1.3mm	200	60	4	68.3	67.0	69.8
Bagasse	<1.3mm	220	360	6	53.6	53.4	66.3
Bagasse	<1.3mm	240	120	6	47.0	46.8	67.3
Carrot	Dried	180	60	6	35.1	35.5	53.3
Carrot	Dried	200	60	6	37.6	38.8	62.5
Carrot	Dried	220	60	6	43.3	44.8	74.6
Food AD + fibres	Dried	220	60	4	75.0	74.3	81.4
Rye AD	Dried	180	60	8	68.3	72.0	85.4
Rye AD	Dried	200	60	8	68.3	70.3	90.9
Rye AD	Dried	215	60	15	60.0	41.7	53.5
Rye AD	Dried	215	60	4	64.2	68.9	89.9
Rye AD	Dried	215	90	8	58.3	62.3	80.2
Rye AD	Dried	250	60	8	42.7	48.5	74.8
Minced beef	Raw	180	60	2	10.9	16.3	28.9
Minced beef	Raw	220	60	2	7.9	12.2	20.6
Minced beef	Cooked	180	60	2	10.5	11.3	23.3

Minced beef	Cooked	200	60	2	8.4	9.0	22.1
Minced beef	Cooked	220	60	2	1.5	1.6	4.2
Olive cake	<1mm	200	60	6	60.2	63.3	71.8
Olive cake	Pellets	200	60	4	50.1	54.1	64.2
Olive cake	pellets	200	60	6	50.9	54.7	65.0
Olive cake	pellets	200	60	6	48.4	55.5	62.1
Olive cake	pellets	225	60	6	46.7	53.5	62.5
Olive cake	Pellets	225	60	4	50.9	55.0	69.6
Olive cake	Pellets	240	120	1	41.9	44.4	68.9
Rice	Grains	180	60	2	18.6	27.8	23.0
Rice	Grains	200	60	2	34.6	51.9	57.9
Rice	Grains	220	60	2	46.9	70.7	79.8
Rice	Grains	220	60	2	46.4	69.8	80.0
Sewage	Dried	180	240	4	62.8	52.2	-
Sewage	Dried	200	60	4	63.3	53.3	-
Sewage	Dried	200	120	4	61.7	50.5	-
Sewage	Dried	200	120	4	64.9	55.6	-
Sewage	Dried	200	240	4	61.7	48.5	-
Sewage	Dried	200	60	6	62.8	50.7	-

Sewage	Dried	200	60	6	62.0	52.3	-
Sewage	Dried	200	120	6	64.0	52.2	-
Sewage	Dried	200	240	6	62.4	50.1	-
Sewage	Dried	200	240	8	58.6	46.9	-
Sewage	Dried	200	120	8	60.6	49.6	-
Sewage	Dried	200	60	8	60.9	48.6	-
Sewage	Dried	220	240	4	60.9	48.0	-
Sunflower	<1mm	240	120	6	43.0	45.5	62.1
Sunflower	<1mm	240	120	6	44.4	48.6	58.6

Legend: AR – as received basis, DAF – dry, ash free basis, C – carbon basis, AD – anaerobic digestate

Appendix 2 HTC proximate analysis data

Non-waste biomass feedstock

Biomass	Particle size	Proximate analysis (%)					
		M	VM	FC	A	VM (DAF)	FC (DAF)
Brites wood	Pellets	7.5 ± 0.2	74.5 ± 1.0	17.6 ± 0.7	0.4 ± 0.1	80.9	19.1
Jatropha	<1mm	1.9 ± 3.1	78.4 ± 2.5	13.7 ± 0.8	5.9 ± 0.3	85.1	14.9
Miscanthus	Pellets	6.4 ± 0.1	67.2 ± 0.8	21.7 ± 0.4	4.7 ± 0.5	75.6	24.4

Legend: M – moisture, VM – volatile matter, FC – fixed carbon, A – ash, DAF – dry, ash free basis

Non-waste biomass biocoal

Biomass	Particle size	Temperature (°C)	Time (min)	W/B	Proximate analysis (%)					
					M	VM	FC	A	VM (DAF)	FC (DAF)
Brites Wood	Pellets	200	60	4	2.3 ± 0.2	77.8 ± 1.2	19.3 ± 0.7	0.5 ± 0.2	80.1	19.9
Brites Wood	Pellets	225	60	4	1.9 ± 0.1	71.6 ± 0.3	25.7 ± 0.3	0.8 ± 0.2	73.6	26.4
Brites wood	<212µm	250	60	2	5.2 ± 0.2	53.2 ± 1.5	41.3 ± 3.5	0.3 ± 2.5	56.3	43.7
Brites wood	<1mm	250	60	2	2.8 ± 0.3	56.9 ± 8.4	39.1 ± 7.7	1.2 ± 1.0	59.3	40.7
Brites wood	<1mm	250	60	6	3.0 ± 0.5	60.7 ± 9.5	38.5 ± 4.6	-2.2 ± 7.1	61.2	38.8
Brites wood	pellets	250	60	4	2.0 ± 0.1	52.3 ± 0.2	45.0 ± 0.5	0.7 ± 0.5	53.7	46.3
Jatropha	<1mm	200	60	4	1.5 ± 0.1	84.2 ± 0.5	12.7 ± 0.5	1.6 ± 0.1	86.9	13.1
Jatropha	<1mm	240	120	6	1.0 ± 0.1	80.8 ± 1.5	14.0 ± 1.5	4.3 ± 0.1	85.2	14.8
Miscanthus	<1mm	200	60	4	3.3 ± 0.0	76.5 ± 0.8	17.8 ± 0.1	2.4 ± 0.8	81.1	18.9
Miscanthus	<1mm	200	60	4	3.2 ± 0.5	75.1 ± 0.4	18.0 ± 0.3	2.1 ± 0.2	79.3	19.0
Miscanthus	Pellets	200	60	6	2.4 ± 1.9	77.5± 1.8	18.0 ± 0.3	2.1 ± 0.2	81.2	18.8
Miscanthus	Pellets	200	60	4	3.1 ± 0.1	74.5 ± 0.5	20.0 ± 0.4	2.4 ± 0.2	78.8	21.2

Miscanthus	Pellets	200	240	4	2.9 ± 0.1	74.3 ± 1.2	20.0 ± 0.7	2.7 ± 0.5	78.7	21.2
Miscanthus	Pellets	200	240	6	2.1 ± 1.1	75.8 ± 1.2	19.6 ± 0.1	2.5 ± 0.9	79.3	20.5
Miscanthus	Pellets	225	150	5	2.1 ± 0.1	68.4 ± 0.7	27.2 ± 0.8	2.3 ± 0.2	71.5	28.5
Miscanthus	Pellets	225	30	4	2.0 ± 0.5	75.5 ± 1.2	19.8 ± 0.2	2.6 ± 0.6	79.1	20.8
Miscanthus	Pellets	225	30	6	2.0 ± 0.6	76.3 ± 1.0	19.6 ± 0.5	2.1 ± 0.2	79.6	20.4
Miscanthus	Pellets	225	30	2	1.6 ± 0.7	69.9 ± 0.2	25.5 ± 0.3	3.1 ± 0.3	73.3	26.8
Miscanthus	Pellets	250	60	4	1.6 ± 0.6	60.4 ± 1.9	33.9 ± 0.5	4.1 ± 1.7	64.4	35.6
Miscanthus	Pellets	250	240	6	1.4 ± 0.1	51.6 ± 2.7	43.2 ± 2.6	3.8 ± 0.3	54.4	45.6
Miscanthus	Pellets	250	60	6	1.2 ± 0.0	61.7 ± 0.4	33.6 ± 0.3	3.5 ± 0.2	64.7	35.3
Miscanthus	Pellets	250	240	6	1.3 ± 0.1	50.1 ± 0.1	42.6 ± 0.2	6.0 ± 0.3	54.0	46.0
Miscanthus	Pellets	250	240	4	1.0 ± 0.8	52.3 ± 1.9	41.4 ± 2.2	5.3 ± 0.4	55.8	44.2

Legend: M – moisture, VM – volatile matter, FC – fixed carbon, A – ash, DAF – dry, ash free basis

Waste biomass feedstock

Biomass	Particle size	Proximate analysis (%)					
		M	VM	FC	A	VM (DAF)	FC (DAF)
Bagasse	<1.3mm	2.8 ± 2.4	82.1 ± 3.4	11.7 ± 0.8	3.4 ± 0.2	87.5	12.5
Carrot[1]	As received	90.7	8.4	2.7	0.7	75.7	24.3
Carrot[1]	Dried (calculated)	0.0	71.2	22.9	5.9	75.7	24.3
Food AD + fibres	As received	2.4 ± 3.0	75.1 ± 1.8	15.5 ± 1.7	7.1 ± 0.8	82.9	17.1
Rye AD	Dried	3.7 ± 1.7	67.8 ± 0.8	19.5 ± 0.6	9.0 ± 2.0	77.6	22.4
Mince[1]	Cooked	7.1	78.2	12.7	2.0	86.1	13.9
Olive cake	Pellets	6.2 ± 0.5	65.1 ± 0.1	22.1 ± 0.4	6.6 ± 0.9	74.6	25.4
Sewage Sludge[1.2]	Dried	2.0	60.5	7.5	30.0	89.0	11.0
Sunflower shell	<1mm	5.2 ± 1.1	72.1 ± 2.4	19.2 ± 0.8	3.5 ± 0.5	79.0	21.0

Legend: M – moisture, VM – volatile matter, FC – fixed carbon, A – ash, DAF – dry, ash free basis, AD – anaerobic digestate

[1] Single determination

[2] VM determination performed at 850°C rather than 700°C

Waste biomass biocoal

Biomass	Particle size	Temperature	Time (min)	W/B	M	VM	FC	A	VM (DAF)	FC (DAF)
Bagasse	<1.3mm	200	60	4	2.3 ± 1.7	77.5 ± 2.8	14.5 ± 3.1	5.7 ± 0.8	84.2	15.8
Bagasse	<1.3mm	220	360	6	0.2 ± 0.0	58.5 ± 0.6	35.0 ± 0.3	6.3 ± 0.6	62.6	37.4
Bagasse	<1.3mm	240	120	6	0.9 ± 0.2	53.5 ± 0.4	40.1 ± 0.0	5.6 ± 0.2	57.2	42.8
Carrot	Dried	180	60	6	3.0 ± 0.4	60.5 ± 1.6	33.2 ± 1.4	3.3 ± 1.0	64.6	35.4
Carrot	Dried	200	60	6	2.5 ± 0.7	55.7 ± 0.4	40.2 ± 0.4	1.7 ± 0.0	58.1	41.9
Carrot	Dried	220	60	6	2.2 ± 0.2	52.4 ± 0.1	43.4 ± 0.1	2.0 ± 0.1	54.7	45.3
Rye AD	Dried	180	60	8	2.4 ± 2.2	79.0 ± 6.5	13.0 ± 1.2	5.7 ± 6.6	85.9	14.1
Rye AD	Dried	200	60	8	0.8 ± 1.3	70.5 ± 1.4	19.4 ± 1.0	9.3 ± 1.0	78.4	21.6
Rye AD	Dried	215	60	15	1.7 ± 1.6	73.6 ± 0.8	17.4 ± 0.9	7.3 ± 1.4	80.9	19.1
Rye AD	Dried	215	60	4	1.1 ± 0.2	71.3 ± 7.3	20.3 ± 2.8	7.4 ± 4.3	77.9	22.1
Rye AD	Dried	215	90	8	0.8 ± 0.1	72.8 ± 4.8	19.9 ± 0.2	6.6 ± 4.9	78.5	21.5
Rye AD	Dried	250	60	8	0.3 ± 0.1	56.3 ± 0.4	31.3 ± 1.0	12.1 ± 0.7	64.2	35.8

Food AD + fibres	Dried	220	60	4	1.1 ± 2.0	73.5 ± 2.7	16.3 3.6	9.2 ± 1.9	81.9	18.1
Mince	Mince	180	60	2	0.6 ± 0.0	93.1 ± 0.4	4.5 ± 0.3	1.8 ± 0.1	95.3	4.7
Mince	Cooked, dried	180	60	2	1.2 ± 0.3	84.2 ± 0.1	13.0 ± 0.1	1.7 ± 0.0	86.7	13.4
Mince	Cooked, dried	200	60	2	1.0 ± 0.1	90.3 ± 1.0	7.5 ± 0.9	1.2 ± 0.1	92.3	7.7
Olive cake	<1mm	200	60	6	2.5 ± 0.7	63.5 ± 3.0	25.3 ± 3.2	8.6 ± 2.2	71.5	28.5
Olive cake	pellets	200	60	6	2.0 ± 0.7	66.7 0.8	27.0 ± 1.5	4.3 ± 1.4	71.2	28.8
Olive cake	pellets	225	60	6	1.7 ± 0.3	64.4 ± 0.6	29.0 ± 0.6	5.0 ± 0.7	69.0	31.0
Olive cake	Pellets	225	60	4	1.0 ± 0.7	65.4 ± 2.0	28.9 ± 0.6	4.8 ± 1.2	69.4	30.6
Olive cake	Pellets	240	120	1	0.4 ± 0.1	55.8 ± 0.5	36.6 ± 0.5	7.2 ± 0.4	60.4	39.6
Rice	Grains	180	60	2	1.9 ± 0.5	73.7 ± 0.4	23.4 ± 0.2	1.0 ± 0.1	75.9	24.1
Rice	Grains	200	60	2	2.2 ± 0.3	52.9 ± 0.3	44.5 ± 0.3	0.4 ± 0.2	54.3	45.7
Rice	Grains	220	60	2	1.8 ± 0.2	48.7 ± 0.2	49.2 ± 0.2	0.3 ± 0.1	49.7	50.3
Rice	Grains	220	60	2	2.0 ± 0.2	48.6 ± 0.1	49.1 ± 0.1	0.3 ± 0.1	49.7	50.3
Sewage Sludge[1]	Dried	180	240	4	2.3 ± 0.1	47.6 ± 1.0	8.9 ± 0.6	41.3 ± 0.7	84.2	15.8
Sewage Sludge[1]	Dried	200	60	4	2.3 ± 0.3	44.8 ± 1.9	12.4 ± 2.2	40.5 ± 1.2	78.4	21.6
Sewage Sludge[1]	Dried	200	120	4	2.0 ± 0.2	43.3 ± 2.6	12.3 ± 0.7	42.4 ± 2.8	77.8	22.2

Sewage Sludge[1]	Dried	200	120	4	2.0 ± 0.2	48.3 ± 0.2	9.9 ± 0.2	39.8 ± 0.3	83.0	17.0
Sewage Sludge[1]	Dried	200	240	4	2.0 ± 0.0	42.2 ± 1.6	11.2 ± 2.5	44.5 ± 1.2	79.0	21.0
Sewage Sludge[1]	Dried	200	60	6	2.2 ± 0.4	44.7 ± 3.5	10.3 ± 1.8	42.9 ± 2.1	81.3	18.7
Sewage Sludge[1]	Dried	200	60	6	2.4 ± 0.7	47.4 ± 3.6	10.0 ± 2.1	40.2 ± 5.3	82.6	17.4
Sewage Sludge[1]	Dried	200	120	6	2.6 ± 0.6	43.5 ± 2.4	12.0 ± 2.6	41.9 ± 3.8	78.4	21.6
Sewage Sludge[1]	Dried	200	240	6	2.0 ± 0.2	43.2 ± 2.8	11.5 ± 1.7	43.3 ± 1.0	79.0	21.0
Sewage Sludge[1]	Dried	200	240	8	1.8 ± 0.2	43.3 ± 3.6	11.1 ± 2.3	43.8 ± 1.5	79.5	20.5
Sewage Sludge[1]	Dried	200	120	8	2.0 ± 0.6	47.0 ± 2.9	8.7 ± 1.5	42.3 ± 2.4	84.4	15.6
Sewage Sludge[1]	Dried	200	60	8	2.1 ± 0.4	46.6 ± 0.2	7.8 ± 0.7	43.5 ± 0.3	85.7	14.3
Sewage Sludge[1]	Dried	220	240	4	1.5 ± 0.1	44.2 ± 1.2	9.3 ± 0.8	45.0 ± 0.8	82.6	17.4
Sunflower shell	<1mm	240	120	6	0.7 ± 0.2	60.1 ± 2.1	36.5 ± 2.5	2.7 ± 0.8	62.2	37.8

Legend: M – moisture, VM – volatile matter, FC – fixed carbon, A – ash, DAF – dry, ash free basis, AD – anaerobic digestate

[1]VM determination performed at 850°C rather than 700°C

Appendix 3 HTC elemental analysis data

Non-waste biomass feedstock

Biomass	Particle size	Elemental composition (%)		
		C	H	N
Soft wood	Pellets	48.0	6.6	0.2
Jatropha	<1mm	59.6	9.9	7.0
Miscanthus	Pellets	48.0	6.5	0.5

Non-waste biomass biocoal

Biomass	Particle size	Temperature (°C)	Time (min)	W/B	Elemental composition (%)		
					C	H	N
Soft wood	<1mm	200	60	6	52.2	5.9	0.3
Soft wood	Pellets	200	60	4	52.8	5.9	0.2
Soft wood	Pellets	225	60	4	57.4	5.8	0.2
Soft wood	<212µm	250	60	2	67.3	5.5	0.4
Soft wood	<1mm	250	60	2	67.1	5.4	0.4
Soft wood	<1mm	250	60	6	65.5	5.3	0.3
Soft wood	pellets	250	60	4	69.4	5.2	0.3
Jatropha	<1mm	200	60	4	64.4	8.5	2.2
Jatropha	<1mm	240	120	6	74.5	11.6	3.8
Jatropha	<1mm	240	120	6	67.2	9.0	2.5
Miscanthus	<1mm	200	60	4	50.5	6.1	0.5
Miscanthus	<1mm	200	60	4	50.1	6.1	0.5

Miscanthus	<1mm	200	60	6	50.7	6.1	0.4
Miscanthus	Pellets	200	60	6	50.8	6.1	0.4
Miscanthus	Pellets	200	60	4	50.4	5.7	0.5
Miscanthus	Pellets	200	240	4	52.9	6.1	0.5
Miscanthus	Pellets	200	240	6	52.7	6.0	1.0
Miscanthus	Pellets	225	30	4	52.9	6.0	0.5
Miscanthus	Pellets	225	30	6	52.9	6.1	0.6
Miscanthus	Pellets	225	150	5	58.0	6.1	0.6
Miscanthus	Pellets	225	30	2	55.1	5.9	0.5
Miscanthus	Pellets	250	60	4	64.2	6.1	0.7
Miscanthus	Pellets	250	240	6	69.5	5.7	0.9
Miscanthus	Pellets	250	60	6	63.0	5.6	0.6
Miscanthus	Pellets	250	240	7	67.7	5.3	0.8
Miscanthus	Pellets	250	240	4	69.4	5.7	0.8

Waste biomass feedstock

Biomass	Particle size	Elemental composition (%)		
		C	H	N
Olive cake	Pellets	45.1	6.3	1.6
Bagasse	<1.3mm	49.5	8.1	0.4
Sunflower shell	<1mm	50.5	8.3	2.0
Rice	Grains	39.6	6.9	1.3
Mince	Cooked, dried	25.5	9.6	6.1
Carrot	Chopped	3.5	9.7	0.1
Rye AD	Dried	38.4	5.2	2.2
Food AD + fibres	As received	42.6	5.9	2.1

Waste biomass biocoal

Biomass	Particle size	Temperature (°C)	Residence time (min)	W/B	Elemental composition (%)		
					C	H	N
Bagasse	<1.3mm	200	60	4	50.5	5.9	0.5
Bagasse	<1.3mm	220	360	6	61.2	5.3	0.5
Bagasse	<1.3mm	240	120	6	70.8	7.1	0.8
Carrot	Dried	180	60	6	57.1	5.7	1.5
Carrot	Dried	200	60	6	62.6	5.6	1.8
Carrot	Dried	220	60	6	64.8	5.5	1.5
Rye AD	Dried	180	60	8	48.0	6.1	1.2
Rye AD	Dried	200	60	8	51.1	6.1	1.6
Rye AD	Dried	215	60	15	51.3	5.9	1.4
Rye AD	Dried	215	60	4	52.6	5.8	1.7
Rye AD	Dried	215	90	8	52.5	5.8	1.6
Rye AD	Dried	250	60	8	59.4	5.4	2.0
Food AD + fibres	Dried	220	60	4	46.3	5.6	2.0
Mince	Raw	180	60	2	67.7	10.0	4.3
Mince	Raw	220	60	2	66.2	10.2	2.9
Mince	Cooked	180	60	2	56.6	7.9	12.6

Mince	Cooked	200	60	2	67.2	9.7	6.7
Mince	Cooked	220	60	2	69.0	10.8	4.4
Olive cake	<1mm	200	60	6	52.6	6.0	2.0
Olive cake	pellets	200	60	6	56.3	6.2	1.5
Olive cake	pellets	200	60	6	56.5	6.1	1.5
Olive cake	Pellets	200	60	4	56.5	6.2	1.6
Olive cake	pellets	225	60	6	60.1	6.2	1.7
Olive cake	pellets	225	60	6	59.1	6.1	1.6
Olive cake	Pellets	225	60	4	60.4	6.3	1.8
Olive cake	Pellets	240	120	1	72.6	8.4	3.1
Rice	Grains	180	60	2	48.8	6.5	3.4
Rice	Grains	200	60	2	66.1	5.2	3.5
Rice	Grains	220	60	2	67.3	5.0	2.6
Rice	Grains	220	60	2	68.2	5.0	2.3
Sewage (Dried)	As received	180	240	4	34.3	4.4	2.3
Sewage (Dried)	As received	200	60	4	38.3	5.0	3.3
Sewage (Dried)	As received	200	120	4	35.1	4.6	3.1
Sewage (Dried)	As received	200	240	4	37.9	4.8	2.9
Sewage (Dried)	As received	200	60	6	34.5	4.0	3.0

Sewage (Dried)	As received	200	60	6	38.1	5.3	3.8
Sewage (Dried)	As received	200	120	6	37.9	5.0	2.6
Sewage (Dried)	As received	200	240	6	35.0	4.3	2.9
Sewage (Dried)	As received	200	240	8	33.5	4.1	2.7
Sewage (Dried)	As received	200	120	8	35.0	4.4	2.9
Sewage (Dried)	As received	200	60	8	34.3	4.4	3.0
Sewage (Dried)	As received	220	240	4	39.3	5.0	3.3
Sunflower shell	<1mm	240	120	6	73.0	8.1	4.0
Sunflower shell	<1mm	240	120	6	66.7	6.1	1.5